



**The architecture of chemical and electrical synapses
of horizontal cell dendrites in the mouse retina**

Von der Fakultät für Mathematik und Naturwissenschaften der
Carl von Ossietzky Universität Oldenburg zur
Erlangung des Grades und Titels eines

Doktors der Naturwissenschaften (Dr. rer. nat.)

angenommene Dissertation

Von Matteo Spinelli
Geboren am 7. Juli 1985 in Pisa, Italien

Gutachterin: Prof. Dr. Ulrike Janssen-Bienhold

Weitere Gutachter: in: Prof. Dr. Karl-Wilhelm Koch

Prof. Dr. Arne Nolte

Tag der Disputation: 18.12.2024

I am a slow walker, but I never walk back.

Abraham Lincoln

Given how much is now known, it might be fair to ask,
are we finished with the retina, or are there more surprises on the horizon?

Helga Kolb, 2003

Table of contents

Summary	IV
Zusammenfassung	VII
Acknowledgements	X
List of abbreviations.....	XII
List of figures	XIV
List of tables	XVI
1. Introduction	1
1.1 The mammalian retina	2
1.2 The cellular components of the outer retina	4
1.2.1 Photoreceptors.....	4
1.2.2 Horizontal cells.....	7
1.2.3 Bipolar cells.....	9
1.3 Synaptic architecture of the outer retina	11
1.3.1 Chemical synapses.....	11
1.3.2 Electrical synapses (Connexins).....	14
1.3.3 Electrical coupling in the outer retina.....	16
1.3.4 Zonula Occludens-1 in the outer retina	18
2. Aims of the study	19
2.1 Project 1: Spatial organization of desmosome-like junctions and gap junctions in the outer plexiform layer of the mouse retina	20
2.2 Project 2: Analysis of a possible mutual interaction between electrical and chemical synapses at the desmosome-like junction level in the OPL of mouse retina	21
2.3 Project 3: The distinct distribution of horizontal cell gap junctions across the retina ..	22
3. Methods	23
3.1 Experimental animals	23
3.2 Tissue preparation	24
3.2.1 Retinal preparation for whole-mounted retinas.....	25
3.2.2 Brushing technique for whole-mounted retinas	26
3.2.3 Retina preparation for vertical sections	29

3.3	Immunohistochemistry	29
3.3.1	Immunolabeling of whole-mounted retinas	30
3.3.2	Immunolabeling of vertical sections	31
3.3.3	Primary and secondary antibodies	31
3.4	Image acquisitions and analysis	33
3.5	Statistical analysis	37
4.	Results	38
4.1	Spatial organization of desmosome-like junctions and gap junctions in the outer plexiform layer of the mouse retina	38
4.1.1	The cone pedicle markers	38
4.1.2	The distinct distribution patterns of the AMPA subunits GluA2, GluA2/3 and Glu4	40
4.1.3	Desmosome-like junctions in the mouse retina	47
4.2	Analysis of a possible mutual interaction between electrical and chemical synapses at the level of desmosome-like junctions in the OPL of the mouse retina	49
4.2.1	Analysis of the Cx57 and ZO-1 staining patterns in GluA2/4 KO animals.....	49
4.2.2	Analysis of the expression patterns of glutamate receptors and ZO-1 in Cx57 KO animals.....	55
4.2.3	Spatial interaction between ZO-1 and Cx57 OPL of the mouse retina.....	59
4.3	Horizontal cells gap junctions across the retina	60
4.3.1	Distribution of horizontal cells in the mouse retina	60
4.3.2	Asymmetric expression of Cx57 across the retina	63
4.3.3	Clustering of ZO-1 and GluA2 across the retina.....	67
5.	Discussion	70
5.1	The AMPA subunits GluA2, GluA2/3 and GluA4 show distinctive distribution patterns in the OPL of the mouse retina	70
5.2	Mouse desmosome-like junctions architecture	75
5.3	The interplay between desmosome-like junctions and gap-junctions in the mouse retina	78
5.4	The dorso-ventral density gradient of horizontal cells is reflected in distinctive changes of dendritic gap junctions	85
5.5	Conclusion and focus points	88
6.	References	89

7. Appendix	109
7.1 Materials	109
7.1.1 Mouse lines.....	109
7.1.2 Devices	109
7.1.3 Consumables.....	110
7.1.4 Chemicals and kits.....	110
7.1.5 Solutions and buffers	111
7.1.6 Primers.....	112
7.1.7 Software.....	112
7.2 Experimental protocols	113
7.2.1 Colocalization analysis protocol.....	113
7.2.2 Anti-Cx57 antibodies validation	113
7.2.3 Immunostaining protocols	115
7.2.4 Horizontal cell quantification and retina reconstructions	116
7.2.5 Genotyping protocols.....	116
7.3 Supplemental material	118
7.3.1 Updated nomenclature for ionotropic glutamate receptors	118
7.3.2 Staining pattern of the anti-GluA2 rabbit monoclonal antibody	119
7.3.3 Cx50 immunoreactivity was unchanged in Cx57-deficient mouse retinas	120
7.4 Publication	121
8. Erklärung	156

Summary

The retina is a thin layer of neuronal tissue located at the back of the eyeball, forming part of the central nervous system. It is responsible for detecting light and converting it into neural signals, which are then processed and transmitted to specific central targets that support various functions, including visual perception (Dhande et al., 2015).

Visual information processing in the retina begins at the first synaptic layer, known as the outer plexiform layer (OPL). Here, signal processing is dominated by horizontal cells, a class of inhibitory interneurons that modulate the synaptic contacts between photoreceptor terminals and their postsynaptic neurons. Triad ribbon synapses are structurally and functionally unique; they form synaptic complexes in which the horizontal cell processes and ON bipolar cell dendrites invaginate into the axon terminals of photoreceptors (Rao-Mirotnik et al., 1995; Sterling and Matthews, 2005). Horizontal cells receive glutamatergic input from photoreceptors via ionotropic AMPA-type glutamate receptors (GluAs) (Hack et al., 2001; Haverkamp et al., 2001a; Wässle, 2004), and provide both feedback inhibition to photoreceptors and feedforward inhibition to bipolar cells. That way, horizontal cells affect the center/surround receptive field of the downstream neurons, as well as contribute to the light adaptation of the retina (for review, see Thoreson and Mangel, 2012). Interestingly, GluAs are not only expressed at the tips of invaginating horizontal cells dendrites but also more proximally at the so-called desmosome-like junctions which are formed between their dendrites ~ 1-2 μm beneath the cone pedicle (Haverkamp et al., 2000). It has been shown in primate retinas that GluAs occur in close spatial association with electrical synapses (gap junctions) between horizontal cells at these sites (Puller et al., 2009). There, mutual interactions between electrical and chemical synapses may exist (Pereda, 2014), similar to what has been shown at the level of mouse retinal amacrine cells (Kothmann et al., 2012). Gap junctions are clusters of intercellular channels that facilitate the exchange of ions and small metabolites between adjacent cells (Söhl et al., 2005). In the mouse retina, horizontal cell dendrites are homologously coupled by gap junctions via connexin57 (Cx57) in the proximal part of the OPL, providing an extensively coupled network which enables them to collect light information over a large area of the retina (Hombach et al., 2004; Shelley et al., 2006; Janssen-Bienhold et al., 2009). The extent of gap junctional coupling is regulated by ambient light levels (Xin and Bloomfield, 1999). However, the precise distribution of GluA subunits in mouse horizontal cells is still unclear, and the potential interaction between electrical and chemical synapses at the desmosome-like junction level remains unknown.

Therefore, in the context of this thesis, immunofluorescence and confocal microscopy were used to investigate the exact spatial distribution of AMPA-type glutamate receptor subunits, whether they are expressed at the putative desmosome-like junctions beneath the cone

pedicles, and if they form functional synaptic complexes with electrical synapses at these sites. AMPA-type glutamate receptors mediate most of the excitatory synaptic transmission in the central nervous system. They possess a flexible quaternary organization formed by four core subunits, GluA1-4, whose specific combinations influence their kinetic properties (Boulter et al., 1990; Keinänen et al., 1990; Greger et al., 2017). The glutamatergic input of mouse horizontal cells is mediated exclusively by AMPA-type receptors (Schubert et al., 2006; Ströh et al., 2013), containing the subunits GluA2 and GluA4 (Hack et al., 2001; Ströh et al., 2018). The staining patterns of GluAs in the OPL revealed distinct distributions. The GluA2/3 immunoreactivity exhibited a punctate pattern in the distal OPL and at the invaginating tips of horizontal cell dendrites, but a much finer and barely detectable pattern below the cone pedicle. GluA2 immunoreactivity was observed at the invaginating tips of horizontal cell dendrites and along the distal OPL, at rods level. Interestingly, clusters of GluA2 were detected beneath the cone pedicle at the putative level of the desmosome-like junctions. In contrast, the GluA4 subunit displayed a fine punctate distribution in the OPL, without forming clusters beneath the cone pedicle, suggesting its association, mostly at the tips of horizontal cell processes. Overall, the results highlighted the presence of AMPA-type receptor subunits beneath the cone pedicle, with GluA2 being the primary candidate for cluster formation at the putative desmosome-like junctions. Cx57-containing gap junctions were also detected in this area suggesting a conserved pattern of the spatial organization of the two types of cell-cell junctions in mammalian horizontal cells. Given the observed distribution patterns of GluA2 and Cx57 beneath the cone pedicle, the second project of this thesis aimed to determine whether a mutual interaction between electrical and chemical synapses exists at the level of desmosome-like junctions. The use of powerful tools, such as transgenic mice in which one line specifically lacked Cx57-containing gap junctions and another line lacked GluA2 and GluA4 subunits in horizontal cells, revealed altered expression of dendritic gap junctions, resulting in a pronounced reduction of Cx57 immunofluorescence in GluA2/4-deficient mice. This suggests that, either directly or indirectly, the expression of Cx57-containing gap junctions is functionally dependent by the operation of AMPA-type receptor-mediated glutamatergic input in horizontal cell dendrites.

The expression pattern of the scaffolding protein zonula occludens-1 (ZO-1) was analyzed to gain further insight into the synaptic architecture at horizontal cell desmosome-like junctions and gap junctions. ZO-1 is known to interact with electrical synapses (Giepmans, 2004; Li et al., 2004c; Flores et al., 2008), and is expressed at gap junctions beneath cone pedicles in horizontal cells (Puller et al., 2009). In the mouse retina, it colocalizes with Cx57 at dendro-dendritic gap junctions of horizontal cells and is closely associated with glutamate receptors in the primate retina (Puller et al., 2009). Surprisingly, in the third project of this thesis, Cx57 and ZO-1 were observed to colocalize beneath cone pedicles in the dorsal retina, while no such

colocalization was found in the ventral retina, due to a marked reduction in Cx57 clustering on horizontal cell dendrites beneath cone pedicles in the ventral region. This spatially distinct association between gap junction and tight junction proteins below cone pedicles appeared to correlate with the transition zone of short-wavelength sensitive S-opsin expression of cone photoreceptors, which forms a dorso-ventral gradient across the mouse retina (Applebury et al., 2000; Nadal-Nicolás et al., 2020), and corresponds to the visual horizon of the mouse. These results suggest a distinct functional organization of electrical synapses between horizontal cell dendrites across the retina which may be dictated by certain features of the visual environment (Baden et al., 2013; Qiu et al., 2021).

Finally, the qualitative analysis of GluA subunits and the quantification of Cx57-positive plaques and ZO-1-positive plaques beneath the cone pedicle, were accompanied by a large-scale analysis of the horizontal cell density distribution across complete mouse retinas to elaborate on existing data (Camerino et al., 2021), in collaboration with Lucia Lindenthal, Christoph Block and Asli Pektaş. The density of horizontal cells was notably low in the far dorsal retina, exhibiting a steep increase toward the central-dorsal region, where it remains elevated through to the ventral retina. These findings suggest that the asymmetrical organization of horizontal cells and gap junctions along the dorso-ventral axis, as well as their change at the mouse S-opsin transition zone, may represent a functional adaptation to the visual environment occurring at the first synaptic layer of the mouse visual system.

Zusammenfassung

Die Netzhaut ist eine dünne Schicht aus neuronalem Gewebe, die sich auf der Rückseite des Auges befindet und Teil des zentralen Nervensystems ist. Sie ist für die Erkennung von Licht und dessen Umwandlung in neuronale Signale zuständig, die dann verarbeitet und an bestimmte zentrale Hirnregionen weitergeleitet werden, die verschiedene Funktionen, einschließlich der visuellen Wahrnehmung, unterstützen (Dhande et al., 2015).

Die visuelle Informationsverarbeitung in der Netzhaut beginnt in der ersten synaptischen Schicht, der äußeren plexiformen Schicht (OPL). Hier wird die Signalverarbeitung von Horizontalzellen (HZ) dominiert, einer Klasse von hemmenden Interneuronen, die die synaptischen Kontakte zwischen Photorezeptorendigungen und ihren postsynaptischen Neuronen modulieren. Solch sogenannte „triad ribbon synapses“ sind strukturell und funktionell einzigartig; sie formen synaptische Komplexe, bei denen die Fortsätze der HZ und die Dendriten der ON-Bipolarzellen in die Axonendigungen der Photorezeptoren invaginieren (Rao-Mirotznik et al., 1995; Sterling and Matthews, 2005). HZ erhalten über ionotrope Glutamatrezeptoren vom AMPA-Typ (GluAs) glutamatergen Input von Photorezeptoren (Hack et al., 2001; Haverkamp et al., 2001a; Wässle, 2004) und vermitteln sowohl eine Rückkopplungshemmung für Photorezeptoren als auch eine Vorwärtshemmung für Bipolarzellen. Auf diese Weise beeinflussen die HZ die rezeptiven Felder der nachgeschalteten Neuronen, indem sie über laterale Hemmung an der Entstehung des Zentrum-Umfeld-Antagonismus in der Netzhaut beteiligt sind. HZ tragen außerdem zur Lichtadaptation der Retina bei (für eine Übersicht siehe (Thoreson and Mangel, 2012)). Interessanterweise werden GluAs nicht nur an den Spitzen der invaginierenden Dendriten der HZ exprimiert, sondern auch weiter proximal an den sogenannten Desmosomen-ähnlichen Verbindungen („desmosome-like junctions“, DLJ), die sich zwischen ihren Dendriten etwa 1-2 µm unterhalb der Zapfenterminalien („pedicles“) bilden (Haverkamp et al., 2000). In der Netzhaut von Primaten wurde gezeigt, dass GluAs in enger räumlicher Anordnung mit elektrischen Synapsen (Gap junctions) zwischen HZ an diesen Stellen auftreten (Puller et al., 2009). Möglicherweise bestehen dort gegenseitige Wechselwirkungen zwischen elektrischen und chemischen Synapsen (Pereda, 2014), ähnlich wie es für die Amakrinzellen der Mäusenetzhaut gezeigt wurde (Kothmann et al., 2012). Gap junctions sind Ansammlungen von interzellulären Kanälen, die den Austausch von Ionen und kleinen Stoffwechselprodukten zwischen benachbarten Zellen erleichtern (Söhl et al., 2005). In der Mäusenetzhaut sind die Dendriten der HZ durch Gap junctions über Connexin57 (Cx57) im proximalen Teil der OPL homolog gekoppelt und bilden so ein weitreichend gekoppeltes Netzwerk, welches es ihnen ermöglicht, Lichtinformationen über einen großen Bereich der Netzhaut zu sammeln (Hombach et al., 2004; Shelley et al., 2006; Janssen-Bienhold et al., 2009). Das Ausmaß der

elektrischen Kopplung zwischen HZ wird durch die Lichtverhältnisse in der Umgebung reguliert (Xin and Bloomfield, 1999). Die genaue Verteilung der GluA-Untereinheiten in den HZ der Maus ist jedoch noch immer unklar, sowie die putative Interaktion zwischen elektrischen und chemischen Synapsen auf Ebene der DLJ. Deshalb wurden im Rahmen dieser Arbeit Immunfluoreszenz und konfokale Mikroskopie eingesetzt, um die genaue räumliche Verteilung der Glutamaterezeptor-Untereinheiten vom AMPA-Typ zu untersuchen und festzustellen, ob sie an vermuteten DLJ unterhalb der Zapfenterminalien exprimiert werden und ob sie an diesen Stellen funktionelle synaptische Komplexe mit elektrischen Synapsen bilden.

Glutamaterezeptoren vom AMPA-Typ vermitteln den größten Teil der erregenden synaptischen Übertragung im zentralen Nervensystem. Sie besitzen eine flexible quartäre Struktur, die durch die Kombination von vier Untereinheiten der AMPA-Subtypen GluA1-4 entsteht. Deren spezifische Kombinationen beeinflussen die kinetischen Eigenschaften der Rezeptoren (Boulter et al., 1990; Keinänen et al., 1990; Greger et al., 2017). Der glutamaterge Eingang auf HZ der Maus wird ausschließlich durch Rezeptoren vom AMPA-Typ vermittelt (Schubert et al., 2006; Ströh et al., 2013), die die Untereinheiten GluA2 und GluA4 enthalten (Hack et al., 2001; Ströh et al., 2018). In der vorliegenden Arbeit zeigten die Färbemuster von GluAs in der OPL unterschiedliche Verteilungen. Die GluA2/3-Immunreaktivität wies ein punktförmiges Muster in der distalen OPL und an den invaginierenden Spitzen der Dendriten der HZ auf, aber ein viel feineres und kaum nachweisbares Muster unterhalb der Zapfenterminalien. Die GluA2-Immunreaktivität wurde an den invaginierenden Spitzen der Dendriten der HZ und entlang der distalen OPL auf Stäbchenebene beobachtet. Interessanterweise wurden Cluster von GluA2 unterhalb der Zapfenterminalien auf der vermuteten Ebene der DLJ entdeckt. Im Gegensatz dazu zeigte die Untereinheit GluA4 eine feine punktuelle Verteilung in der OPL, ohne Cluster unterhalb der Zapfenterminalien zu bilden. Dies deutet darauf hin, dass GluA4 hauptsächlich an den Spitzen der Fortsätze von HZ vorkommt. Insgesamt unterstreichen die Ergebnisse das Vorhandensein von Rezeptoruntereinheiten des AMPA-Typs unterhalb der Zapfenterminalien, wobei GluA2 der Hauptkandidat für die Clusterbildung an den mutmaßlichen DLJ ist. In diesem Bereich wurden auch Cx57-haltige Gap junctions entdeckt, was auf ein konserviertes Muster der räumlichen Organisation beider Arten von Zell-Zell-Verbindungen in Dendriten von HZ von Säugetieren hindeutet. Angesichts der beobachteten Verteilungsmuster von GluA2 und Cx57 unterhalb der Zapfenterminalien zielte das zweite Projekt dieser Arbeit darauf ab, festzustellen, ob eine gegenseitige Wechselwirkung zwischen elektrischen und chemischen Synapsen auf der Ebene der DLJ besteht. Durch den Einsatz verschiedener transgener Mauslinien, bei denen zum einen das HZ spezifische Cx57 fehlte und zum anderen GluA2- und GluA4-Untereinheiten selektiv in HZ ausgeschaltet wurden, konnte eine veränderte Expression dendritischer Gap junctions festgestellt werden. Diese betraf die GluA2/4-defizienten Mäuse in deren Retinen eine ausgeprägte Verringerung der Cx57-Immunfluoreszenz in der

proximalen OPL beobachtet werden konnte. Dies deutet darauf hin, dass die Präsenz von Cx57-haltigen Gap junctions in diesem subzellulären Kompartiment entweder direkt oder indirekt von der Funktion des AMPA-Rezeptor-vermittelten glutamatergen Inputs in HZ-Dendriten abhängig ist. Das Expressionsmuster des Gerüstproteins Zonula Occludens-1 (ZO-1) wurde analysiert, um weitere Einblicke in die detaillierte synaptische Architektur an DLJs und Gap junctions an Dendriten von HZ zu gewinnen. Es ist bekannt, dass ZO-1 mit elektrischen Synapsen interagiert (Giepmans, 2004; Li et al., 2004c; Flores et al., 2008) und an Gap junctions unterhalb der Zapfenterminalien in HZ exprimiert wird (Puller et al., 2009). In der Mausretina kolokalisiert es mit Cx57 an dendro-dendritischen Gap junctions von HZ und in der Primatenretina ist es eng mit Glutamatrezeptoren assoziiert (Puller et al., 2009). Interessanterweise wurde im dritten Projekt dieser Arbeit eine Kolokalisation von Cx57 und ZO-1 unter den Zapfenterminalien in der dorsalen Retina beobachtet, während in der ventralen Retina keine derartige Kolokalisation gefunden wurde, was auf eine deutliche Verringerung der Cx57-Präsenz auf Dendriten von HZ unter den Zapfenterminalien in der ventralen Region zurückzuführen ist. Dieses spezifische Verteilungsmuster von Gap junction (Cx57)- und Tight junction (ZO-1)-Proteinen unterhalb der Zapfenterminalien korreliert mit der Übergangszone der S-Opsin-exprimierenden Zapfenphotorezeptoren, die einen dorso-ventralen Gradienten über die Mausretina bilden (Applebury et al., 2000; Nadal-Nicolás et al., 2020) und zur Bildung des visuellen Horizonts der Maus beitragen. Diese Ergebnisse deuten auf eine unterschiedliche funktionelle Organisation der elektrischen Synapsen zwischen den Dendriten von HZ in unterschiedlichen Arealen der Netzhaut hin, die möglicherweise durch bestimmte Merkmale der visuellen Umgebung bestimmt wird (Baden et al., 2013; Qiu et al., 2021). Abschließend wurden die qualitative Analyse der GluA-Untereinheiten und die Quantifizierung der Cx57 und ZO-1-positiven Strukturen unterhalb der Zapfenterminalien von einer umfassenden Analyse der Verteilung von HZ in der gesamten Netzhaut der Maus begleitet, u.a. auch um bestehende Daten zu ergänzen (Camerino et al., 2021). In diesem Projekt wurden die Daten in Zusammenarbeit mit Lucia Lindenthal, Christoph Block und Asli Pektas erhoben und ausgewertet. Sie zeigen, dass die Dichte der HZ in der äußeren dorsalen Retina besonders niedrig ist, zur zentral-dorsalen Region hin signifikant zunimmt und bis in die ventrale Retina hinein erhöht bleibt. Diese Ergebnisse deuten darauf hin, dass die asymmetrische Verteilung von HZ und Gap junctions entlang der dorso-ventralen Achse sowie ihre Veränderung in der S-Opsin-Übergangszone der Maus strukturell-funktionelle Anpassungen an die Bedingungen der visuellen Umgebung repräsentieren, die bereits in der ersten synaptischen Schicht des visuellen Systems der Maus erfolgen.

Acknowledgements

I am deeply aware that this achievement is not mine alone but the result of the consistent support, guidance, and motivation I have received from numerous people over all these years.

I am extremely grateful to apl. Prof. Dr. Ulrike Janssen-Bienhold, who believed in me from the very beginning, for giving me the chance to work on the fascinating topic of retinal research. Her unwavering support and encouragement helped me to believe in myself, encouraging both independence and a critical perspective on my work and scientific findings. Her depth of knowledge and commitment to excellence have been invaluable, guiding me at every step of my research journey. Her patience and empathy provided comfort during moments of doubt, instilling in me the confidence and resilience needed to persevere and grow.

I am equally grateful to Dr. Christian Puller for his invaluable insights and patience, and constant support as my project leader over the years. Despite no longer being present in the lab, he consistently supervised my progress, offering correction, direction, and thoughtful suggestions that were essential in shaping this research. His constructive feedback and critical insights continually challenged me to think more deeply and refine my work, ultimately bringing my research to a level of rigor and clarity that I am truly proud of. I am deeply grateful for the opportunity to learn from his expertise and guidance.

I would like to thank Prof. Dr. Karl-Wilhelm Koch for providing a second opinion and reviewing this thesis.

I am extending my thanks to apl. Prof. Dr. Karin Dedek, for her support, guidance, and the depth of advice she generously provided during the collaboration and valuable support in preparing the publication. Conversely, I am thankful to Prof. Dr. Martin Greschner for welcoming me into his lab, for the support he provided throughout my research, and for his valuable input on the publication.

I am indebted to many of my colleagues and researchers that supported me for this long time. Special thanks go to Bettina Kewitz for her extraordinary technical support and to Dr. Patrick Dömer for his countless and valuable advice, which extended beyond the professional sphere. I would like to express my gratitude to Christoph Block for his invaluable collaboration and great support, which has been immensely helpful on numerous occasions. I am thankful to Dr.

Alejandra Acevedo Harnecker for the successful collaboration on the research project. I would like to thank Lucia Lindenthal and Asli Pektaş for their contributions to the laboratory work.

All my thanks to my lovely colleagues Dipti Ranjan Pradhan, Max Manackin and Dr. Malte Ahlers for their wonderful support, willingness and valuable suggestions in various situations throughout this journey.

A warm thank you goes to my colleagues and friends, Domna Zourelidou, Malien Laurien, Manisha Kumari, Faiza Altaf and Anders Frederiksen, for the many good times we had together. I am thankful to my ever-present friends, Tamara Hirschfeld and Dr. Ashwin Hariharan, met at the start of this journey and whom I hope to carry with me into the future.

I would like to thank my former colleagues Dr. Sabrina Duda and Dr. Lena Nemitz for their help at the beginning of this experience. Thanks to Nicole Iben and Dr. Simeon Helgers for their help and suggestions in the lab and the nice working atmosphere .

I extend my gratitude to Dr. Kristin Tietje for her great support and amazing work as scientific manager and coordinator, the German Research Foundation (DFG) and the Research Training Group (RTG).

This journey would not have been possible without the unwavering support of my mother and my brothers. Thank you for your endless patience, sacrifices, and unconditional belief in me. Your words of encouragement have been my anchor during challenging and dark times, especially during moments when I felt lost and uncertain. Thank you for reminding me to breathe, to calm down, and keep moving forward.

List of abbreviations

°C	Degree Celsius
µg	Microgram
µl	Microliter
µm	Micrometer
µm ²	Square micrometer
AC	Amacrine cell
AMPA	α-amino-3-hydroxy-5-methyl-4-isoxazolepropionic acid
ANOVA	Analysis of variance
BC	Bipolar cell
bp	base pairs
BSA	Bovine serum albumin
CaBP	Calcium binding protein
CNS	Central nervous system
Cre	Cre-recombinase (Cre- <i>loxP</i> System)
CtBP2	C-terminal binding protein 2
Cx	Connexin
dk	Donkey
Fig.	Figure
Fiji	Fiji Is Just ImageJ
Flox	flanked by <i>loxP</i> sites (floxed)
g	Gram
GABA	γ-aminobutyric acid
GC	Ganglion cell
GCL	Ganglion cell layer
GluA	AMPA glutamate receptor
GluK	Kainate glutamate receptor
gp	Guinea pig
gt	Goat
h	hour
HC	Horizontal cell
IgG	Immunoglobulin G
IgM	Immunoglobulin M
IHC	Immunohistochemistry
ILM	Inner limiting membrane

INL	Inner nuclear layer
IPL	Inner plexiform layer
IS	Inner segment
KO	Knock-out
MAGUK	Membrane-associated guanylate kinase
mg	Milligram
mGluR	Metabotropic glutamate receptor
min	Minute
ml	Milliliter
mM	Millimolar
ms	Mouse
n.s.	Non-significance
NDS	Normal donkey serum
nm	Nanometer
NMDA	N-methyl-D-aspartate
OLM	Outer limiting membrane
ONL	Outer nuclear layer
OPL	Outer plexiform layer
OS	Outer segment
PB	Phosphate buffer
PBS	Phosphate buffered saline
PCR	Polymerase chain reaction
PDZ	PSD95/DLG/ZO-1 binding motif
PFA	Paraformaldehyde
pH	Potential of hydrogen
PNA	Peanut agglutinin
PR	Photoreceptor
PSD-95	Postsynaptic density protein 95
rb	Rabbit
RGC	Retinal ganglion cell
rpm	Revolutions per minute
ROI	Region of interest
RT	Room temperature
TBS	Tris-buffered saline
TX-100	Triton X-100
ZO-1	Zonula occludens-1
WT	Wilde-type

List of figures

Figure 1: Schematic structure of the mammalian retina.....	2
Figure 2: Schematic structure of rod and cone photoreceptors	5
Figure 3: Schematic structure of the synaptic terminal of cones.....	7
Figure 4: Morphology of a B-type horizontal cell.....	8
Figure 5: Mouse retina bipolar cells and their connectivity	10
Figure 6: Laminated location of ionotropic glutamate receptors at the cone pedicle	13
Figure 7: Structural organization of gap junctions	14
Figure 8: Layered organization of the mouse retina focusing on the OPL.....	27
Figure 9: The integrity of the OPL is to be maintained following the brushing technique	28
Figure 10: Imaging strategy and layer-specific visualization.....	34
Figure 11: Illustration of the acquisition strategy in whole-mounted retinas.....	36
Figure 12: Organization of photoreceptor terminals in the OPL and their markers.....	39
Figure 13: GluK1 and PNA as cone pedicle base markers	40
Figure 14: Different expression patterns of GluAs in the OPL of mouse retina	41
Figure 15: GluA4 expression in three horizontal planes of the OPL	42
Figure 16: GluA2/3 expression in the three horizontal planes of the OPL	44
Figure 17: GluA2 clusters at the putative desmosome-like junctions	45
Figure 18: GluA2 distribution on horizontal cells	46
Figure 19: Cx57 is closely associated with GluA2 at the level of the desmosome-like junctions	48
Figure 20: ZO-1 and the GluA2 subunit are closely associated at the desmosome-like junctions	49
Figure 21: Absence of GluA2 and GluA4 in horizontal cells affects ZO-1 and Cx57 expression at desmosomal-like junctions	51
Figure 22: Effects of GluA2/4-deficiency on ZO-1 and Cx57 expression at desmosomal-like junctions detected by using a different mix of antibodies	53
Figure 23: Expression of ZO-1 and Cx57 at the cone pedicle appear to be affected by GluA2/4 deficiency in horizontal cells.....	54
Figure 24: Comparison of GluA4 and ZO-1 expression pattern in WT and Cx57-KO retinas	56
Figure 25: Comparison of GluA2/3 and ZO-1 expression patterns in WT and Cx57-KO retinas.....	57
Figure 26: Comparison of GluA2 and ZO-1 expression patterns in WT and Cx57-KO retinas.....	58

Figure 27: The ZO-1 expression pattern is affected in GluA2/4 KO in HCs of the mouse retina..... 59

Figure 28: Association and colocalization of Cx57 and ZO-1..... 60

Figure 29: Calbindin immunoreactivity of horizontal cells in mouse retina 61

Figure 30: Horizontal cell density shows a distinct dorso-ventral gradient 62

Figure 31: Spatial localization of horizontal cell gap junctions 64

Figure 32: Clusters of ZO-1 and Cx57 and their level of colocalization differ between dorsal and ventral retina..... 65

Figure 33: Clusters of ZO-1 and Cx57 change at the S-opsin transition zone..... 66

Figure 34: Distinctive clustering of ZO-1 in the dorsal and ventral mouse retina..... 68

Figure 35: Patterns of GluA2 immunoreactivity reveal no obvious differences between the dorsal and ventral retina..... 69

Figure 36: Connexin57 antibody validation 114

Figure S1: Anti-GluA2 rabbit monoclonal staining pattern in the OPL of the mouse retina 119

Figure S2: Cx50 immunoreactivity is unchanged in Cx57-deficient mice 120

List of tables

Table 1: Primary antibodies and their dilutions	32
Table 2: Secondary antibodies and their dilutions	33
Table 3: Reagents and their dilutions	33
Table 4: Mouse line used in this study.....	109
Table 5: Devices used	109
Table 6: Consumables used	110
Table 7: Chemicals and kits used in this study.....	110
Table 8: Solutions and buffer used in this study	111
Table 9: Primers used for mouse genotyping	112
Table 10: Software used in this study	112
Table 11: Immunostaining protocol for vertical sections	115
Table 12: Immunostaining protocol for whole-mounted retinas.....	115
Table 13: Pipetting scheme for DNA extraction	116
Table 14: Thermocycler setting for DNA extraction	116
Table 15: Cx57 <i>Cre</i> PCR protocol	117
Table 16: Cx57 <i>LacZ</i> PCR protocol	117
Table 17: GluA2/GluA4 PCR protocol	117
Table S1: NC-IUPHAR recommended and previous nomenclature of ionotropic glutamate receptor subunits.	118

1. Introduction

Vision is one of the primary senses that humans rely on to navigate the world, make decisions, and perform complex tasks. Memories and learning processes are strongly influenced by vision.

The entire visual system is organized into a complex architecture of interconnected functional units and specialized processing centers, orchestrated by an equally majestic neural circuitry that characterizes and links these centers. Accordingly, the concept about how information processing in the visual system is managed entails the existence of several parallel pathways that carry different information, interact with one another at different levels and thereby create a coherent visual image.

The visual perception process begins in the retina. The retina is the sensory organ responsible for converting light into neuronal signals and sending visual information to the brain.

In the past, the mechanisms of visual perception were considered analogous to those of a camera. However, the similarities to a camera are limited to the presence of the lens in the eye that projects an inverted image onto the retina.

The retina is part of the central nervous system (CNS), with a proper cellular and synaptic organization. Instead of functioning as a simple feature detector like a camera, the retina collects, decomposes, and processes a wide range of aspects of the visual environment including colors, contrast, motion and shapes, and ensures their perception under different light conditions.

As part of CNS the retina incorporates highly complex synaptic contacts organized in a layered, anatomically well-ordered arrangement. In this way, the retina is a valuable model, not only to understand the mechanisms of sensory transduction, but also for studying the information processing in more complex neuronal circuits.

Over the past few decades, the visual system and the retina have been extensively studied in primates, such as macaques and humans, as well as in other animal models. Nevertheless, several questions regarding complete functional pathways and their cellular organization are still under debate. In this context this thesis focuses on the outer retina, particularly on the cellular components and synaptic architecture.

In the introduction a brief overview of the entire retinal structure and retinal pathways will be given (see Chapter 1.1), followed by a description of the present state of knowledge about the structure and components involved in information processing in the outer retina (see Chapter 1.2 and 1.3).

1.1 The mammalian retina

The retina represents the initial stage of visual processing. In vertebrates, the retina and optic nerve, like the rest of the CNS, originate from the neural tube, specifically as an outgrowth of the embryonic forebrain. Therefore, the retina is a part of the CNS (Stenkamp, 2015).

The retina is a light-sensitive organ located at the back of the eyeball, approximately 200 μm thin, with two main functions. First, it transduces light into electrical signals. Second, it decomposes and transfers visual information. The specially designed neuronal circuitry of the retina breaks down the visual scene into fundamental component, relaying this information in parallel to the brain for further processing (Kolb, 2003).

The mammalian retina is best characterized as a well-organized laminar structure, consisting of three cellular layers divided by two synaptic or plexiform layers. The light entering the eyeball must pass through the entire tissue before reaching the outer segments of the photoreceptors where it is transduced into an electrical signal. Different neuronal cell classes occur in the retina: photoreceptors, horizontal cells, bipolar cells, amacrine cells and ganglion cells (Fig. 1).

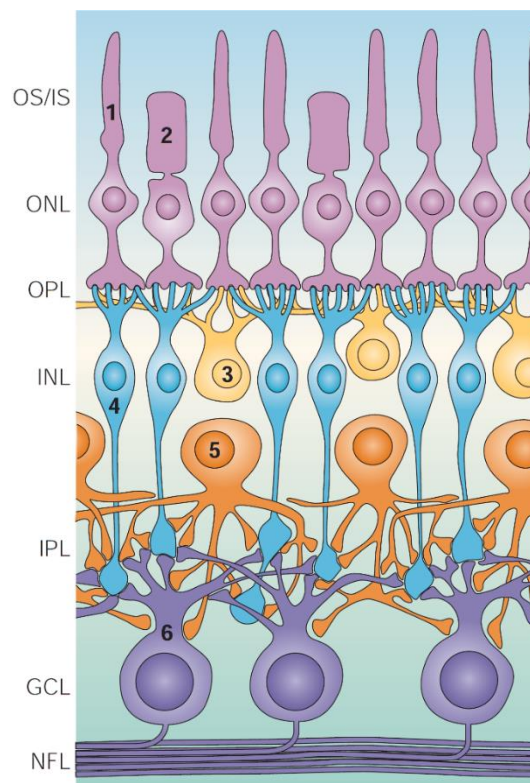


Figure 1: Schematic structure of the mammalian retina

Six classes of neurons are listed by numbers 1-6: rods (1), cones (2), horizontal cells (3), bipolar cells (4), amacrine cells (5) and retinal ganglion cells (6). They are arranged in discrete layers indicated on the left side: outer and inner segments of photoreceptors (OS/IS), outer nuclear layer (ONL), outer plexiform layer (OPL), inner nuclear layer (INL), inner plexiform layer (IPL), ganglion cell layer (GCL) and nerve fiber layer (NFL), modified from (Wässle, 2004).

The cell bodies of rod and cone photoreceptors (PRs) are localized in the outer nuclear layer (ONL). In the second cell layer, called the inner nuclear layer (INL) lie the cell bodies of horizontal cells (HCs), bipolar cells (BCs) and amacrine cells (ACs). Finally, the ganglion cell layer (GCL) contains the cell bodies of ganglion cells (GCs). The spaces between these three layers are the outer plexiform layer (OPL) and the inner plexiform layer (IPL). The OPL contains the synaptic contacts between photoreceptor terminals, the processes of HCs and the dendrites of BCs, while in the IPL the axon terminals of BCs are connected to the neurites of ACs and GC dendrites. On the surface of the inner retina, the axons of the GCs form the nerve fiber layer (NFL), where they bundle together to then form the optic nerve which transfers the information to the visual centers of the brain (Wässle, 2004).

At the photoreceptor terminals, the light-evoked signals are transferred onto the downstream target neurons. Horizontal cells provide lateral interaction in the OPL and modulate the transfer of information between photoreceptors and bipolar cells (see Chapter 1.2.2). Cone and rod bipolar cells receive visual signals and split them into two major sets of visual pathways: ON and OFF. These parallel circuits are then duplicated tangentially, across the extent of the retina, to build the visual field (Wässle and Boycott, 1991). The information is transferred through these pathways to specific sublayers in the IPL. Amacrine cells are the inhibitory lateral elements in the IPL and integrate signals between bipolar cells and ganglion cells (Masland, 2012a). Unlike horizontal cells, they are a very diverse family of at least 45 different cell types (Masland, 2012b). Amacrine cells can be organized into groups based on their size (narrow-, medium-, and wide-field) axonal and dendritic architecture (e.g., mono- or bistratified), neurotransmitter content (glycine, GABA, and acetylcholine) and neuromodulator (dopamine and serotonin) (Kolb, 1997; Masland, 2012a). The dendrites of ganglion cells gather signals from amacrine cells and bipolar cells, and their axons transmit the signal to different areas of the brain. Approximately 30 types of ganglion cells can be classified based on at least four distinct criteria in the mammalian retina. The axons of these cells, which form the optic nerve, represent the sole route by which information can be transmitted from the retina to the brain (for review, see Sanes and Masland, 2015).

Like the rest of the CNS, the mammalian retina comprises neurons and glia. Müller cells are the most abundant glial elements, followed by astrocytes and microglia. Müller glia maintains retinal homeostasis and provides structural support to photoreceptors. Their cell bodies are placed in the INL, and they extend processes which take part in forming the outer limiting membrane (OLM) above the ONL, and the inner limiting membrane (ILM) below the NFL (for review, see Vecino et al., 2016).

1.2 The cellular components of the outer retina

The retina, with its intricately wired neurons and discrete layers, serves as the initial site for feature extraction of the visual information, while image decoding occurs in more complex centers within the visual system. The transmission of signals from photoreceptors to bipolar cells to ganglion cells defines the so-called vertical pathways of information processing. These pathways are modulated in the outer retina by horizontal cells and in the inner retina by amacrine cells (for review, see Diamond, 2017). Thus, the complexity of these circuits is increased by the morphologically and functionally complex synapses, within the outer plexiform layer (OPL), and the various subtypes of cells in the inner retina. Moving forward, this section of the introduction will focus on the architecture of the cellular components in the outer plexiform layer.

1.2.1 Photoreceptors

Information processing in the retina starts with the sampling of the light by photoreceptors. In the vertebrate retina there are two types of photoreceptors. Rods and cones are organized in a similar structure which consists of three distinct compartments (Fig. 2). The outer segment (OS), located at a distal end, is specialized in signal transduction. The central component is the inner segment (IS), which contains the nucleus of the cell and most of the cellular components responsible for biochemical processes. The third compartment located at the proximal end is the synaptic terminal, which establishes connections with horizontal cells and bipolar cells. In the mammalian retina, the distal end of photoreceptors lies directly in front of the pigment epithelial layer, which provides a regular stream of nutrients and supports the physiological recycling of the membrane of the outer segments, during the phototransduction (for review, see Fu and Yau, 2007). While the biochemical mechanisms of phototransduction are not discussed in this text, it is important to note some key functional aspects of photoreceptors to better understand the following topics.

Although the two types of photoreceptors share structural similarities, they exhibit different functional properties which are reflected in their respective neuronal systems. Rods are highly sensitive to light and are responsible for dim light vision (scotopic vision), while cones are responsible for daylight and color vision (photopic vision), but are less sensitive to light (Baylor et al., 1979; Fu and Yau, 2007; Ingram et al., 2016). Additionally, rods have a low temporal resolution due to their slow response and long integration time. Because this type of photoreceptor expresses only one type of pigment, the “rod system” is defined as achromatic. Cones, on the other hand, have high temporal resolution, with rapid responses and short integration times. Most mammals have two types of cones which express two different pigments: green-sensitive and blue-sensitive opsins (for review, see Jacobs, 1993, 2009;

Puller and Haverkamp, 2011a). Mice are dichromats and in addition to a medium (M) wavelength-sensitive opsin peaking at 510 nm (green), they have a short (S) wavelength-sensitive opsin peaking at 360 nm in the UV range (Jacobs et al., 2004; Nikonov et al., 2006; Fu and Yau, 2007).

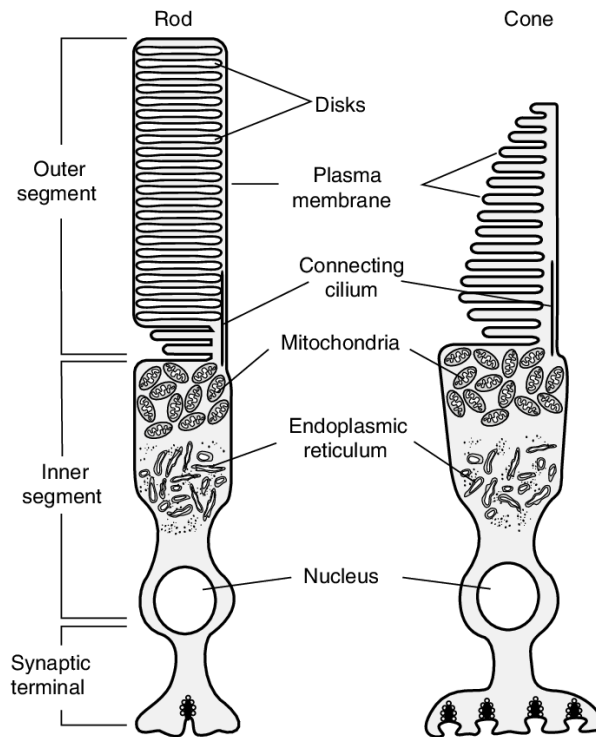


Figure 2: Schematic structure of rod and cone photoreceptors

Both types of photoreceptors include an outer segment and an inner segment that are linked to each other by a cilium, and a synaptic terminal. The first compartment contains membranous discs where photopigments are stored. Endoplasmic reticulum, mitochondria and nucleus are in the inner segment. The end foot of photoreceptors makes synaptic contacts with their specific neuronal targets (modified from (Cote, 2006).

Most of mouse cones co-express both M- and S-opsins, distributed in a dorso-ventral gradient with higher M-opsin expression in the dorsal and S-Opsin in the ventral retina (Applebury et al., 2000). Only few cones express exclusively S-opsin (known as “true S-cones”) and they are mostly concentrated in the ventral retina (Haverkamp et al., 2005; Nadal-Nicolás et al., 2020). Thereby, the “cone system” enables color vision and improves the ability to detect shapes and details, thanks in part to its specific connectivity patterns of the different cone types. Most mammals have retinas with higher density in rods, although the number of rods and cones varies considerably among them (for review, see Peichl, 2005). Mice are a nocturnal species with retinas predominantly composed of rods and only 3% cones (Nikonov et al., 2006).

Like in other sensory systems, the photoreceptors of the retina do not generate action potentials, but they respond to light with a gradual modification of their membrane potentials. Both rods and cones release neurotransmitter in the dark, when the membrane is depolarized by an influx of sodium and calcium ions across the cell membranes. Upon exposure to light,

ion channels in the cell membrane of photoreceptors undergo a closure process, which causes the cells to enter a hyperpolarized state, thereby reducing the release of neurotransmitter. Consequently, the degree of hyperpolarization determines the amount of neurotransmitter released. Photoreceptors show graded membrane potentials according to the inverse of light intensities. Light-evoked changes in the membrane potentials spread from the outer segment to the synaptic terminal where voltage-gated calcium ion channels, clustered at the active zone, are equivalently activated in a light-dependent manner and subsequently, trigger the vesicular Ca^{2+} -dependent release of neurotransmitter (Morgans, 2000).

The synaptic terminals of the photoreceptors lie in the OPL, and they are characterized by the presence of an organelle known as synaptic ribbon, which represents the synaptic machinery for transmitter release. Synaptic ribbons extend from the active zones into the synaptic terminal and are surrounded by numerous docked synaptic vesicles, prepared for exocytosis (Schmitz, 2009). At this specific chemical synapse, the peculiar disposition of vesicles enables a rapid and sustained release of the neurotransmitter, which can be continuously adapted to changes in membrane potential (Sterling and Matthews, 2005). Photoreceptor synaptic vesicles are filled with glutamate via the vesicular glutamate transporter vGluT1 (Haverkamp et al., 2003). Rod and cone axon terminals are quite different. Rod terminals are large, spherical, and are typically called rod spherules. Cone axon terminals are giant synapses, long and flat and are called cone pedicles. In contrast to rod spherules, which only own a single ribbon (Tsukamoto et al., 2001), cone pedicles usually have multiple ribbon release sites (Fig. 3 B). The number of ribbons varies between species. While mouse cones contain approximately 10 ribbons, cones in the peripheral monkey retina feature more than 50 ribbons (for review, see Sterling and Matthews, 2005).

The photoreceptor terminal plasma membrane contains an arciform density to which ribbons are hooked. The arciform density is curved towards the inside of the presynaptic terminal and the synaptic ribbon assumes a shape like a curved plate. In rod spherules it is bent like a horseshoe and commonly cracks in two parts (Migdale et al., 2003). This invagination creates a postsynaptic cavity that is occupied by the invaginating processes of horizontal and bipolar cells (Fig. 3 A). Thereby, two morphologically distinct types of synaptic contacts occur at the photoreceptor terminals. Laterally to the presynaptic ribbon, two invaginating horizontal cell processes are positioned, while centrally below the ribbon, one or two invaginating ON bipolar cell dendrites are located. This synaptic arrangement is also known as a triad synaptic complex (Rao-Mirotnik et al., 1995; Haverkamp and Wässle, 2000; Haverkamp et al., 2000; Li et al., 2016). In contrast, OFF bipolar cells form the flat basal contact (non-invaginating) at the base of the photoreceptors (Haverkamp and Wässle, 2000; Haverkamp et al., 2000).

In this manner, at the synaptic terminals of rods and cones, the light-evoked signals are transferred onto bipolar and horizontal cells (Fig. 3 A). The following chapter will address synaptic communication at this level in greater detail.

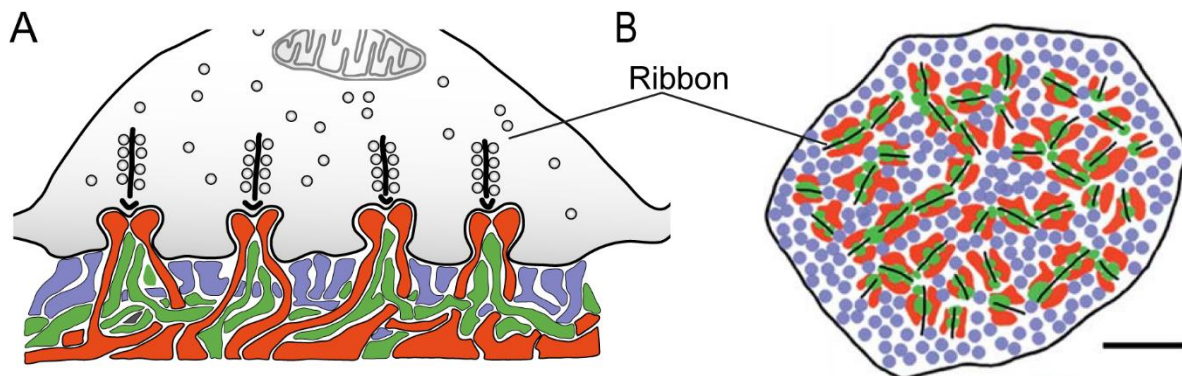


Figure 3: Schematic structure of the synaptic terminal of cones

A: Vertical view of the cone pedicle. The triad synapse consists of the presynaptic ribbon surrounded by synaptic vesicles and opposed to the invaginating dendrites of horizontal cell (red) and ON-cone bipolar cell (green). OFF-cone bipolar cell dendrites make flat contacts at the pedicle base (purple). **B:** Horizontal view of a macaque cone pedicle base. Ribbons (black lines), horizontal cell processes (red), ON-cone bipolar cells dendrites (green) form a triad each one. OFF-cone bipolar cells (purple) contact the cone pedicle base. Scale bar in B, 20 μm , applies to B. Modified from (Wässle, 2008; Puller et al., 2009).

1.2.2 Horizontal cells

Photoreceptors convey light-evoked information to bipolar and horizontal cells at triad ribbon synapses established within the outer plexiform layer (OPL) (Dowling and Boycott, 1966). Horizontal cells are laterally interconnected GABAergic interneurons and although their morphology varies widely between species, their general role in signal processing remains constant.

Most mammals possess two horizontal cell types: the axon-less A-type and the axon-bearing B-type (Kolb et al., 1980; Peichl and González-Soriano, 1994). Rod-dominated retinas, such as the mouse and rat retina, with around 1-3% cones (Peichl, 2005), lack the axon-less A-type horizontal cell (Suzuki and Pinto, 1986; Peichl and González-Soriano, 1994). The axon-bearing B-type horizontal cells (Fig. 4) have a densely branched dendritic tree with fine dendrites and an axon terminal system distant (several hundred microns) from the dendritic structure. Dendrites of mouse horizontal cells carry clusters of terminals that synapse exclusively with cones (Feigenspan and Babai, 2015) while the axon terminal system has unclustered terminals that exclusively contact rods (Peichl and González-Soriano, 1994). The B-type axon differs from typical axons by not relaying information from dendrites and soma to the axon terminal system. It remains electrically isolated from the dendritic segment, possibly due to its thin and long structure, which limits its ability to conduct the graded potentials.

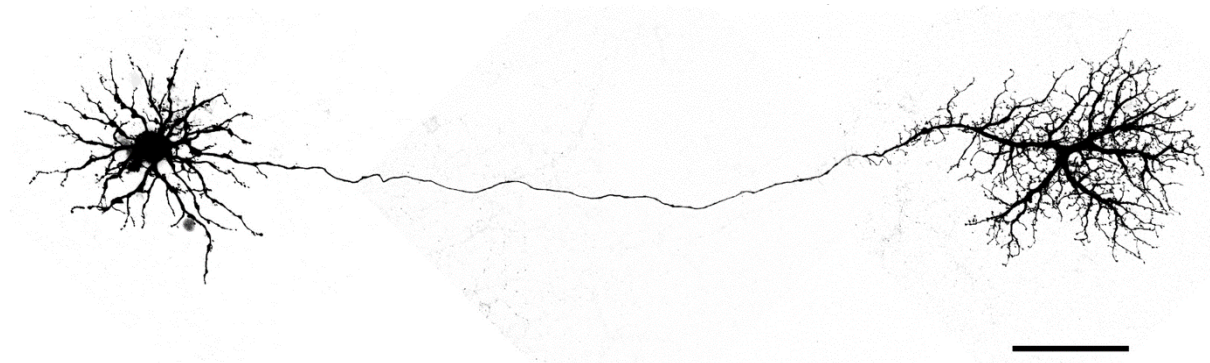


Figure 4: Morphology of a B-type horizontal cell

A single axon-bearing horizontal cell from rabbit retina. The cell body, with somatic dendrites is on the left side, connected by a very fine axon to the axon terminal system, on the right. Scale bar 100 μm . (modified from (Pan et al., 2012).

The B-type axon terminal system in mouse consists of an independent rod horizontal cell and does not contribute to dendritic signaling (Trümpler et al., 2008; Peichl, 2010).

As with OFF bipolar cells, horizontal cells are hyperpolarized by light or depolarized in darkness, which is the reason they are referred to as OFF cells. They receive glutamatergic input from photoreceptors through the α -amino-3-hydroxy-5-methyl-4-isoxazole-propionic acid (AMPA)-type receptors, specifically subunits GluA2 and GluA4 (Hack et al., 2001; Ströh et al., 2013, 2018). Due to extensive coupling through gap junctions, which allows electrical and metabolic communication (Bloomfield and Völgyi, 2009), the receptive fields of horizontal cells are much larger than their dendritic fields (Kaneko, 1971; Dacheux and Raviola, 1982; Bloomfield et al., 1995; Shelley et al., 2006). The extent of electrical coupling depends on the light adaptation state of the retina (Xin and Bloomfield, 1999; Baldrige, 2001). Mouse horizontal cells express two distinct gap junction subunits. The dendritic arbor and the axon terminal system each form independent, electrically coupled networks via connexin57 (Janssen-Bienhold et al., 2009). The axo-axonal network is instead electrically coupled via connexin50 (Dorgau et al., 2015). Chapter 1.3 will cover the spatial organization and function of electrical and chemical synapses in the outer plexiform layer.

Horizontal cells play a key role in shaping visual information processing in the outer mammalian retina, crucial for functions such as light adaptation, contrast enhancement, and color discrimination. Horizontal cells modulate the synaptic communication between photoreceptors and bipolar cells, providing negative feedback (Wu, 1992; Kamermans et al., 2001; Hirasawa and Kaneko, 2003; Kemmler et al., 2014) and feedforward (Yang and Wu, 1991; Fahey and Burkhardt, 2003) at the triad synaptic complex, respectively. Two other forms of lateral interaction in the outer retina have also been described. These include negative feedback from horizontal cells to rods (Thoreson et al., 2008), and local positive feedback from horizontal cells to cones (Jackman et al., 2011). Lateral inhibition generate a center-surround

organization of the receptive field, which is important for noise reduction, spatial discrimination, and edge detection (for review, see VanLeeuwen et al., 2009; Thoreson and Mangel, 2012). In addition, it is assumed that horizontal cells contribute to the downstream organization of the receptive field, including surround properties of retinal ganglion cells (Chaya et al., 2017; Drinnenberg et al., 2018; Ströh et al., 2018).

At the triad synapse, signaling and communication between photoreceptors and horizontal cells is reciprocal. The mechanism by which the photoreceptor output is regulated by negative feedback from horizontal cells is controversial and may differ between species (Thoreson and Mangel, 2012). Three different mechanisms have been suggested: GABA (gamma-aminobutyric acid) release from the horizontal cells (Wu, 1992), changes in the proton concentration in the synaptic cleft (Hirasawa and Kaneko, 2003) and finally the ephaptic modulation of the photoreceptor membrane potential via hemichannels (Kamermans et al., 2001). However, studies suggest that all three mechanisms are involved in negative horizontal cell feedback with different response modulation (Kramer and Davenport, 2015), and that GABA binding to GABA auto-receptors on horizontal cells modulates pH- and hemichannel-mediated feedback (Kemmler et al., 2014; Grove et al., 2019). In addition, feedforward signaling to bipolar cells is also mediated via GABA release (Dowling et al., 1966; Marchiafava, 1978; Yang and Wu, 1991). Both, ON and OFF bipolar cells express ionotropic GABA(A) chloride-permeable receptors on their dendrites (Greferath et al., 1994; Vardi and Sterling, 1994). Depending on their intracellular dendritic chloride concentration, activation of the GABA(A) receptors results in a depolarization of the ON bipolar cells and a hyperpolarization of the OFF bipolar cells (Vardi et al., 2000b; Duebel et al., 2006; Puller et al., 2014). Thus, GABA mediates opposite polarity - excitatory and inhibitory - which shape the receptive field organization of bipolar cells. However, it is also well known that lateral interaction in the inner plexiform layer via amacrine cells, strongly contributes to the center/surround organization of bipolar cells (for review, see Lukasiewicz, 2005; Marco et al., 2013; Diamond, 2017; Franke et al., 2017).

1.2.3 Bipolar cells

Bipolar cells are the output from the OPL. They are glutamatergic neurons that collect, shape and relay in turn, visual information from the photoreceptors to ganglion and amacrine cells in the inner retina. The morphology and connectivity of bipolar cells change across species based on their natural habitat (for review, see Euler et al., 2014). These cells and their connections determine which signal from the primary sensory neurons is directed to the higher specialized downstream network. The mouse retina contains 14 different types of bipolar cells, of which one contacts mainly rod terminals (rod bipolar cell) and 13 types mainly contact cone terminals (cone bipolar cells; Fig. 5) (Shekhar et al., 2016; Tsukamoto and Omi, 2017).

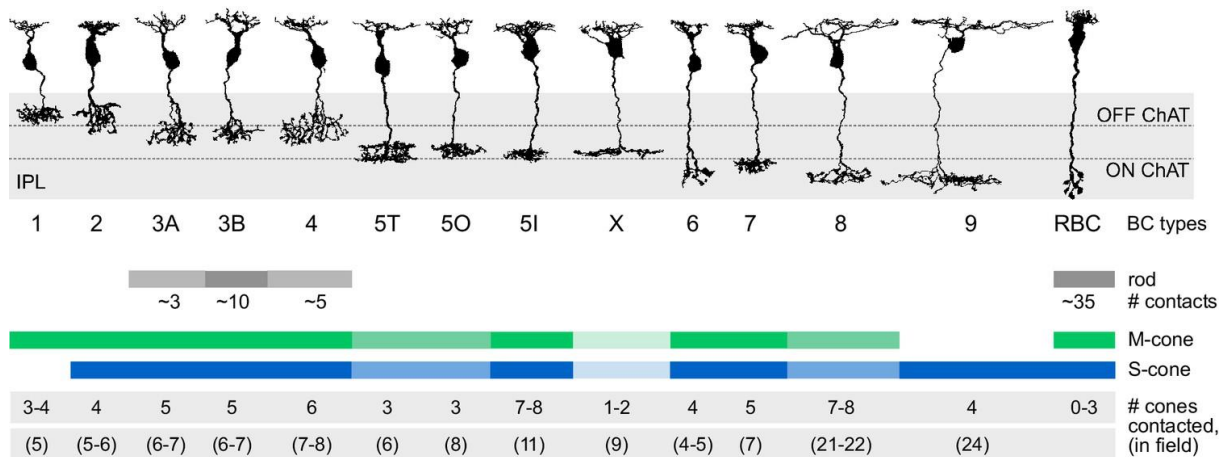


Figure 5: Mouse retina bipolar cells and their connectivity

Examples of different types of bipolar cells found in the mouse retina are presented, along with the number of cones in their dendritic fields and the photoreceptors they connect with (Behrens et al., 2016).

Type 1 cone bipolar cells establish exclusively connections with M-cones, while type 9 cone bipolar cells are specifically linked to S-cones. Other types of cone bipolar cells form connections with both types of cones (Behrens et al., 2016). Additionally, type 3a, 3b, and 4 cone bipolar cells have been observed to make additional contacts with rods (Mataruga et al., 2007; Haverkamp et al., 2008; Behrens et al., 2016), and rod bipolar cells have been found to establish additional contacts with both S- and M-cones (Behrens et al., 2016). The latest discovered bipolar cell type, type 1b, functions as a glutamatergic monopolar interneuron (GluMI) and does not receive direct inputs from photoreceptors (Della Santina et al., 2016).

Bipolar cells can be categorized into ON and OFF types based on their light responses. ON bipolar cells, including types 5t, 5o, 5i, X, 6, 7, 8, 9, and rod bipolar cells, depolarize in response to light stimulation, whereas OFF bipolar cells, such as types 1a, 1b, 2, 3a, 3b, and 4, hyperpolarize. This polarity distinction arises from the expression of different glutamate receptors at the dendritic terminals of the bipolar cells. ON cone bipolar cells and rod bipolar cells express metabotropic glutamate receptor 6 (mGluR6 also known as GRM6) (Nomura et al., 1994; Masu et al., 1995), while OFF bipolar cells express ionotropic glutamate receptors (AMPA and kainate receptors) (DeVries, 2000; Hack et al., 2001; Puller et al., 2013; Puthussery et al., 2014). Upon light exposure, reduced glutamate release from photoreceptors deactivates mGluR6 in ON bipolar cells, leading to the opening of a non-selective cation channel (TRPM1-transient receptor potential cation channel subfamily M member 1) (Morgans et al., 2010). Conversely, ionotropic glutamate receptors in OFF bipolar cells are closed upon reduced glutamate release from photoreceptors.

Furthermore, ON and OFF bipolar cells exhibit distinct axonal stratification within the inner plexiform layer (IPL) of the retina. The axon terminals of ON bipolar cells stratify in the inner

half of the IPL, where they form synapses with ON ganglion cells, while the axon terminals of OFF bipolar cells stratify in the outer half of the IPL, forming synapses with OFF ganglion cells. The synaptic output of bipolar cells, known as a dyad, consists of bipolar cell presynaptic ribbons and two post-synaptic elements. These post-synaptic elements can either be two processes from amacrine cells or a combination of one process from an amacrine cell and one process from a ganglion cell (Dowling and Boycott, 1965; Raviola and Dacheux, 1987; Ghosh et al., 2001).

Functional properties of bipolar cells are strongly influenced by inhibitory signals from amacrine cells at their axon terminals. Recent findings have shown that both ON- and Off-center bipolar cells exhibit similar responses or not, based on the level of antagonistic interaction between amacrine (Franke et al., 2017). The influence of amacrine cells is substantial enough to cause bipolar cells to respond to light stimuli, even in the absence of dendritic input, like the glutamatergic monopolar interneuron that exhibits similarities to type 1 and type 2 bipolar cells in its terminal system.

1.3 Synaptic architecture of the outer retina

Synaptic organization in the outer plexiform layer (OPL) plays a crucial role in signal transmission, decoding visual information, and providing raw data for downstream signal processing.

At the triad synapse, synaptic communication is mediated by glutamate released from the presynaptic photoreceptors, and the expression of metabotropic or ionotropic glutamate receptors at the postsynaptic dendrites (for review, see Wässle, 2004). Additionally, different cell types are electrically coupled via gap junctions, providing a direct and rapid neuronal communication in the OPL (for review, see Söhl et al., 2005).

The following sections report insight into the mechanisms of signal transmission, addressing both chemical and electrical synapses (see Chapters 1.3.1 and 1.3.2). The electrical coupling in the outer retina (see Chapter 1.3.3) and finally the spatial location of a tight junction-associated protein ZO-1 (see Chapter 1.3.4).

1.3.1 Chemical synapses

Glutamate mediates its excitatory effects by activating members of the ionotropic (iGluR) and metabotropic glutamate receptor (mGluR) families. Metabotropic GluRs activate in turn an intracellular second messenger signal cascade via the interaction with a membrane-bound G proteins (for review, see Pin and Duvoisin, 1995). ON bipolar cells express the metabotropic glutamate receptor 6 (mGluR6 – GRM6) on the vertical walls of the invaginating dendrites at the photoreceptor triad synapse (Vardi et al., 2000a).

Ionotropic GluRs are responsible for most of the fast excitatory transmission in the central nervous system and consist of homo- or heteromeric integral membrane protein complexes that bind glutamate and form nonselective cation channels (Dingledine et al., 1999). Based on their pharmacological and electrophysiological properties, iGluRs can be classified into N-methyl-D-aspartate (NMDA) and non-NMDA receptors, which are further divided into AMPA (α -amino-3-hydroxy-5-methyl-4-isoxazolepropionic acid) receptors and kainate (2-carboxy-3-carboxymethyl-4-isopropenyle-pyrrolidine) receptors (for review, see Traynelis et al., 2010). Since NMDA receptors have not been analyzed in this thesis, they will not be presented in more detail.

In previous studies outdated terminology was used for the different ionotropic glutamate subunits. However, a revision of the nomenclature occurred in 2009, resulting in the subunits being recognized by alternative names in contemporary literature (Collingridge et al., 2009). The most up-to-date nomenclature is used in this work, and a table with previous terms is provided in the Appendix – Supplemental material (see Chapter 7.3).

AMPA and kainate receptors show distinct kinetics and roles in synaptic transmission.

AMPA-type glutamate receptors (GluAs) are integral transmembrane proteins assembled by GluA1–GluA4 subunits as a tetrameric complex and they mediate fast excitatory synaptic transmission. With their rapid recovery from desensitization, AMPA receptors drive transient visual stimuli (for review see, Hollmann and Heinemann, 1994). However, subunit composition affects affinity, kinetics, ionic permeability, and channel conductance, leading to receptors with “sui generis” characteristics (for review, see Guo and Ma, 2021). The calcium ion (Ca^{2+}) conductance of AMPA receptors changes based on the inclusion of the GluA2 subunit within the tetrameric complex. When the GluA2 subunit is part of AMPA receptors, it inhibits the entry of cations like Ca^{2+} and Zn^{2+} , resulting in different kinetic behavior (Hack et al., 2001; Stincic and Frerking, 2015). The GluA2 subunit typically has a positively charged arginine (R) residue at the Q/R site, which is not originally encoded at the genomic level, but is created by RNA editing (Sommer et al., 1991). This editing process is essential for determining the permeability of AMPA receptors to calcium ions, as well as influencing their functional properties and overall role in synaptic transmission. (Kawahara et al., 2003, 2004a, 2004b; Liu and Zukin, 2007).

Kainate-type glutamate receptors (GluKs) include low-affinity kainate receptor subunits GluK1–GluK5 and high-affinity receptor subunits KA1 and KA2 (Haverkamp et al., 2001b). Kainate receptors are also characterized by a fast signal transmission but with a slower recovery from desensitization thus driving sustained signaling (DeVries, 2000).

In the mammalian retina, both AMPA and kainate receptors subunits are expressed in horizontal and bipolar cells (Vardi et al., 1998; Haverkamp et al., 2001a, 2001b). Each ribbon synapse receives the invaginating dendrites of horizontal and bipolar cells, while OFF-cone bipolar cells contact the cone at the so called “flat-contacts”. The laminar distribution of

dendrites forms a series of bands where different glutamate receptors are expressed beneath the cone pedicle (Fig. 6). OFF bipolar cells express GluK1 at the base of the cone pedicles (Haverkamp et al., 2000, 2001b, 2003). Horizontal cells express AMPA-type subunits such as GluA2, GluA2/3 and GluA4 at two different locations at the cone pedicle. The first location or upper band, at the invaginating tips close to the cone synaptic ribbon, whereas the second location or lower band, 1.5 μm below the cone pedicle base, at the desmosome-like junctions. Desmosome-like junctions represent adjacent postsynaptic densities formed by horizontal cell dendrites. These occur beneath the cone pedicle and at the interface between connecting horizontal cell dendrites in the triads (Haverkamp et al., 2000, 2001a). Therefore, glutamate released from the cone pedicle acts not only through direct contact, but it extends even through diffusion to glutamate receptor clusters at the desmosome-like junctions.

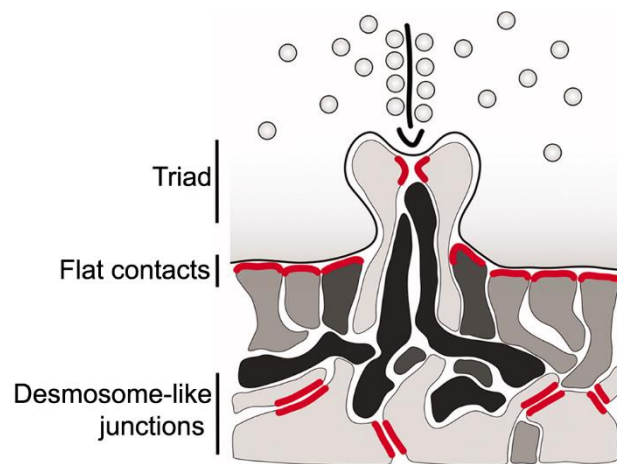


Figure 6: Laminated location of ionotropic glutamate receptors at the cone pedicle

Example from primate retina. AMPA-type glutamate receptors are expressed on the top, at the invaginating horizontal cells dendrites and at the desmosome-like junctions in a band 1-2 μm underneath the cone pedicle. Within this stratification, kainate-type glutamate receptors are expressed by OFF-cone bipolar cells at the cone pedicle base. Modified from (Puller and Haverkamp, 2011b).

It is well known that in primate retina GluAs are expressed below the cone pedicles at the desmosome-like junctions between horizontal cells (Haverkamp et al., 2000, 2001a, 2001b; Puller et al., 2009). Furthermore, accumulation of GluAs was also found below the cone pedicle in the rabbit retina (Pan and Massey, 2007). Consequently, the presence of GluA receptors in horizontal cells beneath the cone pedicle, alongside their conventional localization at the invaginating dendritic tips, seems to be a defining characteristic of the connectivity of horizontal cells in various mammalian species.

1.3.2 Electrical synapses (Connexins)

Electrical synaptic transmission plays a focal role in the intercellular communication of the retina, where each of the five distinct neuronal types is interconnected via gap junctions expressing a variety of connexin proteins (Söhl and Willecke, 2003; Söhl et al., 2005). This variety of electrical synapses among different classes of neurons highlights their crucial role in the transmission and processing of visual information (for review, see Völgyi et al., 2013).

Gap junction channels are the functional units of electrical synapses. They consist of two hemichannels, also known as connexons, that link together adjacent neurons (Fig. 7). Connexons are assembled from six transmembrane protein subunits called connexins (Cx). Their arrangement forms a central pore that facilitates the passive diffusion of cations and anions, secondary messengers (cAMP and IP3), and small metabolites (saccharides, nucleotides, and amino acids) by means of electrical and metabolic coupling up to a molecular weight of 1 kDa (for review, see Goodenough et al., 1996; Kumar and Gilula, 1996; Evans and Martin, 2002). The presence of extracellular loops on each connexin ensures the intermolecular docking of two opposing hemichannels. Gap junction channels can occur in two ways: homotypic and heterotypic. Homotypic channels are characterized by identical connexons, while heterotypic channels have different connexons. Additionally, connexons can be composed of one or multiple connexin isoforms, resulting in either homomeric or heteromeric channels (for review, see (Bloomfield and Völgyi, 2009)). Multiple gap junction channels aggregate to form a gap junction plaque, which typically contains channels with the same connexin subunit composition. However, bihomotypic gap junctions, have also been observed. Bihomotypic gap junctions consist of distinct connexins, like Cx36 and Cx45, which coexist within a single plaque, but form separate homotypic channels. In the retina, these structures permit Cx36 and Cx45 to form connections within separate domains, enabling specialized signal transmission in the inner plexiform layer (Li et al., 2008).

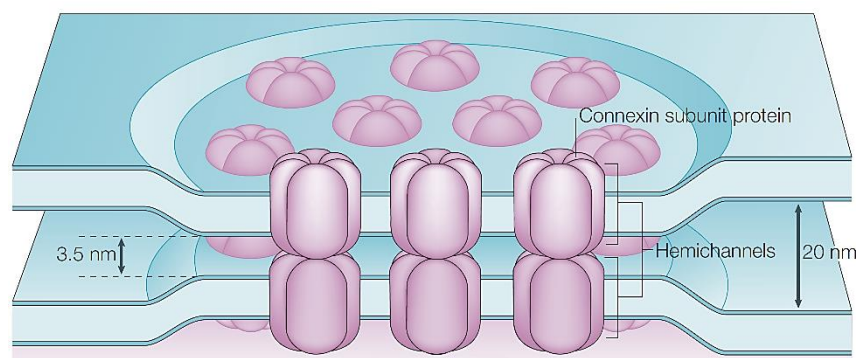


Figure 7: Structural organization of gap junctions

Hemichannels on each side dock with each other to form conductive channels between two neighboring cells. Six connexin subunits are arranged to form a central pore in the hemichannel. Clusters of these channels are called gap junctional plaques (modified from (Söhl et al., 2005)).

Approximately 20 different connexin isoforms have been identified in humans and mice, each exhibiting distinctive conductance or gating properties (Willecke et al., 2002; Söhl and Willecke, 2003; Völgyi et al., 2013). Two nomenclature systems are currently in use for connexin proteins and their genes. Connexins have been named according to the species from which they are derived and their abbreviated theoretical molecular mass (in kDa). Alternatively, connexins have been divided into subgroups (α , β or γ) according to their degree of sequence similarity and the length of the cytoplasmic domains. In this nomenclature, different connexins are abbreviated with the acronym "Gj" for gap junction, and numbered consecutively in the order of their discovery (Söhl and Willecke, 2003).

The subunit composition of the gap junction channel determines its physiological properties, such as permeability and gating (Maeda and Tsukihara, 2011). Like ion channels, the conductance and gating characteristics of gap junctions are influenced by various physiological factors and agents.

The adaptability of electrical coupling between cells plays a crucial role in the response of neuronal networks and the regulation mechanisms can be classified according to different time frames (for review see, Bloomfield and Völgyi, 2009; O'Brien and Bloomfield, 2018).

Short-term plasticity within communicating neuronal networks is mediated by changes in the current across the gap junction. This involves passive currents, such as those from potassium or chloride channels, as well as active conductance from sodium channels, which collectively modulate the junctional current (Curti and Pereda, 2004; Trenholm et al., 2013).

Post-translational phosphorylation is a widely used mechanism that modulates conductance gating of gap junction channels, as well as trafficking, assembly and disassembly of connexons and gap junction channels within the cell and cell membrane (Laird, 2006; Bloomfield and Völgyi, 2009). The intracellular C-terminal domain of the connexins is the main target for protein kinases (Lampe and Lau, 2000, 2004), that in turn are regulated by calcium-calmodulin, cAMP, cGMP and neuromodulators. In the retina light adaptation and circadian rhythm cause significant changes in coupling between neurons by activating neurotransmitter and neuromodulator receptors like dopamine, adenosine, glutamate, or nitric oxide (NO). These changes occur through intracellular signaling cascades predominantly via cyclic nucleotides, leading to post-translational modifications of the gap junction forming proteins usually through reversible phosphorylation (for review, see Bloomfield and Völgyi, 2009; O'Brien, 2014; O'Brien and Bloomfield, 2018). A well-known mechanism of modulation of gap junction conductance through intracellular pathways, is the one mediated by dopamine. Briefly, dopamine is released by dopaminergic amacrine cells following light exposure and prolonged darkness at night (Weiler et al., 1997; Ribelayga and O'Brien, 2017). Activation of D1-receptors expressed by horizontal cells and some amacrine cell subtypes leads to the intracellular activation of adenylate cyclase and an increase of the intracellular cAMP concentration. This in turn results

in the activation of cAMP-dependent protein kinase, the phosphorylation of connexins and a reduction in the conductance of gap junctions coupling horizontal cells (Piccolino et al., 1984; Lasater, 1987; He et al., 2000). Different retinal cell classes express different dopamine receptor isoforms (D1-D5) and for this reason the respective cellular response to dopamine is dependent on the intracellular signaling cascade activated by the specific D-receptor (Dowling, 1991; Urschel et al., 2006).

In addition, it is well known that a high concentration of cytosolic calcium reduces electrical coupling by closing the gap junctions (Rose et al., 1977; Peracchia, 1978). This modulation is among others dependent on calmodulin, which interacts directly with connexins subunits (Peracchia, 2020) or involves the activation of the calcium/calmodulin dependent protein kinase II (CaMKII) (Kothmann et al., 2012). Finally, changes in intracellular pH can also alter the gating properties of connexins, leading to a reduction of gap junction permeability by acidification while conductance increase is mediated by alkalinization (Spray et al., 1981; Church and Baimbridge, 1991).

All these mechanisms are mediated by intracellular second messengers and involve structural modifications or fine intracellular changes. Therefore, they require longer periods of time, typically seconds to minutes, compared to those described for short-term plasticity. Changes in the expression level of connexins are instead considered long-term plasticity mechanisms taking minutes to hours to be effective. Circadian changes enable the signaling pathways to achieve different states at various times during the day, resulting, for example, in a minimum level of coupling for photoreceptors at dawn (Li et al., 2013; Zhang et al., 2015; O'Brien, 2017). These multiple mechanisms likely represent distinct pathways that are influenced by common environmental factors. Gradual changes, such as variations in protein expression levels, are well-suited for adapting to slower, long-term shifts in environmental conditions, like the daily cycle of ambient light. In contrast, rapid responses to sudden changes, such as moving from darkness into bright light, are more efficiently managed by faster mechanisms, such as alterations in channel gating.

1.3.3 Electrical coupling in the outer retina

In the mouse retina, connexin45 (Cx45) and connexin36 (Cx36) are the two most abundant connexins (Bloomfield and Völgyi, 2009; Sigulinsky et al., 2020). In the outer plexiform layer, photoreceptors are electrically coupled through Cx36. Previous studies have shown both homologous cone-cone and heterologous rod-cone coupling (Bloomfield and Völgyi, 2009). However, a recent study has demonstrated that heterologous rod-cone communication by Cx36 is the predominant form of electrical coupling between photoreceptors (Ishibashi et al., 2022). The connection between photoreceptors via gap junction plays several functional roles. Cone-cone coupling reduces electrical noise, increasing the signal-to-noise ratio (Hornstein et

al., 2005; Jin et al., 2015). Compared to other retinal gap junctions this coupling is not affected by light (DeVries et al., 2002). Electrical coupling between rods and cones allows for the crossover of rod signals into the cone pathway, providing a secondary rod pathway that can be modulated by light intensity and circadian rhythm (Jin and Ribelayga, 2016; Ishibashi et al., 2022).

Mouse axon-bearing horizontal cells are extensively coupled by gap junctions, resulting in a receptive field that is larger than their dendritic field (Bloomfield et al., 1995; Shelley et al., 2006; Zhang et al., 2011). Consequently, the strength of coupling determines the spatial extent of feedback signals to photoreceptors (Dacheux and Raviola, 1982; Bloomfield et al., 1995). The dendritic arbor and axon terminal system form separate, large networks connected electrically via connexin57 (Cx57) gap junctions (Hombach et al., 2004; Pan and Massey, 2007). Cx57 is specifically expressed at the dendro-dendritic and axo-axonal horizontal cell gap junction (Janssen-Bienhold et al., 2009). Electrical coupling of the dendritic network occurs beneath the cone pedicles, near the desmosome-like junctions, where horizontal cell dendrites converge before invaginating into the cones (Puller et al., 2009). Connexin50 (Cx50) has also been observed in the axon terminals of mouse horizontal cells (Dorgau et al., 2015).

Horizontal cell coupling is modulated by ambient light in a triphasic manner (Xin and Bloomfield, 1999; Bloomfield and Völgyi, 2009). In mesopic light conditions, horizontal cells display strong coupling, resulting in signal transmission over long distances within the OPL. In photopic or scotopic light conditions, gap junctions close, resulting in horizontal cells which act as smaller inhibitory units. This is advantageous because, in the first case, the reduced coupling in turn reduces the surround signal and enhances light sensitivity at the expense of contrast detection. Conversely, in bright light, the decreased coupling among horizontal cells improves local contrast detection (Shimizu and Stopfer, 2013). This modulation is regulated by retinal dopamine (Perlman and Ammermüller, 1994; He et al., 2000), retinoic acid (Weiler et al., 1999, 2000; Pottek and Weiler, 2000), and nitric oxide levels (Lu and McMahon, 1997; Pottek et al., 1997; Xin and Bloomfield, 2000). These neuromodulators collectively reduce horizontal cell coupling, indicating the presence of multiple distinct pathways for modulation in response to dark and light conditions.

Horizontal cell coupling can be modulated by altering the expression levels of the gap junction proteins. Previous studies have shown that dark adaptation reduces connexin57 (Cx57) expression in the mouse retina (Kihara et al., 2006) which corresponds to a decrease in the number of Cx57-immunoreactive plaques (Janssen-Bienhold et al., 2009).

Unlike horizontal cell coupling, the electrical coupling observed between bipolar cells is notably weaker. As a result, these cells display significantly smaller receptive fields that can be modulated by gap junction permeability (Zhang and Wu, 2009; Arai et al., 2010). On the other hand, OFF-cone bipolar cells may not support effective electrical coupling. They might instead

play a role in chemical or metabolic coupling between subcellular compartments. (Fournel et al., 2021). In the OPL OFF bipolar cell dendrites are homologously coupled via Cx36 and Cx45 (Feigenspan et al., 2004; Hilgen et al., 2011).

1.3.4 Zonula Occludens-1 in the outer retina

Gap junction proteins are known for their interactions with other membrane-associated proteins, which exert regulatory influences on cell communication. The structural protein zonula occludens-1 (ZO-1) has been found to interact with several connexins at gap junctions (Giepmans, 2004; Li et al., 2004b; Flores et al., 2008; Lynn et al., 2012). ZO-1 is a member of the membrane associated guanylate kinase homologs family (MAGUK) and was originally described in peripheral endothelial cells as cytoplasmatic scaffolding protein at adherent and tight junctions (for review, see Stevenson et al., 1986; Hartsock and Nelson, 2008). MAGUK proteins are characterized by the presence of different binding domains, including the PDZ (PSD95, DLG and ZO-1) domains (for review, see González-Mariscal et al., 2000), SH3 (Src Homology 3) domain (Nomme et al., 2011), and a GUK (guanylate kinase) domain (Fanning et al., 1998). These domains are essential for spatially clustering and anchoring transmembrane proteins to specific subcellular components. They act as a scaffold, organizing structurally diverse, but functionally connected proteins in tight proximity. In doing so, ZO-1 particularly links tight junction (claudins and occludins) and gap junction proteins to the actin cytoskeleton (Fanning et al., 1998; Hartsock and Nelson, 2008) and proteins implicated in signaling cascades (Li et al., 2004c; Rash et al., 2004; Tetenborg et al., 2020). In the mouse retina, ZO-1 was observed to be associated with Cx36 in both the OPL and IPL, as well as with Cx45 in the IPL, suggesting a regulatory role at the appropriate gap junctions (Li et al., 2004b, 2008; Ciolofan et al., 2006, 2007). At the same time, it has been shown how the spatial distribution of ZO-1 is restricted to specific locations within the OPL. Here, ZO-1 colocalized with Cx36, which plays a role in the formation of gap junctions between dendrites of OFF bipolar cells and photoreceptor terminals adjacent to the cone pedicles (Feigenspan et al., 2004; Jin et al., 2020). Additionally, ZO-1 is expressed at gap junctions beneath the cone pedicle in a type-specific manner by horizontal cells. In the mouse retina, it is associated with Cx57 at dendro-dendritic gap junctions of horizontal cells, while in the rabbit retina, it is linked with Cx50 in axonless A-type horizontal cells, forming a rim around the Cx50 plaques, both beneath the cone pedicle and at large plaques. In macaques, ZO-1 is also located below the cone pedicle at the level of desmosome-like junctions on the dendrites of H1 horizontal cells where it was clustered in tight proximity to GluAs (Puller et al., 2009). Based on these observations a multifunctional role has been suggested for ZO-1, both as a scaffolding protein for connexins and as a link between the cytoskeleton and transmembrane proteins at the border of the desmosome-like junctions area (Puller et al., 2009).

2. Aims of the study

Signal processing in neuronal networks deeply depends on the precise timing and interplay between excitation and inhibition at the synaptic connections between cells. The synaptic architecture and components supporting intercellular communication play a critical role in processing and signaling. A crucial aspect of the sensory systems, such as the retina, is its capacity to adjust to the changes in the surrounding environment. This adaptation optimizes the signaling range and the ability to distinguish relevant information under different ambient conditions, thereby improving the overall functionality of the sensory system.

Horizontal cells are the class of inhibitory interneurons that dominate signal processing in the outer retina, where the first synaptic connections of the entire visual system are formed between the photoreceptors and their postsynaptic cells.

Synaptic transmission in the OPL relies on the neurotransmitter glutamate and a distinctive distribution of metabotropic and ionotropic glutamate receptors. Furthermore, intercellular communication via electrical synapses which includes scaffolding proteins, that stabilize the synaptic structures, are essential components of the neuronal network.

Although much has been observed regarding the localization of synaptic components in the OPL and several studies have given architectural representations of their distribution in different species, a more detailed analysis of their spatial distribution and interactions is still needed. This is particularly true for animal models such as mice, which have become an important tool for understanding the visual system in recent decades.

The role of horizontal cells has been extensively studied. Nevertheless, numerous questions persist regarding their specific function and the intricate structure of the synaptic networks they establish. Therefore, this thesis aims to further investigate the molecular components whereby horizontal cells contribute to the signaling in the outer retina. In the first two projects the spatial distribution of glutamate receptor subunits and electrical synapses, as well as some synaptic components of horizontal cells were analyzed. In the third section, the distribution of gap junctions between horizontal cells is analyzed, along with density and electrical coupling analysis, based on collaborative work with Dr. Alejandra Acevedo Harnecker, Dr. Prof. Karin Dedek, Dr. Martin Greschner and Christoph Block, that has been recently published (see attached article). These findings will be presented in the results.

2.1 Project 1: Spatial organization of desmosome-like junctions and gap junctions in the outer plexiform layer of the mouse retina

In the mammalian retina horizontal cells (HCs) receive glutamatergic input from photoreceptors via ionotropic glutamate receptors (Haverkamp et al., 2000, 2001a; Hack et al., 2001). The dendrites of horizontal cells in the primate retina express glutamate receptors hot spots at two postsynaptic locations. These locations are at the invaginating processes that are opposed to the presynaptic ribbons and more proximally, at the so-called desmosome-like junctions, which are formed between their dendrites ~1.5 μm beneath the cone pedicle (Haverkamp et al., 2000). Also in primates, it has been shown that AMPA-type glutamate receptors (GluAs) occur in close spatial association with electrical synapses (gap junctions) between HCs at these sites (Puller et al., 2009). In the rodent retina horizontal cells express different types of ionotropic glutamate receptors including kainate- and AMPA-type receptors (Brandstätter et al., 1997; Hack et al., 2001), but not NMDA-type receptors (Schubert et al., 2006). More specifically, studies on mouse HCs have shown that specific AMPA-type glutamate receptors subunits, GluA2 and GluA4, mediate the glutamatergic light responses from photoreceptors (Ströh et al., 2013, 2018). Additionally the accumulation of GluAs below the cone pedicle was also observed in the rabbit retina (Pan and Massey, 2007). Finally, the axon-bearing B-type horizontal cell forms axo-axonal and dendro-dendritic networks coupled by gap junctions via connexin57 (Cx57) in the mouse retina (Hombach et al., 2004; Janssen-Bienhold et al., 2009). However, it remains unclear in the mouse retina whether GluAs are expressed at the desmosome-like junction level and their function at this level.

This project aims to investigate the detailed spatial distribution of horizontal cell glutamate receptor subunits in the mouse retina. Questions aimed to be answered with this project were, whether these subunits are expressed at the desmosome-like junctions beneath the cone pedicles, and how their spatial association with gap-junction proteins (Cx57) is organized at this level. The goal is to gain more insight into the distribution patterns of components of chemical and electrical synapses in the OPL and to check whether these are preserved among different mammals.

2.2 Project 2: Analysis of a possible mutual interaction between electrical and chemical synapses at the desmosome-like junction level in the OPL of mouse retina

Horizontal cells possess specialized postsynaptic structures situated approximately 1.5 μm beneath the cone pedicle at the level of desmosome-like junctions. Desmosomes are easily identifiable by electron microscopy, consisting of electron-dense plaques adjacent to the plasma membrane, separated by an intermediate dense line marking the extracellular space. At this level horizontal cell dendrites form specific “contact points” where glutamate receptors were identified as further post-synaptic densities on HCs (Haverkamp et al., 2000, 2001a, 2001b). The close spatial association of GluA subunits and gap junctions, between HC dendrites at this level, suggested that reciprocal interactions between electrical and chemical synapses might exist (Puller et al., 2009). There is further evidence indicating that the close interaction of chemical and electrical synapses is essential for the proper functioning of the neuronal system (for review, see Pereda, 2014). A well-known example of mutual interaction between the two types of synapses has been described for the auditory afferents. Here, so-called mixed synapses have been detected on Mauthner cells of teleost fishes, where reciprocal influence between glutamatergic synapses via NMDA receptors and Cx35-containing gap junctions was found by means of anatomical and physiological experiments (Pereda et al., 2004; Faber and Pereda, 2018). In the mouse retina, mutual interaction between electrical and chemical synapses has been described at the level of the All amacrine cells (Kothmann et al., 2012). Here, Cx36 gap junctions are expressed between All type ACs, and their local conductance is modulated via activation of non-synaptic NMDA receptors. Calcium influx, in turn leads to the activation of Ca^{2+} -Calmodulin-dependent kinase II, phosphorylation of Cx36 and increase in electrical coupling between All-amacrine cells.

In this context, the second chapter of this thesis aims to analyze a possible mutual interaction of electrical and chemical synapses at the level of the desmosome-like junctions in the OPL. To address this question, comparative qualitative analysis has been performed exploiting valuable tools such as transgenic mice. Specifically, the study analyzed the effect of Cx57-knockout on the expression of GluAs in the OPL of the mouse retina, and vice versa evaluated the expression of Cx57 in GluA2/GluA4-deficient mice, respectively.

2.3 Project 3: The distinct distribution of horizontal cell gap junctions across the retina

The mouse retina has been thought to be relatively homogeneous, lacking a specialized area such as fovea or area centralis. Over the past decades, however, variations in cellular distributions and regional circuits have been observed. This may represent adaptive mechanisms to the visual statistics of the animal and thus provide behavioral benefits (for review, see Heukamp et al., 2020). Among the observed variations, the different distributions of the opsins in the mouse retina represent a well-established example for a topographic specialization. Short-wavelength-sensitive opsins are sparse in the dorsal half of the retina and dominate the ventral half, whereas middle-wavelength sensitive opsins dominate the dorsal retina, forming opposite gradients of green and UV opsin expression (Applebury et al., 2000; Haverkamp et al., 2005; Nikonov et al., 2006; Wang et al., 2011; Warwick et al., 2018). Cones and bipolar cells in the dorsal retina are tuned to green light, while those in the ventral retina are tuned to UV light (Baden et al., 2013; Szatko et al., 2020). Consequently, retinal ganglion cells (RGCs) in the dorsal retina are more sensitive to green light, whereas those in the ventral retina are more sensitive to UV light (Wang et al., 2011; Chang et al., 2013; Szatko et al., 2020). A recent study has identified a functional gradient in retinal ganglion cells, whereby the receptive field surround structure shows a dorso-ventral change in amplitude and spatial extent, exhibiting remarkable asymmetries in the visual horizon (Gupta et al., 2023). Nevertheless, a clear understanding of the circuitry involved in this regional distribution is still missing. Amacrine cells contribute to the formation of RGC receptive field surrounds (for review, see Diamond, 2017), however it is worth noting that horizontal cells also play a significant role in establishing RGC receptive fields, including their surround properties (Chaya et al., 2017; Drinnenberg et al., 2018; Ströh et al., 2018). Thereby, horizontal cells may contribute to the variation of the ganglion cell receptive fields across the retina.

In collaboration with the students Asli Pektaş, Lucia Lindenthal and Dr. Alejandra Acevedo and Christoph Block, we focused on the topographic distribution and synaptic connectivity of horizontal cells within the retina. Specifically, a detailed analysis of the horizontal cell distribution across the retina, as well as the analysis of the gap junction (Cx57) distribution and their functional electrical coupling across the retina was addressed. Further a comprehensive analysis of the morphology of horizontal cells in the dorsal and ventral part of the mouse retina is presented in the manuscript (see Section 7.4 – Publication).

3. Methods

This work focused exclusively on the mouse as the animal model for the studies of the retina. Over the last few decades, the use of the mouse as a model to better understand how vision works, has increased considerably. This is due to the small dimensions of the animal, fast reproduction, low cost, and a stable tolerance to genetic modification. As such, the mouse retina, and the mouse visual system generally, has become a valid tool exploited for studies that extend to the mammalian central nervous system.

The following chapter not only would provide a comprehensive description of the methodologies used in all projects, but also highlights technical issues and outlines for applied solutions used for the protocols. The mouse lines, devices, consumables, chemicals, kits, and software used in this work are listed in Section 7.1 (Materials). Experimental protocols are reported in detail in Section 7.2 (Experimental protocols).

3.1 Experimental animals

All the procedures conducted in this study were approved by the local animal care committee (*Niedersaechsisches Landesamt fuer Verbraucherschutz und Lebensmittelsicherheit*) and the experiments complied with the guideline for the welfare of experimental animals issued by the European Communities Council Directive of 24 November 1986 (86/609/EEC) and the laws of the Federal Government of Germany (*Tierschutzgesetz*; BGB1. I S. 1206, 1313 and BGB1. I S. 1934) for experimental animals.

Mice were housed under standard conditions, including a 12-hour light-dark cycle with water and food ad libitum. Animals aged between 2 and 6 months of either sex were used for the experiments. All mouse lines have the genetic background of the C57BL6/6J inbred strains or were backcrossed into the C57BL6/6J background for at least three generations.

Wild-type C57BL6/6J have been used to investigate the spatial distribution of the ionotropic glutamate receptors, tight junction protein zonula occludens-1, different connexins on mouse horizontal cells and the main cellular and synaptic components that characterize the OPL.

To further investigate the spatial relationships and putative mutual interactions between electrical synapses (containing connexins) and chemical synapses (containing glutamate receptors) different sets of mouse lines were used. To study if the selective ablation of the ionotropic glutamate receptor subunits GluA2 and GluA4 in horizontal cells, could affect the expression of connexin 57 (Cx57) in the OPL, $GluA2^{fl/fl}/GluA4^{fl/fl};Cx57^{+/Cre}$ animals were used (Ströh et al., 2013, 2018). In these transgenic mice the Cre-LoxP system, which excises the targeted gene in specific tissues or cell populations, has been applied. Briefly, exon 11 of the *GluA* gene was flanked by *loxP* sites, which allows the ablation of the gene by the Cre

recombinase (Cre). Cre instead, was expressed under the cell specific Cx57 promoter in mouse horizontal cells (Hombach et al., 2004; Janssen-Bienhold et al., 2009; Ströh et al., 2018). Mice not expressing Cre recombinase (GluA2^{fl/fl}/GluA4^{fl/fl}:Cx57^{+/+}) and mice expressing only Cre (Cx57^{+Cre}), were both used as controls and crossed to generate the double knockout GluA2^{fl/fl}/GluA4^{fl/fl}:Cx57^{+Cre} mouse line. Conversely, the Cx57^{LacZ/LacZ} mouse line was used to evaluate if the expression patterns of the ionotropic glutamate receptors (specifically, the AMPA-type subunits GluA2 and GluA4) in the OPL, were affected by lack of Cx57. Here, the Cx57 coding region was replaced with the *LacZ* gene reporter by homologous recombination (Hombach et al., 2004), and Cx57^{+/+} littermates were used as control. The same mouse line was also used to validate the immunoreactivity of the new guinea pig polyclonal anti-Cx57 antibodies (anti-bodies validation, see Section 7.2.2; Appendix – Experimental protocols). The correct genotype of the transgenic mice was monitored by PCR genotyping technique. The list of primers used for the PCR is reported in Section 7.1.6 (Appendix – Material) while the PCR protocols are described in Section 7.2.5 (Appendix – Experimental protocols).

3.2 Tissue preparation

Immunohistochemistry represents one of the most widely used methods for ex-vivo anatomical studies. This approach has been applied extensively to provide qualitative and quantitative information on neurons and their cellular components.

Neuroanatomical images obtained by immunohistochemistry are in turn qualitatively compared and/or analyzed depending on the purpose of the study. However, to achieve these results, tissues must be previously handled and exposed to a non-physiological environment. Fixation is a reliable procedure to preserve the morphological properties of the tissues at that specific life-like state and preserves them from mechanical, chemical, and osmotic stress during all the steps of the tissue preparation (Stradleigh and Ishida, 2015).

In this study, fixation was obtained by a crosslinking, non-coagulating chemical, that gives structural support without changing the overall of the cellular components. Aldehydes are the most common crosslinking fixatives and paraformaldehyde (PFA) is generally used for light microscopy analysis.

Animals were sacrificed by cervical dislocation, in the middle of the day (during the light cycle) under room lights. Eyes were then rapidly collected and opened along the ora serrata at the border of the cornea. The lens and vitreous body were removed in phosphate-buffered saline (PBS) or in 0,1 M phosphate buffer (PB) and the resulting posterior eyecups were immersion-fixed. Buffers and PFA were kept in the fridge at +4°C up to the time of the enucleation. For the whole-mounted retinas used for quantification and colocalization analysis between ZO-1 and Cx57 (Project 3), eyecups were fixed in PB containing 2% PFA and 3% sucrose for 20

minutes at room temperature (RT). For all the other experiments, eyecups were fixed in PBS containing 2% PFA, at RT for 20 min (see Section 7.1.5; Appendix – Materials). At the end of the fixation time, fixative solutions were removed to stop crosslinking, and eyecups were immediately immersed into the respective buffer, fixative-free, and washed at least three times for a minimum of 10 minutes each one. Studies using brief and mild fixations have reported that immunostaining intensity is reduced by longer fixations (Haverkamp and Wässle, 2000; Hack et al., 2001). Then, retinas were cryoprotected in sucrose solutions (30% w/v), overnight at 4°C and stored at -20°C in 30% sucrose until use. Cryoprotectants such as sucrose disrupt the interactions between polar water molecules preventing ice crystals formation in tissues when water freezes and expands. At the same time, fast freezing thawing cycles (1-3 times maximum) were useful prior to immunolabeling incubations for whole-mounted retinas, to increase the antibodies penetration. “Brushed” whole-mounted retinas (see Section 3.2.2) required only the freezing step for their storage at -20°C.

Part of this research project benefited from the collaboration with Prof. Karin Dedek and Dr. Alejandra Acevedo Harnecker. Retinal horizontal cells labelled with dye by single cell injections or intracellular tracer-dye injections with biotin for the electrical coupling study, have been provided by Alejandra Harnecker (for further details, please refer to “Material and methods” section of the attached article). Retinas in which horizontal cells were injected with neurobiotin and intended for immunostaining, were handed over to me and fixed in dark condition, using the same fixation protocol used for the whole-mounted retinas. Briefly, tissue was fixed in PBS containing 2% PFA for 20 minutes, washed three times in PBS for 10 min minimum each time and kept overnight at 4°C in the sucrose solution (30% w/v). Then stored at -20°C in the same cryoprotectant solution until used.

One of the key points in this study is the methodology applied to dissect the retinas for spatial orientation. This methodology not only allowed for higher accuracy and reliability between experiments, but also made it possible to share tissues that required different processing by different researchers. Moreover, precise retinal orientation and accuracy of the relief cuts were useful when images of entire flat whole-mounted retinas were reconstructed in their three-dimensional structure using specific software and algorithms (see Section 7.2.4; Appendix – Experimental protocols). The following sections explain all these technical aspects in more detail.

3.2.1 Retinal preparation for whole-mounted retinas

The choroid fissure is a developmental remnant from the circumferential growth path of the eyecup. In the developing retina, it exists as a gap between the two halves of the eyecup through which retinal vessels enter and ganglion cell axons exit, to form what will be the optic nerve later (for review, see Lamb et al., 2007). Once the edges of the retina join, the choroid

fissure fuses, and all that remains is a line visible under a light microscope on the back of the sclera, running from the nasal to the temporal edge of the eyecup. Due to their intrinsic formation during development, deep anatomical landmarks based on the choroid fissure, show to be more reliable and accurate for orienting the retina (Stabio et al., 2018).

For the preparation of whole-mounted retinas, all the following steps were performed in a Petri dish containing PBS or PB as buffer. After removing the retina from the cryoprotectant solution, the choroid fissure was identified on the sclera thanks to its more transparency compared to the rest of the dark epithelium. A total of four radial relieving cuts were made and the longest one along the temporal fissure, nearing the optic nerve. A second cut along the nasal fissure and the last two in the middle of the dorsal and ventral side of the retina. The tissue was then mounted on a nitrocellulose filter membrane (Millipore) with the ganglion cell layer (GCL) up. The resulting flattened whole-mounted retina resembled a clover plant, where each cloverleaf represents a retina quadrant: temporal-dorsal, temporal-ventral, nasal-dorsal and nasal ventral. Whenever possible, a further landmark was established on the dorsal-nasal quadrant via a minor incision along the rim of the retina. All the reference points on the retina were useful for monitoring the orientation in each step: from the tissue preparation to image acquisition with various microscopes or eventually for retina reconstructions (for further details on the reconstruction protocol, please refer to the attached article).

3.2.2 Brushing technique for whole-mounted retinas

The outer plexiform layer (OPL) of the mammalian retina is situated in a relatively medial position among the different retinal layers. In the mouse retina, the OPL represents one of the thinnest layers (Ferguson et al., 2013, 2014). The OPL is inserted between two layers of greater thickness such as, the inner nuclear layer (INL) below and the outer nuclear layer (ONL) above. Both layers are densely packed by the cell bodies of horizontal cells, amacrine cells, bipolar cells, and photoreceptors, respectively. Therefore, immunohistochemistry and optimal antibody penetration to mark specific targets at this level, becomes particularly challenging for whole-mounted retinas. The duration and temperature (room temperature or +4°C) at which antibodies are incubated have a significant impact on the immunostaining result. However, to enhance the penetration of the antibodies and detect specific antigens, the tissue must first be permeabilized, especially after fixation with cross-linking agents such as formaldehyde. Permeabilization can be performed by freeze/thaw cycles upon cryoprotection steps or by including in the immunostaining protocol, the addition of detergents such as Triton-X 100 as described before. Nevertheless, both procedures have their drawbacks, as the formation of ice crystals during the freeze-thaw process can lead to rupture of cell membranes, and the Triton-X 100, as a non-selective detergent may extract proteins along with the lipids.

Hence, an alternative preparation protocol for flat whole-mounted retinas was established as part of this thesis project, to improve antibody penetration and therefore achieve better antigen detection in the OPL.

An alternative to the method described above was to place the retina on the filter membrane with the photoreceptor layer facing upward instead of the ganglion cell layer. In this orientation, it was possible to gently remove the entire layers distal to the OPL (ONL, inner and outer segments) using a simple, fine brush (Fig. 8).

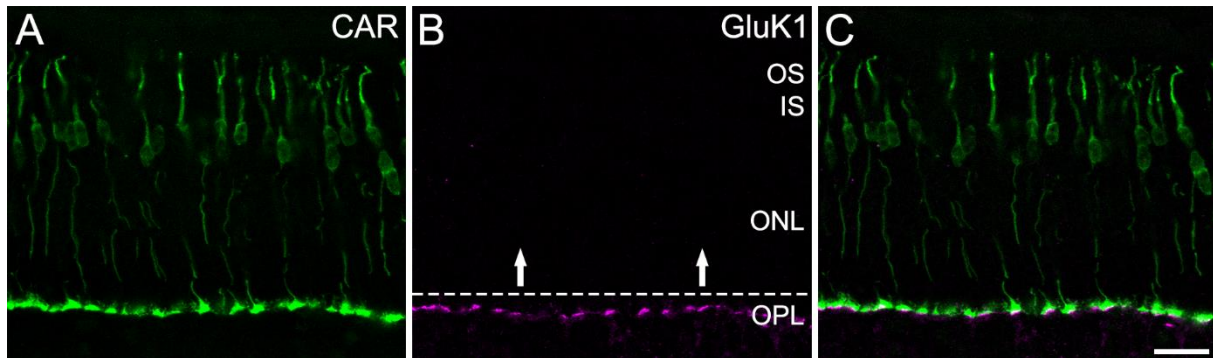


Figure 8: Layered organization of the mouse retina focusing on the OPL

A-C: Maximum intensity projection of a confocal stack ($\sim 4 \mu\text{m}$) from a vertical cryosection, labeled against cone photoreceptors (CAR) and the base of the cone pedicles in the OPL (GluK1), as shown in C. Dashed line indicates the approximate level achieved by the brushing technique and the removal of the layers above the OPL (arrows). OS, outer segments; IS, inner segments; ONL, outer nuclear layer; OPL, outer plexiform layer. Scale bar: $20 \mu\text{m}$ in C, applies to A-C.

The intact retina presents a shiny, whitish surface. As the brushing process continues, the color changes due to the retina becoming thinner and more transparent, and the blackness of the cellulose filter becoming stronger. The outer- and inner segments of the photoreceptors, which are the most superficial, are also the most delicate and easiest to remove. Below, a more intense brushing is needed to remove the outer nuclear layer. However, close to the outer plexiform layer, retina tissue becomes more compact, resistant, and darker, indicating the point at which further brushing is no longer required. Accordingly, the entire surface of the retina was subjected to brushing, with particular attention paid to thinner or already compromised regions, such as the most peripheral region (ciliary marginal zone) and the optic disk at the center.

To roughly estimate the preserved structural integrity of the OPL following the brushing technique, whole-mounted retinas were labeled for markers that are typically located in the distal part of the OPL, specifically at the border of the brushed surface (Fig. 9). Connexin36-positive gap junctions are expressed between cone and rod photoreceptors, and they could be detected following “brushing”, in the upper part of the OPL (Feigenspan et al., 2004; Jin et al., 2020; Ishibashi et al., 2022). In the same way, the antibody against the C-terminal-binding protein 2 (CtBP2) labels the synaptic ribbons of both photoreceptors (Schmitz et al., 2000; tom Dieck et al., 2005). The CtBP2 staining pattern was homogeneous on the surface of the retina

after applying the brushing protocol. In combination with the cone pedicle marker, cone arrestin (CAR) (Zhu et al., 2002; Ishibashi et al., 2022) and the tight junction protein zonula-occludens-1 (ZO-1) (Ciolofan et al., 2006, 2007; Puller et al., 2009) respectively, this antibody combination allows the assessment of the structural integrity of the entire thickness of the OPL.

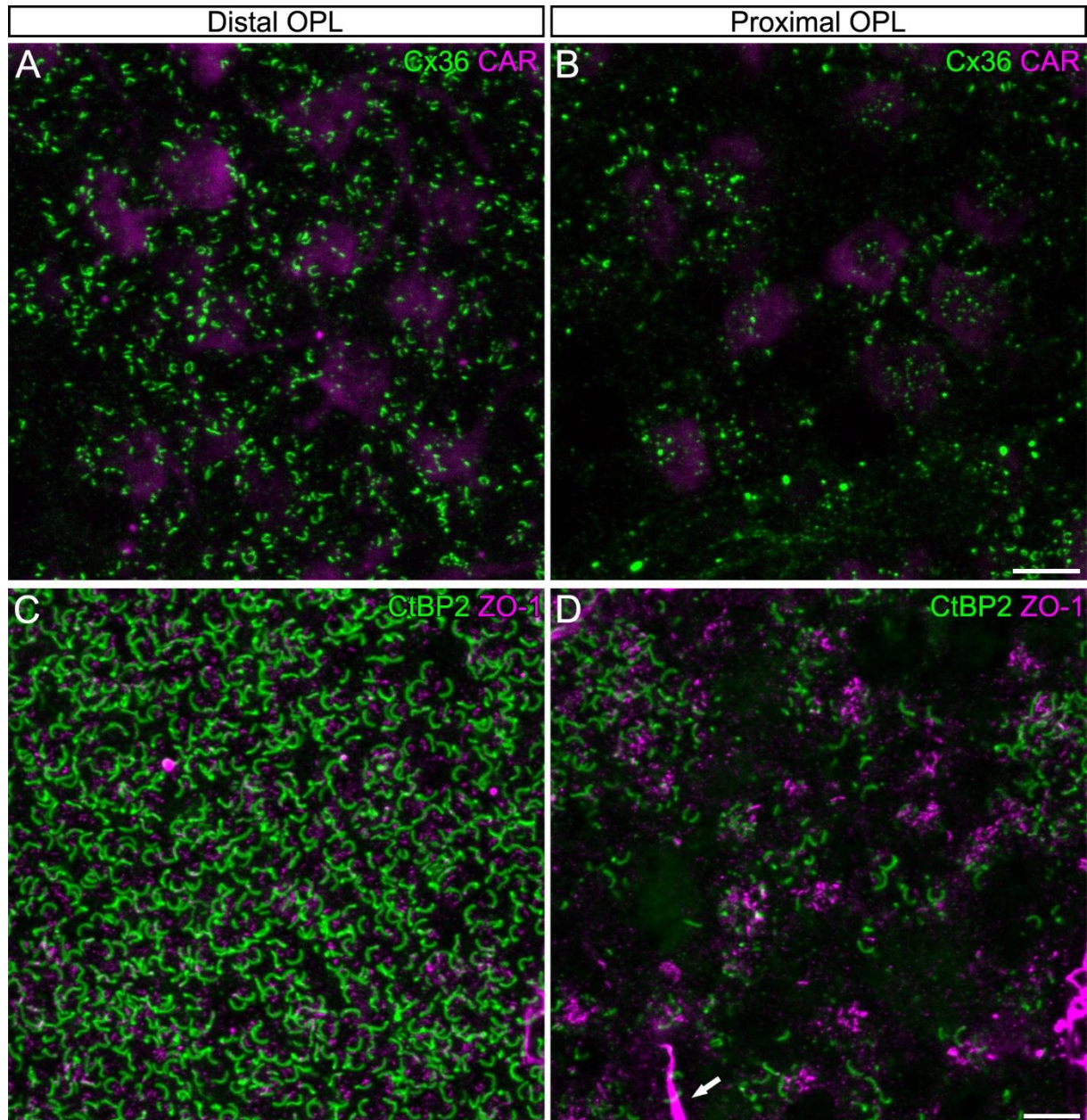


Figure 9: The integrity of the OPL is to be maintained following the brushing technique

A-B: Maximum projections of confocal image stacks from the distal OPL (A) (Z-steps 3-15/38, Z-size ~ 2.6 μm) and the proximal OPL (B) (Z-steps 20-35/38, Z-size ~ 3.2 μm) of a brushed whole-mounted retina, double labeled against connexin 36 (Cx36) and the cone arrestin (CAR). **C-D:** Maximum projections of confocal image stacks from the distal OPL (C) (Z-steps 5-14/24, Z-size ~ 2 μm) and the proximal OPL (D) (Z-steps 17-24/24, Z-size ~ 1.6 μm) of a brushed whole-mounted retina, double labeled against synaptic ribbons (C-terminal-binding protein 2 – CtBP2) and the tight junction protein zonula-occludens-1 (ZO-1). Scale bars: 5 μm in B, applies to A-B and in D, applies to C-D.

Thereby, the brushing technique for whole-mounted retinas, represents a promising approach to addressing the issue of the antibody penetration, without compromising the structural integrity of the outer plexiform layer/ synaptic network. This is particularly the case on the more inner side of the OPL. This protocol was used for most of the whole-mounted retinas and for the immuno stainings performed on retinas after intracellular tracer-dye injections of horizontal cells. Obviously, such technique was not employed when the labeling of the photoreceptor outer segments with opsin markers was needed.

3.2.3 Retina preparation for vertical sections

Vertical sections were obtained from flat-mounted retinas or directly from the eyecups. In the first case, the stored tissue was thawed and placed in a Petri dish containing the same cryoprotectant solution used for storage, as the retina was frozen again in the next step.

Retinas were dissected and flattened as described previously, keeping track of the spatial orientation. Afterward, the tissue was placed in a cryomatrix (Tissue-Tek O.C.T. compound) at room temperature for at least 20 minutes and finally placed on a microscope slide. From here, the retina was gently placed on a flat surface made by the frozen cryomatrix solution and then completely embedded. Dorso-ventral marks allowed a correct alignment on the cryostat sample plate and each vertical section was thus oriented on the slide as well.

In the case of starting from an eyecup, after identification of the choroid fissure on the back of the sclera, a small incision was made on the cornea-scleral border as landmark, to distinguish between temporal and nasal side of the retina. Eyecups were then embedded and frozen in Tissue-Tek placed on an aluminum block cooled with liquid nitrogen and subsequently vertically sectioned. Cryostat sections of 20 μm thickness were mounted on adhesion microscope slides (SuperFrost Plus™) and dried for 40-45 minutes on a heating plate at around 36°C. Afterwards, slides were directly used for immunofluorescence staining or stored at -20°C for later use.

3.3 Immunohistochemistry

Immunohistochemistry (IHC) is a consolidated routine technique used to study expression and cellular localization of proteins in the mouse retina. For indirect immunofluorescence staining so called “primary antibodies” are used, each of which binds to a specific antigen to form an antibody-antigen complex through noncovalent interactions. Each antibody molecule recognizes a specific region of the antigen, known as an epitope. The signal can be amplified by indirect immunofluorescence in which fluorophores are conjugated to “secondary antibodies”, which in turn bind to the primary antibody-antigen complex (Burnett, 1997). This method preserves spatial resolution while increasing sensitivity to low-concentration antigens.

This indirect method enables an amplification of the signal since several secondary antibodies may be connected to each primary antibody. All the experiments performed in the present study are based on the immunofluorescence technique.

3.3.1 Immunolabeling of whole-mounted retinas

Once placed and flattened on the nitrocellulose filter paper, retinas were washed several times for at least one hour in PBS or in a tris-buffered saline (TBS) solution, containing 0,3% Triton X-100 (TX-100). For convenience, rinses and incubations with antibodies were performed in 10 mm diameter micro dishes, so that small volumes of 150-200 µl could be used for immuno incubations. During the incubation periods the dish was sealed with parafilm to avoid tissue drying.

Whole-mounted retinas were incubated at room temperature for 2-3 days in a mixture of primary antibodies in the proper incubation solution to receive double-, triple- or quadruple-labelling data. Primary antibodies used in this study are listed below in Table 1. The incubation solution was the same for the primary and secondary antibodies and was consisting of PBS buffer containing 5% normal donkey serum (NDS), 1% bovine serum albumin (BSA) and 1% Triton X-100, or TBS buffer containing 5% Chemi-BLOCKER (CB), 0,3% Triton X-100 and 0,02% sodium azide. Serums such as NDS, BSA and ChemiBLOCKER are generally added to block non-specific binding sites and facilitate the specificity between the antibody and its target. Permeabilization of the cell membrane is useful to improve the efficiency of the antibodies. Triton is a common non-ionic and non-denaturing surfactant used as a mild detergent for permeabilization of cells for immunofluorescence stainings. Sodium azide is used to protect the sample from bacterial contamination during longer incubation times.

Following incubation with primary antibodies, tissues were washed 3 times for 5 minutes each time and then another 3 times for 15 min each time, with the specific buffer. The solution containing the appropriate secondary antibodies (Tab. 2) was centrifuged for 5 minutes at 13,000 rpm, as additives are often included in the secondary antibody stocks to maintain the structural stability and efficacy of the antibodies. Reagents (Tab. 3), such as PNA or streptavidin, were employed as secondary antibodies and underwent the same step. By centrifuging the antibody incubation solution and by careful pipetting the supernatant onto the sample, it is possible to remove the additives and possible aggregates from the solution, which otherwise disturbs high resolution of confocal microscopy.

Finally, retina wholemounts were washed as mentioned before and mounted on slides with VECTASHIELD (mounting medium). Spacers between glass slides and coverslips were used to avoid squeezing of the tissue and the coverslip was sealed with nail polish to prevent leaking. The sample was then stored at 4°C in the darkness and the acquisition of images at the confocal or epifluorescence microscope was performed at least the day after.

3.3.2 Immunolabeling of vertical sections

For immunolabeling of the vertical sections, a small incubation area was created around the vertical cryostat sections using a water repellent barrier pen. Slides were washed three times for at least 10 min each with buffer (PBS or TBS Tx-100 0.3%) to remove the embedding material (cryomatrix). Sections were incubated overnight at room temperature with a mixture of primary antibodies (Tab. 1), in PBS containing 5% NDS, 1% BSA and 0,5% of Triton X-100, or in TBS containing 5% CB, 0,3% Triton X-100 and 0,02% sodium azide. The incubation was performed in a chamber containing a wet wipe to prevent the tissue from drying and from light exposure. Next day, sections were rinsed in buffer and subsequently incubated for 90 minutes at room temperature with secondary antibodies (Tab. 2), diluted in the same incubation solutions used for incubations with primary antibodies.

During incubation with the secondary antibodies, the following washing steps and after mounting the sections in Aqua-Polymount (mounting medium), slides were kept in a dark environment and stored at 4°C until further image acquisition.

3.3.3 Primary and secondary antibodies

For these projects, different combinations of monoclonal and polyclonal antibodies were used, depending on their availability and suitability for multiple targets in the retinal sections or wholemounts. Antibodies are either polyclonal or monoclonal. Polyclonal antibodies refer to a mixture of heterogeneous immunoglobulins produced by different plasma B cells. They can recognize different epitopes of the same antigen. Monoclonal antibodies are generated by a single clone of plasma B cells. Unlike polyclonal antibodies, which are produced in live animals, monoclonal antibodies are produced *ex vivo* using cell-culture techniques. They can recognize the same epitope of an antigen.

In this study, three different antibodies against Cx57 were used (Tab 1). The two new guinea pig polyclonal anti-Cx57 antibodies were generated against two C-terminal peptides of mouse Cx57 (for further details, please refer to Section 7.2.2; Appendix – Experimental protocols). Both peptides CSM and PGS, were used for Cx57 detection and for convenience are referred in the text as Cx57 guinea pig antibody.

All used antibodies were immunoglobulins of class G (IgG), except for the immunoglobulin of class M (IgM) used to identify the protein connexin 50 (Cx50) on the mouse horizontal cells. In some experiments, the reagent lectin peanut agglutinin (PNA) conjugated to a fluorophore (Alexa-568 or Alexa-647) was used to specifically mark the cone pedicle base in the OPL. For the tracing experiments performed to analyze coupling between mouse horizontal cells, injected neurobiotin was detected with streptavidin conjugated with Alexa-568 (Tab. 3).

Table 1: Primary antibodies and their dilutions

Antibody	Host, type	Dilution	Immunogen	Source, Catalog
Calbindin	rb, polyclonal	1:2000	Recombinant protein of rat calbindin D-28K	Swant, CB-38A
	gp, polyclonal	1:500	Recombinant protein of human calbindin D-28K	Synaptic System, 214 005
	ms, monoclonal	1:1000	calbindin D-28K purified from chicken gut	Swant, CB300
Cone arrestin	rb, polyclonal	1:1000	C-terminal region of mouse cone arrestin.	Chemicon, AB15282
CtBP2	rb, polyclonal	1:1000	Synthetic peptide of rat Ribeye aa. 974-988	Synaptic System, 193003
	ms, monoclonal	1:1000	Mouse CtBP2 aa. 361-445	BD Transduction Lab, 612044
Cx36 (1E5H5)	ms, monoclonal	1:500	Synthetic C-terminal peptide of rat and mouse	Invitrogen, 37-4600
Cx50 IgM (C6)	ms, monoclonal	1:5000(w)/ 1:1000(c)	urea/alkali stripped sheep lens membranes	Invitrogen, 33-4300
Cx57 (PGS)	gp, polyclonal	1:500(w)/1:100(c)	PGSRKASFLSRLMSEK	This study
Cx57 (CSM)		1:200(w)/1:100 (c)	CSMSMILELSSIMKK	This study
Cx57	rb, polyclonal	1:500	CSMSMILELSSIMKK	(Janssen-Bienhold et al., 2009)
GluA2 (1K4)	rb, monoclonal	1:500	C-terminal of GluA2, cytoplasmatic domain	Sigma-Aldric; ZooMAb®, ZRB1008
GluA2 (6C4)	ms, monoclonal	1:100	Fusion protein of N-terminal region of GluA2	Invitrogen, 32-0300
GluA2/3	rb, polyclonal	1:1000	Synthetic peptide of rat GluA2 aa. 864-883	Sigma-Aldric, 07-598
GluA4	rb, polyclonal	1:5000	Synthetic C-terminal peptide	Chemicon, AB1508
GluK1 (C18)	gt, polyclonal	1:2000	C-terminal of human GluK1	Santa Cruz Biot. sc-7616
GluK1 (E12)	ms, monoclonal	1:2000	C-terminal of human GluK1 aa. 869-918	Santa Cruz Biot. sc-393420
PSD95 (K28/43)	ms, monoclonal	1:5000	Fusion protein of human PSD-95 aa. 77-299	NeuroMab, 75-028
S-Opsin	gt, polyclonal	1:10000	N-terminal of the of human OPN1SW	Santa Cruz Biot. sc-14363
ZO-1	ms, monoclonal	1:100	human recombinant zonula occludens-1 aa. 334–634	Zymed, 33-9100
	rb, polyclonal	1:100	human zonula occludens-1 cDNA aa. 463–1109	Zymed, 61-7300

Table 1: primary antibodies used in this study

Working dilutions were used for labelling of cryosections (c) and whole-mounted retinas (w) if different and depending on conditions. The “host” refers to the species of the animal from which the primary antibodies were produced: mouse (ms), guinea pig (gp), goat (gt), rabbit (rb). Amino acid (aa).

Table 2: Secondary antibodies and their dilutions

Conjugate	Type	Dilution	Source, catalog
Alexa Fluor 405	Donkey anti-mouse	1:500	Jackson ImmunoResearch, 715-475-150
Alexa Fluor 488	Donkey anti-mouse		Invitrogen / Molecular probes, A21202
	Donkey anti-mouse-IgM		Jackson ImmunoResearch, 715-545-140
	Donkey anti-rabbit		Invitrogen / Molecular probes, A21206
	Donkey anti-guinea pig		Jackson ImmunoResearch, 706-545-148
Alexa Fluor 568	Donkey anti-mouse		Invitrogen / Molecular probes, A10037
	Donkey anti-rabbit		Invitrogen / Molecular probes, A10042
CF568	Donkey anti-guinea pig		Sigma, SAB4600469
Alexa Fluor 647	Donkey anti-mouse		Invitrogen / Molecular probes, A31571
	Donkey anti-rabbit		Invitrogen / Molecular probes, A31573
	Donkey anti-goat		Invitrogen / Molecular probes, A21447

Table 3: Reagents and their dilutions

Name	Dilution	Source, catalog
Peanut Agglutinin-586 (PNA-568)	1:250	ThermoFisher, L32458
Peanut Agglutinin-647 (PNA-647)		ThermoFisher, L32460
Streptavidin-568		Invitrogen, S11226

3.4 Image acquisitions and analysis

The confocal approach is suitable for imaging analysis because the light source and a spatial pinhole system facilitate the elimination of out-of-focus light from the specimen, even across different depth planes. To avoid the so called “crosstalk” between channels, sequential scanning of different wavelengths was performed by stack or by frame. For qualitative-comparative analysis and colocalization analysis, optimizing scanning settings, including sampling size, laser power, gain and offset (background level), were crucial in achieving the optimal signal-to-noise ratio (SNR). Acquiring with the most efficient SNR is important for a proper signal intensity and avoiding saturation or underexposure of the immunoreactive target, so that it can be properly evaluated (Bolte and Cordelières, 2006).

The outer plexiform layer (OPL) is inherently stratified, with distinct proteins and structures distributed across different depths. To fully capture the spatial arrangement of the immunoreactive targets within this layered architecture, imaging from the distal to the deeper proximal regions of the OPL was sometimes necessary. Figure 10 below, shows the imaging strategy used for the retina and explains the corresponding images elaborated upon in the text. Confocal image Z-stacks were typically scanned at $\sim 0.2 \mu\text{m}$ intervals, resulting in approximately 55 focal planes to cover the entire OPL, which spans about $11 \mu\text{m}$ in thickness (Fig. 10 B). To effectively visualize these stacked images, projected focal planes from different levels of the full acquisition stack are presented. Consequently, most images depict various levels of the OPL above, at, and below the cone pedicle base (Fig. 10 C), providing a more

comprehensive representation of the sample at different depths (Fig. 10 D). This approach also helps to flatten any tissue irregularities. In contrast, some images are shown as single optical sections, corresponding to individual focal planes, which offer the most precise depiction of spatial organization within a very confined volume.

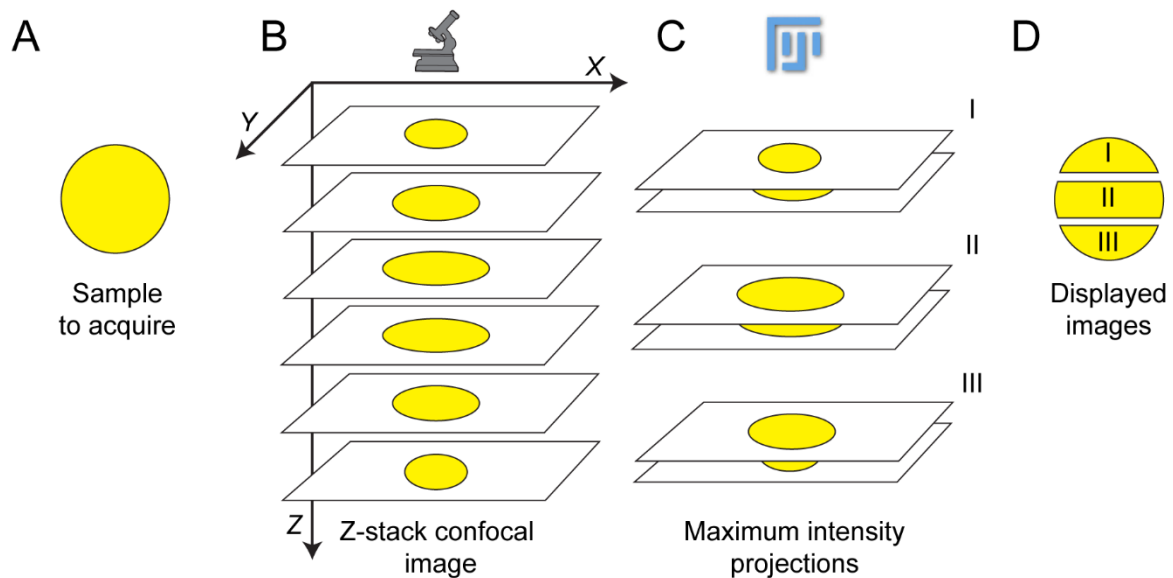


Figure 10: Imaging strategy and layer-specific visualization

A: Schematic of the imaging strategy for capturing the spatial distribution of targets within the stratified mouse retina. **B:** Confocal Z-stacks were acquired at different Z-increments (Z-step size), covering the entire thickness of the region **C-D:** Projected focal planes from different levels of the original Z-stack provide a detailed view of the retinal layers. Select images shown as single optical sections for precise structural visualization.

Based on the tissue preparation protocol for immunostaining, the orientation of the OPL during the subsequent confocal imaging step could change. This variability was simply due to the positioning of the retina on the filter paper, whether it was laid on the ganglion cell layer or the photoreceptor layer. To maintain clarity and consistency, however, all images - whether from vertical sections or whole-mounted retinas - are presented with the same orientation: the distal OPL is positioned at the top or in the upper panels, while the proximal OPL is shown at the bottom or in the lower panels. It is important to note that the sequence of planes within a single Z-stack is proper for each individual acquisition. These sequences are reported in their original order throughout the thesis to provide a clear representation of the different layer arrangements within the OPL.

Confocal micrographs of fluorescent specimens were taken using a Leica TCS SL (SP2 or SP8) confocal laser scanning microscope. Scanning was performed with a PL APO 63X/1.32 oil-immersion objective or with an HC PL APO CS2 63X/1.4 oil-immersion objective at different image resolutions and a z-axis increment in a range of 0.1 – 0.3 μm .

During microscope acquisition, particular care was taken to ensure correct retina orientation. Different microscopes use different approaches or technologies to display and manipulate the sample. Thanks to the retina landmarks, made during tissue preparation and the overview function of the microscope (Navigator system, Leica SP8), it was possible to acquire with confidence in specific areas of interest and in relation to the entire sample.

The epifluorescence Leica DM6 B microscope, equipped with motorized stage and a HCX PL FLUOTAR 20X/0.5 air-objective was used to acquire images of whole-mounted retinas used for the large-scale quantification of the horizontal cells. For this project I collaborated with Lucia Lindenthal and Asli Pektaş. Christoph Block was responsible for the visualization and data curation of these analysis (see Section 7.2.4; Appendix – Experimental protocol). For this analysis, I provided the whole-mounted retinas for the immunostaining and perform the image acquisitions. Since these results are closely related with the horizontal cell gap junction project, they will be presented in the results section and discussed later.

In project three, a quantitative analysis of the immunoreactivity of the gap-junction protein connexin57 (Cx57) and the tight-junction protein zonula occludens-1 (ZO-1) was conducted beneath single cone pedicles across the retina. Colocalization between Cx57 and ZO-1 was also analyzed in the same area (see Section 7.2.1; Appendix – Experimental protocols). Colocalization can be described as the simple spatial overlap or co-occurrence of two components. The two probes not only overlap with one another, but they are distributed together within and along specific structures. Merging or superimposing images of each probe may show areas whose color reflects the combination of both probes (Dunn et al., 2011). Colocalization analysis relies on the fact that both targets are labeled with different fluorochromes and acquired with their specific wavelength of light. Regarding the information gathered through this methodology, resolution of the light microscopy represents a physical limitation, thus it is not possible to determine molecular interactions. Nevertheless, fluorescence colocalization is useful to observe close association between two different proteins within a specific cellular location.

To evaluate the colocalization level between Cx57 and ZO-1 across the retina, each whole mounted retina was sampled in ~ 8 fields, corresponding to the intersections of the four cardinal directions and two eccentricities each (dorsal-temporal, dorsal nasal, ventral temporal, and ventral nasal; see Fig. 11). Eccentricities were defined between center and the retina edges: in the middle, approximately 50% away from the optic nerve head and at peripheral, 75% away from the optic nerve.

Confocal stacks were acquired from three different retinas, at a z-increment of 0.1 – 0.3 μm . The total z-size was chosen to fully capture the entire thickness of the ZO-1 cluster below the cone pedicle (Puller et al., 2009), which typically included 20-25 consecutive optical sections. The area defined by each cone pedicle was represented by a circular region of interest (ROI)

of 7 μm of diameter, which surrounded the ZO-1 cluster. Background and contrast were adjusted as described below, and global threshold was independently applied. Colocalization between Cx57 and ZO-1 was estimated by the “colocalization highlighter” plugin in Fiji (MBF collection, (Collins, 2007; Tetenborg et al., 2017)). The resulting 8-bit z-stack images displaying the colocalized area, were used to calculate the colocalization area below the cone pedicle, with the “analyze particles” function in Fiji.

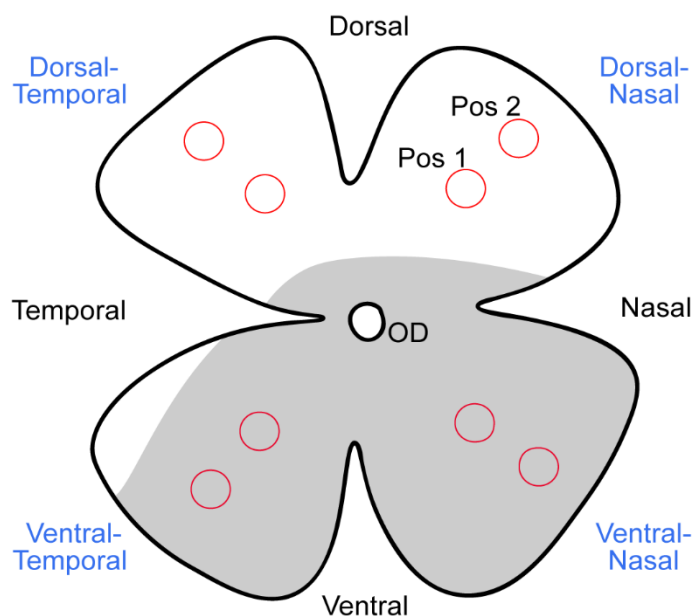


Figure 11: Illustration of the acquisition strategy in whole-mounted retinas

The retina was divided into a dorsal peripheral area and a ventral peripheral area based on the S-opsin gradient (grey area) and then subdivided into ~ 4 ROIs on each side. The distance from the optic disc (OD) was approximately at 50% (Pos1) and 75% (Pos2) of eccentricity.

As control, Cx57 image z-stack channel of each ROI, was vertically flipped and the colocalization analysis repeated (Puller et al., 2007). Simultaneously, the positive area of Cx57 and ZO-1 was measured in the same ROIs with the “analyze particles” function in Fiji. Colocalization areas smaller than 0.01 μm^2 were excluded from the analysis. For the quantification of the individual immunostainings, particles with a size smaller than 0.04 μm^2 were excluded from the analysis. The detailed script for the immunoquantitative and colocalization analyses is presented in section 7.2.1 (Appendix – Experimental protocols). The area measurements were normalized (Results – Project 3) to account for differences between the samples regarding staining intensity and the relative background staining levels.

Fiji is an open source image processing platform based on ImageJ (Schindelin et al., 2012). This software is commonly used for image analysis due to its versatility and numerous tools. It relies on the scientific community for the proper functioning of its protocols.

Microscope images shown in this work are presented as maximum intensity projections of image stacks, unless stated otherwise. Some images were further processed with Fiji for

visualization purpose, using the “subtract background” (rolling ball) plugin and the “enhance contrast” plugin with 0.01% saturation. Brightness and contrast of the final images were adjusted using Adobe Photoshop CS6, while Adobe Illustrator was occasionally used for the illustrations and graphs.

3.5 Statistical analysis

For project three, statistical analyses were performed using GraphPad Prism 9 on normalized ZO-1 and Cx57 immunostaining data from three different retinas. One-way ANOVA Tukey for multiple comparison was used to compare the colocalization area between the four different groups dorsal peripheral, ventral peripheral and the corresponding two flip controls. An unpaired, two-tailed Mann Whitney test was used instead, to compare the difference of the immunoreactive areas of Cx57 and ZO-1 from the same regions where the colocalization analysis have been performed. A p -value < 0.05 was considered statistically significant. Quantitative data were obtained from 3 different retinas including 144 pedicles from the dorsal peripheral area and 131 pedicles from the ventral peripheral area, presented as median and quartiles.

4. Results

4.1 Spatial organization of desmosome-like junctions and gap junctions in the outer plexiform layer of the mouse retina

4.1.1 The cone pedicle markers

To accurately determine the exact spatial expression patterns of glutamate receptor subunits, electrical synapses and their associated structural proteins in horizontal cells (HCs), it was first necessary to identify those structures that served as reference points in the outer plexiform layer (OPL). Therefore, an antibody detecting the mouse cone arrestin (CAR) was used to label cones in their entirety, from the outer segments to the synaptic terminals (Fig. 12 D, F) (Zhu et al., 2002; Ishibashi et al., 2022).

Maximum projections (Z-size, see Fig.12) of image stacks acquired from vertical cryosections of the OPL, show a series of cone pedicles aligned in a rather orderly manner. At the same time, an antibody directed against PSD-95 (postsynaptic density protein 95) was used to label the membranes of cone and rod terminals. In the OPL, PSD-95 immunoreactivity is uniquely present at the presynaptic terminals (Koulen et al., 1998). In the mouse retina, the number of rods is significantly higher than that of cones (Jeon et al., 1998; Nikonov et al., 2006), and their terminals occupy the space between and above the cone pedicles (Fig. 12 A-C). Thus, in the OPL, cone pedicles and rod spherules can be identified by their size, location and structure.

The space underneath the cone pedicles is occupied by the dendrites of HCs and bipolar cells (BCs) and the rare processes of interplexiform amacrine cells (ACs) (Haverkamp et al., 2000). The glutamate receptor GluK1 is a kainate receptor subunit expressed at the dendrites of OFF-cone bipolar cells at the flat contacts of each cone pedicle (DeVries and Schwartz, 1999; Haverkamp et al., 2001b, 2003; Puller et al., 2013). Therefore, an antibody against this glutamate receptor subunit was used to label and map the position of the cone pedicle bases (Fig. 12 D-F; G-I). In whole-mounted retinas, clusters of GluK1 at the flat contacts of the pedicles reveal the mosaic of cones (Fig. 12 J-L). Furthermore, the thin layering of the GluK1 clusters observed by fluorescence microscopy allows for a valuable determination of the spatial distribution of synaptic components at the cone terminal. In a similar way, the lectin peanut agglutinin (PNA) was used in several experiments as an alternative to the GluK1 antibody. From a variety of species, including chick, human, monkey and fish, PNA has been shown to locate exclusively at cone photoreceptor terminals and associated with the central elements of the triad, the invaginating dendrites of ON-cone bipolar cells (Blanks and Johnson, 1984; Haverkamp et al., 2001a; Wässle et al., 2009).

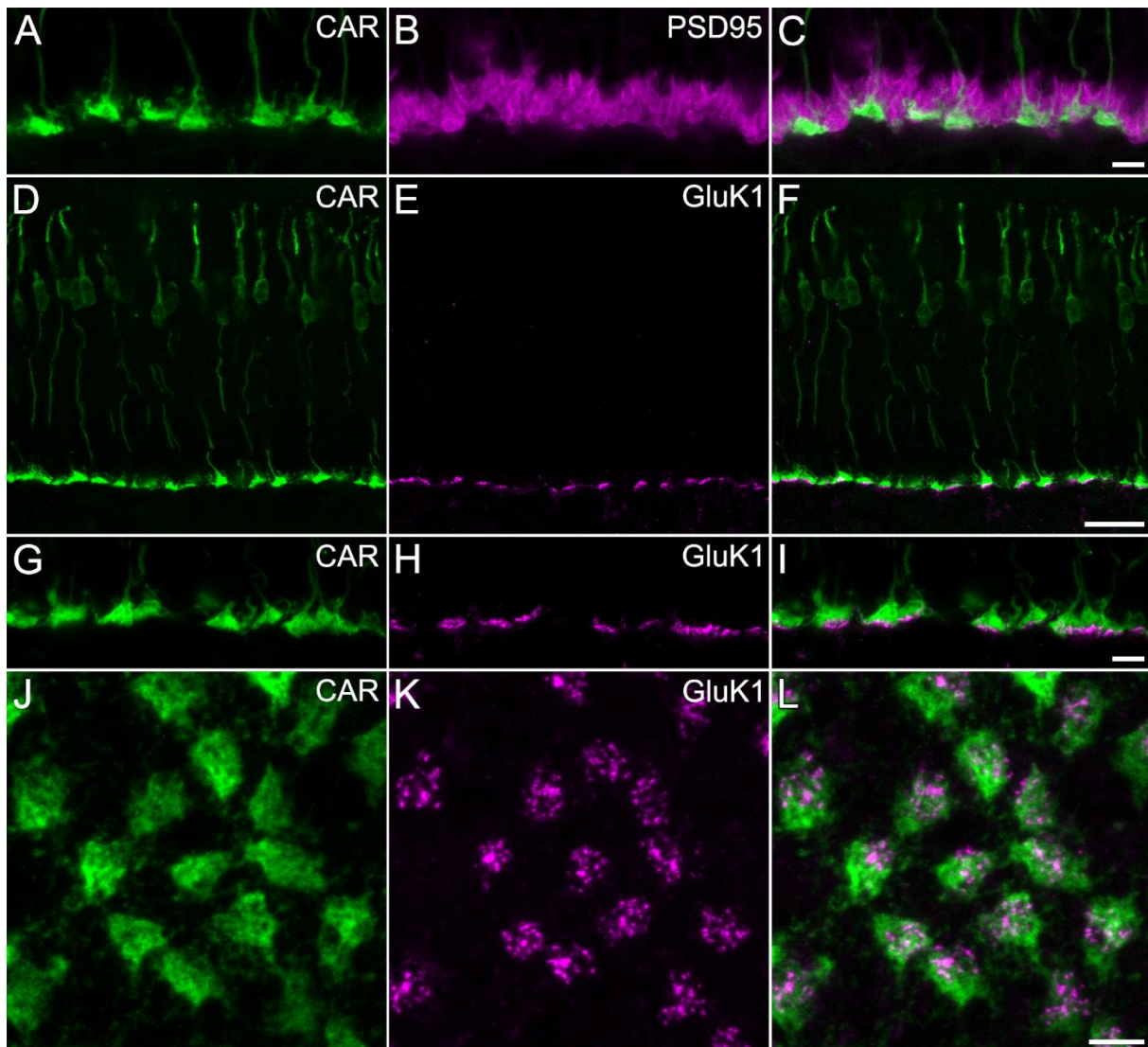


Figure 12: Organization of photoreceptor terminals in the OPL and their markers

A-C: Projection of confocal image stacks (Z-size $\sim 4\mu\text{m}$) of a vertical cryosection double labeled for detecting cone arrestin (CAR) and the postsynaptic density protein 95 (PSD95), that in the retina mark the presynaptic terminals of photoreceptors. **D-F:** Projection of confocal image stacks (Z-size $\sim 3\mu\text{m}$) of a vertical cryosection double labeled for CAR and the kainate receptor subunit 1 (GluK1). **G-I:** Projection of confocal image stacks (Z-size $\sim 3.4\mu\text{m}$), focusing on the cone pedicles and GluK1 clusters. **J-L:** Confocal image stacks (Z-steps 1-38/38, Z-size $\sim 7\mu\text{m}$) of the OPL of a whole-mounted retina showing the distribution of CAR- and GluK1-immunoreactivity in the horizontal plane. Scale bars: $5\mu\text{m}$ in C, applies to A-B; $20\mu\text{m}$ in F, applies to E-F; $5\mu\text{m}$ in I, applies to G-I; $5\mu\text{m}$ in L, applies to J-L.

In previous studies, PNA was used to label invaginations at the cone pedicles in the mouse retina, similar to the situation described in monkey cones (Haverkamp et al., 2001b; Mataruga et al., 2007). The expression patterns in the mouse retina showed that both GluK1 and PNA clusters are aligned in regular arrays at the cone pedicle base, almost overlapping when observed at low magnification (Fig. 13 A-C). However, higher magnification images (Fig. 13 D-F) revealed what has been anticipated before (see scheme Fig. 3) as the laminated distribution of dendritic processes at the cone pedicle.

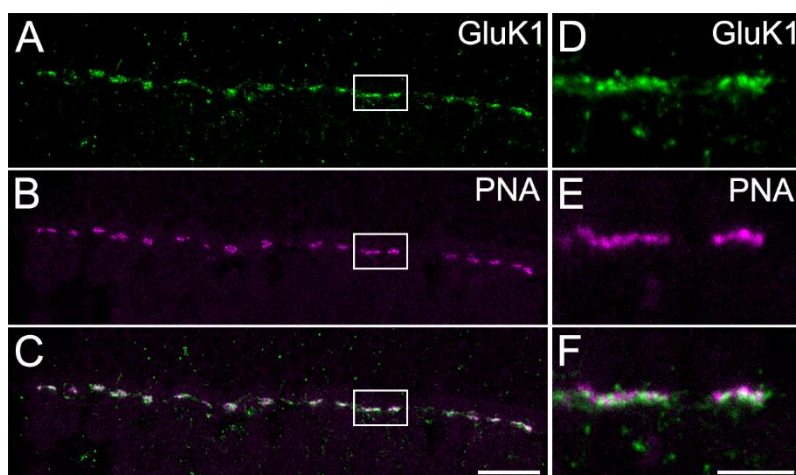


Figure 13: GluK1 and PNA as cone pedicle base markers

A-C: Maximum projections of confocal image stacks (Z-size $\sim 3.2 \mu\text{m}$) of a vertical cryosection double labeled for detecting the kainate receptor subunit 1 (GluK1) and the Alexa-568 conjugated peanut agglutinin (PNA) in the OPL. Rectangles indicate an example of two pedicles of which higher magnifications are shown in **D-F**. Scale bars: $20 \mu\text{m}$ in C, applies to A-C; $5 \mu\text{m}$ in F, applies to D-F.

PNA labeling forms a band that is slightly above the GluK1-immunoreactive clusters and maintains consistent length across the pedicles. This is because GluK1 is expressed by OFF-cone bipolar cells at the flat contacts, while ON-cone bipolar cell dendrites are involved in the triad just above. In this way, both the GluK1 antibody and PNA can be used as reliable markers for the cone pedicle base and more importantly as an excellent reference to describe the distribution of the synaptic components in the OPL.

4.1.2 The distinct distribution patterns of the AMPA subunits GluA2, GluA2/3 and Glu4

To investigate the spatial distribution patterns of the AMPA-type receptor subunits (GluAs) on the horizontal cells in more detail, vertical cryosections of the mouse retina were double labeled for the subunits GluA2, GluA2/3 and GluA4, together with a cone pedicle base marker, either anti-GluK1 or PNA (Fig. 14).

The immunoreactivity patterns of the three GluAs exhibited an extensive distribution within the OPL, and their association with both cone and rod photoreceptor terminals. However, the staining patterns showed a distinct spatial organization for each subunit. The monoclonal antibody directed against the GluA2 subunit (Fig. 14 A-C), robustly stained the lateral elements of the rod spherule triads in the distal part of the OPL. Here, the staining pattern of GluA2 sometimes appears in the shape of a coffee bean or the equal sign (=) (Fig. 14 A, arrowhead). At the cone pedicle level, two distinct bands or strata were observed, which also showed strong GluA2 Immunoreactivity (Fig. 14 A-C). The upper band, above the GluK1 cluster was generally brighter and clearly defined. Related to its position, the upper band identified the GluA2

expression at the invaginating tips at the triads in cone pedicles. The second strata, beneath the cone pedicle base, appeared wider in height, but retained its brightness and showed a more triangular shape facing downward. This suggested the presence of GluA2 subunit aggregates underneath the cone pedicle at the putative desmosome-like junctions, which have prior been described between horizontal cell dendrites in the macaque retina (Haverkamp et al., 2000, 2001a), and rabbit retina (Pan and Massey, 2007).

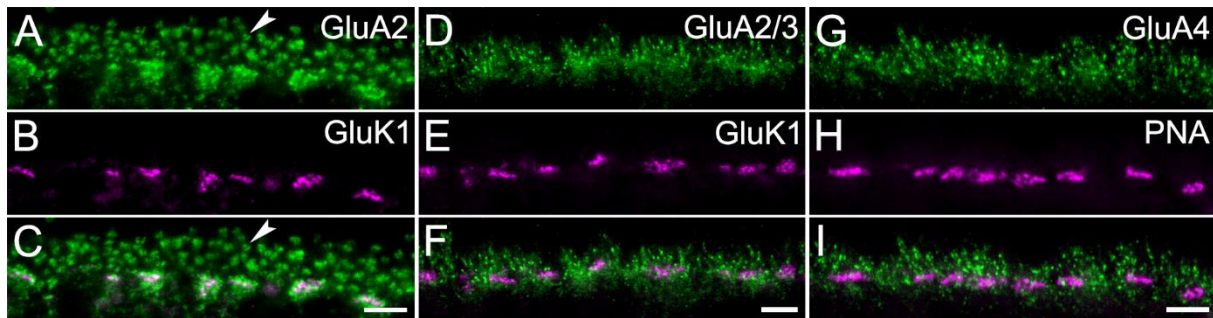


Figure 14: Different expression patterns of GluAs in the OPL of mouse retina

Projections of confocal image stacks obtained from vertical cryosections double labeled for the AMPA-type receptor subunit 2 (GluA2) with the typical shape at rods level (arrowhead), and GluK1 (in **A-C**; Z-size 3 μ m), the subunits GluA2/3 and GluK1 (in **D-F**; Z-size \sim 1.8 μ m), and the subunit GluA4 and PNA (in **G-I**; Z-size \sim 1.6 μ m) are shown. The distinct distribution patterns of the different AMPA-receptor subunits become particularly evident in (C, F and I). Scale bars: 5 μ m in C, applies to A-C; 5 μ m in F, applies to D-F; 5 μ m in I, applies to I-G.

The two polyclonal antibodies recognizing GluA2/3 and GluA4 subunits showed completely different staining patterns. According to the manufacturer's datasheet, the antiserum against GluA2/3 (Fig. 14 D-F) is supposed to recognize both AMPA receptor subunits, GluA2 and GluA3. The immunoreactive labelling of mouse retina sections exhibited a finer, more punctate distribution pattern mostly restricted to the distal part of the OPL and only sparse puncta in the proximal OPL below the cone pedicle (Fig. 14 F). This immunoreactivity pattern appeared similar to the distribution pattern of the GluA4 subunit (Fig. 14 G-I), which also showed a finer punctate immunoreactivity pattern, but a general lack of labeled clusters beneath the cone pedicles, like those observed for GluA2-immunoreactivity (compare Fig. 13 C, F and I). The abundance of puncta in the distal area of the OPL, above the cone pedicle base, suggested the association of GluA4 with the tips of horizontal cell axon terminals invaginating into rod spherules.

To better understand the spatial distribution of AMPA receptor subunits and confirm what was observed on vertical sections, whole-mounted retinas were immunolabeled with the same three different antibodies. In confocal microscopy, flat, whole-mounted retinas allow for the observation of the labeled targets throughout the focus planes of the Z-axis. Figure 15 shows examples of maximum Z-stack projections (Z-size \sim 2.6 μ m, distal OPL; Z-size \sim 2 μ m, pedicle base; Z-size \sim 1 μ m, proximal OPL) at three different levels of the OPL. Fine puncta of GluA4-

immunoreactivity were observed in the distal part of the OPL (Fig. 15 A-C), suggesting their association with the rod terminals. At this level, the pedicle base marker GluK1 is barely visible due to its location at a different plane, deeper in the OPL. At the cone pedicle base level (Fig. 15 D-F), GluA4 puncta were observed in the space between cone pedicles, as rod spherules are still present at this level. Additionally, more pronounced labelling was also located at the invaginating dendrites of horizontal cells, both inside and around the GluK1 clusters.

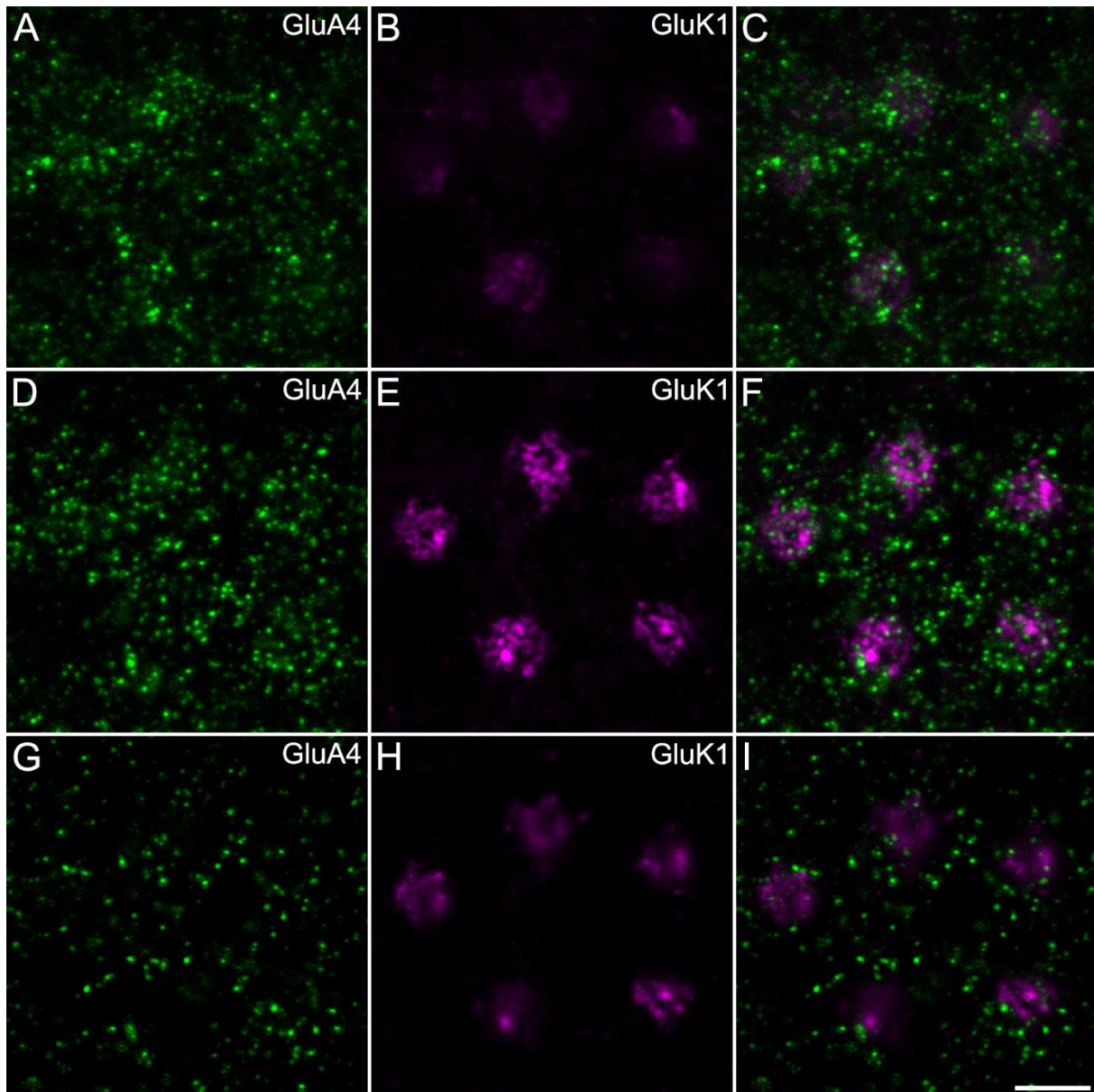


Figure 15: GluA4 expression in three horizontal planes of the OPL

Horizontal view of maximum projections of a whole-mounted retina double labeled to visualize GluA4 and GluK1. **A-C**: At the distal OPL it is possible to observe GluA4 immunoreactivity at the level of rods, with GluK1-immunoreactivity located slightly below (Z-steps 1-13/29, Z-size ~ 2.6 μm). **D-F**: As in A-C, but GluA4-labelling is presented at the level of the HCs invaginating dendrites (Z-steps 14-23/29, Z-size ~ 2 μm). **G-I**: As in D-F but approximately 1 μm below the cone pedicle base (Z-steps 25-29/29, Z-size ~ 1 μm). Scale bar: 5 μm in I, applies to A-I.

Beneath the base of the cone pedicle (Fig. 15 G-I), the clusters of GluK1 are out of focus, so their staining intensity appears lower again. The five pedicles shown in the image are slightly oblique, resulting in a fine deviation of the plane of focus of each pedicle. Nevertheless, GluA4 labeling was absent in the area beneath the pedicle, but still sparse in the space between them where rods are located.

In a similar way, whole-mounted retinas were double labeled for the GluA2/3 subunits and the cone pedicle base marker GluK1. The distribution of these markers was qualitatively analyzed across the thickness of the OPL. Figure 16 provides an example of this distribution at three distinct levels within the OPL (see Fig 16, figure legend). Prominent GluA2/3 immunoreactivity was present at the level of the tips of the processes of HC axon terminals invaginating into rod spherules (Fig. 16 A-C, distal OPL). In this instance, the sample was not entirely flat, as evidenced by some GluK1 clusters being out of focus due to their location deeper within the OPL. Conversely, other clusters are slightly above this plane, making it challenging to achieve clear discrimination during confocal imaging. As a result, the number of optical planes had to be increased to capture the full depth of the region of interest. At rods level, the staining pattern was characterized by a relatively uniform distribution of puncta, comparable to the observed pattern of GluA4-immunoreactivity (see Fig. 15 A-C). However, upon qualitative observations, the size of the GluA2/3 puncta appeared to be occasionally larger when compared to the GluA4 puncta at this level. In contrast, the puncta were observed to be generally smaller at a lower level, particularly in the region of the pedicle bases, identified by the GluK1 clusters (Fig. 16 D-F). Beneath the cone pedicles, in the proximal OPL (Fig. 16 G-I), GluA2/3-immunoreactivity was observed to be generally decreased, with sparse and fine puncta which were challenging to image using the confocal setup. However, the polyclonal anti-GluA2/3 antibody was not able to provide enough visible clusters below the cone pedicle, neither in vertical cryosections nor in whole-mounted retinas. Moreover, the lack of accumulation of the receptor subunits was not observed even when different antibody concentrations or incubation protocols were used (data not shown). Therefore, it is reasonable to assume that the polyclonal anti-GluA2/3 antibodies might have a preferential affinity for the GluA3 subunit rather than the GluA2, since its immunoreactivity pattern is clearly distinguishable from the immunoreactivity pattern revealed by the monoclonal anti-GluA2 antibody.

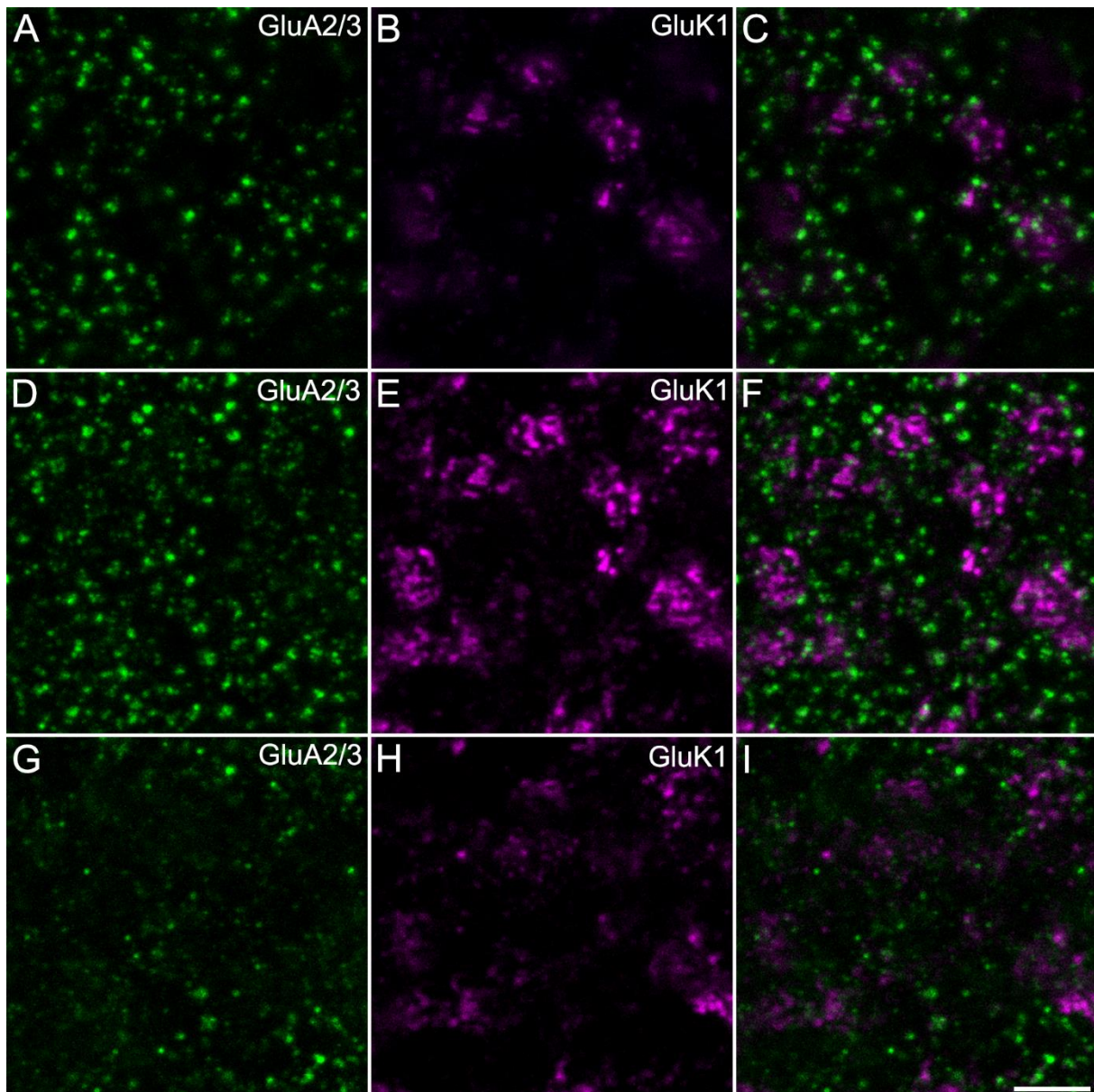


Figure 16: GluA2/3 expression in the three horizontal planes of the OPL

Horizontal view of maximum projections of a whole-mounted retina double labeled to visualize GluA2/3 and GluK1. **A-C**: At the distal OPL it is possible to observe GluA2/3 immunoreactivity at the level of rods, with GluK1-immunoreactivity located slightly below (Z-steps 27-38/40, Z-size ~ 1.2 μm). **D-F**: As in A-C, but GluA2/3-labelling is presented at the level of the HCs invaginating dendrites (Z-steps 14-27/40, Z-size ~ 1.3 μm). **G-I**: As in D-F but approximately 1 μm below the cone pedicle base (Z-steps 3-14/40, Z-size ~ 1.1 μm). Scale bar: 5 μm in I, applies to A-I.

In further analyses of GluA-receptors distribution in the OPL, particular focus was placed on the GluA2 subunit. Immunolabeling in vertical cryosections revealed the presence of GluA2 clusters beneath the cone pedicles. This observation suggests that GluA2 may play a key role in the formation of a complex structure at the putative desmosome-like junctions in the mouse retina. Immunostaining experiments on whole-mounted retinas confirmed the stratified staining pattern of GluA2 found in vertical sections (see Fig. 14 A-C) at the pedicle base (Fig. 17 A-C). The horizontal view from whole-mounted retinas provides a more detailed illustration of the

clustering of glutamate receptor subunits below the cone pedicles. By changing the focal plane, the two strata at the pedicle base could be distinguished (Fig. 17 D-F).

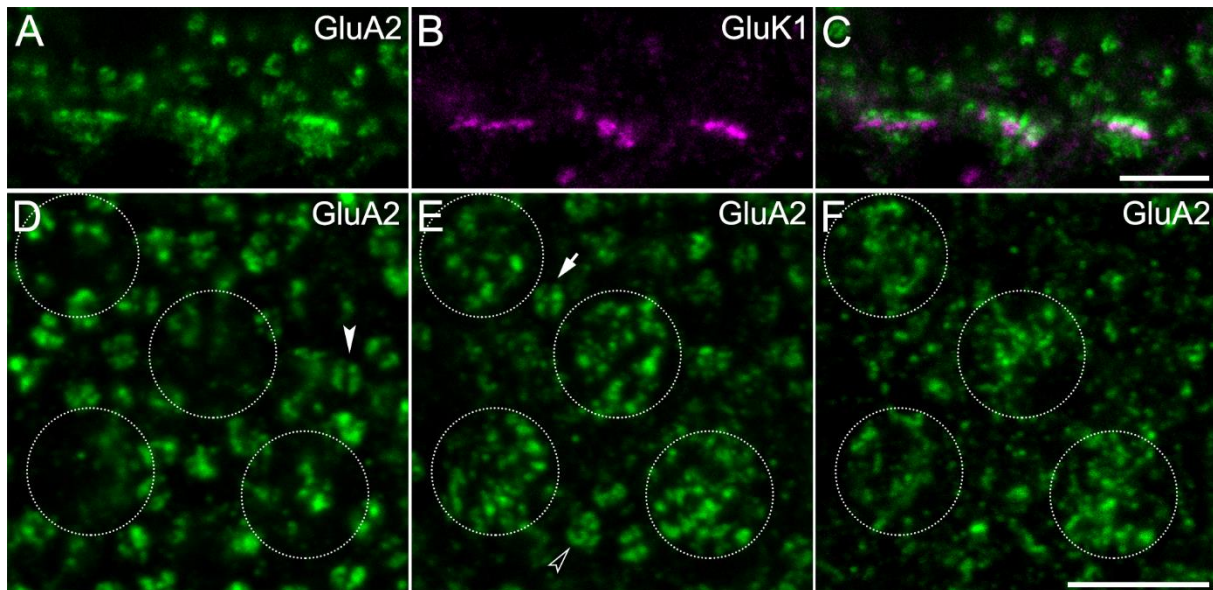


Figure 17: GluA2 clusters at the putative desmosome-like junctions

A-C: Maximum projections (Z-size $\sim 0.8 \mu\text{m}$) of confocal stacks taken from a vertical cryosection double labeled to detect the subunit GluA2 and the cone pedicle marker GluK1. **D-F:** Part of a whole-mounted retina labeled for the subunit GluA2. Maximum projections were chosen to cover the distal OPL (D; Z-steps 1-7/34, Z-size $\sim 1.4 \mu\text{m}$), the OPL at the level where HC processes invaginate the cone pedicle (E; Z-steps 8-16/34, Z-size $\sim 1.8 \mu\text{m}$), and the OPL beneath cone pedicles (F; Z-steps 17-28/34, Z-size $\sim 2.4 \mu\text{m}$). Filled arrowhead in D, indicates the “coffee bean” shape of GluA2 staining at the level of rods. Open arrowhead in E, indicates “horseshoe” shape and the arrow indicates quaternary structure of GluA staining at rods. Circles indicate pedicle positions based on PNA staining (not shown here to make it more understandable). Scale bars: $5 \mu\text{m}$ in C, applies to A-C; $5 \mu\text{m}$ in F, applies to D-F.

In whole-mounted retinas, the GluA2-immunoreactivity exhibited the distinctive “coffee bean” shape in the distal part of the OPL, (Fig. 17 D, filled arrowhead), suggesting its expression at the two lateral elements aligned at the synaptic ribbon of rod terminals. However, it is important to mention the occasional presence of horseshoe-shaped structures (Fig. 17 E, open arrowhead), which are characteristic for ribbon immuno-stainings observed in rod spherules (Haverkamp et al., 2001a, 2001b). Additionally, some of these “coffee beans” displayed a cut along their longitudinal axes, assuming in that way, a quaternary form (Fig. 17 E, arrow).

In whole-mounted retinas, as well as in vertical cryosections, two different bands of GluA2 immunoreactivity were discernible at the cone pedicle base. The upper band was best characterized as a punctate cluster located directly above the pedicle base (compare Fig. 17 A-C, E), indicative for the expression of GluA2 at the invaginating dendrites of horizontal cells. The second band was observed to extend deeper beneath the base of the cone pedicle and appeared to be organized in a punctate and striped configuration (Fig. 17A-C, F).

In previous studies performed with the primate retina (Haverkamp et al., 2000, 2001a), it has been shown that at the desmosome-like junctions the AMPA-subunit clusters are lying on a single plane and aligned at the base of the cone pedicles, thus entitled “band”. In contrast, the pattern of GluA2 immunoreactivity beneath the cone pedicle in the mouse retina was observed to be different, exhibiting a tendency to form a structure that could be compared to a “bouquet of flowers” (Fig. 18 B, E arrowheads). Thereby, the upper portion of the structure followed the extension of the cone pedicle base and narrowing instead towards the proximal retina (Fig. 18 G). To further describe the spatial organization of the GluA2 at the pedicle base and its organization on horizontal cells, triple labeling experiments using antibodies directed against the subunit GluA2, the subunit GluK1 and calbindin (CaBP) were performed on vertical cryosections. The calcium binding protein calbindin is present in mouse horizontal cells and labels all the cellular compartments (Fig. 18 A, C, F, H), including the cell body, dendrites and axons (Röhrenbeck et al., 1987; Haverkamp and Wässle, 2000). Figure 18 shows two examples of vertical cryosections.

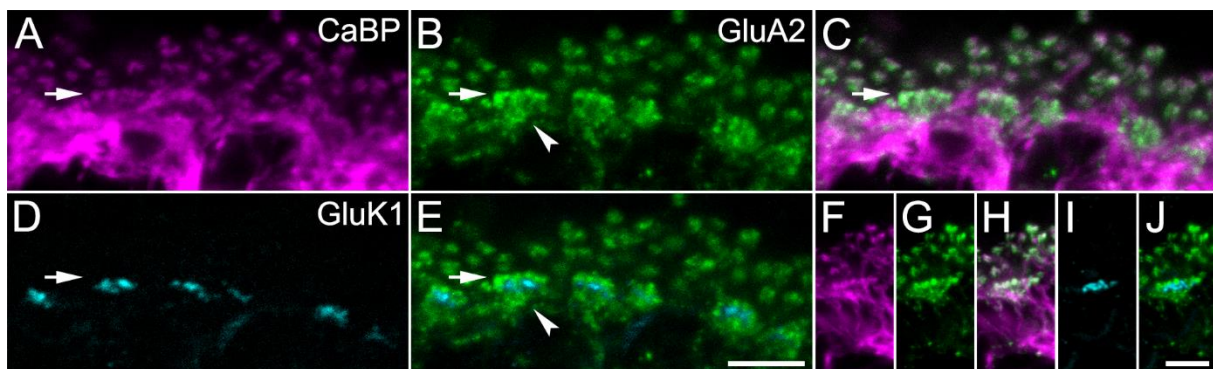


Figure 18: GluA2 distribution on horizontal cells

A-E: Maximum projections (Z-size ~ 2.2 μm) of confocal stacks generated from a vertical cryosection labeled against the calcium binding protein calbindin (CaBP, A, C), the subunit GluA2 (B-C, E) and the cone pedicle marker GluK1 (D, E). Arrows indicate the level of invaginating tips of horizontal cells at the cone pedicles, while arrowheads indicate the “bouquet of flowers” shape of GluA2 staining. **F-J:** As in A-E, max projections (Z-size ~ 1.8 μm) of confocal stacks taken from another vertical cryosection, but with a focus on a single cone pedicle. Scale bars: 5 μm in E, applies to A-E; 5 μm in J, applies to F-J.

On triple-labeled vertical retinal sections it became obvious, that the band containing GluA2 clusters overlap with the invaginating dendritic tips of calbindin positive HCs at the cone pedicles (Fig. 18 A; arrow), thus confirming the expression of this AMPA subunit at that specific location (Fig. 18 A-C). Below the base of the cone pedicles (Fig. 18 D; GluK1) the GluA2 clusters were more extending downwards to the border between proximal OPL and the inner nuclear layer and small GluA2 immunoreactive puncta were often found distributed along the branches of the horizontal cell dendrites (Fig. 18 B, C, F, H), assuming the typical shape of a “bouquet of flowers” (Fig. 18 B, E arrowheads, H).

Overall, GluA2/3 and GluA4 showed a punctate immunofluorescence in the OPL, with a greater number of fine puncta observed for the GluA4 subunit. Moreover, both staining patterns were observed to be wide and sparse in the distal OPL, suggesting that processes associated with rod spherules. The GluA4 subunit was typically absent in the region below the cone pedicles, whereas the GluA2/3 exhibited a staining pattern characterized by fine puncta. On the other hand, the GluA2 subunit was observed to be expressed on dendrites and axon terminals of horizontal cells within the invaginations at rod spherules and cone pedicles. At the latter, GluA2 appeared clustered in two layers, above and below the cone pedicle base. The upper punctate band was located at the horizontal cell dendritic tips and the lower at the level of the putative desmosome-like junctions.

4.1.3 Desmosome-like junctions in the mouse retina

It has been previously described in the mammalian retina that the additional post-synaptic structure at the desmosome-like junctions corresponds to a specialized area in which glutamate receptors are closely associated with gap junctions and the tight junction protein zonula occludens-1 (ZO-1) on horizontal cell dendrites, located below the pedicle (Haverkamp et al., 2000; Puller et al., 2009).

To address this hypothesis in the mouse retina, whole-mounted retinas were double labeled for GluA2 and HC specific gap junctions containing connexin57 (Cx57; Fig. 19). Cx57 is exclusively employed for the electrical coupling via mouse horizontal cell dendrites (Hombach et al., 2004; Shelley et al., 2006; Janssen-Bienhold et al., 2009; Puller et al., 2009).

Confocal maximum projections of different consecutive focus planes acquired from a single Z-stack (Fig. 19 A-I), show the spatial distribution of the two synaptic components from the distal to the proximal OPL. Extending across the distal OPL, the GluA2 staining pattern was characterized by the typical “coffee beam” shape (Fig. 19 A, C). At this OPL level, tiny and faint stained puncta of Cx57 were distributed more homogeneously (Fig 19 B, C). At a lower OPL level, clusters of GluA2 were identified at the invaginating tips, at the cone pedicle base (Fig. 19 D, F), but here Cx57 puncta were only rarely found in proximity to GluA2 cluster (Fig. 19E, F, K, L). A higher magnification image of a single GluA2 cluster at the level of the invaginating dendritic tips of HCs (Fig. 19 J, L), reveals an irregular punctate structure in which it is still possible to observe a pairing tendency of these puncta, that recalls the two invaginating lateral elements. The lower GluA2 strata was found approximately 1-2 μm beneath the cone pedicles indicative for its presence at the sites of the putative desmosome-like junctions between mouse horizontal cell dendrites (Fig. 19 G, I, M, O). Here, Cx57-immunoreactive plaques were observed in close association with the GluA2 clusters (Fig. 19 H, I, N, O), pointing to the presence of a desmosomal-like junction structure being also present at this site in the mouse retina.

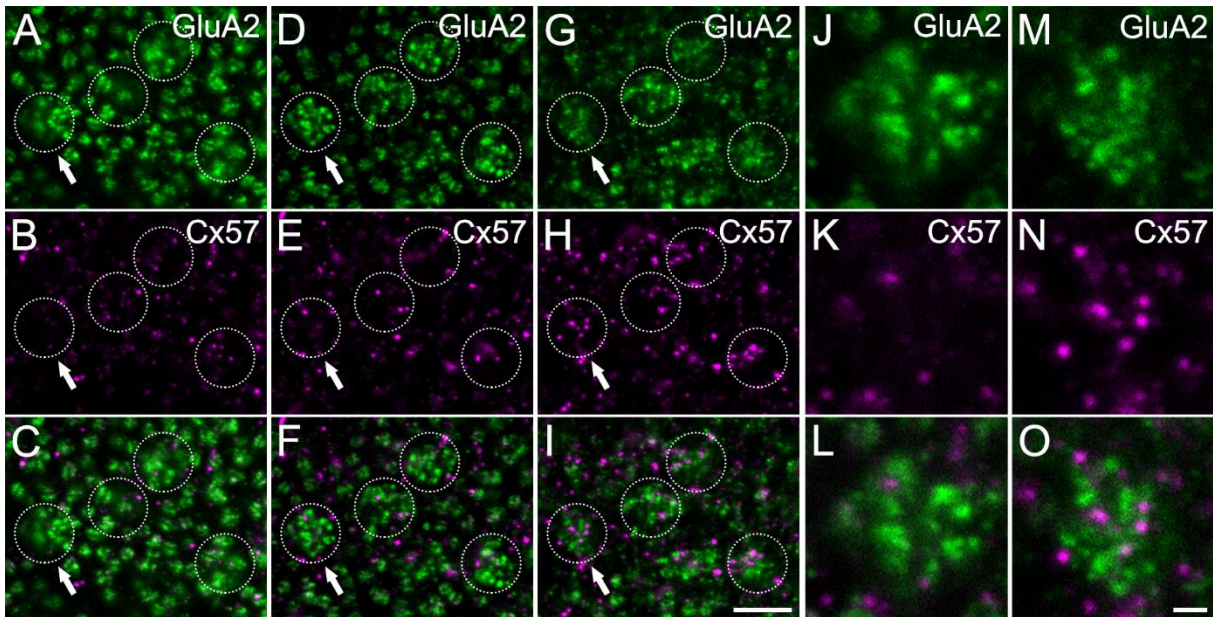


Figure 19: Cx57 is closely associated with GluA2 at the level of the desmosome-like junctions

A-I: Maximum projections of confocal image stacks from a whole-mounted retina double labeled with antibodies recognizing GluA2 and Cx57. Maximum projections were chosen to cover the distal OPL at the putative rods level (A-C; Z-steps 21-31/43, Z-size ~ 2.2 μm), at the invaginating dendritic tips (D-F; Z-steps 12-17/43, Z-size ~ 1.2 μm) and the proximal OPL beneath the cone pedicles (G-I; Z-steps 2-9/43, Z-size ~ 1.6 μm). Pedicle positions were identified by the GluA2 clusters and indicated by dashed circles. Arrows indicate an example pedicle of which a magnified version of the corresponding channels is shown in **J-O**: Maximum projections at the invaginating dendritic tips (J-L; Z-steps 17-18/43, Z-size ~ 0.4 μm) and beneath the cone pedicle (M-O; Z-steps 5-6/43, Z-size ~ 0.4 μm). Scale bars: 5 μm in I, applies to A-I; 1 μm in O, applies to J-O.

The expression pattern of the tight-junction protein zonula occludens-1 (ZO-1) was analyzed to gain further insight into the synaptic architecture of the desmosome-like junctions within the dendritic HC network. ZO-1 has been shown to interact with various connexins at electrical synapses (Giepmans, 2004; Li et al., 2004b; Flores et al., 2008; Lynn et al., 2012) and to be expressed at gap junctions below the cone pedicle in a type-specific manner by horizontal cells (Puller et al., 2009). As described in more detail later in this thesis (see project 3), in the mouse retina, ZO-1 colocalized with Cx57 at dendro-dendritic gap junctions of horizontal cells and has been observed in close opposition with glutamate receptors in the primate retina (Puller et al., 2009). In accordance with these insights, mouse whole-mounted retinas immunostained for the GluA2 subunit and the scaffolding protein ZO-1 revealed the spatial relationship between the two components below the cone pedicle (Fig. 20). The ZO-1 staining pattern exhibited distinct, string-like clusters situated beneath the cone pedicle (Fig. 20 C) and further tiny immunoreactive puncta among the clusters. Although ZO-1 expression was shown on horizontal cells at the same level of the desmosome-like junctions, ZO-1 was not colocalized with the AMPA receptor subunit GluA2, as shown here in retinal whole mounts (Fig. 20 B-D).

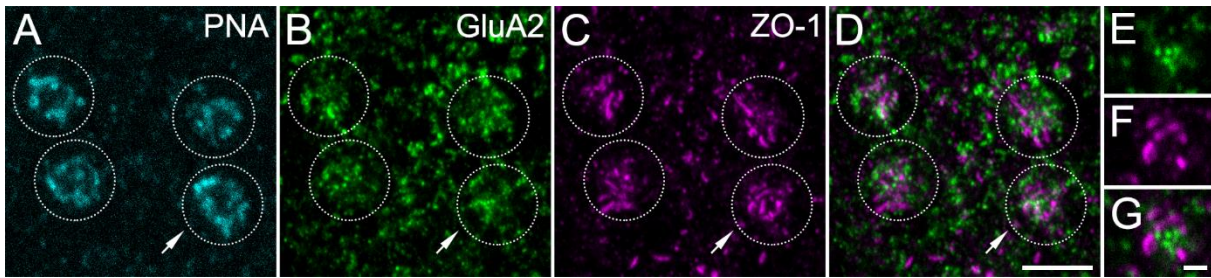


Figure 20: ZO-1 and the GluA2 subunit are closely associated at the desmosome-like junctions
A-D: Horizontal view of a whole-mounted retina triple labeled for the pedicle base marker PNA, the GluA2 subunit, and the tight junction protein zonula occludens-1 (ZO-1). Maximum projections (Z-steps 17-34/37, Z-size $\sim 3.5 \mu\text{m}$) were chosen to cover the proximal OPL beneath cone pedicles. Circles indicate pedicle positions (PNA max projection: Z-steps 7-22/37, Z-size $\sim 3.3 \mu\text{m}$). Arrows indicate an example pedicle of which single optical sections (Z-step 25/37, Z-size $\sim 0.2 \mu\text{m}$) of the corresponding channels are shown in **E-G**. Scale bars: $5 \mu\text{m}$ in D, applies to A-D; $1 \mu\text{m}$ in G, applies to E-G.

However, ZO-1 and GluA2 clusters were found in proximity at the putative desmosome-like junctions (Fig 20 E-G). The single optical section (Fig. 20 E-G) reveals a distinct arrangement of the two proteins, where the GluA2 cluster (Fig. 20 E) is encircled by ZO-1 string-like plaques (Fig. 20 F, G). This specific organization at the desmosome-like junction, in which ZO-1 is presumably positioned at the border of the junctional plaque, has been previously observed in the rabbit and monkey retina, suggesting a unique role for ZO-1 at this site (Puller et al., 2009). Taken together, these results show that the expression patterns of GluA subunits in horizontal cells are more complex than expected from previous studies (Ströh et al., 2013). Interestingly, the presented data clearly demonstrate the accumulation of AMPA-type glutamate receptors, specifically of the GluA2 subunit, underneath the cone pedicle. As it is well known from studies of other mammalian species that desmosome-like junctions are present between horizontal cell dendrites at this site. The findings presented in this chapter also indicate that this synaptic specialization is also present in OPL of the mouse retina. Additionally, they suggest that specifically GluA2 subunits are closely associated with Cx57-containing gap junctions and the scaffold protein ZO-1 at this site.

4.2 Analysis of a possible mutual interaction between electrical and chemical synapses at the level of desmosome-like junctions in the OPL of the mouse retina.

4.2.1 Analysis of the Cx57 and ZO-1 staining patterns in GluA2/4 KO animals

The previous chapter demonstrated the accumulation of the GluA2 AMPA receptor subunit beneath the cone pedicle at the putative desmosome-like junctions, highlighting its proximity to Cx57-containing gap junctions between horizontal cell dendrites. In addition, a preliminary

investigation of the spatial localization of the tight junction protein ZO-1 was performed to further investigate the synaptic structure at the cone pedicle in the mouse retina in more detail. The co-occurrence of closely associated chemical and electrical synapses at the same synaptic sites has been documented in other neuronal system (for references, see (Pereda et al., 2004; Pereda, 2014; Jabeen and Thirumalai, 2018)). This led to the hypothesis that connexins and GluAs form interconnected complexes at the desmosome-like junctions, which would enable mutual interactions between electrical and chemical synapses and subsequently allow the system a more precise and finer tuning and regulation of synaptic signal transduction (Puller et al., 2009). To further test this hypothesis, different mouse lines were employed in the present study, including $\text{GluA2}^{\text{fl/fl}}\text{-GluA4}^{\text{fl/fl}}\text{:Cx57}^{+/Cre}$, $\text{Cx57}^{+/Cre}$, and $\text{GluA2}^{\text{fl/fl}}\text{-GluA4}^{\text{fl/fl}}\text{:Cx57}^{+/+}$. In a qualitative manner, it was evaluated whether the selective ablation of GluA2 and GluA4 in HCs affected the expression pattern of Cx57-positive gap junctions in the OPL. Therefore, whole-mounted retinas from the three different genotypes were double labeled for Cx57 and ZO-1. To eliminate any potential discrepancies in the outcomes of the immunostainings due to variations in experimental conditions, the experiments were always conducted on retinas of the three different genotypes simultaneously, using the same buffers, incubation solutions and times for all of them. Moreover, the experiments were performed exploiting two different anti-Cx57 antibodies, the new polyclonal anti-Cx57 antibodies raised in guinea pig, and presented in the context of this study for the first time (Fig. 21), and the established polyclonal anti-Cx57 raised in rabbit (Janssen-Bienhold et al., 2009; Puller et al., 2009; Ströh et al., 2013), (Fig. 22). Retinas from $\text{GluA2}^{\text{fl/fl}}\text{-GluA4}^{\text{fl/fl}}\text{:Cx57}^{+/+}$ mice are considered to be wild type phenotype in this study, given the absence of the horizontal cell-specific Cre recombinase and the regular expression of glutamate receptor subunits (for further details, please refer to Chapter 3). In wild type ($\text{GluA2}^{\text{fl/fl}}\text{-GluA4}^{\text{fl/fl}}\text{:Cx57}^{+/+}$) whole-mounted retinas, immunoreactivities for Cx57 and ZO-1 showed the typical staining patterns for the tight-junction protein ZO-1, characterized by clusters made up of string-like structures, and plaques for the gap junction protein Cx57, and both were located 1-2 μm below the cone pedicle base (Fig. 21 A-C). It is important to note that ZO-1 is also located at the tight junctions between vascular endothelial cells (Tornavaca et al., 2015). Therefore, ZO-1 immunoreactivity was strongly detected also by the tight junctions of the blood vessels (Fig. 21 A, C open arrowheads).

Both ZO-1 and Cx57 immunoreactivities were found to be largely overlapping pattern (colocalized) at the desmosome-like junctions (Fig. 21 C), confirming previous observations in the mouse retina (Puller et al., 2009). In the $\text{Cx57}^{+/CRE}$ mouse line, the Cre expression is restricted to horizontal cells, but the glutamate receptors are not excised, because the corresponding gene sequences are not *loxP*-flanked. Thus, possible effects on immunoreactivity patterns could only be related to the absence of one Cx57 allele. Accordingly, significant reduction of Cx57 immunoreactivity has been reported in $\text{Cx57}^{+/CRE}$ retinas (Ströh et

al., 2013). In the present study, as illustrated in figure 21 D-F, Cx57 immunoreactivity was observed to colocalize with ZO-1, which exhibited a tendency to form more compact clusters. Additionally, the string-like clusters of ZO-1 were still present beneath the cone pedicles of this genotype.

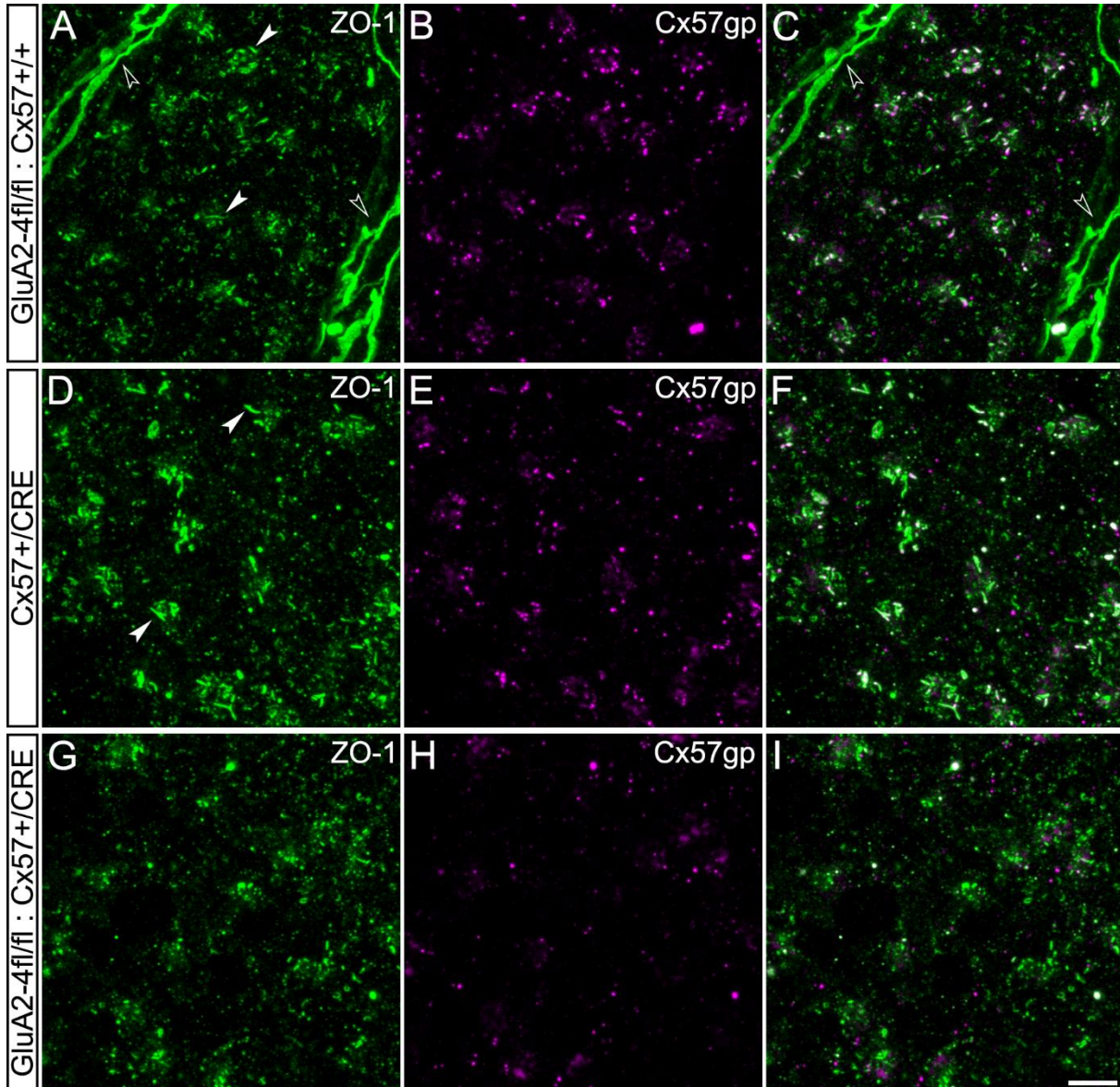


Figure 21: Absence of GluA2 and GluA4 in horizontal cells affects ZO-1 and Cx57 expression at desmosomal-like junctions

Projections of confocal stacks generated from the OPL of whole-mounted retinas immunolabeled for ZO-1 and Cx57. The new anti-Cx57 antibody, raised in guinea pig (gp) was used in this experiment. The immunolabeling was performed on GluA2^{fl/fl}-GluA4^{fl/fl};Cx57^{+/+} **A-C** (Z-steps 19-50/64, Z-size ~ 6.4 μ m), on Cx57^{+/Cre} mice **D-E** (Z-steps 19-36/44, Z-size ~ 3.6 μ m) and GluA2/4-deficient mice (GluA2^{fl/fl}-GluA4^{fl/fl};Cx57^{+/Cre}; **G-I** (Z-steps 20-30/31 S-size ~ 2.2 μ m). Filled arrowheads indicate the characteristic string-like structures of ZO-1 plaques. Open arrowheads indicate blood vessels in the OPL indicating additional cross-reactivity of the anti-ZO-1 antibodies with ZO-1 in endothelial cells Scale bar: 5 μ m in I, applies to, A-I.

Thus, the retinas of the two genotypes used as controls showed the same patterns for ZO-1 immunoreactivity and the Cx57^{+/Cre} retinas displayed the expected reduction in Cx57 expression. In contrast, the situation was markedly different in retinas lacking GluA2 and GluA4 subunits (GluA2^{fl/fl}-GluA4^{fl/fl}:Cx57^{+/Cre}, Fig. 21 G-I). Here, the organized ZO-1-positive string-like structures, which were present in the retinas of the two controls (GluA2^{fl/fl}-GluA4^{fl/fl}:Cx57^{+/+} and Cx57^{+/CRE} mice), were absent (compare Fig. 21 A, D, G). Instead, the ZO-1 staining appeared more punctate, showing more delicate accumulations below the pedicles in GluA2^{fl/fl}-GluA4^{fl/fl}:Cx57^{+/Cre} retinas (Fig. 21 G). ZO-1 clusters beneath the cone pedicles were still discernible, though they appeared smaller and more finely punctate. This is likely due to the remaining ZO-1 being associated with Cx36 at the OFF bipolar cells, specifically at the flat contacts on the pedicle base (Feigenspan et al., 2004; Puller et al., 2009). Another striking observation was, that although the GluA2^{fl/fl}-GluA4^{fl/fl}:Cx57^{+/Cre} mice still possess a single Cx57 allele, like the Cx57^{+/CRE} mouse line, the retinas of this genotype obviously revealed an even stronger reduction, almost absence, of Cx57 plaques at the putative desmosome-like junctions below the cone pedicles (Fig. 21 H). In line with this finding, the previously observed colocalization of ZO-1 and Cx57 seen in the controls (GluA2^{fl/fl}-GluA4^{fl/fl}:Cx57^{+/+}, Cx57^{+/CRE}) at these sites was also absent (Fig. 21 I).

For evaluation of the striking, new observations presented in Figure 21, the same experiments were repeated with the already established rabbit anti-Cx57 polyclonal antibody (Fig. 22). Notably, the use of anti-Cx57 from rabbit necessitates the use of a monoclonal anti-ZO-1 from mouse, rather than the previously used rabbit antibody. Furthermore, the use of different combinations of antibodies targeting the same proteins is a very reliable approach for evaluating such fine overlapping and specific staining patterns, like those shown in Figure 21. As summarized in Figure 22 A-I, the use of a mouse monoclonal anti-ZO-1 antibody and the rabbit polyclonal anti-Cx57 antibodies on whole-mounted retinas of the two controls (GluA2^{fl/fl}-GluA4^{fl/fl}:Cx57^{+/+} and Cx57^{+/CRE} mice) confirmed the immunoreactivity patterns of ZO-1 (compare Figs. 21 and 22 A, D, G) and Cx57 (compare Figs. 21 and 22 B, E, H), as well as the colocalization of both proteins in the OPL of both control genotypes (compare Figs. 21 and 21 C, F) and the absence of colocalization in the OPL of GluA2^{fl/fl}-GluA4^{fl/fl}:Cx57^{+/Cre} retinas (compare Figs. 21 I and 22 I). Again, the clusters of ZO-1 were organized in string-like structures below the cone pedicles where they colocalized with Cx57 plaques in the two control retinas (Figs 22 A, C and D, F) and, punctate patterns, lacking string-like structures, with smaller and compact accumulations were found in the GluA2/4-deficient retinas. Additionally, there was pronounced reduction in Cx57 plaques beneath the pedicle in the latter genotype.

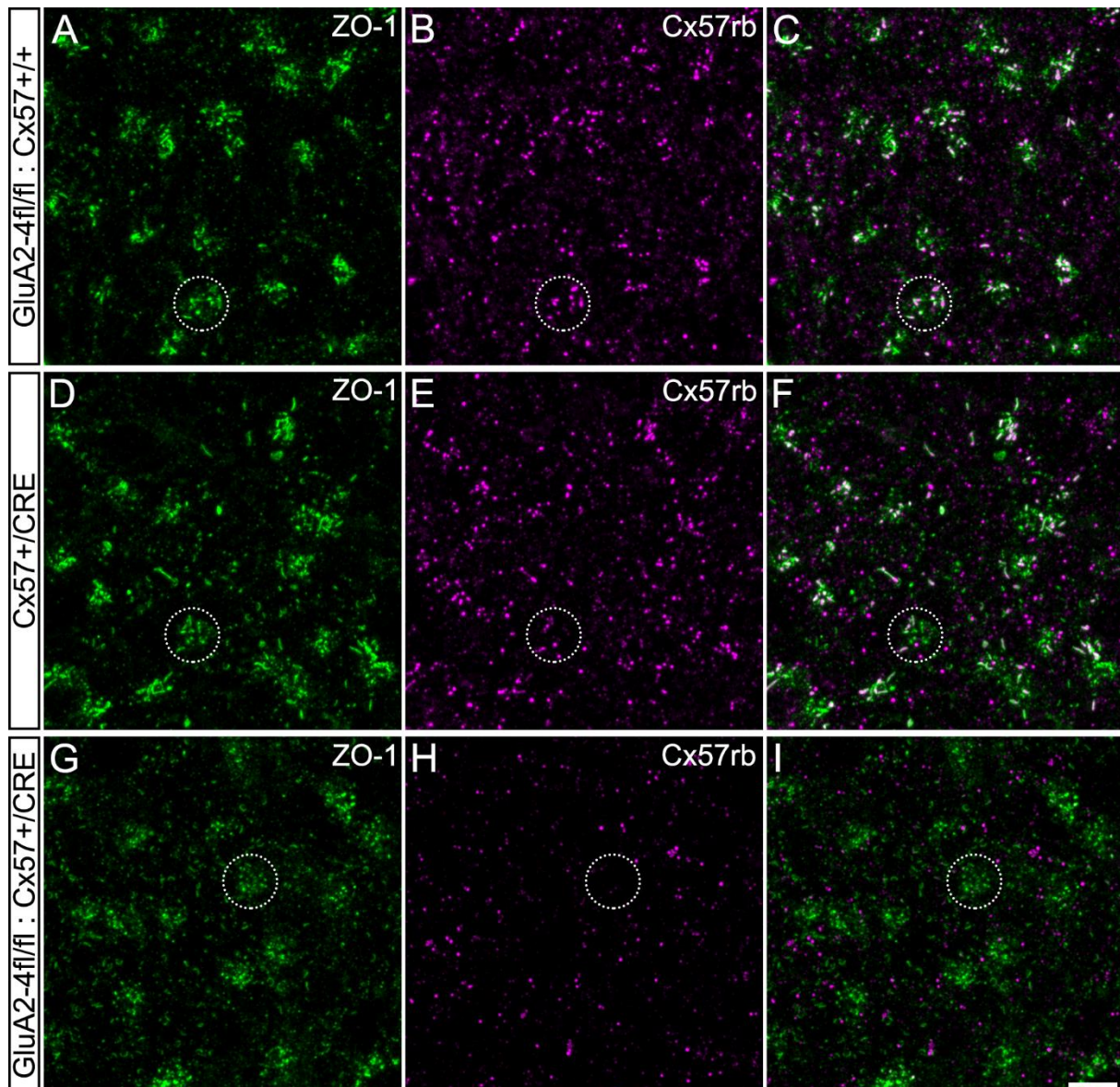


Figure 22: Effects of GluA2/4-deficiency on ZO-1 and Cx57 expression at desmosomal-like junctions detected by using a different mix of antibodies

Projections of confocal stacks generated from the OPL of whole-mounted retinas immunolabeled with monoclonal mouse anti-ZO-1 and polyclonal rabbit anti-Cx57. Immunolabeling was performed on GluA2^{fl/fl}-GluA4^{fl/fl};Cx57^{+/+} **A-C** (Z-steps 14-30/33, Z-size ~ 3.4 μ m), on Cx57^{+/Cre} mice **D-E** (Z-steps 10-36/36, Z-size ~ 5.4 μ m) and GluA2/4-deficient mice (GluA2^{fl/fl}-GluA4^{fl/fl};Cx57^{+/Cre}) **G-I** (Z-steps 13-30/32, Z-size ~ 3.6 μ m). Circles indicate an example pedicle of which x/y-projections are shown in Figure. 23. Scale bar: 5 μ m in I, applies to, A-I.

For a more detailed presentation of the fine differences between the different genotypes, examples of x/y-projections (or 3D renderings) of three pedicles taken from the three different retinas, as indicated by dotted circles in Figure 22 are shown in Figure 23. X/y-projections were generated by rotating the confocal image stacks (Fig. 23, figure legend for Z-size) on the X-axis of the images to obtain an orthogonal view of the optical sections. This lateral visualization improves the understanding of the staining patterns of ZO-1 and Cx57 beneath the cone pedicle.

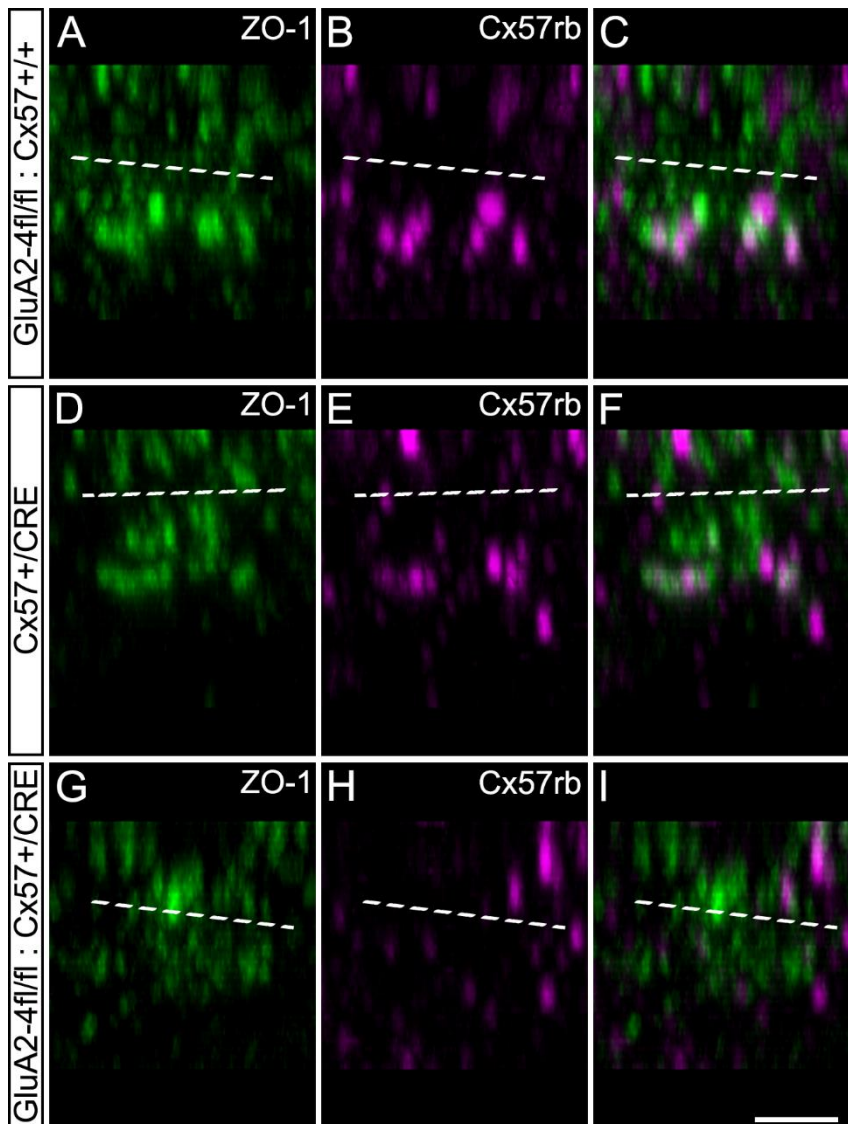


Figure 23: Expression of ZO-1 and Cx57 at the cone pedicle appear to be affected by GluA2/4 deficiency in horizontal cells

X/y-projections of confocal stacks taken from single pedicles of the whole-mounted retinas shown in Figure 22 (circles) and immunolabeled for ZO-1 and Cx57. As described in Figure 22, immunolabeling was performed on $\text{GluA2}^{\text{fl/fl}}\text{-GluA4}^{\text{fl/fl}}\text{:Cx57}^{+/+}$ **A-C** (Z-size $\sim 6.6 \mu\text{m}$), on $\text{Cx57}^{+/CRE}$ mice **D-E**; (Z-size $\sim 7.2 \mu\text{m}$) and GluA2/4 -deficient mice ($\text{GluA2}^{\text{fl/fl}}\text{-GluA4}^{\text{fl/fl}}\text{:Cx57}^{+/CRE}$) **G-I** (Z-size $\sim 6.4 \mu\text{m}$). Dashed lines indicate pedicle base positions detected by PNA staining (not shown). The pedicle position in D-F was estimated from the image stack. Scale bar: $5 \mu\text{m}$ in I, applies to, A-I.

ZO-1 formed prominent clusters below the pedicle, and a string-like pattern remained discernible, as well as the close association between ZO-1 and Cx57, in both $\text{GluA2}^{\text{fl/fl}}\text{-GluA4}^{\text{fl/fl}}\text{:Cx57}^{+/+}$ (Fig. 23 A, C) and $\text{Cx57}^{+/CRE}$ (Fig. 23 D, F) retinas. In GluA2/4 -deficient retinas, orthogonal views revealed the more punctate and reduced labeling of ZO-1 (Fig. 23 G, I), along with a significant reduction in Cx57 immunoreactivity (Fig. 23 H). Consequently, the typical organization between ZO-1 and Cx57 observed in the retinas of the two control genotypes, was missing. These findings provide the initial insight into the impact of the elimination of

AMPA-type receptor subunits GluA2 and GluA4 have on the expression of Cx57 and the synaptic organization within the OPL of the mouse retina.

Finally, mouse horizontal cells express two distinct types of connexins. Electrical coupling at the dendrites and at the thin axon terminals of HCs is exclusively supported by Cx57, whereas Cx50-containing gap junctions are expressed on the thick proximal axon terminals of these cells (Dorgau et al., 2015). Vertical cryosections immunolabeled for Cx50 revealed no apparent reorganization or compensatory changes beneath the cone pedicle in Cx57 KO retinas (see Fig. S2 – Section 7.3.3 – Supplemental material), confirming that the two gap junctions are regulated differently and independently (Dorgau et al., 2015).

4.2.2 Analysis of the expression patterns of glutamate receptors and ZO-1 in Cx57 KO animals

Based on the previous observations, the following experiments aimed to qualitatively analyze the synaptic architecture at horizontal cell desmosome-like junctions in retinas lacking Cx57. Therefore, immunolabeling of the tight-junction protein ZO-1 and the glutamate receptor subunits GluA2, GluA2/3 and GluA4, were performed on retinas of the Cx57-knockout mouse line, and its wildtype litter mates. Transgenic mice in which the Cx57 gene was replaced by the LacZ reporter gene, are Cx57 knockout (KO; Cx57^{LacZ/LacZ}) animals, which have been intensively studied and exhibited reduced coupling between horizontal cells (Hombach et al., 2004; Shelley et al., 2006) (for further details, please refer to Chapter 3).

To analyze the expression patterns of the different AMPA receptor subunits in the OPL of this specific transgenic mouse line in more detail, the whole-mounted retinas of wild type (WT) and Cx57 KO animals were double-labeled for the glutamate receptor subunit GluA4 and ZO-1. To obtain a comprehensive representation of the synaptic components, image acquisitions were focused to capture the entire thickness of the ZO-1 cluster beneath the cone pedicle, hence image stack projections show the 3-4 μm of the proximal OPL, below the cone pedicle level. As previously outlined, the GluA4 staining pattern in the WT retina was characterized by fine puncta, distributed uniformly throughout the OPL (Fig. 24 A) and ZO-1 clusters were organized in string-like plaques below the cone pedicle (Fig. 24 B). In the absence of Cx57 (Fig. 24 D-F), the GluA4 immunoreactivity (Fig. 24 D, F) showed a distribution qualitatively comparable with the WT condition (Fig. 24 A, C). No obvious changes or different distributions at the pedicle base were observed in Cx57 KO mice. Nevertheless, ZO-1 displayed a slight tendency to form more compact clusters, which were typically distinguished by a more punctate pattern. Therefore, no other significant or notable differences in the distribution and expression of ZO-1 were observed in the OPL of Cx57-deficient mice and their WT littermates.

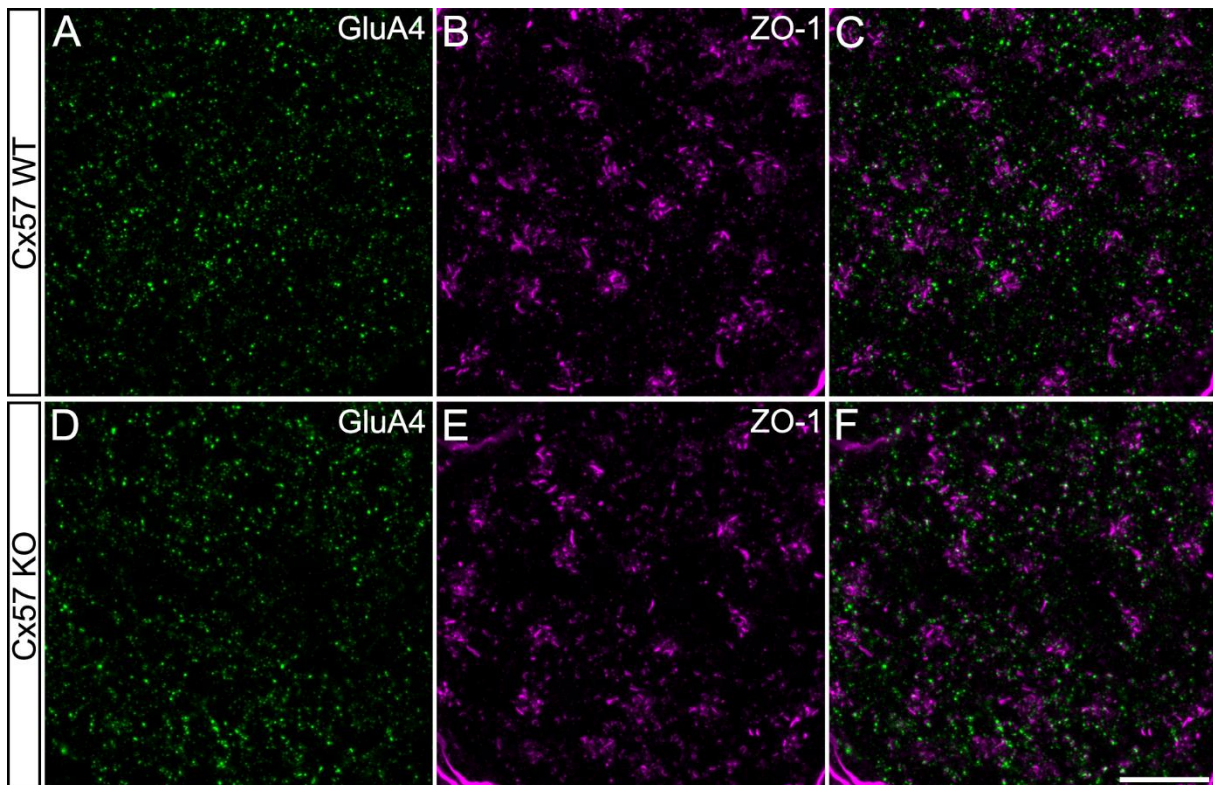


Figure 24: Comparison of GluA4 and ZO-1 expression pattern in WT and Cx57-KO retinas

A-D: Maximum projections (Z-steps 21-36/44, Z-size $\sim 3.2 \mu\text{m}$) of a confocal stack from a whole-mounted retina of a WT (Cx57^{+/+}) animal double-labeled for the subunit GluA4 and ZO-1. **D-F:** Maximum projections (Z-steps 13-28/31, Z-size $\sim 3.2 \mu\text{m}$) as shown in A-D, but generated from a Cx57 KO animal (Cx57^{LacZ/LacZ}). Scale bar: 10 μm in F, applies to, A-F.

Next, whole-mounted retinas of WT and Cx57 KO mice were immunostained for the GluA2/3 subunits and ZO-1, and qualitative analyses were conducted to detect potential changes in the staining patterns. GluA2/3 immunoreactivity in Cx57 KO mice (Fig. 25 D-F) showed a distribution at the proximal OPL, comparable to the control (Fig. 25 A-C). No obvious, new arrangements were disclosed at the pedicle base. As previously described, ZO-1 clusters were observed to be more compact, exhibiting a tendency towards a less string-like structure organization, in puncta (Fig. 25 E).

Finally, the experiments were repeated with a focus on the GluA2 receptor subunit. Whole-mounted retinas of WT and KO animals were immunostained for GluA2 and ZO-1 (Fig. 26). In both genotypes, clusters of GluA2 subunits (Fig. 26 A, D, example of clusters are indicated by circles) were found beneath the cone pedicles in close association with ZO-1 at the level of the desmosome-like junctions (Fig. 26 C, F, example of clusters are indicated by circles). Except for confirming the more compact ZO-1 clusters (Fig. 26 B, E), no obvious changes in the spatial distribution of GluA2 subunits were discerned. Furthermore, it was difficult to roughly ascertain whether there were qualitative shifts in the amount of GluA2 immunoreactivity beneath the cone pedicles in response to the knockout of Cx57.

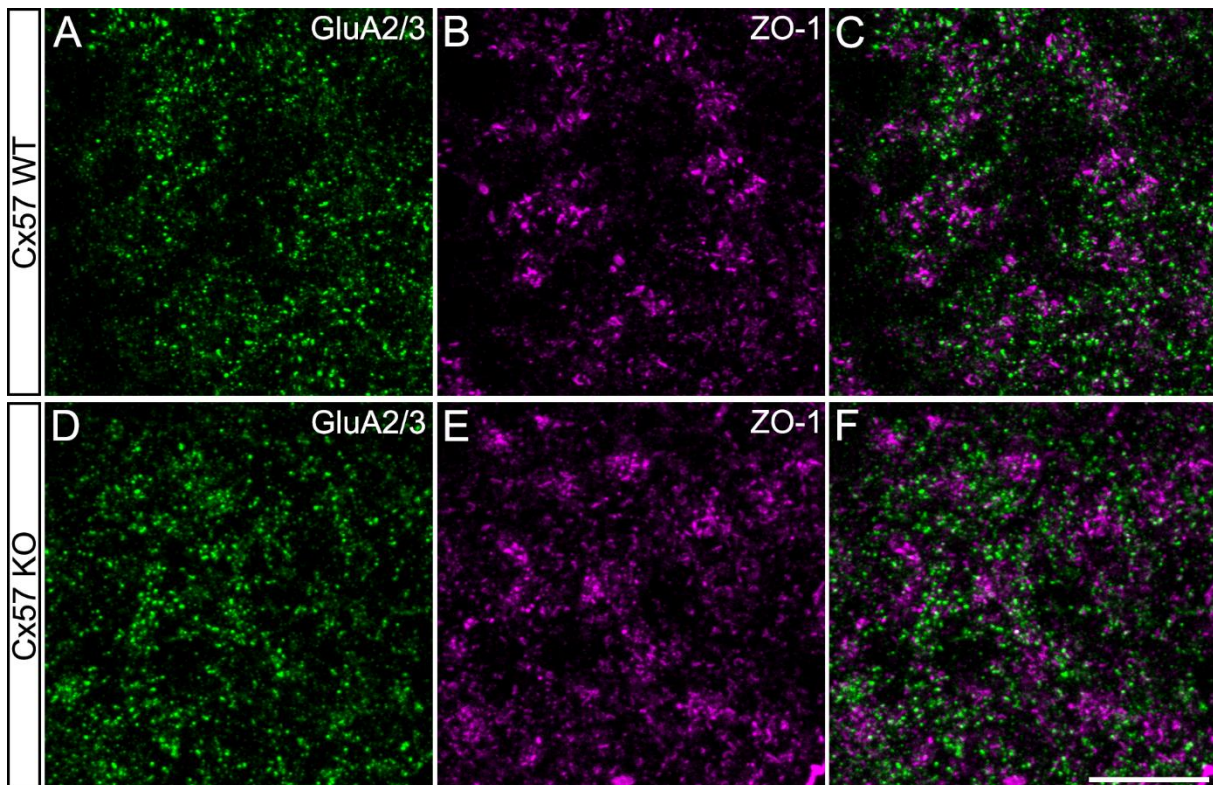


Figure 25: Comparison of GluA2/3 and ZO-1 expression patterns in WT and Cx57-KO retinas
A-D: Maximum projections (Z-steps 19-35/36, Z-size ~ 3.4 μm) of confocal images generated from a whole-mounted retina of a WT (Cx57^{+/+}) animal double-labeled for detecting the subunits GluA2/3 and ZO-1. **D-F:** Maximum projections as shown in A-D (Z-steps 16-32/43, Z-size ~ 3.4 μm), however, generated from the retina of a Cx57 KO animal (Cx57^{LacZ/LacZ}). Scale bar: 10 μm in F, applies to, A-F.

Taken together, these qualitative experimental observations draw attention to the idea, that the observed spatial proximity between GluAs and gap junctions, at the level of desmosome-like junctions in the mouse retina may provide the bases for mutual interaction of both types of synapses at this site and thus, a fine tuning of signal transduction at the first retinal synapse. As opposed to the unaffected expression patterns of glutamate receptors in the proximal OPL following the selective ablation of Cx57, a striking reduction, if not complete absence, of CX57-positive gap junctions, was observed beneath the cone pedicles when both subunits GluA2 and GluA4 were selectively knocked out in horizontal cells of the mouse retina (see Fig. 21 G-I and Fig. 22 G-I). These results suggest a complex interaction between the two distinct synaptic proteins within the synaptic architecture of the mouse retina. Consequently, it is important to closely examine the functional roles that the GluA2 and GluA4 receptor subunits may play in the expression and localization of Cx57-containing gap junctions beneath the cone pedicle, particularly at the desmosome-like junctions. It has been shown that the tight-junction protein ZO-1 is not only distributed in a type-specific manner, but is also confined to the dendro-dendritic gap junctions between horizontal cells of the mammalian retina (Puller et al., 2009).

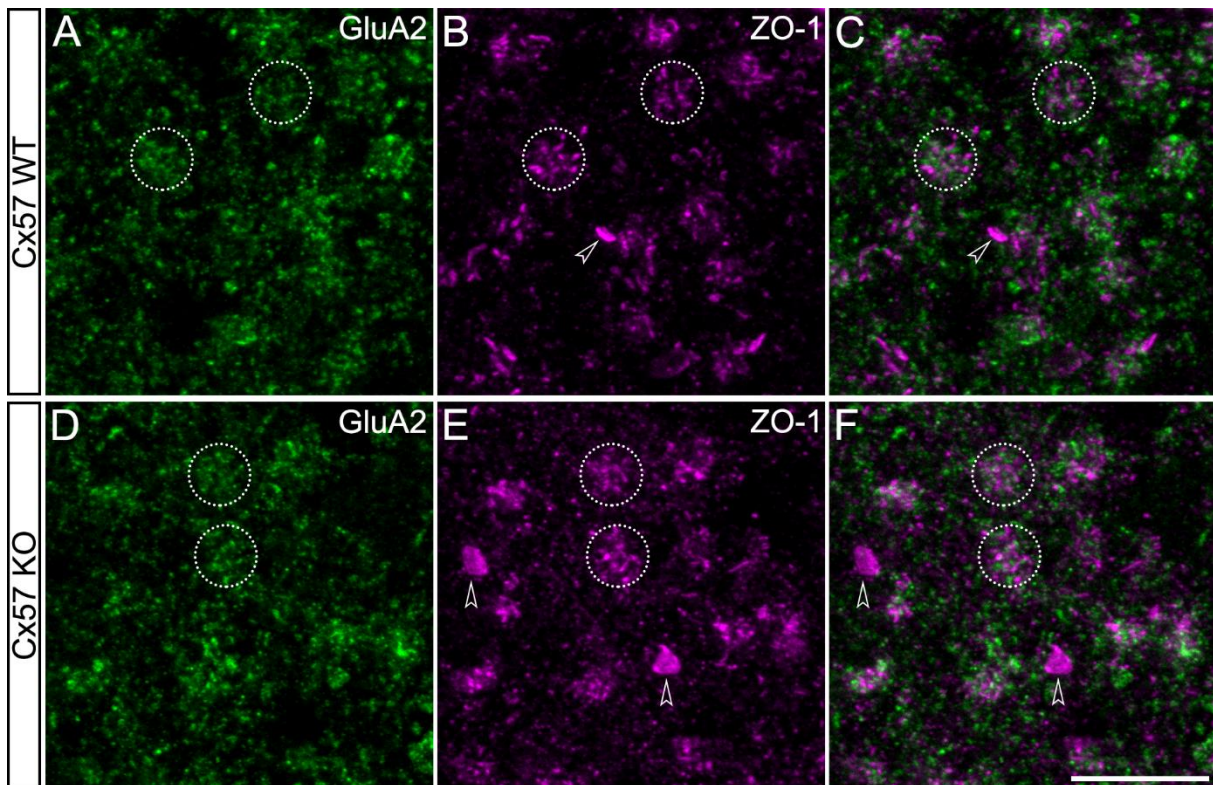


Figure 26: Comparison of GluA2 and ZO-1 expression patterns in WT and Cx57-KO retinas

A-D: Maximum projections (Z-steps 18-32/38, Z-size $\sim 3 \mu\text{m}$) of a confocal images generated from a whole-mounted retina of a WT animal ($\text{Cx57}^{+/+}$) double-labeled for the subunit GluA2 and ZO-1. **D-F:** Maximum projections (Z-steps 23-31/39, Z-size $\sim 2 \mu\text{m}$) generated as those shown in A-D, but, from a Cx57 KO animal ($\text{Cx57}^{\text{LacZ/LacZ}}$). Example of clusters of associated GluA2 and ZO-1 are indicated by circles. Open arrowheads indicate blood vessels in the OPL indicating additional cross-reactivity of the anti-ZO-1 antibodies with ZO-1 in endothelial cells. Scale bar: $10 \mu\text{m}$ in F, applies to, A-F.

Light microscopy analysis conducted in this study raised the question whether ZO-1 may have a specific function at the desmosome-like junctions. In this respect, the distribution patterns of ZO-1 were analyzed and compared in three different types of mice, wildtype C57/BL6, $\text{Cx57}^{\text{LacZ/LacZ}}$ (Cx57KO) and $\text{GluA2}^{\text{fl/fl}}\text{-GluA4}^{\text{fl/fl}}\text{:Cx57}^{+/Cre}$, to gain more insight into the effects of the selective knockouts on ZO-1 expression in the OPL. The typical expression pattern of ZO-1 in the wildtype mouse retina (C57/BL6, Fig. 27 A) displays clusters of string-like plaques that are well-defined beneath the cone pedicles. This characteristic structure of ZO-1 plaques was only slightly affected when only one or both Cx57 alleles were knocked out in the $\text{Cx57}^{\text{LacZ/LacZ}}$ mice (Fig. 27 B; see also Fig. 21 E and Fig. 22 E). In contrast the selective ablation of both receptor subunits, GluA2 and GluA4, from HCs led to a clear change of the ZO-1 immunoreactivity pattern in the retina of these transgenics, with a drastic decrease of ZO-1 positive structures and the loss of all the features observed in the BL6 mice (compare Fig. 27 C and A). These findings point to a specific role of ZO-1 at the desmosome-like junctions and to its likely interaction at least with glutamate receptors at this specific synaptic site.

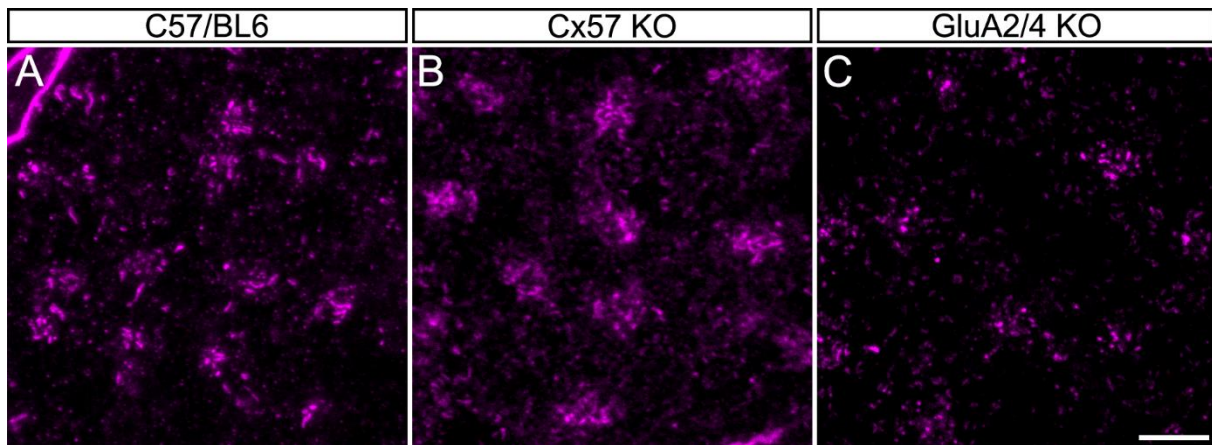


Figure 27: The ZO-1 expression pattern is affected in GluA2/4 KO in HCs of the mouse retina
 Projections of confocal stacks from whole-mounted retinas stained for ZO-1. Immunolabeling was performed on retinas from C57/BL6 mice **A** (Z-steps 25-48/58, Z-size $\sim 4.8 \mu\text{m}$), Cx57 KO mice (Cx57^{LacZ/LacZ}) **B** (Z-steps 16-21/26, Z-size $\sim 1.2 \mu\text{m}$), and double GluA2/4 KO (GluA2^{fl/fl}-GluA4^{fl/fl}; Cx57^{+Cre}) **C** (Z-steps 8-30/32, Z-size $\sim 4.6 \mu\text{m}$). Scale bars: $5 \mu\text{m}$.

4.2.3 Spatial interaction between ZO-1 and Cx57 OPL of the mouse retina

The ZO-1 expression pattern in the mouse retina and its association with connexins was already described in both OPL and IPL (Li et al., 2004b, 2008; Ciolofan et al., 2006, 2007; Puller et al., 2009). Significant insights into the potential functions of ZO-1 were provided by Puller et al. (2009), who studied the giant gap-junctional plaques of A-type horizontal cells in the rabbit retina. They observed that ZO-1 formed a fence-like boundary around Cx50 rather than overlapping with it directly. In the present study, light microscopy analysis of ZO-1 and Cx57 demonstrated colocalization between the two proteins, in addition to close proximity (Fig. 28 A-C), confirming previous findings observed in the mouse retina (Puller et al., 2009). Despite the small size of gap junctions and the resolution limits of confocal microscopy, single optical sections shown in Figure 28 (D-F and G-I) suggest a close association where ZO-1 basically follows the border of the gap junction plaques. In the first example (Fig. 28 D-F), ZO-1 immunoreactivity forms a structure that almost completely encloses the two plaques of Cx57-containing gap junctions, bringing the proteins to the same level (Fig. 28 F). The second example (Fig. 28 G-I) illustrates how the small Cx57 plaque slightly overlaps the ZO-1 string-like structure, with partial colocalization. These observations may indicate a similar mechanism to that described for the giant gap-junctional plaques in the rabbit retina, highlighting the role of ZO-1 at the desmosome-like junctions and its interactions with gap junctions at this site.

A further interesting observation was the occasional presence of ZO-1 string-like plaques located beyond the area defined by the ZO-1 clusters. Additionally, these structures were generally found at a more proximal level, deeper below the cone pedicle. Similar ZO-1-positive structures have been described in the monkey retina, where they are restricted to H1 dendrites (Puller et al., 2009). Thus, the ZO-1-positive string-like plaques observed in the more proximal

OPL of the mouse retina in this study suggest the existence of an additional conserved pattern of ZO-1 organization in the retinal OPL across species.

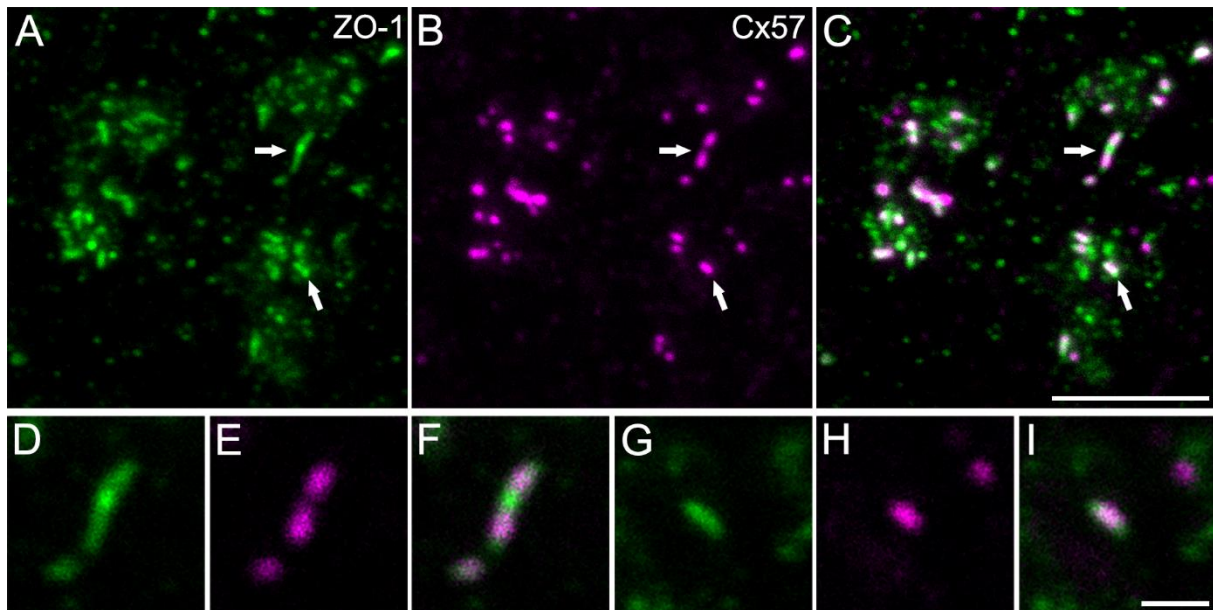


Figure 28: Association and colocalization of Cx57 and ZO-1

A-C: Maximum projection (Z-steps 24-47/58, Z-size $\sim 4.8 \mu\text{m}$) from a whole-mounted retinas double labeled for ZO-1 and Cx57. Arrows indicate plaques of ZO-1 and Cx57 in close association, which are shown as single optical sections of $\sim 0.2 \mu\text{m}$ of the corresponding channels in **D-F** for the upper arrow (Z-step 44) and in **G-I** for the lower arrow (Z-step 26). Scale bars: $5 \mu\text{m}$ in C, applies to A-C; $1 \mu\text{m}$ in I, applies to D-I.

4.3 Horizontal cells gap junctions across the retina

4.3.1 Distribution of horizontal cells in the mouse retina

Although the mouse retina lacks a specialized area like the fovea in primates, it exhibits significant topographic variation in the density distribution of its cellular components. From the well-known opsins expression patterns in cone photoreceptors to the more complex and diverse distribution of retinal ganglion cells (RGCs), these variations may provide benefits for several behavioral requirements (for review, see Heukamp et al., 2020). The acknowledgment of these insights has been of fundamental importance in all the analyses conducted within the context of this study.

There is evidence from previous studies indicating that horizontal cells density varies across different retinal regions in the mouse (Camerino et al., 2021). Consequently, a part of this thesis involved a collaborative effort with Lucia Lindenthal, Asli Pektaş, and Christoph Block, to ascertain the density profile of the horizontal cells across the entire mouse retina. Whole-mounted retinas were labeled with antibodies recognizing calbindin (CaBP; Fig. 29) to identify the entire structure, soma included, of horizontal cells (Röhrenbeck et al., 1987; Haverkamp

and Wässle, 2000). Confocal images of whole-mounted retinas labeled with a horizontal cell marker reveal the rounded cell bodies of horizontal cells, along with the intricate network of their dendritic and axonal terminal processes in the background. The horizontal cell bodies are situated in the distal inner nuclear layer (INL) (Haverkamp and Wässle, 2000; Masland, 2001), and the CaBP-positive somas, reveals the mosaic distribution across the entire retina enabling accurate cell counting.

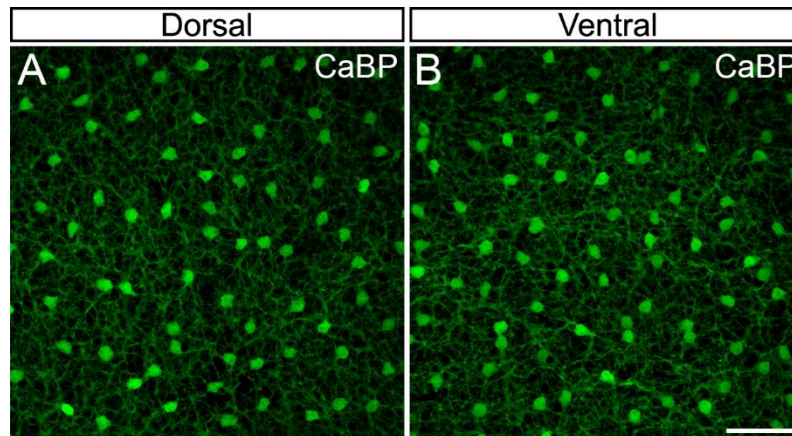


Figure 29: Calbindin immunoreactivity of horizontal cells in mouse retina

A-B: Projections of confocal image stacks of dorsal (A; Z-steps 16-56/65, Z-size $\sim 8.2 \mu\text{m}$) and ventral (B; Z-steps 1-34/44, Z-size $\sim 10.2 \mu\text{m}$) whole-mounted retinas labelled against calbindin (CaBP), used for the quantification of the horizontal cells across the entire retina. Scale bar: $50 \mu\text{m}$ in B, applies to A-B. Immunostaining and acquisitions performed by Lucia Lindenthal, (see attached article).

The positions of all immunolabeled horizontal cell bodies were meticulously marked on a merged microscopic tile scan of the flattened retina using the software Fiji (Fig. 30 A) with each dot representing the location of a horizontal cell body. The cloverleaf-shaped tissue was reconstructed as a hemispherical structure using the software Retistruct (Sterratt et al., 2013; Duda et al., 2023) and the local density was calculated on the sphere and shown in an azimuthal equal distance projection (Fig. 30 B-C). Additionally, retinas were immunostained with an antibody targeting the short-wavelength sensitive S-opsin to delineate the transition zone of opsin expression, which indicates the visual horizon on the retina (Nadal-Nicolás et al., 2020; Qiu et al., 2021; Gupta et al., 2023). S-opsin expression is high in the ventral retina and sharply decreases towards the dorsal retina at the transition zone, allowing the border of this separation to be identified at low magnification. In Figure 30 the transition zone is indicated by lines and is notably positioned above the optic disc crossing the peripheral ends of the lower leaflets in the retinal whole-mount preparation (see also Fig. 33 A, D for representative microscopic images).

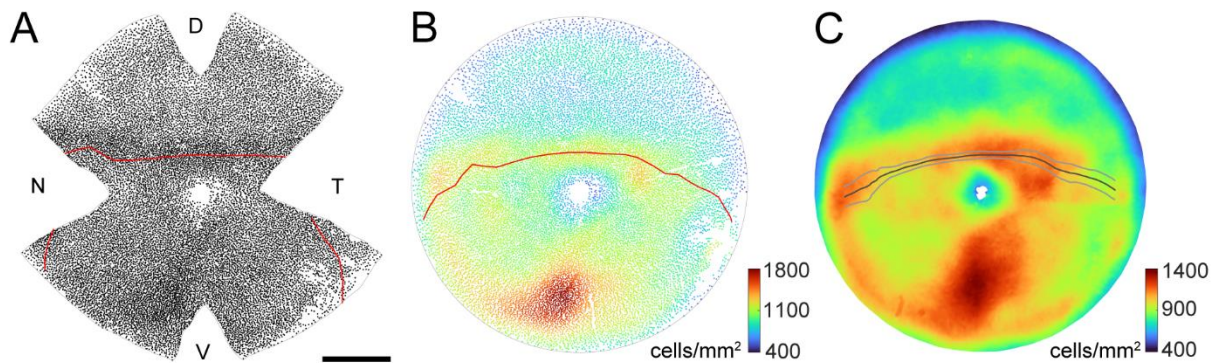


Figure 30: Horizontal cell density shows a distinct dorso-ventral gradient

A: Cloverleaf of a whole-mounted retina from the left eye, where each dot represents the cell body position of a horizontal cell marked with CaBP. The red lines in A and B mark the S-opsin transition zone (see also Fig. 32). D, dorsal; V, ventral; N, nasal; T, temporal. **B:** Azimuthal equal-distance projection of the reconstructed retinal sphere of the data shown in A. The color of the dots represents the local density of the corresponding cell body position. **C:** Horizontal cell density distribution (17650 ± 1412 , $n=5$ retinas). Black line, mean S-opsin transition zone, gray lines, SD ($n=5$). Color bars in B and C indicate cells/mm². Scale bar: 50 μ m in A. Project in collaboration with Lucia Lindenthal, Asli Pektaş, and Christoph Block (see attached article).

The average of five retinas (Fig. 30 C; 17650 ± 1412 , see attached article) showed a distinct dorso-ventral gradient of HCs across the mouse retina, with low density in the dorsal and high density in the ventral retina. The gradient displayed several notable features, with the most significant being the pronounced change in the area identified as the S-opsin transition zone. Furthermore, two regions of high density, or hotspots, were identified. The first was a small area on the temporal side of the retina, near the optic disc. The second was a larger area extending across the ventral retina mostly on the temporal side. Overall, this pattern of HC distribution closely mirrored the density gradient observed for several types of mouse ganglion cells (Dräger and Olsen, 1981; Salinas-Navarro et al., 2009; Duda et al., 2023) and mouse cone photoreceptors (Ortín-Martínez et al., 2014; Nadal-Nicolás et al., 2020). A common decrease in HC density towards the peripheral areas of the retina was also evident (Jeon et al., 1998; Wässle, 2004).

My contribution to the study of the horizontal cell density across the mouse retina, included the tissue preparation, immunostainings, image acquisitions and processing, and supervision of the master students. Lucia Lindenthal performed some of the immunostainings and cell counting. Asli Pektaş also performed parts of the cell counting and Christoph Block provided significant computational data processing for generation of appropriate graphical abstracts. For more details regarding the morphological analysis performed on the horizontal cells across the retina, please refer to the manuscript attached to this thesis.

4.3.2 Asymmetric expression of Cx57 across the retina

In the following chapter some of the results summarized in the published manuscript (see Section 7.4 – Publication) will be presented and discussed together with some additional findings, including qualitative analysis of the expression pattern of ZO-1 and GluAs across the retina, which are not included in the manuscript.

To investigate the precise spatial distribution of horizontal cell glutamate receptor subunits and their potential role in forming specific functional synaptic complexes with electrical synapses at desmosome-like junctions, special emphasis was placed on analyzing the distribution of Cx57, particularly in relation to the gradient of horizontal cells. Therefore, the analysis focused on determining the amount of Cx57 present on HC dendrites in a distinct volume beneath each cone pedicle base, across the retina. By this means, Cx57-containing gap junctions present on HC axon terminals, where it is expressed together with Cx50-containing gap junctions (Dorgau et al., 2015), was excluded from the analysis (Fig. 31). At HC axon terminals connexins are exclusively associated with rod photoreceptor terminals and do not influence dendritic signaling (Trümpler et al., 2008).

As described in the previous chapters, Cx57-immunoreactive plaques were observed to cluster in the proximal OPL in regular arrays, below the cone pedicles (Fig. 31 A-C). In this experiment horizontal cells were injected with the neuroanatomical tracer neurobiotin, a small amino derivative of biotin used as an intracellular label for neurons. This technique allows the visualization of even the finest architecture of cells and the identification of gap junction coupling between cells (Vaney, 1991; Bloomfield et al., 1995; He et al., 2000; Pan and Massey, 2023). As shown in Figure 31, neurobiotin-injected cells revealed the structural composition of individual dendrites of several horizontal cells that converge beneath the cone pedicle to form a terminal cluster, in the proximal part of the OPL (Fig. 31 F, I), before their tips invaginate into the pedicle at the ribbon synapse (Fig. 31 D, G). In combination with immunolabeling for detection of Cx57, this approach allowed to determine the exact location of horizontal cell gap junctions on their dendrites. Cx57-immunoreactive plaques were observed to colocalize with neurobiotin-filled horizontal cell dendrites at a level $\sim 1\text{-}2\ \mu\text{m}$ below the cone pedicle base, a site where the putative desmosome-like junctions are supposed to be localized. Here, Cx57 was previously found closely associated with the GluA receptors subunits (see Fig. 19, Section 4.1.3) and to colocalize with ZO-1 at this level, on the horizontal cell dendrites (see Fig. 28 Section 4.2.3).

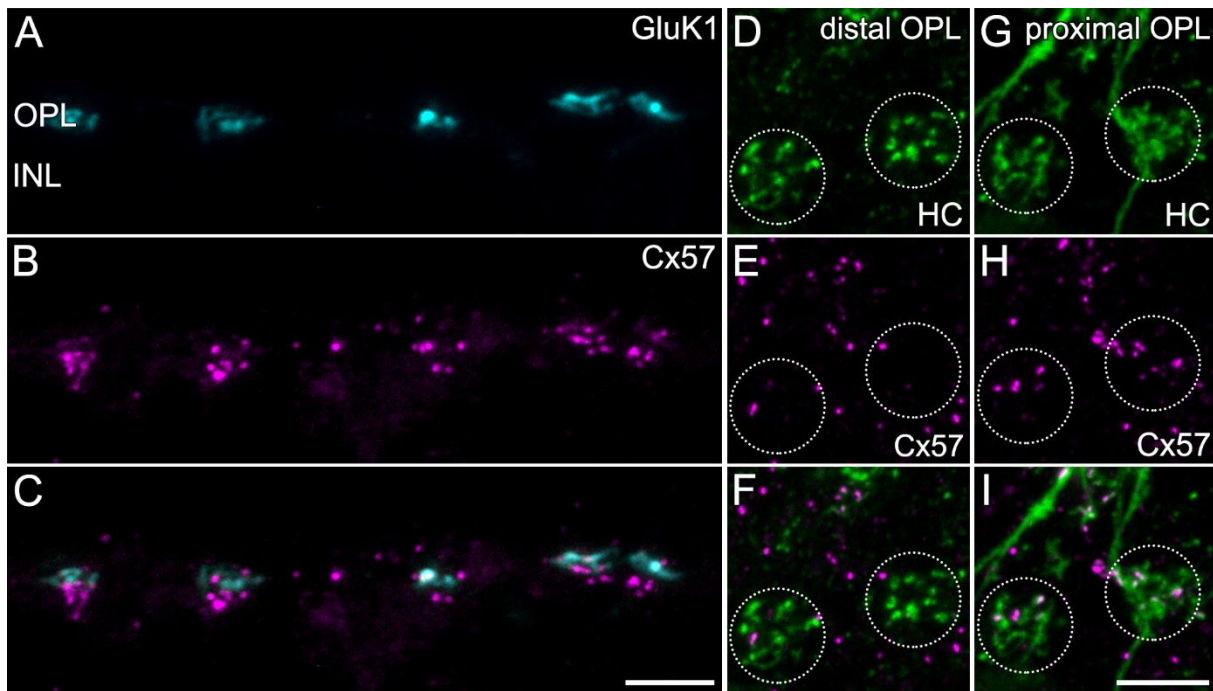


Figure 31: Spatial localization of horizontal cell gap junctions

A-C: Projections of confocal image stacks (Z-steps 5-20/24, Z-size $\sim 3.2 \mu\text{m}$) of a vertical cryostat section double labeled for the kainate receptor subunit 1 (GluK1) and Cx57. **D-F:** D-F Maximum intensity projections of confocal image stacks (Z-steps 8-12/56, Z-size $\sim 1 \mu\text{m}$) taken from a whole-mounted retina labeled with antibodies against Cx57 and with Alexa Fluor 568-conjugated streptavidin after microinjection of neurobiotin into a horizontal cell (neurobiotin, injections by Alejandra Acevedo, see attached article). The distribution of Cx57 is shown at the tips of horizontal cell (HC) dendrites invaginating into two cone pedicles (position refers to the distal OPL). Pedicle positions were identified by these clusters of invaginating dendritic tips and are indicated by dotted circles. **G-I:** Images refer to the pedicles encircled in D-F but are taken from a position 1-2 μm beneath the same pedicle (position refers to the proximal OPL; Z-steps 14-23/56, Z-size $\sim 2 \mu\text{m}$). INL, inner nuclear layer; OPL, outer plexiform layer. Scale bars: 10 μm in C, applies to A-C; 5 μm in I, applies to D-I.

Interestingly, counterstaining of Cx57 and ZO-1 across different retinal regions revealed a previously unrecognized pattern in the localization of these two proteins. Images acquired from the dorsal side of the triple-labeled retinas showed the staining patterns in their typical conformation. ZO-1-immunoreactivity was characterized by large and string-like organized clusters beneath the pedicle (Fig. 32 B, D, F, H). Cx57-positive plaques were clustered below the pedicle and largely colocalized with ZO-1 at this level (Fig. 32 C, D, G, H). However, from the same whole-mounted retinas, a completely different picture became obvious when image stacks were acquired from the ventral retina (Fig. 32 I-L, M-P). Although the general distribution of the cone pedicle marker GluK1 remained rather consistent across retinal regions (Fig. 32 A, E, I, M), ZO-1 exhibited a less dense clustering, and lacked the characteristic string-like structures both beneath the pedicle and the ones beyond cone base area between clusters (Fig. 32 J, L, N, P). However, most striking was that the Cx57 immunoreactive plaques beneath the pedicle appeared drastically reduced in the ventral retina when compared to the dorsal part

(compare Fig. 32 C, G and K, O), and colocalization with ZO-1 was nearly absent (compare Fig. 32 D, H and L, P).

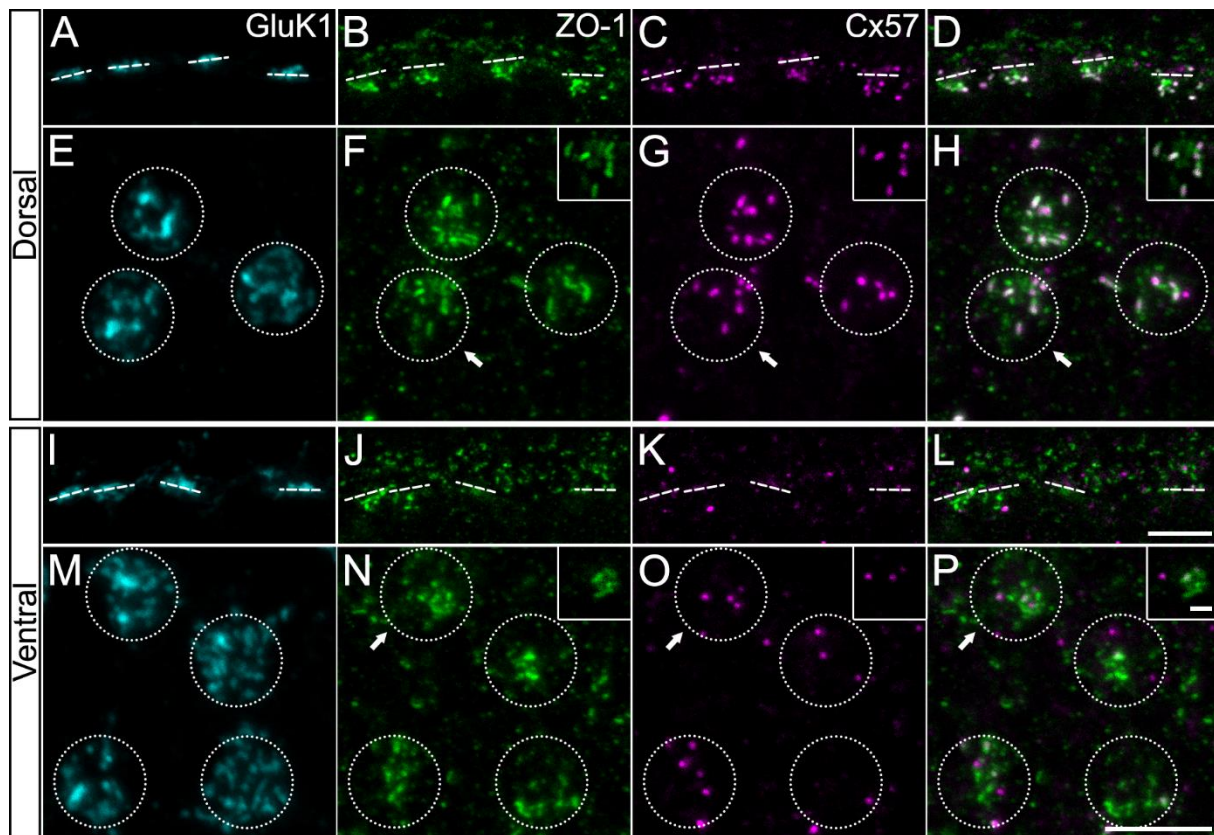


Figure 32: Clusters of ZO-1 and Cx57 and their level of colocalization differ between dorsal and ventral retina

A-D: Maximum projections (Z-steps 15-30/30, Z-size $\sim 3.2 \mu\text{m}$) of confocal stacks from a vertical cryosection of the dorsal retina triple-labeled against GluK1, ZO-1, and Cx57. Dashed lines indicate pedicle positions marked by GluK1 staining. **E-H:** Projections (Z-steps 30-45/58, Z-size $\sim 3.2 \mu\text{m}$) of confocal stacks taken from the dorsal half of a whole-mounted retina. Maximum projections were chosen to cover the proximal OPL beneath cone pedicles. Circles indicate pedicles positions. Arrows indicate example pedicles of which single optical sections (Z-step 35/58, Z-size $\sim 0.2 \mu\text{m}$) of the corresponding channels are shown in the box (top right). **I-L:** Images were taken as described for A-D, but from the ventral retina (Z-steps 8-22/29, Z-size $\sim 2.8 \mu\text{m}$). **M-P:** Images were taken as described for E-H, but from the ventral retina (Z-steps 21-33/46, Z-size $\sim 2.4 \mu\text{m}$). Single optical sections of pedicles from the ventral area shown in the box (Z-step 29/46, Z-size $\sim 0.2 \mu\text{m}$). Scale bars: $5 \mu\text{m}$ in L, applies to A-D and I-L; $5 \mu\text{m}$ in P, applies to E-H and M-P; $1 \mu\text{m}$ in box P, applies for single optical section boxes in E-H and M-P.

To better understand the distinction in the patterning between the dorsal and ventral regions, the spatial distributions of ZO-1 and Cx57 were studied in greater detail at the S-opsin transition zone, which is thought to represent the visual horizon in mice. Therefore, whole-mounted retinas were immunolabeled for ZO-1, Cx57, the cone pedicle marker GluK1, and for the short-wavelength sensitive opsin. Doing so, confocal image stacks were acquired from whole-mounted retina above and below the S-opsin transition zone and kept the same x/y position, but changing the Z-level, focusing at the OPL (Fig. 33 A-C).

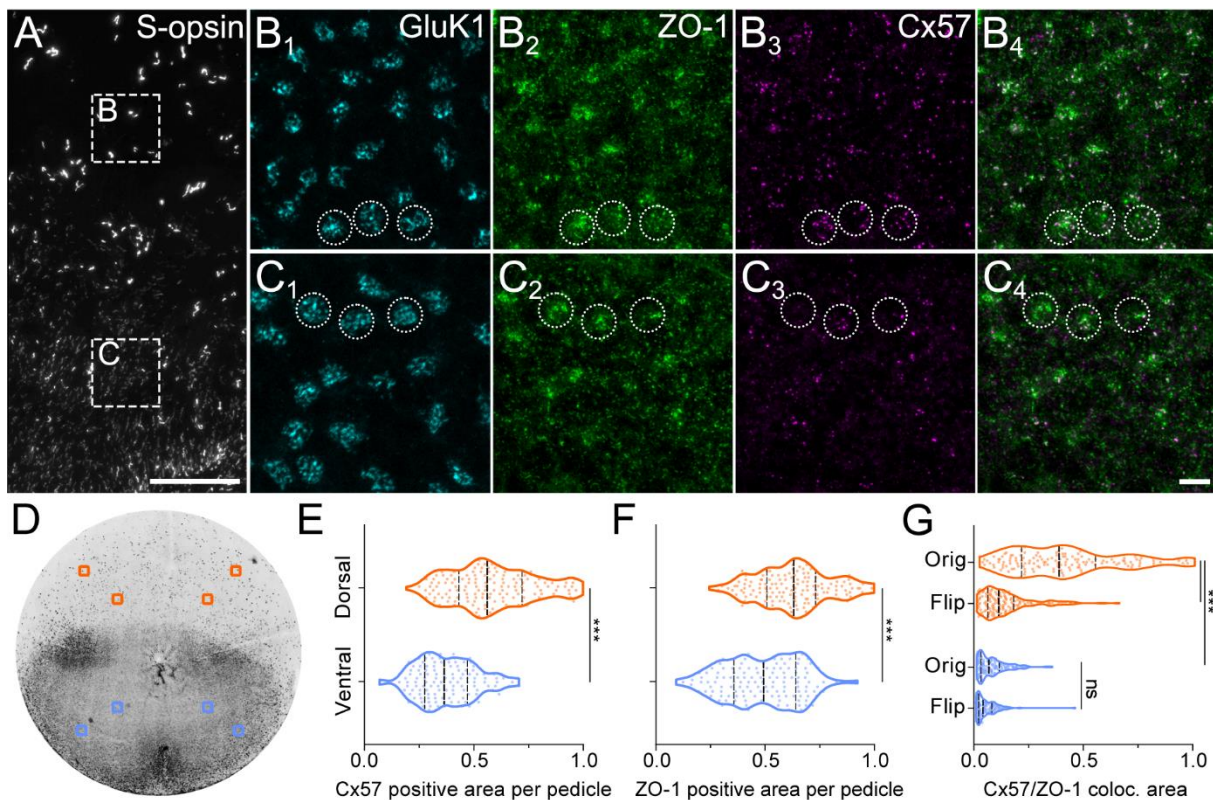


Figure 33: Clusters of ZO-1 and Cx57 change at the S-opsin transition zone

A-C: Maximum projections (Z-steps 18-25/30, Z-size $\sim 4 \mu\text{m}$) of confocal image stacks taken from the region of the short-wavelength sensitive (S)-opsin transition zone. The retinal whole-mount was quadruple-labeled with antibodies against S-opsin (A), GluK1 (B₁, C₁), ZO-1 (B₂, C₂), and Cx57 (B₃, C₃). In A, cone outer segments positive for S-opsin at the transition zone are shown. Boxes B and C indicate regions where higher magnification confocal image stacks (B₁-B₄ and C₁-C₄) were acquired. B₁-B₄ show GluK1, ZO-1, and Cx57 immunoreactivities revealed at the level of the OPL in the position of box B (in A), dorsal to the transition zone (Z-steps 11-25/38, Z-size $\sim 3 \mu\text{m}$). Three examples of pedicles are indicated by circles. C₁-C₄ represent equivalent images taken from the area C on the ventral side of the transition zone (Z-steps 12-23/36, $\sim 2.4 \mu\text{m}$). **D** Azimuthal equal-distance projection of tile scans of a complete, whole-mounted retina immunolabeled against S-opsin. Boxes indicate the locations where image stacks were acquired for the quantification of Cx57 and ZO-1 immunostaining. **E-G** Quantification of the immunolabeled areas (μm^2 normalized) of Cx57 and ZO-1 and their level of colocalization per circular region of interest (ROI) beneath each pedicle. Measurements were pooled across dorso-peripheral locations (orange, all upper boxes in D combined) and the ventro-peripheral locations (blue, all lower boxes in D combined). Dashed lines in violin plots show median and quartiles. Each data point represents the measurement in a ROI beneath one pedicle. Orig: colocalization analyzed in the original ROI image stack, Flip: control measurements in which case one channel per ROI was vertically flipped. *** $p < 0.001$; ns, not significant. Scale bars: $100 \mu\text{m}$ in A; $5 \mu\text{m}$ in C₄, applies to B₁-C₄. Azimuthal equal-distance projection, plotted by Christoph Block (see article attached).

As summarized in Figure 33, the distinct immunostainings revealed an evident shift from dense Cx57 clustering and strong colocalization with ZO-1 to significantly reduced Cx57 levels and a lack of colocalization within the transition zone, spanning only a few hundred microns (Fig. 33 A-C). Based on these observations, an acquisition protocol was established to obtain data from specific regions of whole-mounted retinas. This protocol aimed to quantify the colocalization between ZO-1 and Cx57, as well as their respective immunoreactive positive areas, from

image stacks collected from regions of interest (ROIs) beneath each cone pedicle (“proximal OPL” as shown in Figure 31 G-I, for further details, please refer to Chapter 2 - materials and methods). Data were collected and pooled together from four locations in both dorsal and ventral peripherals of entire retinas immuno labeled for ZO-1, Cx57 and a cone pedicle base marker (either PNA or GluK1). Thresholding and normalization were applied to image stacks to account for varying signal-to-noise ratios in the three retinas. The areas were measured within ROIs beneath a given pedicle (Fig. 33 D; 3 retinas, 144 dorsal pedicles, 131 ventral pedicles). Analysis showed that ZO-1 and Cx57 positive areas were reduced by 22% and 35%, respectively, from the dorsal to the ventral retina (Fig. 33 E, F). Additionally, colocalization of ZO-1 and Cx57 decreased by 84% from the dorsal to ventral regions of the retina (Fig. 33 G). These results confirmed the previous qualitative observations that ZO-1 was less clustered and Cx57 was drastically reduced at the ventral cone pedicle, leading to a significant reduction in colocalization. As control for colocalization, the analysis was repeated in the same ROI of a given pedicle but with one channel of the image stack vertically flipped. The colocalization in the flip control of the dorsal retina was significantly reduced by 73%, indicating that the observed overlap in the original image was not a random occurrence. In the ventral retina, colocalization in control measurements was reduced by 45%. This reduction was not significant since the amount of colocalization of ventral pedicles was low.

Together, these results led to the conclusion that there is a dorso-ventral asymmetrical distribution of the two previously described components at the putative desmosome-like junctions beneath the pedicle. ZO-1 and Cx57 were observed to shift at the S-opsin transition zone and this change coincided with the steepest change in the HC gradient at the visual horizon of the mouse.

The asymmetrical distribution of Cx57-containing gap junctions was found to be reflected in a distinct electrical coupling between horizontal cells. These experiments were conducted in collaboration with Alejandra Acevedo, and for further details, please refer to the attached manuscript (Appendix 7.4).

4.3.3 Clustering of ZO-1 and GluA2 across the retina

In the present study, an accumulation of GluA2 below the cone pedicle base and at the desmosome-like junctions between horizontal cells has been demonstrated (for further details, please refer to Chapter 4.1). Furthermore, GluA2 was observed to be closely associated with Cx57 and ZO-1, of which the last-named proteins in turn exhibited a distinct asymmetrical distribution across the retina. As ZO-1 can be regarded as an important scaffolding component involved in protein-protein interactions at the desmosome-like junctions, and its distribution differs between dorsal and ventral retina in accordance with the distribution of Cx57, the next consequent step was, to analyze whether this also holds for ZO1 and GluA2 at these specific

synaptic sites. Therefore, a comprehensive qualitative microscopic analysis of the staining patterns of these two synaptic components was conducted to reveal possible changes in the distribution of GluA2 across the retina.

As found in previous experiments, the clustering of ZO-1 differed between the dorsal and ventral retinas at the sites of the desmosome-like junctions beneath the pedicle (Fig. 34). In the dorsal retina, the staining patterns consistently appeared with string-like plaques organized in large clusters beneath the cone pedicle (Fig. 34 A-B). In contrast, in the ventral retina, ZO-1 immunoreactivity appeared more compact as densely and more diffuse packed material beneath the cone pedicle, exhibiting a more punctate pattern rather than an elongated form. Moreover, the ZO-1 stripes extending beyond the area defined by the cluster beneath the pedicle and the underlying ZO-1 cluster, representing ZO-1 positive structures characteristic for the dorsal retina (Fig. 34 B, arrowheads), were generally absent in the ventral side (Fig. 34 C-D). It is worth underlining that the staining pattern of ZO-1, as well as that of Cx57, in the dorsal retina was consistent above the S-opsin transition zone but below this zone, it adopted the ventral pattern (see Fig. 33). This observation highlights an asymmetrical distribution of ZO-1 across the retina.

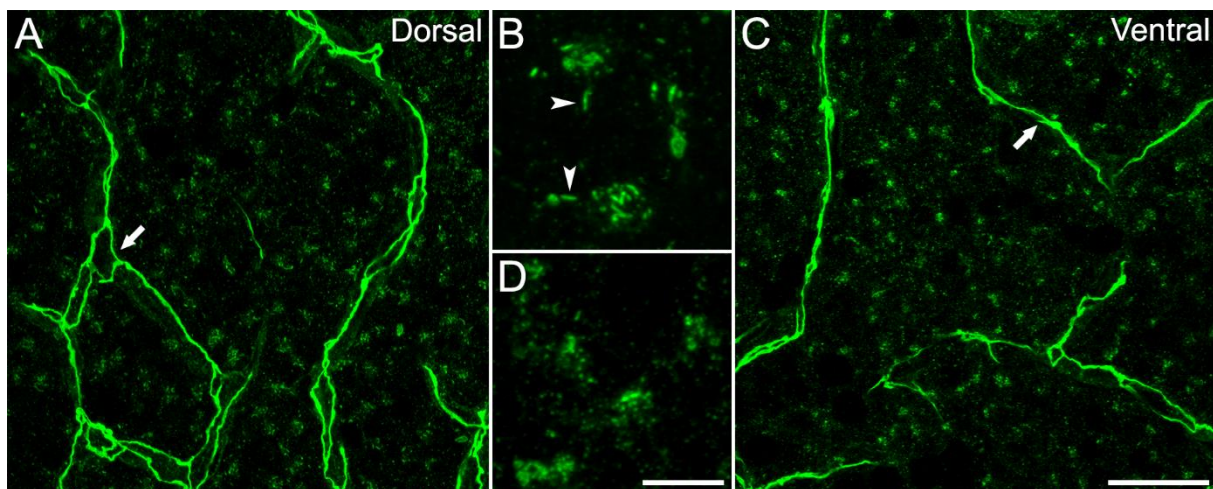


Figure 34: Distinctive clustering of ZO-1 in the dorsal and ventral mouse retina

Maximum projections of confocal image stacks acquired from a whole-mounted retina stained for ZO-1 by means of a polyclonal rabbit anti-ZO-1 antibody. Image stacks were acquired from the same retina from the dorsal side **A-B** (A, Z-steps 21-34/34, Z-size $\sim 2.8 \mu\text{m}$) and from the ventral side **C-D** (C, Z-steps 21-35/35, Z-size $\sim 3 \mu\text{m}$). As an example, magnifications of a few pedicles were acquired from the dorsal side B (Z-steps 19-31/36, Z-size $\sim 2.6 \mu\text{m}$) and ventral side D (Z-steps 24-33/36, Z-size $\sim 2 \mu\text{m}$). Arrows in A and C indicate blood vessels typically detected with ZO-1 antibodies. Arrowheads in B indicate ZO-1 string-like plaques extending beyond the clusters. Scale bars: $20 \mu\text{m}$ in C, applies to A and C; $5 \mu\text{m}$ in D, applies to B and D.

In parallel performed experiments, whole-mounted retinas were double-labeled for ZO-1 and the GluA2 receptor subunit to get deeper insight into the distribution of GluA2 in relation to ZO-1 in the dorsal and ventral retina. As summarized in Figure 35, and in contrast to ZO-1 and

Cx57 immunostaining, the distribution of GluA2 immunoreactivity showed no distinctive changes across the mouse retina. The staining patterns of GluA2 clusters beneath the cone pedicles were qualitatively comparable between the dorsal and ventral retina (Fig. 35 A, D) and colocalization with ZO-1 was rarely detectable (Fig. 35 C, F), indicating their close association at the desmosome-like junction (see Fig. 20). Thus, no further quantitative analysis was performed.

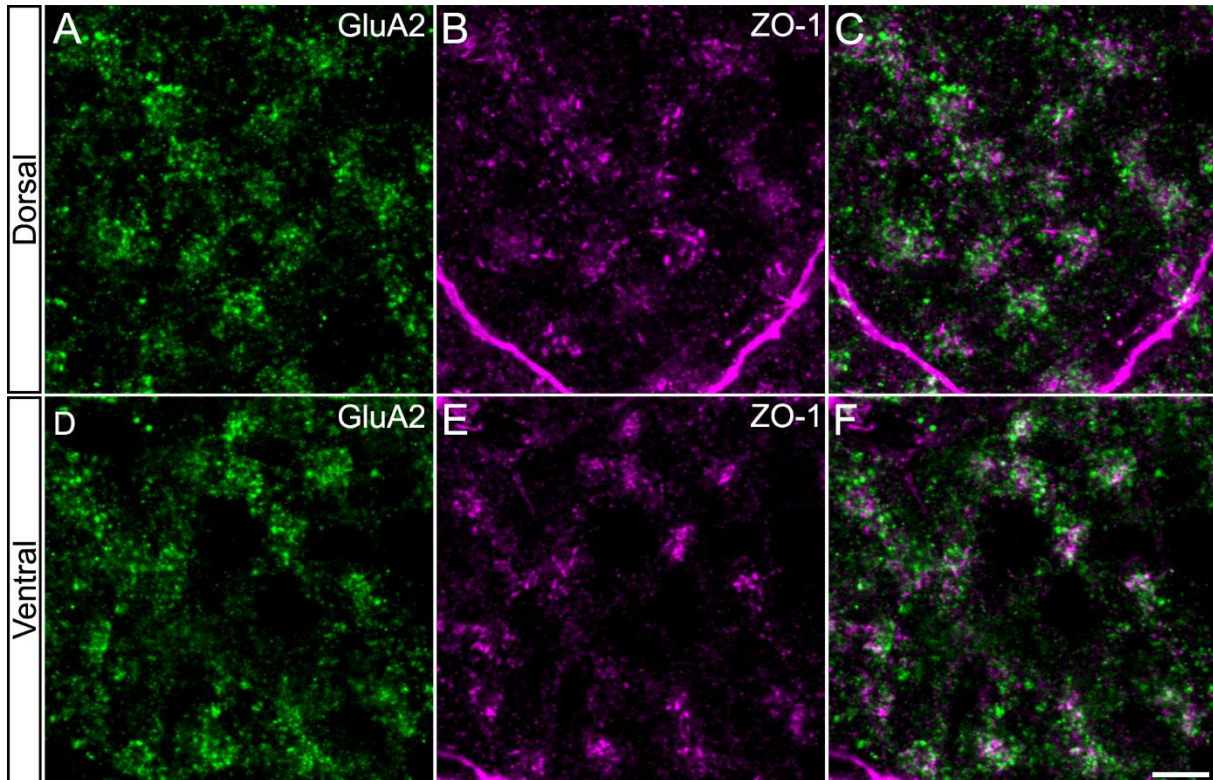


Figure 35: Patterns of GluA2 immunoreactivity reveal no obvious differences between the dorsal and ventral retina

Maximum projections from a whole-mounted retina double-labelled for the glutamate receptor subunit GluA2 and ZO-1. Image stacks were acquired from the dorsal retina **A-C** (Z-steps 16-26/27, Z-size ~ 2.2 μm) and the ventral retina **D-F** (Z-steps 13-20/24, Z-size ~ 1.6 μm). Clustering of both proteins beneath the cone pedicles is obvious, but GluA2 clustering appeared similar in the dorsal and ventral retina. Scale bar: 5 μm in F, applies to A-F.

5. Discussion

The outer plexiform layer (OPL) is the first synaptic layer in retinal information processing and, by extension, the entire visual system. Glutamatergic input to horizontal cells (HCs) is mediated by glutamate receptors (Hack et al., 2001) allowing HCs to provide feedback and feedforward inhibition to photoreceptors and bipolar cells (BCs), respectively (Thoreson and Mangel, 2012). The close association of glutamate receptors with gap junctions at desmosome-like junctions between horizontal cell dendrites, positioned 1-2 μm below the cone photoreceptor terminals (Haverkamp et al., 2000), suggests a calcium dependent mechanism for rapid regulation of signal transmission via gap-junctional coupling, during conditions of retinal adaptation which are not triggered by neuromodulators (Puller et al., 2009). In the mouse retina, horizontal cell dendrites are coupled by gap junctions formed by connexin57 (Cx57), creating a light-dependent, extensively coupled network (Hombach et al., 2004; Janssen-Bienhold et al., 2009). However, the exact distribution of glutamate receptors in this region remains unknown, and potential interactions between electrical and chemical synapses in the OPL of the mouse retina have not yet been fully elucidated.

The recognition of topographic variations in horizontal cells (Camerino et al., 2021), adds another level of complexity to the synaptic architecture at the pedicle base, potentially influencing the receptive fields of downstream neurons - an aspect that remains incompletely understood.

5.1 The AMPA subunits GluA2, GluA2/3 and GluA4 show distinctive distribution patterns in the OPL of the mouse retina

In this doctoral study, the precise spatial distribution of glutamate receptors on horizontal cells in the OPL of the mouse retina was investigated, providing robust evidence for a specific synaptic architecture - the desmosome-like junction - beneath the cone pedicle, that is conserved across different mammalian species.

Previous studies have established that ionotropic glutamate receptors (iGluRs) are localized beneath the cone pedicles at the desmosome-like junctions between horizontal cell dendrites in the primate retina (Haverkamp et al., 2000, 2001a, 2001b; Pan and Massey, 2023), as well as in the rabbit retina (Pan and Massey, 2007). Glutamatergic input into mouse horizontal cells is mediated exclusively by AMPA-type receptors (AMPA receptors) (Ströh et al., 2013, 2018) containing the subunits GluA2 and GluA4 (Hack et al., 2001). Immunohistochemistry and

confocal microscopy analysis carried out in this work revealed distinctive patterns of AMPAR subunits, including GluA2, GluA2/3 and GluA4 within the OPL of the mouse retina. The layered distribution of AMPA receptors at each cone pedicle delineated the general staining patterns of these subunits, mirroring observations previously reported in the primate retina (Haverkamp et al., 2000, 2001a). Immunoreactivities of all three subunits were detected in the distal OPL at the rod spherules and at the tips of horizontal cell dendrites, suggesting their proximity to the synaptic ribbons, where horizontal cells receive a strong glutamatergic input. A third, at a more proximal level, was observed beneath cone pedicles, situated at a depth of 1-2 μm below the synaptic ribbons of cone pedicles, at the desmosome-like junctions between HC dendrites (Haverkamp et al., 2000). Interestingly, light microscopic analysis using different poly- and monoclonal antibodies revealed the unequivocal presence of GluA2 immunoreactivity beneath the cone pedicles at the desmosome-like junctions, when the monoclonal anti-GluA2 antibody was used (see Chapter 4.1 and Fig. 14), while the polyclonal anti-GluA2/3 antibodies revealed no staining at this site, and GluA4 subunits were also not observed at this level in the OPL. GluA subunits display a unique molecular architecture, whereby the cytoplasmic C-terminal domain (CTD) is important for subunit-specific AMPAR-trafficking and synaptic plasticity. Both processes involve protein interactions, that in turn can be modulated by phosphorylation. This modulation process involves different protein kinases and phosphatases (for review, see Shepherd and Huganir, 2007). Moreover, phosphorylation of the CTD of GluAs has been shown to influence receptors characteristics such as channel conductance, peak channel open probability and has an effect on auxiliary subunit enhancement of channel conductance (Derkach et al., 1999; Kristensen et al., 2011).

In this study, distinctive clusters of GluA2 were detected beneath the cone pedicles using a monoclonal antibody raised in mouse. This antibody specifically recognizes the amino acid sequence 175-430 of the extracellular N-terminal domain (NTD) of GluA2. In contrast, the polyclonal antibodies anti-GluA2/3 recognize both GluA2 and GluA3 subunits and is targeting a peptide corresponding to amino acids 864-883 at the CTD of the rat GluA2. As shown in this study, both antibodies exhibited robust patterns of immunoreactivity at the processes of HC axon terminals invaginating the rod spherules (see Fig. 14). But unexpectedly and in contrast to the monoclonal anti-GluA2 antibody, the polyclonal anti-GluA2/3 antibodies failed to reveal clusters of AMPA receptors below the cone pedicles. This outcome was observed despite changes in antibody concentration and some parameters of the immunostaining protocol (data not shown). This result was difficult to explain, because the same polyclonal anti-GluA2/3, however a different production charge, was used in a previous investigation (Ströh et al., 2018) in the $\text{GluA2}^{\text{fl/fl}}\text{-GluA4}^{\text{fl/fl}}\text{:Cx57}^{+\text{Cre}}$ mouse line, to confirm the specific deletion of GluA2 in HCs. They could show that the GluA2/3-immunoreactivities were reduced to background in the GluA2/4-deficient mice, a finding which pointed to the GluA2-specificity of these antibodies in

the mouse and coincidentally indicated that no other GluA subunits (GluA3) were detected by it in this experiment. However, one explanation for the discrepancy in the immunoreactivity patterns revealed by the two antibodies in the present study might be the masking of the epitopes caused by interaction with other membrane standing proteins after insertion of the receptor subunits into the membrane and following fixation of the biological material, respectively (Stradleigh and Ishida, 2015).

This is a known problem when immunocytochemistry is used to detect ionotropic glutamate receptors (Baude et al., 1995; Petralia, 1997), particularly, when antibodies targeting the C-terminal of the receptors are used, as it has been described for the GluA2 CTD, for which masking by its interaction with the anchoring protein GRIP (glutamate receptor interacting protein) is discussed (Dong et al., 1997; Morigiwa and Vardi, 1999).

In this study, a second antibody against GluA2 (Tab. 1) was tested to analyze the spatial distribution of the subunit in the mouse OPL. The rabbit monoclonal anti-GluA2 targets an epitope within 16 amino acids of the cytoplasmic CTD. Immunoreactivity was again observed in the distal OPL at the level of the rods and at the invaginating processes into the cone pedicle. However, no accumulation of GluA2 beneath cone pedicles was detected (Fig. S1 – Supplemental material). On the other side and based on the clear immunoreactivities found with the polyclonal GluA2/3 antibodies in the distal OPL at the level of rod spherules, it is tempting to speculate that the failure of these antibodies to detect GluA2 clusters beneath the cone pedicles is likely not due to epitope masking by a common AMPAR scaffolding-interacting protein, such as GRIP. Instead, it is tempting to speculate that the different binding probabilities of the polyclonal GluA2/3-antibodies in the distal and proximal OPL, at the different HC compartments may be the result of different, intracellularly located protein conformation and channel activity modulating systems (i.e. phosphorylation/dephosphorylation systems) at the specific sites. As these modifications particularly appear at the intracellular CTD of AMPARs (Greger et al., 2017). This argument could also explain the clear labeling of the GluA2 subunits at the desmosome-like junctions by the monoclonal NTD-directed antibody, because the NTD lies extracellular and would more likely be affected in its conformation (epitope binding probabilities) by ligand-binding, assembly processes (Greger et al., 2017) or histological fixation procedures.

Other antibodies that recognize the GluA2 subunit by targeting the NTD, are available on the commercial market. For example, the rabbit polyclonal anti-GluA2 from Alomone Labs (Cat #: AGC – 005) is generated against a peptide [NVGNINNDKKDETYR(C)], corresponding to amino acid residues 179-193 on the NTD of rat GluA2. Immunostainings performed with this antibody should display accumulation of the GluA2 subunit at the desmosome-like junctions. AMPAR responses kinetics are shaped at multiple levels including post-translational modification such as phosphorylation and palmitoylation that occur at the CTD of the subunits

(for reviews, see Greger et al., 2017; Matthews et al., 2021). In the retina, the phosphorylation event represents the final step in the process through which dopamine regulates neuronal circuit functions, in dependence upon the light conditions (for review, see Roy and Field, 2019). It would be valuable to explore whether immunostaining with the anti-GluA2/3 and the monoclonal anti-GluA2 antibodies reveals GluA clusters beneath the pedicle in different light-adapted retinas. An intriguing direction for further investigation would be to conduct the same experiments on retinas adapted to varying light conditions, incorporating the antibody targeting GluA4, given that its epitope is also located at the CTD. Notably, no GluA4 clusters were generally observed beneath the pedicle in this study. Further observations regarding the composition of synaptic glutamate receptors support these experiments. Activity-driven synaptic plasticity is a fundamental feature across the central nervous system, often relying on conserved mechanisms that enable neurons to adapt to dynamic environmental signals (for reviews, see Malinow and Malenka, 2002; Derkach et al., 2007). In retinal ganglion cells (RGCs) for example, this plasticity is reflected by changes in the composition of AMPA-type glutamate receptors, specifically the proportion of surface GluA2-containing AMPARs in On RGCs (Xia et al., 2006, 2007). Changes in the expression of proteins that bind to the glutamate receptors such as GRIP, activity-regulated cytoskeleton-associated protein (Arc), and the protein interacting with C kinase 1 (PCK1), driven by visual activity provide a mechanism through which ambient light can modulate synaptic function, highlighting how external cues influence AMPAR-mediated plasticity (Casimiro et al., 2013).

Unlike other mammals, which possess two types of HCs, the mouse retina contains only one type of HC, which resembles the B-type axon-bearing HC of the rabbit retina (Peichl and González-Soriano, 1994). In the rabbit retina, both the A-type axonless HCs and the B-type HCs exhibit clusters of GluA2/3 and GluA4 on their dendrites, beneath the cone pedicle (Pan and Massey, 2007). Similarly, in the primate retina, both H1 and H2 HCs exhibit the presence of GluA2, GluA2/3 and GluA4 clusters at the desmosome-like junctions (Haverkamp et al., 2000, 2001a). The primate H1 and H2 HCs are both axon bearing: the H1 cell axon terminal exclusively contacts rods, similar to the mouse B-type cell (Pan and Massey, 2007, 2023) and the H2 axon terminal has only sparse collaterals, which contact only cones (Kolb et al., 1980). The H1 HC dendrites contact all red/green cone pedicles but have sparse or no contact with blue cones, whereas H2 cells preferentially target blue cone pedicles while also connecting with all cones within their dendritic field (Dacey et al., 1996; Goodchild et al., 1996). H1 HC dendrites express the kainate subunits GluK2/3 (GluR6/7 old nomenclature) at the desmosome-like junctions, whereas H2 HCs, which mostly innervate S-cones, show no expression of GluK2/3. Finally, B-type HC dendrites in the cat retina express GluA2/3 strongly, GluK2/3 weakly and do not express GluA4, whereas the A-type HCs express all the subunits

strongly (Morigiwa and Vardi, 1999; Qin and Pourcho, 2000). It is worth emphasizing that H2 cells of the primate retina are homologous to cat A-type HCs (Sandman et al., 1996; Peichl et al., 1998; Wässle et al., 2000). However, at S-cone pedicles in the primate retina no predominant expression of GluA4 has been observed, as might be expected (Haverkamp et al., 2001a). AMPARs are tetrameric ion channels that function as homo- or heterotetramers, composed of various combinations of the subunits GluA1-4 (Boulter et al., 1990; Keinänen et al., 1990). Each subunit plays a distinct role in determining channel kinetics, ion selectivity, and receptor trafficking, making heteromerization a crucial factor in the functional diversity of these receptors (Traynelis et al., 2010; Greger et al., 2017). An important consideration is that GluA2 exhibits a significantly higher affinity for GluA3 compared to GluA3 self-assembly, thereby preferentially promoting the formation of GluA2/3 heterodimers (Rossmann et al., 2011; Zhao et al., 2016). This high-affinity interaction ensures that GluA2 is predominantly incorporated into AMPAR heterotetramers, limiting the formation of GluA3 homotetramers. Additionally, Q/R editing of GluA2 (see next section) impedes its ability to form homotetramers, further enhancing the availability of GluA2 for incorporation into GluA2/3 heterodimers and reinforcing the predominance of GluA2-containing receptors in neurons (Greger et al., 2002). Therefore, an exclusive composition of AMPA receptors by GluA2 at desmosome-like junctions, and the resulting more intense labeling compared to the rabbit polyclonal antibody, can be excluded. Depending on their subunit composition, some AMPA receptors may mediate phasic responses, while others may be responsible for more tonic responses to visual stimuli (for review, see Wässle, 2004). The kinetics of synaptic responses, driven by receptor subunit composition, are tailored to the specific roles of the synapse and cell type within the neural circuit (Traynelis et al., 2010). Thus, comparing the distinct distribution patterns of AMPAR subunits observed in this study with previous research on primate and rabbit retinas proves challenging. While GluA2, GluA2/3, and GluA4 were observed at the triads of horizontal cell invaginating processes in both primate and mouse retinas, in the mouse retina, only GluA2 was detected at the desmosome-like junctions, despite the expectation that GluA2/3 should also be present. This result is in contrast to that observed in the primate retina, where all of three subunits were found at the desmosome-like junctions. What is consistent with other mammals is the distinct distribution of AMPA receptors at different levels at the cone pedicle. This suggests that the composition of AMPARs may be modulated to meet the specific needs of visual signal processing in different species. Whether the unique synaptic organization in the mouse retina is related to the presence of a single horizontal cell type, possibly reflecting adaptation to low-light or nocturnal environments dominated by rod photoreceptors (Boije et al., 2016), remains controversial and widely debated (Peichl, 2010).

However, it is plausible to suggest that the distinct AMPA receptor patterns observed in horizontal cells in the context of this thesis work, are specific to the mouse retina, in comparison to what characterizes AMPA receptor distribution in other mammals.

5.2 Mouse desmosome-like junctions architecture

Desmosome-like junctions are distinguished by a distinctive synaptic configuration and the absence of desmosome markers, which indicates that they are not desmosome or adherens junctions (Gumbiner, 1996; Paffenholz et al., 1999). AMPARs are expressed by both horizontal cell members beneath the cone pedicle, where they form two postsynaptic densities that face each other, linked together in the same way as presynaptic and postsynaptic densities in conventional synapses and aggregate at these desmosome-like structures (Haverkamp et al., 2000, 2001a; Puller et al., 2009). Thereby, the glutamate released at the ribbon acts both at the direct synaptic contacts and through diffusion to the deeper GluAs (Rao-Mirotnik et al., 1995, 1998; Haverkamp et al., 2000, 2001a). As a result, variations in the location of AMPA receptors along horizontal cell processes contribute to the complexity of synaptic transmission by introducing subtle timing differences, typically ~ 1 ms (for review, see Barbour and Häusser, 1997; Rusakov et al., 2011). These differences are likely crucial for signal processing, with AMPARs positioned near the photoreceptor ribbon synapse activating earlier than those located at desmosome-like junctions (Hack et al., 2001; Haverkamp et al., 2001a, 2001b). In the primate retina, it has been hypothesized that the GluAs at the desmosome-like junctions solve a logistical problem of “packing” of postsynaptic sites at the synaptic ribbon by adding an additional layer. It is plausible that this solution may also be adopted in the OPL of the mouse retina. Confocal image analysis carried out in this work, revealed a distribution of GluA2 beneath the pedicle that resembled the shape of a “bouquet of flowers,” wherein the GluA2 immunoreactivity narrowed downward in the proximal OPL, along the structure of the fine HC dendrites that invaginate at the base of the cone pedicle. Unlike the broad, aligned bands observed in primates, whole-mounted mouse retinas reveal a more intricate structure that extends and then narrows in depth (see Section 4.1.2). Despite these differences, the crucial arrangement for the desmosome-like junctions appears to be the location below the cone, aligned with the glutamate release site at 1-2 μm from the synaptic ribbon. Furthermore, GluA2 expression was found in the present study, in close association with the dendritic gap junctions of the horizontal cells (Cx57) and the scaffolding protein ZO-1, suggesting a synaptic architecture below the cone pedicle that characterizes dendritic HC connection sites in the retina of many mammals, including mice.

Zonula occludens-1 (ZO-1) belongs to the MAGUK family proteins. It is a membrane-associated scaffolding protein that links junctional membrane proteins to the cytoskeleton and signaling plaque proteins (for reviews, see Hartsock and Nelson, 2008; Paris et al., 2008). However, it also interacts with connexins at electrical synapses (Giepmans, 2004; Lynn et al., 2012). In the OPL of mouse, rabbit and primate retinas, ZO-1 revealed a consistent organization: (I) It is found in association with Cx57 at the dendro-dendritic gap junctions of mouse HCs, (II) with Cx50 of axonless A-type HCs, both below the cone pedicle and at the giant plaques in the rabbit retina and (III) located at the desmosome-like junctions on H1 horizontal cell dendrites in the primate retina (Puller et al., 2009). Thus, a multifunctional role has been suggested for ZO-1 at the desmosome-like junctions, since, as scaffolding protein it is able to interact with connexins via its first and second PDZ domains (Li et al., 2004b; Flores et al., 2008), and simultaneously it can act as a link between the cytoskeleton and the local transmembrane proteins via its GUK domain and its proline-rich C-terminal domain (Fanning et al., 1998). In a model, Puller et al., (2009) suggested that connexins are closely associated with glutamate receptors at desmosome-like junctions, in that manner the gap junction is flanked by a fence-like boundary of tight or adherens junctions, where ZO-1 anchors transmembrane proteins to the cytoskeleton, rather than directly and exclusively interacting with connexins. In support of this hypothesis, electron microscopy studies described that Cx57-immunoreactive gap junctions in mouse horizontal cells are flanked by zonula adherens (Janssen-Bienhold et al., 2009) as shown previously for dendritic gap junctions in cat (Kolb, 1977) and turtle (Kolb and Jones, 1984). Associations between gap junctions and ZO-1 have been also observed at the junctions between primary dendrites of horizontal cells in macaque and rabbit retinas (Puller et al., 2009). In the dorsal retina of the mouse, string-like structures of colocalized ZO-1 and Cx57 were frequently observed, extending beyond the cone pedicle regions and they were generally found at a deeper, more proximal level in the OPL (see Section 4.2.3). Although not exhaustively investigated, these structures appeared to be comparable to those observed in the macaque and rabbit. This analogy is also supported by the observation that, in the superior (dorsal) rabbit retina, the largest gap junctions appeared as "strings" between adjacent dendrites, while rounder structures were more prevalent in the inferior (ventral) retina (O'Brien et al., 2006). Light microscopic analysis of ZO-1 and Cx57 in the present study confirmed the colocalization of these proteins beneath the cone pedicle. However, the observed colocalization between ZO-1 and Cx57 in this study should also be interpreted as a result of the small size of Cx57 plaques and the inherent resolution limitations of confocal microscopy. Consequently, ZO-1 may form these fence-like structures independently, as a tight junction protein, in the mouse retina, rather than interacting exclusively with Cx57. High-resolution fluorescence imaging carried out in this study, sought to represent the potential structural organization of ZO-1 and Cx57 (see Fig 28). Images from the dorsal side of the mouse retina,

where ZO-1 and Cx57 plaques appeared linearly arranged and larger in size, respectively, seemed particularly well-suited to illustrate this association. The ZO-1 structures often appeared to accommodate Cx57-containing gap junctions, suggesting a possible localization of ZO-1 around these regions. A way to address this question and obtain additional information would be to use super resolution fluorescence microscopy (Huang et al., 2010). Conventional fluorescence microscopy is limited by relatively low spatial resolution because of the diffraction of light (Abbe, 1873). Although confocal microscopy, along with advanced laser sources and improved optics, can enhance resolution, the diffraction limit remains about 200–300 nm in the lateral direction and 500–700 nm in the axial direction, which is comparable to or larger than many subcellular structures (Kamasawa et al., 2006; Janssen-Bienhold et al., 2009). With a stimulated emission depletion (STED) microscope, resolution of fluorescently stained structures down to well below 100 nm is possible (Hell and Wichmann, 1994; Klar and Hell, 1999). Other techniques also include the saturated structured-illumination microscopy (SSIM) (Gustafsson, 2005) as well as techniques that are based on the localization of individual fluorescent molecules, such as stochastic optical reconstruction microscopy (STORM) (Rust et al., 2006), or the photoactivated localization microscopy (PALM) (Hess et al., 2006). If ZO-1 is indeed involved in forming tight or adherens junctions around gap junctions, then with increased spatial resolution by an order of magnitude or more over the diffraction limit, the ZO-1 plaques beneath the cone pedicle might appear as ring-shaped or fence-like structures, much like the patterns observed at connexin plaques in rabbit A-type horizontal cells by Puller et al., (2009). Understanding synaptic function and plasticity requires detailed mapping of molecular organization and dynamics at synaptic sites.

Super-resolution fluorescence microscopy meets these needs with molecule-specific contrast, nanometer-scale resolution, and live tissue imaging capabilities (Huang et al., 2010). However, the resolution is limited by the quality of fluorescent probes, and factors such as photobleaching, high-intensity laser requirements, and slower image acquisition times can pose significant challenges.

Finally, ZO-1 expression is not only distributed in a type-specific manner - i.e. primate H1 horizontal cells - but is also restricted to the dendro-dendritic gap junctions in the mouse retina as well (Puller et al., 2009). Previous research on goldfish retinal horizontal cells has shown that dopamine differentially influences connexin density in dendrites versus axon terminals (Baldrige et al., 1987). Specifically, dopamine significantly reduced connexin levels in dendro-dendritic gap junctions, while axo-axonal junctions were less affected. Additionally, another study on vascular endothelial cells have demonstrated that dopamine can alter the permeability of tight junctions by phosphorylation, involving occludin and ZO-1 (Bhattacharya et al., 2008). In regulating endothelial cell–cell junctions, ZO-1 plays a central role by coordinating multiple processes that control adherens junctions and influence endothelial

behavior and function (Tornavaca et al., 2015). These findings suggest that ZO-1 may contribute not only to the structural integrity of gap junctions but also to their regulation through more complex pathways, including modulation by neurotransmitters like dopamine.

5.3 The interplay between desmosome-like junctions and gap-junctions in the mouse retina

The close association of gap junctional plaques and glutamate receptors beneath the cone pedicle observed in different mammals, suggests a potential role for AMPARs in modulating gap junction permeability, facilitating rapid light adaptation independent of neuromodulators like dopamine (Puller et al., 2009). Modulation by glutamate receptor is more spatially restricted and selectively influencing the conductance of nearby gap junctions (Pereda et al., 2004). Thus, in the case of the rabbit retina, giant horizontal cell gap junctions may be predominantly modulated by dopamine, while the smaller dendritic gap junctions beneath the cone pedicles could be influenced by calcium and potentially dopamine as well (Puller et al., 2009).

This thesis demonstrates that in the mouse retina GluA2-subunits containing receptors at desmosome-like junctions, which are located at proximal dendrites of horizontal cells beneath the cone pedicle, are closely associated with Cx57-containing gap junctions. This spatial proximity between GluA2, involved in chemical signaling, and Cx57, involved in electrical signaling, along with the scaffolding protein ZO-1, may indicate potential protein-protein interactions occurring at these sites. To address this topic by means of immunohistochemistry, the contiguous presence of electrical and chemical synapses at desmosome-like junctions, was further verified by immunolabeling the retinas of different transgenic mouse lines with the appropriate antibodies, followed by qualitative analyses. Immunostaining of retinas from the Cx57-deficient mouse line (Hombach et al., 2004), was conducted to assess changes in the expression patterns of glutamate receptor subunits GluA2, GluA2/3, and GluA4. Notably, no significant qualitative differences were observed compared to wild-type tissue. However, ZO-1 immunostaining indicated a trend towards more compact clusters, with fewer string-like structures and a slight shift towards a more punctate pattern (see Section 4.2.2). In Cx57-deficient mice, tracer coupling between horizontal cells was reduced by more than 99%. However, no morphological alterations or impaired development of horizontal cells structure and distribution were observed (Hombach et al., 2004; Shelley et al., 2006). In addition, electron microscopy analysis revealed the presence of numerous sites along adjacent horizontal cell processes that resemble adherent junctions (Janssen-Bienhold et al., 2009).

Finally, the genetic profile of Cx57 KO mice demonstrated the complete absence of mRNA transcripts within the remaining coding regions after the insertion of the LacZ gene reporter sequence (Ciolofan et al., 2007). This experiment rules out the presence of an “incomplete” knock-out of Cx57 in this mouse line and the consequent presence of functionless connexin portions, unrecognized by the antibodies but still capable of interacting with ZO-1 and the desmosome-like junctions through a preserved PDZ binding domain. Taken together, these findings underscore the ambiguity regarding the precise role of ZO-1 at the desmosome-like junctions. As a member of the MAGUK family, ZO-1 contains three PDZ domains that facilitate interactions with various proteins, including those involved in tight junctions, adherens junctions, and gap junctions (González-Mariscal et al., 2000, 2003; Singh et al., 2005). Thereby, a variety of connexins interact with ZO-1 (Giepmans, 2004; Li et al., 2004a, 2004b, 2004c; Flores et al., 2008; Lynn et al., 2012). However, in contrast to other connexins, Cx57 lacks a PDZ binding motif (Ciolofan et al., 2007), suggesting that a classical direct interaction with ZO-1 is unlikely. If ZO-1 and Cx57 had interacted directly, one would expect a noticeable change in the expression pattern of ZO-1 in Cx57-deficient mice. The lack of such changes suggests that ZO-1 may serve additional roles at desmosome-like junctions with Cx57, beyond simply anchoring gap junctions to the cytoskeleton.

The three GluA subunits also did not exhibit significant alterations in their immunostaining patterns, which suggests that the absence of Cx57 gap junctions beneath the cone pedicle does not result in notable spatial or structural consequences for glutamatergic transmission at these specific sites (see Section 4.2.2). A reduction in input resistance resulting from the upregulation of a conductance as a compensation for the absence of Cx57 was observed in dissociated horizontal cells from Cx57 KO mice when compared to wild-type cells (Shelley et al., 2006). However, later studies revealed that horizontal cells from mice with one or two alleles of Cx57 exhibited striking similarities, displaying comparable glutamate dependence and mean resting membrane potential (Ströh et al., 2013).

In contrast, the verification of Cx57 and ZO-1 expression in GluA2/4 KO retinas revealed significant findings. Qualitative analysis showed a striking reduction in both Cx57 and ZO-1 immunoreactivity beneath the cone pedicle (see Section 4.2.1). In this mouse line, Cre recombinase is placed under the control of the Cx57 promoter to specifically excise GluAs sequences in horizontal cells. The expression of a single Cx57 allele reduces horizontal cell electrical coupling and receptive field size (Shelley et al., 2006), as well as the number and area fraction of Cx57 clusters compared to control mice (Ströh et al., 2013). Despite this reduction, immunolabeling of Cx57 and ZO-1 in heterozygous Cx57+/CRE mice continued to show distinct clustering and colocalization beneath the cone pedicles, qualitatively resembling that observed in wild-type mice. Therefore, it is reasonable to presume that the absence of

GluA2 and GluA4 subunits exert a direct or indirect functional impact on the clustering of Cx57 and ZO-1 at the desmosome-like junction. GluA2 and GluA4 subunits are the key components of the glutamatergic input to HCs in the mouse retina, contributing approximately 25% and 75% to the glutamate-induced currents, respectively (Ströh et al., 2013, 2018). Furthermore, based on the findings presented in this thesis and those of previous studies, it is tempting to suggest that the absence of the GluA2 subunit specifically contributes to the impaired expression of ZO-1 and Cx57 beneath the cone pedicle. The present study identified the GluA2 subunit as a potential candidate for the formation of desmosome-like junctions in the mouse OPL. Immunostainings for the GluA2/3 and GluA4 subunits, conducted both in this thesis and in previous studies, have either not detected their presence or shown that they are absent beneath the pedicle. Previous investigations into Cx57 immunoreactivity in GluA4 knockout mice - where GluA4 contributes approximately 75% of the input currents to horizontal cells - revealed a roughly 50% reduction in Cx57 expression area fraction, consistent with the expected impact of a missing allele (Ströh et al., 2013). At the same time, structural and morphological analyses in GluA4- and GluA2/4-deficient mice, conducted using both electron microscopy and immunohistochemistry, were restricted to examining potential alterations at the triad synapse, without assessing changes at the desmosome-like junction level. However, Cx57 immunoreactivity was not analyzed in GluA2/4 deficient mice (Ströh et al., 2018). Interestingly, the same authors have previously reported the effect of the loss of one Cx57 allele on ganglion cell tuning in GluA4^{fl/fl}:+/Cre mice, where glutamate-evoked currents in horizontal cells were reduced by 75% (Ströh et al., 2013). No significant changes in t-OFF RGC responses to frequency or contrast were observed. Concluding that the remaining 25% of photoreceptor input is sufficient for normal visual processing and suggesting that the loss of one Cx57 allele does not account for the observed changes in GluA2/4-deficient mice. Based on these findings, it would be worthwhile to conduct similar experiments and observations using a GluA2-deficient mouse line with the same Cre-recombinase system (GluA2^{fl/fl}:+/Cre) and compare t-OFF RGC responses with the one from GluA4-deficient mice.

The extent to which HC coupling is modulated by dopamine is regulated by both, the circadian rhythm and the light adaptation state of the retina (Tornqvist et al., 1988; Xin and Bloomfield, 1999; He et al., 2000; Ribelayga and O'Brien, 2017; Roy and Field, 2019). For instance, as daylight increases at dawn, dopamine is released by dopaminergic amacrine cells (ACs) (Iuvone et al., 1978) in the inner retina, diffuses to the outer retina, and reduces electrical coupling in the HC network (for review, see Witkovsky, 2004). Activation of D1-receptors enhances adenylate cyclase activity, thereby increasing cAMP content and activating protein kinase A (PKA), which in turn decrease the electrical conductance of gap junction channels by phosphorylation of the connexins (Piccolino et al., 1984; Lasater, 1987; Hampson et al., 1994;

He et al., 2000). Dopamine is also released in the retina upon light exposure (Weiler et al., 1997), but conductance changes in gap junctions between horizontal cells by glutamate or calcium influx may serve as a modulatory mechanism in darkness that compensates for this effect (Solessio and Lasater, 2002; Schubert et al., 2006). The retinal horizontal cell network is also subject to modulation by the neuromodulator nitric oxide (NO) (Pottek et al., 1997; Xin and Bloomfield, 2000). NO decrease the glutamate receptor affinity, leading to suppressed receptor responses. However, at high glutamate concentrations, such as those at the photoreceptor–horizontal cell synapse in the dark, NO increases the maximal glutamate current, resulting in enhanced glutamate-evoked currents and depolarization of the horizontal cell membrane. Overall, NO/PKG and dopamine/PKA modulate both glutamate receptors and gap junction channels in horizontal cells through distinct but potentially overlapping molecular sites, producing significant comodulating effects (McMahon and Schmidt, 1999). Therefore, in addition to dopamine, the close proximity of GluA2 and electrical synapses beneath cone terminals could indeed, modulate horizontal cell coupling, explaining the presence and necessity of a secondary expression location of glutamate receptors at the desmosome-like junctions (Puller et al., 2009).

It is well-established that among the four AMPA receptor subunits, the inclusion of Q/R-edited GluA2 in the formation of homo- or hetero-tetrameric receptors reduces the calcium influx through the channel (for reviews, see Hollmann and Heinemann, 1994; Jonas and Burnashev, 1995; Guo and Ma, 2021). Studies on mouse retinal horizontal cells have shown that kainate receptors contribute to calcium influx (Schubert et al., 2006). However, the calcium influx mediated by kainate receptors was lower than that of AMPAR, likely due to the relatively smaller number of expressed receptor subunits. Despite these observations, GluA2 still accounted for 25% of the photoreceptor inputs in HCs (Ströh et al., 2013, 2018).

The interplay between electrical and chemical synapses is a vast and complex topic, with numerous exceptions and still controversially discussed (for reviews, see Pereda, 2014; Jabeen and Thirumalai, 2018). Based on the findings from the present work, the mechanisms driving the failure of Cx57 and ZO-1 to organize beneath the cone pedicle in the absence of GluA2/4 remain speculative. Furthermore, although the observation of a functional interplay between GluAs and Cx57 at the desmosome-like junctions was evident, proper quantification is still needed to strengthen the qualitative analyses conducted in the project. This would involve precise measurements of the positive area covered by ZO-1 and Cx57 immunostaining within circular ROIs beneath each pedicle, using a method similar to the analysis applied to assess the asymmetrical distribution of Cx57 across the retina (see Section 4.3). One hypothesis is that Cx57 hemichannels and GluA2-containing AMPA receptors are co-transported in the same vesicle to a common destination at the desmosome-like junction.

In the absence of the GluA2 subunit, this transport system becomes incomplete and fails to reach its destination. Consequently, the simultaneous absence of both Cx57 and GluA2-containing receptors at the desmosome-like junction significantly disrupts the organization of ZO-1, affecting its role both as a scaffolding protein and as a connexin anchoring protein. However, co-transport of gap junction components and glutamate receptor subunits in the same vesicle would be highly unusual, since these two proteins undergo different cellular processes and are generally trafficked via distinct mechanisms within neurons. AMPAR are initially translated and inserted into the endoplasmic reticulum (ER), where crucial steps such as folding, dimerization, tetramerization and auxiliary subunit association take place. After export from the ER, AMPARs are typically transported in vesicles that are specifically destined for the postsynaptic membrane. This process involves various proteins that regulate receptor trafficking, insertion, and removal of AMPARs from the synaptic membrane (for reviews, see Malinow and Malenka, 2002; Greger et al., 2017; Matthews et al., 2021). Connexins, on the other hand, are transported via the ER for complete oligomerization and usually via the Golgi apparatus for further post-translational modification before being delivered to the plasma membrane, where they form hemichannels that eventually dock with hemichannels on adjacent cells to form gap junctions (for reviews, see Laird, 2006; Matsuuchi and Naus, 2013; Kirichenko et al., 2021). To date, no specific studies have demonstrated the occurrence of co-transport between glutamate receptors and connexins. Confocal microscopy provides high spatial resolution and optical sectioning but is primarily suited to give structural information and intensity-based fluorescence measurements. In contrast, other imaging techniques can offer insights into molecular interactions and environmental changes within cells. Therefore, an experimental approach to address this question could involve the use of fluorescent-protein-tagged connexins or AMPAR subunits to reveal their trafficking in the mouse retinal HCs (Lauf et al., 2002; Thomas et al., 2005). Other techniques that could be employed include fluorescence resonance energy transfer (FRET), bi-molecular fluorescent complementation (BiFC - (Ciruela, 2008) and fluorescence lifetime imaging microscopy (FLIM) (Datta et al., 2020). FRET allows to detect interactions between molecules that are in close proximity (typically 1-10 nm), providing real-time information about protein-protein interactions, conformational changes, or signaling events within live cells. In contrast, FLIM measures the fluorescence lifetime of excited fluorophores, providing insights into the local micro-environment (e.g., pH, ion concentration, or molecular interactions) and changes in molecular dynamics independent of fluorophore intensity. While both techniques improve our understanding of cellular processes, they also present challenges, including the need for advanced equipment, careful selection of fluorophores, and complex data analysis. Advances in light microscopy imaging, along with the availability of genetically encoded fluorescent proteins, offer the necessary tools to observe the spatial and temporal distribution of protein

interactions within living cells (for review, see Sekar and Periasamy, 2003). Finally, fluorescence recovery after photobleaching (FRAP), is a method for determining interaction and mobility through cell membranes or intracellular structures. Molecules of interest are tagged with fluorescent markers and their location is followed by photobleaching with confocal laser scanning microscopes (Meyvis et al., 1999; Lauf et al., 2002).

Glutamate chemical transmission interacts with electrical synapses at mixed synapses, such as those at the "club endings" on teleost Mauthner cells (Pereda et al., 2004). Activation of these synapses leads to long term potentiation (LTP) of both electrical and glutamatergic components, demonstrating activity-dependent plasticity in both forms of transmission (Yang et al., 1990). Potentiation of electrical transmission is initiated by the activity of the coexisting glutamatergic synapse and require an increase of postsynaptic calcium level and the activation of the calcium/calmodulin-dependent protein kinase II (CaMKII) (Pereda et al., 1998). CaMKII was found to phosphorylate Cx36 at Ser293, enhancing gap junctional coupling within the All mouse retinal amacrine cell network, upon activation of non-synaptic NMDA receptors colocalizing with Cx36 on these cells (Kothmann et al., 2012). CaMKII is an important component of the postsynaptic density at chemical synapses and plays a key role in activity-dependent plasticity mechanisms (Kennedy, 1997). Additionally, CaMKII has been studied in horizontal cells of the carp and mouse retina, where it is implicated in synaptic modulation and plasticity (Liu et al., 2000; Schultz et al., 2004).

Mixed synapses or the co-occurrence of chemical and electrical synapses provide clear evidence that glutamatergic and electrical synapses interact (for review, see Pereda, 2014). Therefore, it is reasonable to conclude that the dendritic gap junctions of mouse retinal horizontal cells, closely associated with desmosome-like junctions, are modulated by calcium influx dependent on glutamatergic signaling. This modulation likely occurs through the activation of CaMKII (Alev et al., 2008; Flores et al., 2010) which, in the absence of GluA2-containing AMPA receptors, is unable to maintain its kinase activity necessary for effectively regulating the structural aggregation of Cx57-containing gap junctions. To prove the role of CaMKII in modulating the aggregation of Cx57, several experimental approaches could be employed: genetic manipulation using a conditional knockout model to delete the CaMKII gene specifically in horizontal cells adopting the Cre-recombinase system under the Cx57 promoter. Alternatively, overexpress a dominant-negative form of CaMKII to disrupt its activity. In both cases, disrupted or altered Cx57 aggregation in these genetically modified animal retinas would indicate a role for CaMKII in the process. Confocal microscopy with CaMKII antibodies could be used to assess its expression and distribution in wild-type and transgenic mouse retinas. An interesting approach for further investigation would be to evaluate horizontal cell

tracer-coupling in GluA2/4-deficient mice while modulating CaMKII activity with an agonist and comparing this coupling to wild-type conditions treated with a CaMKII inhibitor.

Unlike what was observed in Cx57-Cre mice, in GluA2/4-deficient mice, where one allele of Cx57 is retained, Cx57-containing gap junctions fail to cluster and colocalize with ZO-1 beneath the cone pedicle. To better understand the components and mechanisms modulating this interaction, it would be valuable to investigate what contributes to the absence of Cx57 plaques beneath the cone pedicle. Specifically, it would be important to determine whether Cx57 expression is downregulated or if the protein is not correctly accumulated at the desmosome-like junctions. Connexin expression levels can be determined using SDS-PAGE followed by immunoblotting to quantify the protein amount. Additionally, RT-PCR can be employed to detect and quantify Cx57 mRNA, allowing for the evaluation of its expression at the transcriptional level. Based on the results of the experiment, it might be interesting to further investigate the presence of a signaling cascade and transcriptional regulatory pathways triggered by AMPARs in mouse retinal horizontal cells.

It is particularly intriguing that ZO-1 was found significantly reduced to a narrow cluster of puncta, likely associated with Cx36 on OFF-bipolar cells at the base of the cone (Ciolofan et al., 2007; Puller et al., 2009) in GluA2/4 KO mice, while the same ZO-1 showed only a slight alteration in Cx57 complete knockout animals (Cx57-LacZ mouse line). Double labeling of Cx36 and ZO-1 in GluA2/4-deficient mice, may reveal all “remaining” ZO-1 puncta are colocalized with Cx36. ZO-1 is widely expressed in various tissues, including the CNS, where it plays a multifunctional role as a tight junction protein and/or scaffolding protein and/or regulatory component at electrical synapses (Li et al., 2004b, 2008; Rash et al., 2004; Ciolofan et al., 2006, 2007; Puller et al., 2009). ZO-1 may function in neuronal gap junctions similarly to how postsynaptic density proteins operate at glutamatergic synapses. Likewise, electrical synapses require a specific molecular machinery to facilitate the turnover of gap junction channels (Pereda, 2014), ZO-1 could anchor regulatory molecules such as protein kinases like CaMKII and cAMP-dependent protein kinase (Flores et al., 2008), thereby promoting the accumulation of Cx57. Neuronal signaling pathways mediated by PKC (Stuart and Nigam, 1995) or CaMKII (Pereda et al., 2013; Pereda, 2014) may also modulate synaptic strength and plasticity by altering phosphorylation state, localization and function of ZO-1. There is evidence that ZO-1 controls gap junction channel aggregation and turnover at the edges of gap junctions and thereby regulates the size and stability of gap junctions (Hunter et al., 2005). In mouse retinal horizontal cell dendrites, the absence of AMPAR subunits, particularly GluA2 at the desmosome-like junctions, could disrupt the phosphorylation state of the ZO-1/Cx57 complex impairing the organization of ZO-1 string-like structures at the border of this region and in turn

affecting the normal compartmentalization of Cx57-containing gap junctions at the desmosome-like junctions. Further investigations targeting these kinases could elucidate their roles and interactions in synaptic plasticity and the regulation of these synaptic components. Taken together, the findings of the present thesis and their discussion point to the presence of a complex modulation system at the “mixed” desmosome-like junctions. On one hand, the release of neuromodulators like dopamine activates specific metabotropic G protein-coupled receptors (D1-5 dopamine receptors), initiating a signaling cascade through cAMP-PKA that modulates synaptic communication between cells. On the other hand, modulation occurs via a calcium influx-dependent signaling cascade through AMPARs, likely mediated by CaMKII. The kinase activity of CaMKII may facilitate the assembly and regulation of the Cx57/ZO-1 complex at the desmosome-like junctions. However, other calcium-dependent modulation, such as calmodulin, could also be involved (Peracchia, 2020; Tran et al., 2023). As suggested, these two mechanisms of gap junction conductance modulation reflect a global regulatory effective mechanism through neuromodulators, and a local modulation pathway via AMPARs beneath the cone pedicle, which together could explain the precise adaptation of coupling at varying light conditions (Puller et al., 2009).

5.4 The dorso-ventral density gradient of horizontal cells is reflected in distinctive changes of dendritic gap junctions

The following sections will discuss the cell density profile of horizontal cells, with a particular focus on the asymmetrical distribution of Cx57-containing gap junctions between the dorsal and ventral regions of the retina. These findings will be interpreted in relation to the results presented in this thesis. Further conclusions regarding horizontal cell morphology and physiological implications, are provided in the attached article.

This study (HC density project, in collaboration with Lucia Lindenthal, Christoph Block and Asli Pektaş) presented a detailed analysis of the horizontal cell density, which in the further course of the project revealed a significant matching with the synaptic architecture beneath the cone pedicle and an alignment with the topographic specialization of the S-opsin transition zone. Cell density gradients and morphological variations among cell types are well known to exist across the mammalian retina (for reviews, see Baden et al., 2020; Heukamp et al., 2020). Recent findings show that, along with OFF bipolar cells, horizontal cell density varies dorso-ventrally, being lower in the dorsal and higher in the ventral retina (Camerino et al., 2021). However, the observations derived from sampling different retinal regions mostly just revealed a trend in HC distribution. Here, the detailed distribution across the entire retina confirmed this trend and added further attributes. A sharp increase in density was observed at the transition

zone, with lower density towards the dorsal retina above this boundary and higher density towards the ventral retina below it. The close correlation between the HC density and the S-opsin transition zone does not represent only a simple separation between upper/dorsal retina and lower/ventral retina. Instead, it reflects a functional segregation of distinct features that characterize the upper and lower visual fields of the mouse, with the photoreceptor transition zone aligning with the horizon of the visual field (Baden et al., 2013; Nadal-Nicolás et al., 2020; Qiu et al., 2021; Sharpe et al., 2022). This is supported by the fact that the HC density pattern resembled the density gradient of mouse ganglion cells, which show a distinct global density gradient with many more cells found in the ventral retina (Salinas-Navarro et al., 2009; Duda et al., 2023) and mouse photoreceptors (Ortín-Martínez et al., 2014; Nadal-Nicolás et al., 2020). Horizontal cells located above the S-opsin transition zone receive information from the lower visual field, while horizontal cells below the horizon collect information from the upper visual field. The HC density profile revealed a hotspot extending medially at the center of the ventral retina, below the optic disk. This region may overlap with the hotspot of "true S-cones" (expressing only S-opsin) found in the ventral mouse retina. The presence of this S-cone hotspot was interpreted as an evolutionary adaptation to improve color coding in the upper visual field, aligning with the specific habitat and behavior of the animal (Haverkamp et al., 2005; Nadal-Nicolás et al., 2020). The true S-cones are not only defined by their exclusive expression of S-opsin, but they also own a synaptic connectivity with their selective type 9 bipolar cells (for review, see Puller and Haverkamp, 2011a). In primate retina, H2 horizontal cell dendrites contact preferentially S-cones (Dacey et al., 1996; Goodchild et al., 1996; Pan and Massey, 2023). In macaque retina, ZO-1 staining was strongly reduced at the S-cone pedicle (Puller et al., 2009), and in contrast to H1, H2 dendrites do not express the kainate subunits GluK2/3 (GluR6/7 – old nomenclature) (Haverkamp et al., 2000, 2001b). Therefore, it would be very worthwhile to investigate the synaptic architecture of mouse HCs, including the distribution of glutamate receptors, the expression of tight-junction protein ZO-1, and properties of gap junctions, with a particular focus on the HC hotspot in the ventral area. Specifically focusing on the AMPA-type subunits GluA2 and GluA4 at the desmosome-like junctions, as well as on the staining pattern of ZO-1 and Cx57. These kinds of analyses could be performed by targeting the true-blue cone pedicles, exploiting transgenic mouse lines in which S-cone-selective type 9 BCs can be identified, such as the CLM1 mouse line (Berglund et al., 2006; Breuninger et al., 2011).

In muroid species like the rat, mouse, gerbil, and Syrian hamster, only one type of horizontal cell, the axon-bearing B-type, has been identified, with no evidence supporting the existence of a second type (Peichl et al., 1998; Boije et al., 2016). This absence of the A-type horizontal cell, which deviates from the typical mammalian pattern, holds practical significance, because genetically modified mice are widely used to study mammalian retinal wiring and function. This

unique characteristic in mice offers valuable insights into how the presence of one versus two horizontal cell types might influence ganglion cell receptive fields (Peichl, 2010).

In this doctoral project, an asymmetrical density distribution of Cx57-containing gap junctions in horizontal cell dendrites was demonstrated, revealing distinct tracer coupling of HCs between the dorsal and ventral retina (see results in the attached article). In the ventral retina, the reduction of Cx57-positive plaques was observed, along with significant structural changes in ZO-1 arrangement, including a loss of string-like plaques and reduced colocalization with Cx57. These results provide evidence that both synaptic components are differently distributed across the mouse retina, particularly beneath the cone pedicle at the desmosome-like junctions. Immunoreactivity quantifications and colocalization analyses were restricted to the area below the cone pedicle, where horizontal cells dendrites converge to form the terminal cluster. However, it's important to note that a negligible amount of axonal Cx57 might have been included in the measurements. The ZO-1 asymmetry was less pronounced than that of Cx57, likely due to the association of ZO-1 with Cx36-containing gap junctions at OFF-bipolar cells dendritic tips at the flat contacts with the pedicle (Feigenspan et al., 2004; Puller et al., 2009). While no documented increase in Cx36 expression in the ventral retina of mice has been reported, a well-documented increase in OFF bipolar cell dendritic density in the ventral retina has been observed (Camerino et al., 2021; Sharpe et al., 2022). This increase in OFF bipolar cell dendrites was also reflected in the ZO-1 quantification analyses performed in this study. Due to the immediate proximity between ZO1/Cx36 and ZO-1/Cx57 expression layers, was hard to exclude the ZO-1 associated with OFF bipolar cells from the quantifications. However, it is surprising that despite the presumed increase in ZO-1 associated with the increase in OFF bipolar cell dendrites at the pedicle base, the dorsal-ventral difference in synaptic components below the cone pedicle is still strongly significant.

The switch in this asymmetry was observed to occur at the S-opsin transition zone, and the staining patterns of ZO-1 and Cx57 were shown to change a few hundred micrometers from the photoreceptor transition. Consequently, a simple division into dorsal and ventral halves based on the relative position to the optic disc, may not be sufficient for studies on whole-mounted retinas because of the functional regionalization of horizontal cell density and synaptic structure beneath the cone pedicle, with the S-opsin transition zone marking the functional boundary throughout its extent.

The reduction of Cx57 was exclusively accompanied by a change in ZO-1, which exhibited a distinct staining pattern characterized by less dense clustering, smaller accumulations, and the absence of the typical elongated plaques beneath and between pedicles. The absence of Cx57 in Cx57-deficient mice had only a slight effect on ZO-1. Additionally, no significant differences were observed in GluA2 expression at desmosome-like junctions between the dorsal and ventral retina. These findings suggest that the structural organization in ZO-1 clustering, driven

by the reduction of Cx57, alongside the preserved GluA2 expression across the retina, points to the intricate relationship between these proteins in maintaining the structural integrity of desmosome-like junctions in the retina. Finally, the strong reduction of both ZO-1 and Cx57 in GluA2-deficient mice hints at a multi-tasking role for ZO-1, potentially coordinating multiple aspects of junctional organization and stability. Specifically, GluA2 expression at the desmosome-like junctions may play a central role in the formation of these structures beneath the cone pedicle. Furthermore, the possible regulation of ZO-1 in conducting or support gap junction permeability via local calcium-dependent modulation or via global neuromodulation may be a consequence of this process.

5.5 Conclusion and focus points

The findings presented in this study highlight a conserved synaptic architecture beneath the cone pedicle at desmosome-like junctions across various mammalian species. Key features, such as the role of ZO-1 and the spatial organization of gap junctions and glutamate receptors in the outer plexiform layer, have been consistently observed in the retinas of mice, rabbits, and primates. This research dives deeper into the characteristics of the desmosome-like junctions in the mouse retina, addressing previously unresolved questions. While many findings align with those observed in other species, such as the overall synaptic architecture at the cone pedicle, unique aspects, like the asymmetric distribution of Cx57, appear to be adaptations specific to the natural environment of the mouse. This suggests a fundamental functional system shared among mammals, which is then tailored in a species-specific manner to neural circuitry and the visual field demands. Nevertheless, several questions remain open, particularly regarding the mechanisms that orchestrate these synaptic architectures and the synergistic effects of neuromodulators and calcium-dependent modulations. Exploring the calcium permeability of AMPAR subunits, calcium regulation in horizontal cells and its effects on gap junction permeability, as well as the differential impact on the synaptic architecture of dendrites versus axon terminals, alongside the modulatory role of neuromodulators, could offer valuable insights into the functional diversity of horizontal cell circuits in the retina. Particular attention could also be given to the role of ZO-1 in regulating and supporting synaptic function, particularly at S-cone synapses. Together, these analyses would deepen our understanding of the complex mechanisms underlying retinal signal processing.

6. References

- Abbe E (1873) Beiträge zur Theorie des Mikroskops und der mikroskopischen Wahrnehmung. *Arch für Mikroskopische Anat* 9:413–468 Available at: <http://link.springer.com/10.1007/BF02956173>.
- Alev C, Urschel S, Sonntag S, Zoidl G, Fort AG, Höher T, Matsubara M, Willecke K, Spray DC, Dermietzel R (2008) The neuronal connexin36 interacts with and is phosphorylated by CaMKII in a way similar to CaMKII interaction with glutamate receptors. *Proc Natl Acad Sci* 105:20964–20969 Available at: <https://pnas.org/doi/full/10.1073/pnas.0805408105>.
- Applebury M., Antoch M., Baxter L., Chun LL., Falk J., Farhangfar F, Kage K, Krzystolik M., Lyass L., Robbins J. (2000) The Murine Cone Photoreceptor. *Neuron* 27:513–523 Available at: <https://linkinghub.elsevier.com/retrieve/pii/S0896627300000623>.
- Arai I, Tanaka M, Tachibana M (2010) Active Roles of Electrically Coupled Bipolar Cell Network in the Adult Retina. *J Neurosci* 30:9260–9270 Available at: <https://www.jneurosci.org/lookup/doi/10.1523/JNEUROSCI.1590-10.2010>.
- Baden T, Euler T, Berens P (2020) Understanding the retinal basis of vision across species. *Nat Rev Neurosci* 21:5–20 Available at: <http://dx.doi.org/10.1038/s41583-019-0242-1>.
- Baden T, Schubert T, Chang L, Wei T, Zaichuk M, Wissinger B, Euler T (2013) A Tale of Two Retinal Domains: Near-Optimal Sampling of Achromatic Contrasts in Natural Scenes through Asymmetric Photoreceptor Distribution. *Neuron* 80:1206–1217 Available at: <https://linkinghub.elsevier.com/retrieve/pii/S0896627313008611>.
- Baldrige WH (2001) Triphasic adaptation of teleost horizontal cells. *Prog Brain Res* 131:437–449 Available at: <http://www.ncbi.nlm.nih.gov/pubmed/11420961>.
- Baldrige WH, Ball AK, Miller RG (1987) Dopaminergic regulation of horizontal cell gap junction particle density in goldfish retina. *J Comp Neurol* 265:428–436 Available at: <https://onlinelibrary.wiley.com/doi/10.1002/cne.902650310>.
- Barbour B, Häusser M (1997) Intersynaptic diffusion of neurotransmitter. *Trends Neurosci* 20:377–384 Available at: <http://www.ncbi.nlm.nih.gov/pubmed/9292962>.
- Baude A, Nusser Z, Molnar E, McIlhinney RAJ, Somogyi P (1995) High-resolution immunogold localization of AMPA type glutamate receptor subunits at synaptic and non-synaptic sites in rat hippocampus. *Neuroscience* 69:1031–1055 Available at: <https://linkinghub.elsevier.com/retrieve/pii/030645229500350R>.
- Baylor DA, Lamb TD, Yau KW (1979) Responses of retinal rods to single photons. *J Physiol* 288:613–634 Available at: <https://physoc.onlinelibrary.wiley.com/doi/10.1113/jphysiol.1979.sp012716>.
- Behrens C, Schubert T, Haverkamp S, Euler T, Berens P (2016) Connectivity map of bipolar cells and photoreceptors in the mouse retina. *Elife* 5:1–20 Available at: <https://elifesciences.org/articles/20041>.
- Berglund K, Schleich W, Krieger P, Loo LS, Wang D, Cant NB, Feng G, Augustine GJ, Kuner T (2006) Imaging synaptic inhibition in transgenic mice expressing the chloride indicator, Clomeleon. *Brain Cell Biol* 35:207–228 Available at: <http://link.springer.com/10.1007/s11068-008-9019-6>.
- Bhattacharya R, Sinha S, Yang S-P, Patra C, Dutta S, Wang E, Mukhopadhyay D (2008) The neurotransmitter dopamine modulates vascular permeability in the endothelium. *J Mol Signal* 3:14 Available at: <http://www.jmolecularsignaling.com/articles/10.1186/1750-2187-3-14/>.
- Blanks JC, Johnson L V. (1984) Specific binding of peanut lectin to a class of retinal photoreceptor cells. A species comparison. *Invest Ophthalmol Vis Sci* 25:546–557 Available at: <http://www.ncbi.nlm.nih.gov/pubmed/6715128>.
- Bloomfield SA, Völgyi B (2009) The diverse functional roles and regulation of neuronal gap junctions in the retina. *Nat Rev Neurosci* 10:495–506 Available at: <https://www.nature.com/articles/nrn2636>.

- Bloomfield SA, Xin D, Persky SE (1995) A comparison of receptive field and tracer coupling size of horizontal cells in the rabbit retina. *Vis Neurosci* 12:985–999 Available at: https://www.cambridge.org/core/product/identifier/S0952523800009524/type/journal_article.
- Boije H, Shirazi Fard S, Edqvist P-H, Hallböök F (2016) Horizontal Cells, the Odd Ones Out in the Retina, Give Insights into Development and Disease. *Front Neuroanat* 10:1–12 Available at: <http://journal.frontiersin.org/Article/10.3389/fnana.2016.00077/abstract>.
- Bolte S, Cordelières FP (2006) A guided tour into subcellular colocalization analysis in light microscopy. *J Microsc* 224:213–232 Available at: <https://onlinelibrary.wiley.com/doi/10.1111/j.1365-2818.2006.01706.x>.
- Boulter J, Hollmann M, O’Shea-Greenfield A, Hartley M, Deneris E, Maron C, Heinemann S (1990) Molecular Cloning and Functional Expression of Glutamate Receptor Subunit Genes. *Science* (80-) 249:1033–1037 Available at: <https://www.science.org/doi/10.1126/science.2168579>.
- Brandstätter JH, Koulen P, Wässle H (1997) Selective Synaptic Distribution of Kainate Receptor Subunits in the Two Plexiform Layers of the Rat Retina. *J Neurosci* 17:9298–9307 Available at: <https://www.jneurosci.org/lookup/doi/10.1523/JNEUROSCI.17-23-09298.1997>.
- Breuninger T, Puller C, Haverkamp S, Euler T (2011) Chromatic Bipolar Cell Pathways in the Mouse Retina. *J Neurosci* 31:6504–6517 Available at: <https://www.jneurosci.org/lookup/doi/10.1523/JNEUROSCI.0616-11.2011>.
- Burnett R (1997) Immunohistochemistry for light microscopy in safety evaluation of therapeutic agents: an overview. *Toxicology* 119:83–93 Available at: <https://linkinghub.elsevier.com/retrieve/pii/S0300483X96036001>.
- Camerino MJ, Engerbretson IJ, Fife PA, Reynolds NB, Berria MH, Doyle JR, Clemons MR, Gencarella MD, Borghuis BG, Fuerst PG (2021) OFF bipolar cell density varies by subtype, eccentricity, and along the dorsal ventral axis in the mouse retina. *J Comp Neurol* 529:1911–1925 Available at: <https://onlinelibrary.wiley.com/doi/10.1002/cne.25064>.
- Casimiro TM, Nawy S, Carroll RC (2013) Molecular mechanisms underlying activity-dependent AMPA receptor cycling in retinal ganglion cells. *Mol Cell Neurosci* 56:384–392 Available at: <http://dx.doi.org/10.1016/j.mcn.2013.07.010>.
- Chang L, Breuninger T, Euler T (2013) Chromatic Coding from Cone-type Unselective Circuits in the Mouse Retina. *Neuron* 77:559–571 Available at: <http://dx.doi.org/10.1016/j.neuron.2012.12.012>.
- Chaya T, Matsumoto A, Sugita Y, Watanabe S, Kuwahara R, Tachibana M, Furukawa T (2017) Versatile functional roles of horizontal cells in the retinal circuit. *Sci Rep* 7:1–15 Available at: <http://dx.doi.org/10.1038/s41598-017-05543-2>.
- Church J, Baimbridge K (1991) Exposure to high-pH medium increases the incidence and extent of dye coupling between rat hippocampal CA1 pyramidal neurons in vitro. *J Neurosci* 11:3289–3295 Available at: <https://www.jneurosci.org/lookup/doi/10.1523/JNEUROSCI.11-10-03289.1991>.
- Ciolofan C, Li X-B, Olson C, Kamasawa N, Gebhardt BR, Yasumura T, Morita M, Rash JE, Nagy JI (2006) Association of connexin36 and zonula occludens-1 with zonula occludens-2 and the transcription factor zonula occludens-1-associated nucleic acid-binding protein at neuronal gap junctions in rodent retina. *Neuroscience* 140:433–451 Available at: <https://linkinghub.elsevier.com/retrieve/pii/S0306452206002144>.
- Ciolofan C, Lynn BD, Wellershaus K, Willecke K, Nagy JI (2007) Spatial relationships of connexin36, connexin57 and zonula occludens-1 in the outer plexiform layer of mouse retina. *Neuroscience* 148:473–488 Available at: <https://linkinghub.elsevier.com/retrieve/pii/S0306452207007397>.
- Ciruela F (2008) Fluorescence-based methods in the study of protein–protein interactions in living cells. *Curr Opin Biotechnol* 19:338–343 Available at: <https://linkinghub.elsevier.com/retrieve/pii/S0958166908000712>.
- Collingridge GL, Olsen RW, Peters J, Spedding M (2009) A nomenclature for ligand-gated ion channels. *Neuropharmacology* 56:2–5 Available at: <https://linkinghub.elsevier.com/retrieve/pii/S0028390808002293>.

- Collins TJ (2007) ImageJ for microscopy. *Biotechniques* 43:S25–S30 Available at: <http://www.ncbi.nlm.nih.gov/pubmed/17936939>.
- Cote R (2006) Photoreceptor Phosphodiesterase (PDE6). In: *Cyclic Nucleotide Phosphodiesterases in Health and Disease*. CRC Press. Available at: <https://www.taylorfrancis.com/chapters/edit/10.1201/9781420020847-8/>.
- Curti S, Pereda AE (2004) Voltage-Dependent Enhancement of Electrical Coupling by a Subthreshold Sodium Current. *J Neurosci* 24:3999–4010 Available at: <https://www.jneurosci.org/lookup/doi/10.1523/JNEUROSCI.0077-04.2004>.
- Dacey DM, Lee BB, Stafford DK, Pokorny J, Smith VC (1996) Horizontal Cells of the Primate Retina: Cone Specificity Without Spectral Opponency. *Science* (80-) 271:656–659 Available at: <https://www.science.org/doi/10.1126/science.271.5249.656>.
- Dacheux RF, Raviola E (1982) Horizontal cells in the retina of the rabbit. *J Neurosci* 2:1486–1493 Available at: <https://www.jneurosci.org/lookup/doi/10.1523/JNEUROSCI.02-10-01486.1982>.
- Datta R, Heaster TM, Sharick JT, Gillette AA, Skala MC (2020) Fluorescence lifetime imaging microscopy: fundamentals and advances in instrumentation, analysis, and applications. *J Biomed Opt* 25:1 Available at: <https://www.spiedigitallibrary.org/journals/journal-of-biomedical-optics/volume-25/issue-07/071203/Fluorescence-lifetime-imaging-microscopy--fundamentals-and-advances-in-instrumentation/10.1117/1.JBO.25.7.071203.full>.
- Della Santina L, Kuo SP, Yoshimatsu T, Okawa H, Suzuki SC, Hoon M, Tsuboyama K, Rieke F, Wong ROL (2016) Glutamatergic Monopolar Interneurons Provide a Novel Pathway of Excitation in the Mouse Retina. *Curr Biol* 26:2070–2077 Available at: <https://linkinghub.elsevier.com/retrieve/pii/S0960982216306558>.
- Derkach V, Barria A, Soderling TR (1999) Ca²⁺/calmodulin-kinase II enhances channel conductance of α -amino-3-hydroxy-5-methyl-4-isoxazolepropionate type glutamate receptors. *Proc Natl Acad Sci* 96:3269–3274 Available at: <https://pnas.org/doi/full/10.1073/pnas.96.6.3269>.
- Derkach VA, Oh MC, Guire ES, Soderling TR (2007) Regulatory mechanisms of AMPA receptors in synaptic plasticity. *Nat Rev Neurosci* 8:101–113 Available at: <https://www.nature.com/articles/nrn2055>.
- DeVries SH (2000) Bipolar Cells Use Kainate and AMPA Receptors to Filter Visual Information into Separate Channels. *Neuron* 28:847–856 Available at: <https://linkinghub.elsevier.com/retrieve/pii/S0896627300001586>.
- DeVries SH, Qi X, Smith R, Makous W, Sterling P (2002) Electrical Coupling between Mammalian Cones. *Curr Biol* 12:1900–1907 Available at: <https://linkinghub.elsevier.com/retrieve/pii/S0960982202012617>.
- DeVries SH, Schwartz EA (1999) Kainate receptors mediate synaptic transmission between cones and 'Off' bipolar cells in a mammalian retina. *Nature* 397:157–160 Available at: <https://www.nature.com/articles/16462>.
- Dhande OS, Stafford BK, Lim J-HA, Huberman AD (2015) Contributions of Retinal Ganglion Cells to Subcortical Visual Processing and Behaviors. *Annu Rev Vis Sci* 1:291–328 Available at: <https://www.annualreviews.org/doi/10.1146/annurev-vision-082114-035502>.
- Diamond JS (2017) Inhibitory Interneurons in the Retina: Types, Circuitry, and Function. *Annu Rev Vis Sci* 3:1–24 Available at: <https://www.annualreviews.org/doi/10.1146/annurev-vision-102016-061345>.
- Dingledine R, Borges K, Bowie D, Traynelis SF (1999) The glutamate receptor ion channels. *Pharmacol Rev* 51:7–61 Available at: <http://www.ncbi.nlm.nih.gov/pubmed/10049997>.
- Dong H, O'Brien RJ, Fung ET, Lanahan AA, Worley PF, Huganir RL (1997) GRIP: a synaptic PDZ domain-containing protein that interacts with AMPA receptors. *Nature* 386:279–284 Available at: <https://www.nature.com/articles/386279a0>.

- Dorgau B, Herrling R, Schultz K, Greb H, Segelken J, Ströh S, Bolte P, Weiler R, Dedek K, Janssen-Bienhold U (2015) Connexin50 couples axon terminals of mouse horizontal cells by homotypic gap junctions. *J Comp Neurol* 523:2062–2081 Available at: <https://onlinelibrary.wiley.com/doi/10.1002/cne.23779>.
- Dowling JE (1991) Retinal neuromodulation: The role of dopamine. *Vis Neurosci* 7:87–97 Available at: https://www.cambridge.org/core/product/identifier/S0952523800010968/type/journal_article.
- Dowling JE, Boycott BB (1965) Neural Connections of the Retina: Fine Structure of the Inner Plexiform Layer. *Cold Spring Harb Symp Quant Biol* 30:393–402 Available at: <http://symposium.cshlp.org/cgi/doi/10.1101/SQB.1965.030.01.039>.
- Dowling JE, Boycott BB (1966) Organization of the primate retina: electron microscopy. *Proc R Soc London Ser B, Biol Sci* 166:80–111 Available at: <https://royalsocietypublishing.org/doi/10.1098/rspb.1966.0086>.
- Dowling JE, Brown JE, Major D (1966) Synapses of horizontal cells in rabbit and cat retinas. *Science* 153:1639–1641 Available at: <https://www.science.org/doi/10.1126/science.153.3744.1639>.
- Dräger UC, Olsen JF (1981) Ganglion cell distribution in the retina of the mouse. *Invest Ophthalmol Vis Sci* 20:285–293 Available at: <http://www.ncbi.nlm.nih.gov/pubmed/6162818>.
- Drinnenberg A, Franke F, Morikawa RK, Jüttner J, Hillier D, Hantz P, Hierlemann A, Azeredo da Silveira R, Roska B (2018) How Diverse Retinal Functions Arise from Feedback at the First Visual Synapse. *Neuron* 99:117–134.e11 Available at: <https://linkinghub.elsevier.com/retrieve/pii/S0896627318304690>.
- Duda S, Block CT, Pradhan DR, Arzhangnia Y, Greschner M, Puller C (2023) Spatial distribution and functional integration of displaced ipRGCs. *bioRxiv:2023.09.05.556383* Available at: <http://biorxiv.org/content/early/2023/09/05/2023.09.05.556383.abstract>.
- Duebel J, Haverkamp S, Schleich W, Feng G, Augustine GJ, Kuner T, Euler T (2006) Two-Photon Imaging Reveals Somatodendritic Chloride Gradient in Retinal ON-Type Bipolar Cells Expressing the Biosensor Clomeleon. *Neuron* 49:81–94 Available at: <https://linkinghub.elsevier.com/retrieve/pii/S089662730500958X>.
- Dunn KW, Kamocka MM, McDonald JH (2011) A practical guide to evaluating colocalization in biological microscopy. *Am J Physiol Physiol* 300:C723–C742 Available at: <https://journals.physiology.org/doi/10.1152/ajpcell.00462.2010>.
- Euler T, Haverkamp S, Schubert T, Baden T (2014) Retinal bipolar cells: elementary building blocks of vision. *Nat Rev Neurosci* 15:507–519 Available at: <https://www.nature.com/articles/nrn3783>.
- Evans WH, Martin PEM (2002) Gap junctions: structure and function (Review). *Mol Membr Biol* 19:121–136 Available at: <http://www.tandfonline.com/doi/full/10.1080/09687680210139839>.
- Faber DS, Pereda AE (2018) Two Forms of Electrical Transmission Between Neurons. *Front Mol Neurosci* 11:1–11 Available at: <https://www.frontiersin.org/article/10.3389/fnmol.2018.00427/full>.
- Fahey PK, Burkhardt DA (2003) Center-surround organization in bipolar cells: symmetry for opposing contrasts. *Vis Neurosci* 20:1–10 Available at: https://www.cambridge.org/core/product/identifier/S0952523803201012/type/journal_article.
- Fanning AS, Jameson BJ, Jesaitis LA, Anderson JM (1998) The Tight Junction Protein ZO-1 Establishes a Link between the Transmembrane Protein Occludin and the Actin Cytoskeleton. *J Biol Chem* 273:29745–29753 Available at: <https://linkinghub.elsevier.com/retrieve/pii/S0021925819593772>.
- Feigenspan A, Babai N (2015) Functional properties of spontaneous excitatory currents and encoding of light/dark transitions in horizontal cells of the mouse retina. *Eur J Neurosci* 42:2615–2632 Available at: <https://onlinelibrary.wiley.com/doi/10.1111/ejn.13016>.

- Feigenspan A, Janssen-Bienhold U, Hormuzdi S, Monyer H, Degen J, Söhl G, Willecke K, Ammermüller J, Weiler R (2004) Expression of Connexin36 in Cone Pedicles and OFF-Cone Bipolar Cells of the Mouse Retina. *J Neurosci* 24:3325–3334 Available at: <https://www.jneurosci.org/lookup/doi/10.1523/JNEUROSCI.5598-03.2004>.
- Ferguson LR, Dominguez II JM, Balaiya S, Grover S, Chalam K V. (2013) Retinal Thickness Normative Data in Wild-Type Mice Using Customized Miniature SD-OCT Viloslada P, ed. *PLoS One* 8:e67265 Available at: <https://dx.plos.org/10.1371/journal.pone.0067265>.
- Ferguson LR, Grover S, Dominguez II JM, Balaiya S, Chalam K V. (2014) Retinal Thickness Measurement Obtained with Spectral Domain Optical Coherence Tomography Assisted Optical Biopsy Accurately Correlates with Ex Vivo Histology Stieger K, ed. *PLoS One* 9:e111203 Available at: <https://dx.plos.org/10.1371/journal.pone.0111203>.
- Flores CE, Cachepe R, Nannapaneni S, Ene S, Nairn AC, Pereda AE (2010) Variability of Distribution of Ca²⁺/Calmodulin-Dependent Kinase II at Mixed Synapses on the Mauthner Cell: Colocalization and Association with Connexin 35. *J Neurosci* 30:9488–9499 Available at: <https://www.jneurosci.org/lookup/doi/10.1523/JNEUROSCI.4466-09.2010>.
- Flores CE, Li X, Bennett MVL, Nagy JI, Pereda AE (2008) Interaction between connexin35 and zonula occludens-1 and its potential role in the regulation of electrical synapses. *Proc Natl Acad Sci* 105:12545–12550 Available at: <https://pnas.org/doi/full/10.1073/pnas.0804793105>.
- Fournel R, Hartveit E, Veruki ML (2021) Differential Contribution of Gap Junctions to the Membrane Properties of ON- and OFF-Bipolar Cells of the Rat Retina. *Cell Mol Neurobiol* 41:229–245 Available at: <https://link.springer.com/10.1007/s10571-020-00845-y>.
- Franke K, Berens P, Schubert T, Bethge M, Euler T, Baden T (2017) Inhibition decorrelates visual feature representations in the inner retina. *Nature* 542:439–444 Available at: <http://dx.doi.org/10.1038/nature21394>.
- Fu Y, Yau K-W (2007) Phototransduction in mouse rods and cones. *Pflügers Arch - Eur J Physiol* 454:805–819 Available at: <http://link.springer.com/10.1007/s00424-006-0194-y>.
- Fuchs EC, Zivkovic AR, Cunningham MO, Middleton S, LeBeau FEN, Bannerman DM, Rozov A, Whittington MA, Traub RD, Rawlins JNP, Monyer H (2007) Recruitment of Parvalbumin-Positive Interneurons Determines Hippocampal Function and Associated Behavior. *Neuron* 53:591–604 Available at: <https://linkinghub.elsevier.com/retrieve/pii/S0896627307000724>.
- Ghosh KK, Haverkamp S, Wässle H (2001) Glutamate Receptors in the Rod Pathway of the Mammalian Retina. *J Neurosci* 21:8636–8647 Available at: <https://www.jneurosci.org/lookup/doi/10.1523/JNEUROSCI.21-21-08636.2001>.
- Giepmans B (2004) Gap junctions and connexin-interacting proteins. *Cardiovasc Res* 62:233–245 Available at: <https://academic.oup.com/cardiovasces/article-lookup/doi/10.1016/j.cardiores.2003.12.009>.
- González-Mariscal L, Betanzos A, Ávila-Flores A (2000) MAGUK proteins: structure and role in the tight junction. *Semin Cell Dev Biol* 11:315–324 Available at: <https://linkinghub.elsevier.com/retrieve/pii/S1084952100901782>.
- González-Mariscal L, Betanzos A, Nava P, Jaramillo B. (2003) Tight junction proteins. *Prog Biophys Mol Biol* 81:1–44 Available at: <https://linkinghub.elsevier.com/retrieve/pii/S0079610702000378>.
- Goodchild AK, Chan TL, Grünert U (1996) Horizontal cell connections with short-wavelength-sensitive cones in macaque monkey retina. *Vis Neurosci* 13:833–845 Available at: https://www.cambridge.org/core/product/identifier/S0952523800009093/type/journal_article.
- Goodenough DA, Goliger JA, Paul DL (1996) Connexins, connexons, and intercellular communication. *Annu Rev Biochem* 65:475–502 Available at: <https://www.annualreviews.org/doi/10.1146/annurev.bi.65.070196.002355>.
- Greferath U, Grünert U, Müller F, Wässle H (1994) Localization of GABAA receptors in the rabbit retina. *Cell Tissue Res* 276:295–307 Available at: <http://link.springer.com/10.1007/BF00306115>.

- Greger IH, Khatri L, Ziff EB (2002) RNA Editing at Arg607 Controls AMPA Receptor Exit from the Endoplasmic Reticulum. *Neuron* 34:759–772 Available at: <https://linkinghub.elsevier.com/retrieve/pii/S0896627302006931>.
- Greger IH, Watson JF, Cull-Candy SG (2017) Structural and Functional Architecture of AMPA-Type Glutamate Receptors and Their Auxiliary Proteins. *Neuron* 94:713–730 Available at: <http://dx.doi.org/10.1016/j.neuron.2017.04.009>.
- Grove JCR, Hirano AA, de Los Santos J, McHugh CF, Purohit S, Field GD, Brecha NC, Barnes S (2019) Novel hybrid action of GABA mediates inhibitory feedback in the mammalian retina. *PLoS Biol* 17:e3000200 Available at: <https://dx.plos.org/10.1371/journal.pbio.3000200>.
- Gumbiner BM (1996) Cell Adhesion: The Molecular Basis of Tissue Architecture and Morphogenesis. *Cell* 84:345–357 Available at: <https://linkinghub.elsevier.com/retrieve/pii/S0092867400812799>.
- Guo C, Ma Y-Y (2021) Calcium Permeable-AMPA Receptors and Excitotoxicity in Neurological Disorders. *Front Neural Circuits* 15:1–14 Available at: <https://www.frontiersin.org/articles/10.3389/fncir.2021.711564/full>.
- Gupta D, Młynarski W, Sumser A, Symonova O, Svatoň J, Joesch M (2023) Panoramic visual statistics shape retina-wide organization of receptive fields. *Nat Neurosci* 26:606–614 Available at: <https://www.nature.com/articles/s41593-023-01280-0>.
- Gustafsson MGL (2005) Nonlinear structured-illumination microscopy: Wide-field fluorescence imaging with theoretically unlimited resolution. *Proc Natl Acad Sci* 102:13081–13086 Available at: <https://pnas.org/doi/full/10.1073/pnas.0406877102>.
- Hack I, Frech M, Dick O, Peichl L, Brandstätter JH (2001) Heterogeneous distribution of AMPA glutamate receptor subunits at the photoreceptor synapses of rodent retina. *Eur J Neurosci* 13:15–24 Available at: <https://onlinelibrary.wiley.com/doi/10.1111/j.1460-9568.2001.01357.x>.
- Hampson EC, Weiler R, Vaney DI (1994) pH-gated dopaminergic modulation of horizontal cell gap junctions in mammalian retina. *Proceedings Biol Sci* 255:67–72 Available at: <https://royalsocietypublishing.org/doi/10.1098/rspb.1994.0010>.
- Hartsock A, Nelson WJ (2008) Adherens and tight junctions: Structure, function and connections to the actin cytoskeleton. *Biochim Biophys Acta - Biomembr* 1778:660–669 Available at: <https://linkinghub.elsevier.com/retrieve/pii/S0005273607002714>.
- Haverkamp S, Ghosh KK, Hirano AA, Wässle H (2003) Immunocytochemical description of five bipolar cell types of the mouse retina. *J Comp Neurol* 455:463–476 Available at: <https://onlinelibrary.wiley.com/doi/10.1002/cne.10491>.
- Haverkamp S, Grünert U, Wässle H (2000) The Cone Pedicle, a Complex Synapse in the Retina. *Neuron* 27:85–95 Available at: <https://linkinghub.elsevier.com/retrieve/pii/S0896627300000118>.
- Haverkamp S, Grünert U, Wässle H (2001a) The Synaptic Architecture of AMPA Receptors at the Cone Pedicle of the Primate Retina. *J Neurosci* 21:2488–2500 Available at: <https://www.jneurosci.org/lookup/doi/10.1523/JNEUROSCI.21-07-02488.2001>.
- Haverkamp S, Grünert U, Wässle H (2001b) Localization of kainate receptors at the cone pedicles of the primate retina. *J Comp Neurol* 436:471–486 Available at: <https://onlinelibrary.wiley.com/doi/10.1002/cne.1081>.
- Haverkamp S, Specht D, Majumdar S, Zaidi NF, Brandstätter JH, Wasco W, Wässle H, tom Dieck S (2008) Type 4 OFF cone bipolar cells of the mouse retina express calsenilin and contact cones as well as rods. *J Comp Neurol* 507:1087–1101 Available at: <https://onlinelibrary.wiley.com/doi/10.1002/cne.21612>.
- Haverkamp S, Wässle H (2000) Immunocytochemical analysis of the mouse retina. *J Comp Neurol* 424:1–23 Available at: [https://onlinelibrary.wiley.com/doi/10.1002/1096-9861\(20000814\)424:1%3C1::AID-CNE1%3E3.0.CO;2-V](https://onlinelibrary.wiley.com/doi/10.1002/1096-9861(20000814)424:1%3C1::AID-CNE1%3E3.0.CO;2-V).

- Haverkamp S, Wässle H, Duebel J, Kuner T, Augustine GJ, Feng G, Euler T (2005) The Primordial, Blue-Cone Color System of the Mouse Retina. *J Neurosci* 25:5438–5445 Available at: <https://www.jneurosci.org/lookup/doi/10.1523/JNEUROSCI.1117-05.2005>.
- He S, Weiler R, Vaney DI (2000) Endogenous dopaminergic regulation of horizontal cell coupling in the mammalian retina. *J Comp Neurol* 418:33–40 Available at: [https://onlinelibrary.wiley.com/doi/10.1002/\(SICI\)1096-9861\(20000228\)418:1%3C33::AID-CNE3%3E3.0.CO;2-J](https://onlinelibrary.wiley.com/doi/10.1002/(SICI)1096-9861(20000228)418:1%3C33::AID-CNE3%3E3.0.CO;2-J).
- Hell SW, Wichmann J (1994) Breaking the diffraction resolution limit by stimulated emission: stimulated-emission-depletion fluorescence microscopy. *Opt Lett* 19:780 Available at: <https://opg.optica.org/abstract.cfm?URI=ol-19-11-780>.
- Hess ST, Girirajan TPK, Mason MD (2006) Ultra-High Resolution Imaging by Fluorescence Photoactivation Localization Microscopy. *Biophys J* 91:4258–4272 Available at: <https://linkinghub.elsevier.com/retrieve/pii/S0006349506721403>.
- Heukamp AS, Warwick RA, Rivlin-Etzion M (2020) Topographic Variations in Retinal Encoding of Visual Space. *Annu Rev Vis Sci* 6:237–259 Available at: <https://www.annualreviews.org/doi/10.1146/annurev-vision-121219-081831>.
- Hilgen G, von Maltzahn J, Willecke K, Weiler R, Dedek K (2011) Subcellular distribution of connexin45 in OFF bipolar cells of the mouse retina. *J Comp Neurol* 519:433–450 Available at: <https://onlinelibrary.wiley.com/doi/10.1002/cne.22526>.
- Hirasawa H, Kaneko A (2003) pH Changes in the Invaginating Synaptic Cleft Mediate Feedback from Horizontal Cells to Cone Photoreceptors by Modulating Ca²⁺ Channels. *J Gen Physiol* 122:657–671 Available at: <https://rupress.org/jgp/article/122/6/657/44345/pH-Changes-in-the-Invaginating-Synaptic-Cleft>.
- Hollmann M, Heinemann S (1994) Cloned Glutamate Receptors. *Annu Rev Neurosci* 17:31–108 Available at: <http://neuro.annualreviews.org/cgi/doi/10.1146/annurev.neuro.17.1.31>.
- Hombach S, Janssen-Bienhold U, Söhl G, Schubert T, Büssow H, Ott T, Weiler R, Willecke K (2004) Functional expression of connexin57 in horizontal cells of the mouse retina. *Eur J Neurosci* 19:2633–2640 Available at: <https://onlinelibrary.wiley.com/doi/10.1111/j.0953-816X.2004.03360.x>.
- Hornstein EP, Verweij J, Li PH, Schnapf JL (2005) Gap-Junctional Coupling and Absolute Sensitivity of Photoreceptors in Macaque Retina. *J Neurosci* 25:11201–11209 Available at: <https://www.jneurosci.org/lookup/doi/10.1523/JNEUROSCI.3416-05.2005>.
- Huang B, Babcock H, Zhuang X (2010) Breaking the Diffraction Barrier: Super-Resolution Imaging of Cells. *Cell* 143:1047–1058 Available at: <https://linkinghub.elsevier.com/retrieve/pii/S0092867410014200>.
- Hunter AW, Barker RJ, Zhu C, Gourdie RG (2005) Zonula Occludens-1 Alters Connexin43 Gap Junction Size and Organization by Influencing Channel Accretion. *Mol Biol Cell* 16:5686–5698 Available at: <https://www.molbiolcell.org/doi/10.1091/mbc.e05-08-0737>.
- Ingram NT, Sampath AP, Fain GL (2016) Why are rods more sensitive than cones? *J Physiol* 594:5415–5426 Available at: <https://physoc.onlinelibrary.wiley.com/doi/10.1113/JP272556>.
- Ishibashi M, Keung J, Morgans CW, Aicher SA, Carroll JR, Singer JH, Jia L, Li W, Fahrenfort I, Ribelayga CP, Massey SC (2022) Analysis of rod/cone gap junctions from the reconstruction of mouse photoreceptor terminals. *Elife* 11:1–41 Available at: <https://elifesciences.org/articles/73039>.
- Iuvone PM, Galli CL, Garrison-Gund CK, Neff NH (1978) Light Stimulates Tyrosine Hydroxylase Activity and Dopamine Synthesis in Retinal Amacrine Neurons. *Science* (80-) 202:901–902 Available at: <https://www.science.org/doi/10.1126/science.30997>.
- Jabeen S, Thirumalai V (2018) The interplay between electrical and chemical synaptogenesis. *J Neurophysiol* 120:1914–1922 Available at: <https://www.physiology.org/doi/10.1152/jn.00398.2018>.

- Jackman SL, Babai N, Chambers JJ, Thoreson WB, Kramer RH (2011) A Positive Feedback Synapse from Retinal Horizontal Cells to Cone Photoreceptors Rieke F, ed. *PLoS Biol* 9:e1001057 Available at: <https://dx.plos.org/10.1371/journal.pbio.1001057>.
- Jacobs GH (1993) The distribution and nature of colour vision among the mammals. *Biol Rev Camb Philos Soc* 68:413–471 Available at: <https://onlinelibrary.wiley.com/doi/10.1111/j.1469-185X.1993.tb00738.x>.
- Jacobs GH (2009) Evolution of colour vision in mammals. *Philos Trans R Soc B Biol Sci* 364:2957–2967 Available at: <https://royalsocietypublishing.org/doi/10.1098/rstb.2009.0039>.
- Jacobs GH, Williams GA, Fenwick JA (2004) Influence of cone pigment coexpression on spectral sensitivity and color vision in the mouse. *Vision Res* 44:1615–1622 Available at: <https://linkinghub.elsevier.com/retrieve/pii/S0042698904000537>.
- Janssen-Bienhold U, Trümppler J, Hilgen G, Schultz K, Müller LPDS, Sonntag S, Dedek K, Dirks P, Willecke K, Weiler R (2009) Connexin57 is expressed in dendro-dendritic and axo-axonal gap junctions of mouse horizontal cells and its distribution is modulated by light. *J Comp Neurol* 513:363–374 Available at: <https://onlinelibrary.wiley.com/doi/10.1002/cne.21965>.
- Jeon C-J, Strettoi E, Masland RH (1998) The Major Cell Populations of the Mouse Retina. *J Neurosci* 18:8936–8946 Available at: <https://www.jneurosci.org/lookup/doi/10.1523/JNEUROSCI.18-21-08936.1998>.
- Jin N, Zhang Z, Keung J, Youn SB, Ishibashi M, Tian L-M, Marshak DW, Solessio E, Umino Y, Fahrenfort I, Kiyama T, Mao C-A, You Y, Wei H, Wu J, Postma F, Paul DL, Massey SC, Ribelayga CP (2020) Molecular and functional architecture of the mouse photoreceptor network. *Sci Adv* 6:eaba7232 Available at: <https://www.science.org/doi/10.1126/sciadv.aba7232>.
- Jin NG, Chuang AZ, Masson PJ, Ribelayga CP (2015) Rod electrical coupling is controlled by a circadian clock and dopamine in mouse retina. *J Physiol* 593:1597–1631 Available at: <https://physoc.onlinelibrary.wiley.com/doi/10.1113/jphysiol.2014.284919>.
- Jin NG, Ribelayga CP (2016) Direct Evidence for Daily Plasticity of Electrical Coupling between Rod Photoreceptors in the Mammalian Retina. *J Neurosci* 36:178–184 Available at: <https://www.jneurosci.org/lookup/doi/10.1523/JNEUROSCI.3301-15.2016>.
- Jonas P, Burnashev N (1995) Molecular mechanisms controlling calcium entry through AMPA-type glutamate receptor channels. *Neuron* 15:987–990 Available at: <https://linkinghub.elsevier.com/retrieve/pii/089662739590087X>.
- Kamasawa N, Furman CS, Davidson KGV, Sampson JA, Magnie AR, Gebhardt BR, Kamasawa M, Yasumura T, Zumbrennen JR, Pickard GE, Nagy JI, Rash JE (2006) Abundance and ultrastructural diversity of neuronal gap junctions in the OFF and ON sublaminae of the inner plexiform layer of rat and mouse retina. *Neuroscience* 142:1093–1117 Available at: <https://linkinghub.elsevier.com/retrieve/pii/S0306452206010670>.
- Kamermans M, Fahrenfort I, Schultz K, Janssen-Bienhold U, Sjoerdsma T, Weiler R (2001) Hemichannel-mediated inhibition in the outer retina. *Science* 292:1178–1180 Available at: <https://www.science.org/doi/10.1126/science.1060101>.
- Kaneko A (1971) Electrical connexions between horizontal cells in the dogfish retina. *J Physiol* 213:95–105 Available at: <https://physoc.onlinelibrary.wiley.com/doi/10.1113/jphysiol.1971.sp009370>.
- Kawahara Y, Ito K, Sun H, Aizawa H, Kanazawa I, Kwak S (2004a) RNA editing and death of motor neurons. *Nature* 427:801–801 Available at: <https://www.nature.com/articles/427801a>.
- Kawahara Y, Ito K, Sun H, Ito M, Kanazawa I, Kwak S (2004b) Regulation of glutamate receptor RNA editing and ADAR mRNA expression in developing human normal and Down's syndrome brains. *Dev Brain Res* 148:151–155 Available at: <https://linkinghub.elsevier.com/retrieve/pii/S016538060300350X>.

- Kawahara Y, Ito K, Sun H, Kanazawa I, Kwak S (2003) Low editing efficiency of GluR2 mRNA is associated with a low relative abundance of ADAR2 mRNA in white matter of normal human brain. *Eur J Neurosci* 18:23–33 Available at: <https://onlinelibrary.wiley.com/doi/10.1046/j.1460-9568.2003.02718.x>.
- Keinänen K, Wisden W, Sommer B, Werner P, Herb A, Verdoorn TA, Sakmann B, Seeburg PH (1990) A Family of AMPA-Selective Glutamate Receptors. *Science* (80-) 249:556–560 Available at: <https://www.science.org/doi/10.1126/science.2166337>.
- Kemmler R, Schultz K, Dedek K, Euler T, Schubert T (2014) Differential Regulation of Cone Calcium Signals by Different Horizontal Cell Feedback Mechanisms in the Mouse Retina. *J Neurosci* 34:11826–11843 Available at: <https://www.jneurosci.org/lookup/doi/10.1523/JNEUROSCI.0272-14.2014>.
- Kennedy MB (1997) The postsynaptic density at glutamatergic synapses. *Trends Neurosci* 20:264–268 Available at: <https://linkinghub.elsevier.com/retrieve/pii/S0166223696010338>.
- Kihara AH, Mantovani de Castro L, Moriscot AS, Hamassaki DE (2006) Prolonged dark adaptation changes connexin expression in the mouse retina. *J Neurosci Res* 83:1331–1341 Available at: <https://onlinelibrary.wiley.com/doi/10.1002/jnr.20815>.
- Kirichenko EY, Skatchkov SN, Ermakov AM (2021) Structure and Functions of Gap Junctions and Their Constituent Connexins in the Mammalian CNS. *Biochem (Moscow), Suppl Ser A Membr Cell Biol* 15:107–119 Available at: <https://link.springer.com/10.1134/S1990747821020069>.
- Klar TA, Hell SW (1999) Subdiffraction resolution in far-field fluorescence microscopy. *Opt Lett* 24:954 Available at: <https://opg.optica.org/abstract.cfm?URI=ol-24-14-954>.
- Kolb H (1977) The organization of the outer plexiform layer in the retina of the cat: electron microscopic observations. *J Neurocytol* 6:131–153 Available at: <http://link.springer.com/10.1007/BF01261502>.
- Kolb H (1997) Amacrine cells of the mammalian retina: Neurocircuitry and functional roles. *Eye* 11:904–923 Available at: <https://www.nature.com/articles/eye1997230>.
- Kolb H (2003) How the Retina Works. *Am Sci* 91:28 Available at: <https://webvision.med.utah.edu/book/part-i-foundations/how-the-retina-works/>.
- Kolb H, Jones J (1984) Synaptic organization of the outer plexiform layer of the turtle retina: an electron microscope study of serial sections. *J Neurocytol* 13:567–591 Available at: <http://link.springer.com/10.1007/BF01148080>.
- Kolb H, Mariani A, Gallego A (1980) A second type of horizontal cell in the monkey retina. *J Comp Neurol* 189:31–44 Available at: <https://onlinelibrary.wiley.com/doi/10.1002/cne.901890103>.
- Kothmann WW, Trexler EB, Whitaker CM, Li W, Massey SC, O'Brien J (2012) Nonsynaptic NMDA Receptors Mediate Activity-Dependent Plasticity of Gap Junctional Coupling in the All Amacrine Cell Network. *J Neurosci* 32:6747–6759 Available at: <https://www.jneurosci.org/lookup/doi/10.1523/JNEUROSCI.5087-11.2012>.
- Koulen P, Fletcher EL, Craven SE, Brecht DS, Wässle H (1998) Immunocytochemical Localization of the Postsynaptic Density Protein PSD-95 in the Mammalian Retina. *J Neurosci* 18:10136–10149 Available at: <https://www.jneurosci.org/lookup/doi/10.1523/JNEUROSCI.18-23-10136.1998>.
- Kramer RH, Davenport CM (2015) Lateral Inhibition in the Vertebrate Retina: The Case of the Missing Neurotransmitter. *PLoS Biol* 13:e1002322 Available at: <https://dx.plos.org/10.1371/journal.pbio.1002322>.
- Kristensen AS, Jenkins MA, Banke TG, Schousboe A, Makino Y, Johnson RC, Haganir R, Traynelis SF (2011) Mechanism of Ca²⁺/calmodulin-dependent kinase II regulation of AMPA receptor gating. *Nat Neurosci* 14:727–735 Available at: <https://www.nature.com/articles/nn.2804>.
- Kumar NM, Gilula NB (1996) The Gap Junction Communication Channel. *Cell* 84:381–388 Available at: <https://linkinghub.elsevier.com/retrieve/pii/S0092867400812829>.

- Laird DW (2006) Life cycle of connexins in health and disease. *Biochem J* 394:527–543 Available at: <https://portlandpress.com/biochemj/article/394/3/527/44068/Life-cycle-of-connexins-in-health-and-disease>.
- Lamb TD, Collin SP, Pugh EN (2007) Evolution of the vertebrate eye: opsins, photoreceptors, retina and eye cup. *Nat Rev Neurosci* 8:960–976 Available at: <https://www.nature.com/articles/nrn2283>.
- Lampe PD, Lau AF (2000) Regulation of Gap Junctions by Phosphorylation of Connexins. *Arch Biochem Biophys* 384:205–215 Available at: <https://linkinghub.elsevier.com/retrieve/pii/S0003986100921313>.
- Lampe PD, Lau AF (2004) The effects of connexin phosphorylation on gap junctional communication. *Int J Biochem Cell Biol* 36:1171–1186 Available at: <https://linkinghub.elsevier.com/retrieve/pii/S1357272503002644>.
- Lasater EM (1987) Retinal horizontal cell gap junctional conductance is modulated by dopamine through a cyclic AMP-dependent protein kinase. *Proc Natl Acad Sci* 84:7319–7323 Available at: <https://pnas.org/doi/full/10.1073/pnas.84.20.7319>.
- Lauf U, Giepmans BNG, Lopez P, Braconnot S, Chen S-C, Falk MM (2002) Dynamic trafficking and delivery of connexons to the plasma membrane and accretion to gap junctions in living cells. *Proc Natl Acad Sci* 99:10446–10451 Available at: <https://pnas.org/doi/full/10.1073/pnas.162055899>.
- Li H, Zhang Z, Blackburn MR, Wang SW, Ribelayga CP, O'Brien J (2013) Adenosine and Dopamine Receptors Coregulate Photoreceptor Coupling via Gap Junction Phosphorylation in Mouse Retina. *J Neurosci* 33:3135–3150 Available at: <https://www.jneurosci.org/lookup/doi/10.1523/JNEUROSCI.2807-12.2013>.
- Li S, Mitchell J, Briggs DJ, Young JK, Long SS, Fuerst PG (2016) Morphological Diversity of the Rod Spherule: A Study of Serially Reconstructed Electron Micrographs Barnes S, ed. *PLoS One* 11:e0150024 Available at: <https://dx.plos.org/10.1371/journal.pone.0150024>.
- Li X, Ionescu A., Lynn B., Lu S, Kamasawa N, Morita M, Davidson KG., Yasumura T, Rash J., Nagy J. (2004a) Connexin47, connexin29 and connexin32 co-expression in oligodendrocytes and cx47 association with zonula occludens-1 (zo-1) in mouse brain. *Neuroscience* 126:611–630 Available at: <https://linkinghub.elsevier.com/retrieve/pii/S0306452204002490>.
- Li X, Kamasawa N, Ciolofan C, Olson CO, Lu S, Davidson KG V., Yasumura T, Shigemoto R, Rash JE, Nagy JI (2008) Connexin45-Containing Neuronal Gap Junctions in Rodent Retina Also Contain Connexin36 in Both Apposing Hemiplaques, Forming Bihomotypic Gap Junctions, with Scaffolding Contributed by Zonula Occludens-1. *J Neurosci* 28:9769–9789 Available at: <https://www.jneurosci.org/lookup/doi/10.1523/JNEUROSCI.2137-08.2008>.
- Li X, Olson C, Lu S, Kamasawa N, Yasumura T, Rash JE, Nagy JI (2004b) Neuronal connexin36 association with zonula occludens-1 protein (ZO-1) in mouse brain and interaction with the first PDZ domain of ZO-1. *Eur J Neurosci* 19:2132–2146 Available at: <https://onlinelibrary.wiley.com/doi/10.1111/j.0953-816X.2004.03283.x>.
- Li X, Olson C, Lu S, Nagy JI (2004c) Association of connexin36 with zonula occludens-1 in HeLa cells, betaTC-3 cells, pancreas, and adrenal gland. *Histochem Cell Biol* 122:485–498 Available at: <http://link.springer.com/10.1007/s00418-004-0718-5>.
- Liu LO, Li G, McCall MA, Cooper NG. (2000) Photoreceptor regulated expression of Ca²⁺/Calmodulin-dependent protein kinase II in the mouse retina. *Mol Brain Res* 82:150–166 Available at: <https://linkinghub.elsevier.com/retrieve/pii/S0169328X00002035>.
- Liu SJ, Zukin RS (2007) Ca²⁺-permeable AMPA receptors in synaptic plasticity and neuronal death. *Trends Neurosci* 30:126–134 Available at: <https://linkinghub.elsevier.com/retrieve/pii/S0166223607000203>.
- Lu C, McMahon DG (1997) Modulation of hybrid bass retinal gap junctional channel gating by nitric oxide. *J Physiol* 499:689–699 Available at: <https://physoc.onlinelibrary.wiley.com/doi/10.1113/jphysiol.1997.sp021961>.

- Lukasiewicz PD (2005) Synaptic mechanisms that shape visual signaling at the inner retina. *Prog Brain Res* 147:205–218 Available at: <https://linkinghub.elsevier.com/retrieve/pii/S0079612304470162>.
- Lynn BD, Li X, Nagy JI (2012) Under Construction: Building the Macromolecular Superstructure and Signaling Components of an Electrical Synapse. *J Membr Biol* 245:303–317 Available at: <http://link.springer.com/10.1007/s00232-012-9451-5>.
- Maeda S, Tsukihara T (2011) Structure of the gap junction channel and its implications for its biological functions. *Cell Mol Life Sci* 68:1115–1129 Available at: <http://link.springer.com/10.1007/s00018-010-0551-z>.
- Malinow R, Malenka RC (2002) AMPA Receptor Trafficking and Synaptic Plasticity. *Annu Rev Neurosci* 25:103–126 Available at: <https://www.annualreviews.org/doi/10.1146/annurev.neuro.25.112701.142758>.
- Marchiafava PL (1978) Horizontal cells influence membrane potential of bipolar cells in the retina of the turtle. *Nature* 275:141–142 Available at: <https://www.nature.com/articles/275141a0>.
- Marco S Di, Protti DA, Solomon SG (2013) Excitatory and inhibitory contributions to receptive fields of alpha-like retinal ganglion cells in mouse. *J Neurophysiol* 110:1426–1440 Available at: <https://www.physiology.org/doi/10.1152/jn.01097.2012>.
- Masland RH (2001) The fundamental plan of the retina. *Nat Neurosci* 4:877–886.
- Masland RH (2012a) The tasks of amacrine cells. *Vis Neurosci* 29:3–9 Available at: https://www.cambridge.org/core/product/identifier/S0952523811000344/type/journal_article.
- Masland RH (2012b) The Neuronal Organization of the Retina. *Neuron* 76:266–280 Available at: <https://linkinghub.elsevier.com/retrieve/pii/S0896627312008835>.
- Masu M, Iwakabe H, Tagawa Y, Miyoshi T, Yamashita M, Fukuda Y, Sasaki H, Hiroi K, Nakamura Y, Shigemoto R, Takada M, Nakamura K, Nakao K, Katsuki M, Nakanishi S (1995) Specific deficit of the ON response in visual transmission by targeted disruption of the mGluR6 gene. *Cell* 80:757–765 Available at: <https://linkinghub.elsevier.com/retrieve/pii/0092867495903542>.
- Mataruga A, Kremmer E, Müller F (2007) Type 3a and type 3b OFF cone bipolar cells provide for the alternative rod pathway in the mouse retina. *J Comp Neurol* 502:1123–1137 Available at: <https://onlinelibrary.wiley.com/doi/10.1002/cne.21367>.
- Matsuuchi L, Naus CC (2013) Gap junction proteins on the move: Connexins, the cytoskeleton and migration. *Biochim Biophys Acta - Biomembr* 1828:94–108 Available at: <https://linkinghub.elsevier.com/retrieve/pii/S0005273612001721>.
- Matthews PM, Pinggera A, Kampjut D, Greger IH (2021) Biology of AMPA receptor interacting proteins - From biogenesis to synaptic plasticity. *Neuropharmacology* 197:108709 Available at: <https://doi.org/10.1016/j.neuropharm.2021.108709>.
- McMahon DG, Schmidt KF (1999) Horizontal cell glutamate receptor modulation by NO: mechanisms and functional implications for the first visual synapse. *Vis Neurosci* 16:425–433 Available at: https://www.cambridge.org/core/product/identifier/S0952523899163041/type/journal_article.
- Meyvis TK, De Smedt SC, Van Oostveldt P, Demeester J (1999) Fluorescence recovery after photobleaching: a versatile tool for mobility and interaction measurements in pharmaceutical research. *Pharm Res* 16:1153–1162 Available at: <http://www.ncbi.nlm.nih.gov/pubmed/10468014>.
- Migdale K, Herr S, Klug K, Ahmad K, Linberg K, Sterling P, Schein S (2003) Two ribbon synaptic units in rod photoreceptors of macaque, human, and cat. *J Comp Neurol* 455:100–112 Available at: <https://onlinelibrary.wiley.com/doi/10.1002/cne.10501>.
- Morgans CW (2000) Neurotransmitter release at ribbon synapses in the retina. *Immunol Cell Biol* 78:442–446 Available at: <https://onlinelibrary.wiley.com/doi/10.1046/j.1440-1711.2000.00923.x>.

- Morgans CW, Brown RL, Duvoisin RM (2010) TRPM1: The endpoint of the mGluR6 signal transduction cascade in retinal ON-bipolar cells. *BioEssays* 32:609–614 Available at: <https://onlinelibrary.wiley.com/doi/10.1002/bies.200900198>.
- Morigiwa K, Vardi N (1999) Differential expression of ionotropic glutamate receptor subunits in the outer retina. *J Comp Neurol* 405:173–184 Available at: [https://onlinelibrary.wiley.com/doi/10.1002/\(SICI\)1096-9861\(19990308\)405:2%3C173::AID-CNE3%3E3.0.CO;2-L](https://onlinelibrary.wiley.com/doi/10.1002/(SICI)1096-9861(19990308)405:2%3C173::AID-CNE3%3E3.0.CO;2-L).
- Nadal-Nicolás FM, Kunze VP, Ball JM, Peng BT, Krishnan A, Zhou G, Dong L, Li W (2020) True S-cones are concentrated in the ventral mouse retina and wired for color detection in the upper visual field. *Elife* 9:1–30 Available at: <https://elifesciences.org/articles/56840>.
- Nikonov SS, Kholodenko R, Lem J, Pugh EN (2006) Physiological Features of the S- and M-cone Photoreceptors of Wild-type Mice from Single-cell Recordings. *J Gen Physiol* 127:359–374 Available at: <https://rupress.org/jgp/article/127/4/359/42618/Physiological-Features-of-the-S-and-M-cone>.
- Nomme J, Fanning AS, Caffrey M, Lye MF, Anderson JM, Lavie A (2011) The Src Homology 3 Domain Is Required for Junctional Adhesion Molecule Binding to the Third PDZ Domain of the Scaffolding Protein ZO-1. *J Biol Chem* 286:43352–43360 Available at: <https://linkinghub.elsevier.com/retrieve/pii/S0021925820870501>.
- Nomura A, Shigemoto R, Nakamura Y, Okamoto N, Mizuno N, Nakanishi S (1994) Developmentally regulated postsynaptic localization of a metabotropic glutamate receptor in rat rod bipolar cells. *Cell* 77:361–369 Available at: <https://linkinghub.elsevier.com/retrieve/pii/0092867494901511>.
- O'Brien J (2014) The ever-changing electrical synapse. *Curr Opin Neurobiol* 29:64–72 Available at: <http://dx.doi.org/10.1016/j.conb.2014.05.011>.
- O'Brien J (2017) Design principles of electrical synaptic plasticity. *Neurosci Lett* 695:4–11 Available at: <https://linkinghub.elsevier.com/retrieve/pii/S0304394017307371>.
- O'Brien J, Bloomfield SA (2018) Plasticity of Retinal Gap Junctions: Roles in Synaptic Physiology and Disease. *Annu Rev Vis Sci* 4:79–100 Available at: <https://www.annualreviews.org/doi/10.1146/annurev-vision-091517-034133>.
- O'Brien JJ, Li W, Pan F, Keung J, O'Brien J, Massey SC (2006) Coupling between A-Type Horizontal Cells Is Mediated by Connexin 50 Gap Junctions in the Rabbit Retina. *J Neurosci* 26:11624–11636 Available at: <https://www.jneurosci.org/lookup/doi/10.1523/JNEUROSCI.2296-06.2006>.
- Ortín-Martínez A, Nadal-Nicolás FM, Jiménez-López M, Albuquerque-Béjar JJ, Nieto-López L, García-Ayuso D, Villegas-Pérez MP, Vidal-Sanz M, Agudo-Barriuso M (2014) Number and Distribution of Mouse Retinal Cone Photoreceptors: Differences between an Albino (Swiss) and a Pigmented (C57/BL6) Strain. *Chidlow G, ed. PLoS One* 9:e102392 Available at: <https://dx.plos.org/10.1371/journal.pone.0102392>.
- Paffenholz R, Kuhn C, Grund C, Stehr S, Franke WW (1999) The Arm-Repeat Protein NPRAP (Neurojungin) Is a Constituent of the Plaques of the Outer Limiting Zone in the Retina, Defining a Novel Type of Adhering Junction. *Exp Cell Res* 250:452–464 Available at: <https://linkinghub.elsevier.com/retrieve/pii/S0014482799945342>.
- Pan F, Keung J, Kim I, Snuggs MB, Mills SL, O'Brien J, Massey SC (2012) Connexin 57 is expressed by the axon terminal network of B-type horizontal cells in the rabbit retina. *J Comp Neurol* 520:2256–2274 Available at: <https://onlinelibrary.wiley.com/doi/10.1002/cne.23060>.
- Pan F, Massey SC (2007) Rod and cone input to horizontal cells in the rabbit retina. *J Comp Neurol* 500:815–831 Available at: <https://onlinelibrary.wiley.com/doi/10.1002/cne.21127>.
- Pan F, Massey SC (2023) Dye coupling of horizontal cells in the primate retina. *Front Ophthalmol* 3:1–17 Available at: <https://www.frontiersin.org/articles/10.3389/fopht.2023.1173706/full>.
- Paris L, Tonutti L, Vannini C, Bazzoni G (2008) Structural organization of the tight junctions. *Biochim Biophys Acta - Biomembr* 1778:646–659 Available at: <https://linkinghub.elsevier.com/retrieve/pii/S0005273607002908>.

- Peichl L (2005) Diversity of mammalian photoreceptor properties: Adaptations to habitat and lifestyle? *Anat Rec Part A Discov Mol Cell Evol Biol* 287A:1001–1012 Available at: <https://anatomypubs.onlinelibrary.wiley.com/doi/10.1002/ar.a.20262>.
- Peichl L (2010) Morphology of Interneurons: Horizontal Cells. In: *Encyclopedia of the Eye*, pp 74–82. Elsevier. Available at: <https://linkinghub.elsevier.com/retrieve/pii/B9780123742032001792>.
- Peichl L, González-Soriano J (1994) Morphological types of horizontal cell in rodent retinae: A comparison of rat, mouse, gerbil, and guinea pig. *Vis Neurosci* 11:501–517 Available at: https://www.cambridge.org/core/product/identifier/S095252380000242X/type/journal_article.
- Peichl L, Sandmann D, Boycott BB (1998) Comparative Anatomy and Function of Mammalian Horizontal Cells. In: *Development and Organization of the Retina*, pp 147–172. Boston, MA: Springer US. Available at: http://link.springer.com/10.1007/978-1-4615-5333-5_9.
- Peracchia C (1978) Calcium effects on gap junction structure and cell coupling. *Nature* 271:669–671 Available at: <https://www.nature.com/articles/271669a0>.
- Peracchia C (2020) Calmodulin-Mediated Regulation of Gap Junction Channels. *Int J Mol Sci* 21:485 Available at: <https://www.mdpi.com/1422-0067/21/2/485>.
- Pereda AE (2014) Electrical synapses and their functional interactions with chemical synapses. *Nat Rev Neurosci* 15:250–263 Available at: <http://dx.doi.org/10.1038/nrn3708>.
- Pereda AE, Bell TD, Chang BH, Czernik AJ, Nairn AC, Soderling TR, Faber DS (1998) Ca²⁺/calmodulin-dependent kinase II mediates simultaneous enhancement of gap-junctional conductance and glutamatergic transmission. *Proc Natl Acad Sci* 95:13272–13277 Available at: <https://pnas.org/doi/full/10.1073/pnas.95.22.13272>.
- Pereda AE, Curti S, Hoge G, Cachope R, Flores CE, Rash JE (2013) Gap junction-mediated electrical transmission: Regulatory mechanisms and plasticity. *Biochim Biophys Acta - Biomembr* 1828:134–146 Available at: <https://linkinghub.elsevier.com/retrieve/pii/S0005273612001848>.
- Pereda AE, Rash JE, Nagy JI, Bennett MVL (2004) Dynamics of electrical transmission at club endings on the Mauthner cells. *Brain Res Rev* 47:227–244 Available at: <https://linkinghub.elsevier.com/retrieve/pii/S0165017304000748>.
- Perlman I, Ammermüller J (1994) Receptive-field size of L1 horizontal cells in the turtle retina: effects of dopamine and background light. *J Neurophysiol* 72:2786–2795 Available at: <https://www.physiology.org/doi/10.1152/jn.1994.72.6.2786>.
- Petralia RS (1997) Immunocytochemical Localization of Ionotropic Glutamate Receptors (GluRs) in Neural Circuits. In: *The Ionotropic Glutamate Receptors*, pp 219–263. Totowa, NJ: Humana Press. Available at: http://link.springer.com/10.1007/978-1-4612-3962-8_9.
- Piccolino M, Neyton J, Gerschenfeld H (1984) Decrease of gap junction permeability induced by dopamine and cyclic adenosine 3':5'-monophosphate in horizontal cells of turtle retina. *J Neurosci* 4:2477–2488 Available at: <https://www.jneurosci.org/lookup/doi/10.1523/JNEUROSCI.04-10-02477.1984>.
- Pin J-P, Duvoisin R (1995) The metabotropic glutamate receptors: Structure and functions. *Neuropharmacology* 34:1–26 Available at: <https://linkinghub.elsevier.com/retrieve/pii/002839089400129G>.
- Pottek M, Schultz K, Weiler R (1997) Effects of nitric oxide on the horizontal cell network and dopamine release in the carp retina. *Vision Res* 37:1091–1102 Available at: <https://linkinghub.elsevier.com/retrieve/pii/S0042698996002982>.
- Pottek M, Weiler R (2000) Light-adaptive effects of retinoic acid on receptive field properties of retinal horizontal cells. *Eur J Neurosci* 12:437–445 Available at: <https://onlinelibrary.wiley.com/doi/10.1046/j.1460-9568.2000.00918.x>.

- Puller C, de Sevilla Müller LP, Janssen-Bienhold U, Haverkamp S (2009) ZO-1 and the Spatial Organization of Gap Junctions and Glutamate Receptors in the Outer Plexiform Layer of the Mammalian Retina. *J Neurosci* 29:6266–6275 Available at: <https://www.jneurosci.org/lookup/doi/10.1523/JNEUROSCI.5867-08.2009>.
- Puller C, Haverkamp S (2011a) Bipolar cell pathways for color vision in non-primate dichromats. *Vis Neurosci* 28:51–60 Available at: https://www.cambridge.org/core/product/identifier/S0952523810000271/type/journal_article.
- Puller C, Haverkamp S (2011b) Cell-type-specific localization of protocadherin β 16 at AMPA and AMPA/kainate receptor-containing synapses in the primate retina. *J Comp Neurol* 519:467–479 Available at: <https://onlinelibrary.wiley.com/doi/10.1002/cne.22528>.
- Puller C, Haverkamp S, Grünert U (2007) OFF midget bipolar cells in the retina of the marmoset, *Callithrix jacchus*, express AMPA receptors. *J Comp Neurol* 502:442–454 Available at: <https://onlinelibrary.wiley.com/doi/10.1002/cne.21315>.
- Puller C, Haverkamp S, Neitz M, Neitz J (2014) Synaptic elements for GABAergic feed-forward signaling between H1 horizontal cells and blue cone bipolar cells are enriched beneath primate S-cones. *Neuhauss SCF, ed. PLoS One* 9:e88963 Available at: <https://dx.plos.org/10.1371/journal.pone.0088963>.
- Puller C, Ivanova E, Euler T, Haverkamp S, Schubert T (2013) OFF bipolar cells express distinct types of dendritic glutamate receptors in the mouse retina. *Neuroscience* 243:136–148 Available at: <https://linkinghub.elsevier.com/retrieve/pii/S0306452213003096>.
- Puthussery T, Percival KA, Venkataramani S, Gayet-Primo J, Grünert U, Taylor WR (2014) Kainate Receptors Mediate Synaptic Input to Transient and Sustained OFF Visual Pathways in Primate Retina. *J Neurosci* 34:7611–7621 Available at: <https://www.jneurosci.org/lookup/doi/10.1523/JNEUROSCI.4855-13.2014>.
- Qin P, Pourcho RG (2000) AMPA-selective glutamate receptor subunits GluR2 and GluR4 in the cat retina: An immunocytochemical study. *Vis Neurosci* 17:155–155 Available at: https://www.cambridge.org/core/product/identifier/S0952523800171159/type/journal_article.
- Qiu Y, Zhao Z, Klindt D, Kautzky M, Szatko KP, Schaeffel F, Rifai K, Franke K, Busse L, Euler T (2021) Natural environment statistics in the upper and lower visual field are reflected in mouse retinal specializations. *Curr Biol* 31:3233–3247.e6 Available at: <https://doi.org/10.1016/j.cub.2021.05.017>.
- Rao-Mirotnik R, Buchsbaum G, Sterling P (1998) Transmitter Concentration at a Three-Dimensional Synapse. *J Neurophysiol* 80:3163–3172 Available at: <https://www.physiology.org/doi/10.1152/jn.1998.80.6.3163>.
- Rao-Mirotnik R, Harkins AB, Buchsbaum G, Sterling P (1995) Mammalian rod terminal: architecture of a binary synapse. *Neuron* 14:561–569 Available at: <https://linkinghub.elsevier.com/retrieve/pii/0896627395903127>.
- Rash JE, Pereda A, Kamasawa N, Furman CS, Yasumura T, Davidson KG V., Dudek FE, Olson C, Li X, Nagy JI (2004) High-resolution proteomic mapping in the vertebrate central nervous system: Close proximity of connexin35 to NMDA glutamate receptor clusters and co-localization of connexin36 with immunoreactivity for zonula occludens protein-1 (ZO-1). *J Neurocytol* 33:131–151 Available at: <http://link.springer.com/10.1023/B:NEUR.0000029653.34094.0b>.
- Raviola E, Dacheux RF (1987) Excitatory dyad synapse in rabbit retina. *Proc Natl Acad Sci* 84:7324–7328 Available at: <https://pnas.org/doi/full/10.1073/pnas.84.20.7324>.
- Ribelayga CP, O'Brien J (2017) Circadian and Light-Adaptive Control of Electrical Synaptic Plasticity in the Vertebrate Retina. Elsevier Inc. Available at: <http://dx.doi.org/10.1016/B978-0-12-803471-2.00010-2>.
- Röhrenbeck J, Wässle H, Heizmann CW (1987) Immunocytochemical labelling of horizontal cells in mammalian retina using antibodies against calcium-binding proteins. *Neurosci Lett* 77:255–260 Available at: <https://linkinghub.elsevier.com/retrieve/pii/0304394087905088>.

- Rose B, Simpson I, Loewenstein WR (1977) Calcium ion produces graded changes in permeability of membrane channels in cell junction. *Nature* 267:625–627 Available at: <https://www.nature.com/articles/267625a0>.
- Rossmann M, Sukumaran M, Penn AC, Veprintsev DB, Babu MM, Greger IH (2011) Subunit-selective N-terminal domain associations organize the formation of AMPA receptor heteromers. *EMBO J* 30:959–971 Available at: <http://emboj.embopress.org/cgi/doi/10.1038/emboj.2011.16>.
- Roy S, Field GD (2019) Dopaminergic modulation of retinal processing from starlight to sunlight. *J Pharmacol Sci* 140:86–93 Available at: <https://doi.org/10.1016/j.jphs.2019.03.006>.
- Rusakov DA, Savtchenko LP, Zheng K, Henley JM (2011) Shaping the synaptic signal: molecular mobility inside and outside the cleft. *Trends Neurosci* 34:359–369 Available at: <https://linkinghub.elsevier.com/retrieve/pii/S0166223611000397>.
- Rust MJ, Bates M, Zhuang X (2006) Sub-diffraction-limit imaging by stochastic optical reconstruction microscopy (STORM). *Nat Methods* 3:793–796 Available at: <https://www.nature.com/articles/nmeth929>.
- Salinas-Navarro M, Jiménez-López M, Valiente-Soriano FJ, Alarcón-Martínez L, Avilés-Trigueros M, Mayor S, Holmes T, Lund RD, Villegas-Pérez MP, Vidal-Sanz M (2009) Retinal ganglion cell population in adult albino and pigmented mice: A computerized analysis of the entire population and its spatial distribution. *Vision Res* 49:637–647 Available at: <https://linkinghub.elsevier.com/retrieve/pii/S0042698909000224>.
- Sandman D, Boycott BB, Peichl L (1996) The horizontal cells of artiodactyl retinae: A comparison with Cajal's descriptions. *Vis Neurosci* 13:735–746 Available at: https://www.cambridge.org/core/product/identifier/S0952523800008610/type/journal_article.
- Sanes JR, Masland RH (2015) The Types of Retinal Ganglion Cells: Current Status and Implications for Neuronal Classification. *Annu Rev Neurosci* 38:221–246 Available at: <https://www.annualreviews.org/doi/10.1146/annurev-neuro-071714-034120>.
- Schindelin J, Arganda-Carreras I, Frise E, Kaynig V, Longair M, Pietzsch T, Preibisch S, Rueden C, Saalfeld S, Schmid B, Tinevez J-Y, White DJ, Hartenstein V, Eliceiri K, Tomancak P, Cardona A (2012) Fiji: an open-source platform for biological-image analysis. *Nat Methods* 9:676–682 Available at: <https://www.nature.com/articles/nmeth.2019>.
- Schmitz F (2009) The Making of Synaptic Ribbons: How They Are Built and What They Do. *Neurosci* 15:611–624 Available at: <http://journals.sagepub.com/doi/10.1177/1073858409340253>.
- Schmitz F, Königstorfer A, Südhof TC (2000) RIBEYE, a Component of Synaptic Ribbons. *Neuron* 28:857–872 Available at: <https://linkinghub.elsevier.com/retrieve/pii/S0896627300001598>.
- Schubert T, Weiler R, Feigenspan A (2006) Intracellular Calcium Is Regulated by Different Pathways in Horizontal Cells of the Mouse Retina. *J Neurophysiol* 96:1278–1292 Available at: <https://www.physiology.org/doi/10.1152/jn.00191.2006>.
- Schultz K, Janssen-Bienhold U, Gundelfinger ED, Kreutz MR, Weiler R (2004) Calcium-binding protein Caldendrin and CaMKII are localized in spinules of the carp retina. *J Comp Neurol* 479:84–93 Available at: <https://onlinelibrary.wiley.com/doi/10.1002/cne.20314>.
- Sekar RB, Periasamy A (2003) Fluorescence resonance energy transfer (FRET) microscopy imaging of live cell protein localizations. *J Cell Biol* 160:629–633 Available at: <https://rupress.org/jcb/article/160/5/629/33208/Fluorescence-resonance-energy-transfer-FRET>.
- Sharpe ZJ, Shehu A, Ichinose T (2022) Asymmetric Distributions of Achromatic Bipolar Cells in the Mouse Retina. *Front Neuroanat* 15 Available at: <https://www.frontiersin.org/articles/10.3389/fnana.2021.786142/full>.
- Shekhar K, Lapan SW, Whitney IE, Tran NM, Macosko EZ, Kowalczyk M, Adiconis X, Levin JZ, Nemesh J, Goldman M, McCarroll SA, Cepko CL, Regev A, Sanes JR (2016) Comprehensive Classification of Retinal Bipolar Neurons by Single-Cell Transcriptomics. *Cell* 166:1308–1323.e30 Available at: <http://dx.doi.org/10.1016/j.cell.2016.07.054>.

- Shelley J, Dedek K, Schubert T, Feigenspan A, Schultz K, Hombach S, Willecke K, Weiler R (2006) Horizontal cell receptive fields are reduced in connexin57-deficient mice. *Eur J Neurosci* 23:3176–3186 Available at: <https://onlinelibrary.wiley.com/doi/10.1111/j.1460-9568.2006.04848.x>.
- Shepherd JD, Huganir RL (2007) The Cell Biology of Synaptic Plasticity: AMPA Receptor Trafficking. *Annu Rev Cell Dev Biol* 23:613–643 Available at: <https://www.annualreviews.org/doi/10.1146/annurev.cellbio.23.090506.123516>.
- Shimizu K, Stopfer M (2013) Gap junctions. *Curr Biol* 23:R1026–R1031 Available at: <https://linkinghub.elsevier.com/retrieve/pii/S0960982213013420>.
- Shimshek DR, Bus T, Grinevich V, Single FN, Mack V, Sprengel R, Spergel DJ, Seeburg PH (2006) Impaired Reproductive Behavior by Lack of GluR-B Containing AMPA Receptors But Not of NMDA Receptors in Hypothalamic and Septal Neurons. *Mol Endocrinol* 20:219–231 Available at: <https://academic.oup.com/mend/article/20/1/219/2741501>.
- Sigulinsky CL, Anderson JR, Kerzner E, Rapp CN, Pfeiffer RL, Rodman TM, Emrich DP, Rapp KD, Nelson NT, Lauritzen JS, Meyer M, Marc RE, Jones BW (2020) Network Architecture of Gap Junctional Coupling among Parallel Processing Channels in the Mammalian Retina. *J Neurosci* 40:4483–4511 Available at: <https://www.jneurosci.org/lookup/doi/10.1523/JNEUROSCI.1810-19.2020>.
- Singh D, Solan JL, Taffet SM, Javier R, Lampe PD (2005) Connexin 43 Interacts with Zona Occludens-1 and -2 Proteins in a Cell Cycle Stage-specific Manner. *J Biol Chem* 280:30416–30421 Available at: <https://linkinghub.elsevier.com/retrieve/pii/S0021925820794706>.
- Söhl G, Maxeiner S, Willecke K (2005) Expression and functions of neuronal gap junctions. *Nat Rev Neurosci* 6:191–200 Available at: <https://www.nature.com/articles/nrn1627>.
- Söhl G, Willecke K (2003) An Update on Connexin Genes and their Nomenclature in Mouse and Man. *Cell Commun Adhes* 10:173–180 Available at: <http://www.tandfonline.com/doi/full/10.1080/cac.10.4-6.173.180>.
- Solessio E, Lasater EM (2002) Calcium-induced calcium release and calcium buffering in retinal horizontal cells. *Vis Neurosci* 19:713–725 Available at: https://www.cambridge.org/core/product/identifier/S0952523802196039/type/journal_article.
- Sommer B, Köhler M, Sprengel R, Seeburg PH (1991) RNA editing in brain controls a determinant of ion flow in glutamate-gated channels. *Cell* 67:11–19 Available at: <https://linkinghub.elsevier.com/retrieve/pii/009286749190568J>.
- Sonntag S, Dedek K, Dorgau B, Schultz K, Schmidt K-F, Cimiotti K, Weiler R, Lowel S, Willecke K, Janssen-Bienhold U (2012) Ablation of Retinal Horizontal Cells from Adult Mice Leads to Rod Degeneration and Remodeling in the Outer Retina. *J Neurosci* 32:10713–10724 Available at: <https://www.jneurosci.org/lookup/doi/10.1523/JNEUROSCI.0442-12.2012>.
- Spray DC, Harris AL, Bennett MVL (1981) Gap Junctional Conductance Is a Simple and Sensitive Function of Intracellular pH. *Science* (80-) 211:712–715 Available at: <https://www.jstor.org/stable/1685624>.
- Stabio ME, Sondereker KB, Haghgou SD, Day BL, Chidsey B, Sabbah S, Renna JM (2018) A novel map of the mouse eye for orienting retinal topography in anatomical space. *J Comp Neurol* 526:1749–1759 Available at: <https://onlinelibrary.wiley.com/doi/10.1002/cne.24446>.
- Stenkamp DL (2015) Development of the Vertebrate Eye and Retina. In: *Physiology & behavior*, pp 397–414 Available at: <https://linkinghub.elsevier.com/retrieve/pii/S1877117315001088>.
- Sterling P, Matthews G (2005) Structure and function of ribbon synapses. *Trends Neurosci* 28:20–29 Available at: <https://linkinghub.elsevier.com/retrieve/pii/S0166223604003650>.
- Sterratt DC, Lyngholm D, Willshaw DJ, Thompson ID (2013) Standard Anatomical and Visual Space for the Mouse Retina: Computational Reconstruction and Transformation of Flattened Retinae with the Retistruct Package Lapp H, ed. *PLoS Comput Biol* 9:e1002921 Available at: <https://dx.plos.org/10.1371/journal.pcbi.1002921>.

- Stevenson BR, Siliciano JD, Mooseker MS, Goodenough DA (1986) Identification of ZO-1: a high molecular weight polypeptide associated with the tight junction (zonula occludens) in a variety of epithelia. *J Cell Biol* 103:755–766 Available at: <https://rupress.org/jcb/article/103/3/755/13454/Identification-of-ZO-1-a-high-molecular-weight>.
- Stincic TL, Frerking ME (2015) Different AMPA receptor subtypes mediate the distinct kinetic components of a biphasic EPSC in hippocampal interneurons. *Front Synaptic Neurosci* 7:1–11 Available at: http://www.frontiersin.org/Synaptic_Neuroscience/10.3389/fnsyn.2015.00007/abstract.
- Stradleigh TW, Ishida AT (2015) Fixation strategies for retinal immunohistochemistry. *Prog Retin Eye Res* 48:181–202 Available at: <https://linkinghub.elsevier.com/retrieve/pii/S135094621500018X>.
- Ströh S, Puller C, Swirski S, Hölzel M-B, van der Linde LIS, Segelken J, Schultz K, Block C, Monyer H, Willecke K, Weiler R, Greschner M, Janssen-Bienhold U, Dedek K (2018) Eliminating Glutamatergic Input onto Horizontal Cells Changes the Dynamic Range and Receptive Field Organization of Mouse Retinal Ganglion Cells. *J Neurosci* 38:2015–2028 Available at: <https://www.jneurosci.org/lookup/doi/10.1523/JNEUROSCI.0141-17.2018>.
- Ströh S, Sonntag S, Janssen-Bienhold U, Schultz K, Cimiotti K, Weiler R, Willecke K, Dedek K (2013) Cell-Specific Cre Recombinase Expression Allows Selective Ablation of Glutamate Receptors from Mouse Horizontal Cells Reid VM, ed. *PLoS One* 8:e83076 Available at: <https://dx.plos.org/10.1371/journal.pone.0083076>.
- Stuart RO, Nigam SK (1995) Regulated assembly of tight junctions by protein kinase C. *Proc Natl Acad Sci* 92:6072–6076 Available at: <https://pnas.org/doi/full/10.1073/pnas.92.13.6072>.
- Suzuki H, Pinto L (1986) Response properties of horizontal cells in the isolated retina of wild-type and pearl mutant mice. *J Neurosci* 6:1122–1128 Available at: <https://www.jneurosci.org/lookup/doi/10.1523/JNEUROSCI.06-04-01122.1986>.
- Szatko KP, Korympidou MM, Ran Y, Berens P, Dalkara D, Schubert T, Euler T, Franke K (2020) Neural circuits in the mouse retina support color vision in the upper visual field. *Nat Commun* 11:3481 Available at: <https://www.nature.com/articles/s41467-020-17113-8>.
- Tetenborg S, Wang HY, Nemitz L, Depping A, Espejo AB, Aseervatham J, Bedford MT, Janssen-Bienhold U, O'Brien J, Dedek K (2020) Phosphorylation of Connexin36 near the C-terminus switches binding affinities for PDZ-domain and 14–3–3 proteins in vitro. *Sci Rep* 10:1–11 Available at: <https://doi.org/10.1038/s41598-020-75375-0>.
- Tetenborg S, Yadav SC, Hormuzdi SG, Monyer H, Janssen-Bienhold U, Dedek K (2017) Differential Distribution of Retinal Ca²⁺/Calmodulin-Dependent Kinase II (CaMKII) Isoforms Indicates CaMKII- β and - δ as Specific Elements of Electrical Synapses Made of Connexin36 (Cx36). *Front Mol Neurosci* 10:1–15 Available at: <http://journal.frontiersin.org/article/10.3389/fnmol.2017.00425/full>.
- Thomas T, Jordan K, Simek J, Shao Q, Jedeszko C, Walton P, Laird DW (2005) Mechanisms of Cx43 and Cx26 transport to the plasma membrane and gap junction regeneration. *J Cell Sci* 118:4451–4462 Available at: <https://journals.biologists.com/jcs/article/118/19/4451/35210/Mechanisms-of-Cx43-and-Cx26-transport-to-the>.
- Thoreson WB, Babai N, Bartoletti TM (2008) Feedback from Horizontal Cells to Rod Photoreceptors in Vertebrate Retina. *J Neurosci* 28:5691–5695 Available at: <https://www.jneurosci.org/lookup/doi/10.1523/JNEUROSCI.0403-08.2008>.
- Thoreson WB, Mangel SC (2012) Lateral interactions in the outer retina. *Prog Retin Eye Res* 31:407–441 Available at: <http://dx.doi.org/10.1016/j.preteyeres.2012.04.003>.
- tom Dieck S, Altmann WD, Kessels MM, Qualmann B, Regus H, Brauner D, Fejtová A, Bracko O, Gundelfinger ED, Brandstätter JH (2005) Molecular dissection of the photoreceptor ribbon synapse. *J Cell Biol* 168:825–836 Available at: <https://rupress.org/jcb/article/168/5/825/54452/Molecular-dissection-of-the-photoreceptor-ribbon>.

- Tornavaca O, Chia M, Dufton N, Almagro LO, Conway DE, Randi AM, Schwartz MA, Matter K, Balda MS (2015) ZO-1 controls endothelial adherens junctions, cell–cell tension, angiogenesis, and barrier formation. *J Cell Biol* 208:821–838 Available at: <https://rupress.org/jcb/article/208/6/821/38104/ZO-1-controls-endothelial-adherens-junctions-cell>.
- Tornqvist K, Yang X, Dowling J (1988) Modulation of cone horizontal cell activity in the teleost fish retina. III. Effects of prolonged darkness and dopamine on electrical coupling between horizontal cells. *J Neurosci* 8:2279–2288 Available at: <https://www.jneurosci.org/lookup/doi/10.1523/JNEUROSCI.08-07-02279.1988>.
- Tran O, Kerruth S, Coates C, Kaur H, Peracchia C, Carter T, Török K (2023) Ca²⁺-Dependent and -Independent Calmodulin Binding to the Cytoplasmic Loop of Gap Junction Connexins. *Int J Mol Sci* 24:4153 Available at: <https://www.mdpi.com/1422-0067/24/4/4153>.
- Traynelis SF, Wollmuth LP, McBain CJ, Menniti FS, Vance KM, Ogden KK, Hansen KB, Yuan H, Myers SJ, Dingledine R (2010) Glutamate Receptor Ion Channels: Structure, Regulation, and Function Sibley D, ed. *Pharmacol Rev* 62:405–496 Available at: <http://pharmrev.aspetjournals.org/lookup/doi/10.1124/pr.109.002451>.
- Trenholm S, McLaughlin AJ, Schwab DJ, Awatramani GB (2013) Dynamic Tuning of Electrical and Chemical Synaptic Transmission in a Network of Motion Coding Retinal Neurons. *J Neurosci* 33:14927–14938 Available at: <https://www.jneurosci.org/lookup/doi/10.1523/JNEUROSCI.0808-13.2013>.
- Trümppler J, Dedek K, Schubert T, de Sevilla Müller LP, Seeliger M, Humphries P, Biel M, Weiler R (2008) Rod and cone contributions to horizontal cell light responses in the mouse retina. *J Neurosci* 28:6818–6825 Available at: <https://www.jneurosci.org/lookup/doi/10.1523/JNEUROSCI.1564-08.2008>.
- Tsukamoto Y, Morigiwa K, Ueda M, Sterling P (2001) Microcircuits for Night Vision in Mouse Retina. *J Neurosci* 21:8616–8623 Available at: <https://www.jneurosci.org/lookup/doi/10.1523/JNEUROSCI.21-21-08616.2001>.
- Tsukamoto Y, Omi N (2017) Classification of Mouse Retinal Bipolar Cells: Type-Specific Connectivity with Special Reference to Rod-Driven All Amacrine Pathways. *Front Neuroanat* 11:92 Available at: <http://journal.frontiersin.org/article/10.3389/fnana.2017.00092/full>.
- Urschel S, Höher T, Schubert T, Alev C, Söhl G, Wörsdörfer P, Asahara T, Dermietzel R, Weiler R, Willecke K (2006) Protein Kinase A-mediated Phosphorylation of Connexin36 in Mouse Retina Results in Decreased Gap Junctional Communication between All Amacrine Cells. *J Biol Chem* 281:33163–33171 Available at: <https://linkinghub.elsevier.com/retrieve/pii/S0021925820704989>.
- Vaney DI (1991) Many diverse types of retinal neurons show tracer coupling when injected with biocytin or Neurobiotin. *Neurosci Lett* 125:187–190 Available at: <https://linkinghub.elsevier.com/retrieve/pii/030439409190024N>.
- VanLeeuwen M, Fahrenfort I, Sjoerdsma T, Numan R, Kamermans M (2009) Lateral Gain Control in the Outer Retina Leads to Potentiation of Center Responses of Retinal Neurons. *J Neurosci* 29:6358–6366 Available at: <https://www.jneurosci.org/lookup/doi/10.1523/JNEUROSCI.5834-08.2009>.
- Vardi N, Duvoisin R, Wu G, Sterling P (2000a) Localization of mGluR6 to dendrites of ON bipolar cells in primate retina. *J Comp Neurol* 423:402–412 Available at: [https://onlinelibrary.wiley.com/doi/10.1002/1096-9861\(20000731\)423:3%3C402::AID-CNE4%3E3.0.CO;2-E](https://onlinelibrary.wiley.com/doi/10.1002/1096-9861(20000731)423:3%3C402::AID-CNE4%3E3.0.CO;2-E).
- Vardi N, Morigiwa K, Wang T-L, Shi Y-J, Sterling P (1998) Neurochemistry of the mammalian cone `synaptic complex'. *Vision Res* 38:1359–1369 Available at: <https://linkinghub.elsevier.com/retrieve/pii/S0042698998000078>.
- Vardi N, Sterling P (1994) Subcellular localization of GABAA receptor on bipolar cells in macaque and human retina. *Vision Res* 34:1235–1246 Available at: <https://linkinghub.elsevier.com/retrieve/pii/0042698994901988>.

- Vardi N, Zhang L-L, Payne JA, Sterling P (2000b) Evidence That Different Cation Chloride Cotransporters in Retinal Neurons Allow Opposite Responses to GABA. *J Neurosci* 20:7657–7663 Available at: <https://www.jneurosci.org/lookup/doi/10.1523/JNEUROSCI.20-20-07657.2000>.
- Vecino E, Rodriguez FD, Ruzafa N, Pereiro X, Sharma SC (2016) Glia-neuron interactions in the mammalian retina. *Prog Retin Eye Res* 51:1–40 Available at: <http://dx.doi.org/10.1016/j.preteyeres.2015.06.003>.
- Völgyi B, Kovács-öller T, Atlasz T, Wilhelm M, Gábel R (2013) Gap junctional coupling in the vertebrate retina: Variations on one theme? *Prog Retin Eye Res* 34:1–18 Available at: <http://dx.doi.org/10.1016/j.preteyeres.2012.12.002>.
- Wang Y V., Weick M, Demb JB (2011) Spectral and Temporal Sensitivity of Cone-Mediated Responses in Mouse Retinal Ganglion Cells. *J Neurosci* 31:7670–7681 Available at: <https://www.jneurosci.org/lookup/doi/10.1523/JNEUROSCI.0629-11.2011>.
- Warwick RA, Kaushansky N, Sarid N, Golan A, Rivlin-Etzion M (2018) Inhomogeneous Encoding of the Visual Field in the Mouse Retina. *Curr Biol* 28:655-665.e3 Available at: <https://doi.org/10.1016/j.cub.2018.01.016>.
- Wässle H (2004) Parallel processing in the mammalian retina. *Nat Rev Neurosci* 5:747–757 Available at: <https://www.nature.com/articles/nrn1497>.
- Wässle H (2008) Decomposing a Cone's Output (Parallel Processing). In: *The Senses: A Comprehensive Reference*, pp 313–339. Elsevier. Available at: <https://linkinghub.elsevier.com/retrieve/pii/B9780123708809002681>.
- Wässle H, Boycott BB (1991) Functional architecture of the mammalian retina. *Physiol Rev* 71:447–480 Available at: <https://www.physiology.org/doi/10.1152/physrev.1991.71.2.447>.
- Wässle H, Dacey DM, Haun T, Haverkamp S, Grünert U, Boycott BB (2000) The mosaic of horizontal cells in the macaque monkey retina: With a comment on bplexiform ganglion cells. *Vis Neurosci* 17:591–608 Available at: https://www.cambridge.org/core/product/identifier/S0952523800174097/type/journal_article.
- Wässle H, Puller C, Müller F, Haverkamp S (2009) Cone Contacts, Mosaics, and Territories of Bipolar Cells in the Mouse Retina. *J Neurosci* 29:106–117 Available at: <https://www.jneurosci.org/lookup/doi/10.1523/JNEUROSCI.4442-08.2009>.
- Weiler R, Baldrige WH, Mangel SC, Dowling JE (1997) Modulation of endogenous dopamine release in the fish retina by light and prolonged darkness. *Vis Neurosci* 14:351–356 Available at: https://www.cambridge.org/core/product/identifier/S0952523800011470/type/journal_article.
- Weiler R, He S, Vaney DI (1999) Retinoic Acid Modulates Gap Junctional Permeability Between Horizontal Cells Of The Mammalian Retina. *Eur J Neurosci* 11:3346–3350 Available at: <https://onlinelibrary.wiley.com/doi/10.1046/j.1460-9568.1999.00799.x>.
- Weiler R, Pottke M, He S, Vaney DI (2000) Modulation of coupling between retinal horizontal cells by retinoic acid and endogenous dopamine. *Brain Res Rev* 32:121–129 Available at: <https://linkinghub.elsevier.com/retrieve/pii/S0165017399000715>.
- Willecke K, Eiberger J, Degen J, Eckardt D, Romualdi A, Güldenagel M, Deutsch U, Söhl G (2002) Structural and functional diversity of connexin genes in the mouse and human genome. *Biol Chem* 383:725–737 Available at: <https://www.degruyter.com/document/doi/10.1515/BC.2002.076/html>.
- Witkovsky P (2004) Dopamine and retinal function. *Doc Ophthalmol* 108:17–39 Available at: <http://link.springer.com/10.1023/B:DOOP.0000019487.88486.0a>.
- Wu SM (1992) Feedback connections and operation of the outer plexiform layer of the retina. *Curr Opin Neurobiol* 2:462–468 Available at: <https://linkinghub.elsevier.com/retrieve/pii/095943889290181J>.

- Xia Y, Carroll RC, Nawy S (2006) State-Dependent AMPA Receptor Trafficking in the Mammalian Retina. *J Neurosci* 26:5028–5036 Available at: <https://www.jneurosci.org/lookup/doi/10.1523/JNEUROSCI.0169-06.2006>.
- Xia Y, Nawy S, Carroll RC (2007) Activity-Dependent Synaptic Plasticity in Retinal Ganglion Cells. *J Neurosci* 27:12221–12229 Available at: <https://www.jneurosci.org/lookup/doi/10.1523/JNEUROSCI.2086-07.2007>.
- Xin D, Bloomfield SA (1999) Dark- and light-induced changes in coupling between horizontal cells in mammalian retina. *J Comp Neurol* 405:75–87 Available at: [https://onlinelibrary.wiley.com/doi/10.1002/\(SICI\)1096-9861\(19990301\)405:1%3C75::AID-CNE6%3E3.0.CO;2-D](https://onlinelibrary.wiley.com/doi/10.1002/(SICI)1096-9861(19990301)405:1%3C75::AID-CNE6%3E3.0.CO;2-D).
- Xin D, Bloomfield SA (2000) Effects of nitric oxide on horizontal cells in the rabbit retina. *Vis Neurosci* 17:799–811 Available at: https://www.cambridge.org/core/product/identifier/S0952523800175133/type/journal_article.
- Yang X-D, Korn H, Faber DS (1990) Long-term potentiation of electrotonic coupling at mixed synapses. *Nature* 348:542–545 Available at: <https://www.nature.com/articles/348542a0>.
- Yang XL, Wu SM (1991) Feedforward lateral inhibition in retinal bipolar cells: input-output relation of the horizontal cell-depolarizing bipolar cell synapse. *Proc Natl Acad Sci U S A* 88:3310–3313 Available at: <https://pnas.org/doi/full/10.1073/pnas.88.8.3310>.
- Zhang A-J, Wu SM (2009) Receptive Fields of Retinal Bipolar Cells Are Mediated by Heterogeneous Synaptic Circuitry. *J Neurosci* 29:789–797 Available at: <https://www.jneurosci.org/lookup/doi/10.1523/JNEUROSCI.4984-08.2009>.
- Zhang A, Jacoby R, Wu SM (2011) Light- and dopamine-regulated receptive field plasticity in primate horizontal cells. *J Comp Neurol* 519:2125–2134 Available at: <https://onlinelibrary.wiley.com/doi/10.1002/cne.22604>.
- Zhang Z, Li H, Liu X, O'Brien J, Ribelayga CP (2015) Circadian clock control of connexin36 phosphorylation in retinal photoreceptors of the CBA/CaJ mouse strain. *Vis Neurosci* 32:E009 Available at: https://www.cambridge.org/core/product/identifier/S0952523815000061/type/journal_article.
- Zhao H, Peng X, Ma L, Sun M (2016) Design of the multiplexing communication system with non-coherent vortex beams. *Opt Commun* 378:5–9 Available at: <https://linkinghub.elsevier.com/retrieve/pii/S0030401816303649>.
- Zhu X, Li A, Brown B, Weiss ER, Osawa S, Craft CM (2002) Mouse cone arrestin expression pattern: light induced translocation in cone photoreceptors. *Mol Vis* 8:462–471 Available at: <http://www.ncbi.nlm.nih.gov/pubmed/12486395>.

7. Appendix

7.1 Materials

7.1.1 Mouse lines

Table 4: Mouse line used in this study

Mouse line	Source-Reference
C57BL/6J	Thierhaus - Carl von Ossietzky University Oldenburg
Cx57- Cre	(Sonntag et al., 2012; Ströh et al., 2013)
GluA2fl/fl GluA4fl/fl:Cx57 ^{+/+}	(Shimshek et al., 2006; Fuchs et al., 2007; Ströh et al., 2018)
Cx57 ^{LacZ/LacZ}	(Hombach et al., 2004)

7.1.2 Devices

Table 5: Devices used

Device	Model	Producer
Analytical – precision scale	BCE653I – 1S	Sartorius
Analytical – precision scale	BP211D	Sartorius
Analytical – precision scale	TP-103	Denver Instrument
Centrifuge	5417R	Eppendorf
Confocal microscope	Leica TCS SP2	Leica Microsystems
Confocal microscope	Lecia TCS SP8	Leica Microsystems
Cryostat	Leica CM1860	Leica Biosystem
Electrophoresis chamber	Agagel Midi-Wide	Biometra
Epifluorescence microscope	Leica DM6 B	Leica Microsystems
Gel documentation system	Alphamager EP	Alpha Innotech
Magnetic stirrer hot plate	RH basic 2	IKA
Magnetic stirrer hot plate	RCT	IKAMAG
Objective	PL APO 63X/1.32 OIL	Leica Microsystems
Objective	HC PL 20X/0.50 FLUOTAR	Leica Microsystems
Objective	HC PL APO 63X/1.40 OIL CS2	Leica Microsystems
Objective	HCX PL 20X/0.5 FLUOTAR	Leica Microsystems
Orbital shaker	KS 125 basic	IKA
Orbital shaker	Rotamax 120	Heidolph
pH-meter	pH 422	WTW
Power supply for Electrophoresis	Standard Power Pack P25	Biometra
Thermocycler	Mastercycler gradient	Eppendorf
Thermocycler	Vapo.protect	Eppendorf

7.1.3 Consumables

Table 6: Consumables used

Consumable	Producer
Advance PAP-Pen	Daido Sangyo Co.
Blood lancets - Solofix®	Braun
Cover glasses thickness # 1, 21 X 26 mm	Thermo Scientific
Cover glasses thickness # 1, 24 X 32 mm	Thermo Scientific
Cover glasses thickness # 1.5, 22 X 22 mm	Paul Marienfeld GmbH & Co. KG
Microscope slide	Thermo Scientific
Nitrocellulose Filters 0.8µm	Millipore
Pasteur capillary pipettes 150 mm	WU Mainz
Safe-Lock Tubes 2.0 ml	Eppendorf
SafeSeal® Tube 0.5 ml	Carl Roth
SafeSeal® Tube 1.5 ml	Sarstedt
Superfrost™ microscope slides	Epredia

7.1.4 Chemicals and kits

Table 7: Chemicals and kits used in this study

Product	Producer
Agarose	SERVA
ChemiBlocker	Millipore
D(+)-Saccarose	Carl Roth
di-sodium hydrogen phosphate dihydrate	Carl Roth
Fast Gene® Optima PCR HotStart Ready Mix	NIPPON Genetics
KAPA HotStart Mouse Genotyping kit	KAPA Biosystem – Peqlab
Normal Donkey Serum	Rockland Immunochemicals
Nuclease-Free water	Qiagen
Paraformaldehyde	Carl Roth
Potassium chloride	VWR
Potassium dihydrogen phosphate	Carl Roth
Roti® Gel Stain	Carl Roth
Sodium azide	Merck
Sodium chloride	Merck
Sodium dihydrogen phosphate dihydrate	VWR
Tissue-Tek O.C.T. Compound	Sakura Finetek
Tris (hydroxymethyl) – aminomethane (TRIS)	Acros
Triton X-100	Carl Roth
VECTASHIELD Mounting Medium	Vector Laboratories

7.1.5 Solutions and buffers

Table 8: Solutions and buffer used in this study

Buffer and Solution	Composition
Antibody incubation solution in PBS for vertical sections	5% (v/v) normal donkey serum (NDS) 1% (w/v) bovine serum albumin (BSA) 0.5% (v/v) Triton X-100 in PBS pH 7.4
Antibody incubation solution in PBS for whole mounts	5% (v/v) normal donkey serum (NDS) 1% (w/v) bovine serum albumin (BSA) 1% (v/v) Triton X-100 in PBS pH 7.4
Antibody incubation solution in TBS	5% (v/v) ChemiBLOCKER 0.3% (v/v) Triton X-100 0.02% (w/v) NaN ₃ in TBS pH 7.6
Cryoprotectant solution in 0,1 M PB	30% (w/v) Sucrose (D+) in 0.1 M PB pH 7.4
Cryoprotectant solution in PBS	30% (w/v) Sucrose (D+) in PBS pH 7.4
Fixation solution for immunohistochemistry	2% (w/v) Paraformaldehyde (PFA) 3% (w/v) Sucrose in 0.1 PB
Fixation solution for immunohistochemistry	2% (w/v) Paraformaldehyde (PFA) in PBS
Phosphate buffer (PB) 0,1M pH 7.4	0.1 M Na ₂ PO ₄ in ultrapure H ₂ O adjusting the pH to 7.4 by adding 0,1 M NaH ₂ PO ₄
Phosphate buffered saline (PBS) pH 7.4	140 mM NaCl 2.7 mM KCl 1.5 mM KH ₂ PO ₄ 8.1 mM Na ₂ HPO ₄ x 2H ₂ O in ultrapure H ₂ O
TRIS-Acetate-EDTA (TAE) 1X Working solution	40 mM Tris 20 mM Acetic acid 1 mM Na ₂ -EDTA x 2H ₂ O (20 ml 50 x TAE add 1000 ml ultrapure H ₂ O) pH ~ 8.5
TRIS-Acetate-EDTA (TAE) 50X Running buffer for electrophoresis	2 M Tris 1 M Acetic acid 50 mM EDTA pH 8.0 in ultrapure H ₂ O
TRIS-buffered saline with Triton X-100 (TBSTX)	50 mM Tris 1.5% (w/v) NaCl 0.3% (v/v) Triton X-100 Adjusting the pH to 7.6 by adding HCl in ultrapure H ₂ O

7.1.6 Primers

Table 9: Primers used for mouse genotyping

Primer	Sequence (5' to 3')	Amplicon	Reference
Cx57Cre for	CAA TGA GTG GTA GTG GAA GCT TAG	720 bp WT 970 bp Cx57 Cre	(Sonntag et al., 2012; Ströh et al., 2013)
Cx57Cre rev	GGC CCA TAT ACA CCA AAG AAG GG		
Int-Cre rev	TCC ATG AGT GAA CGA ACC TGG TCG		
Lac Z rev	TTC CCA GTC ACG ACG TTG TAA AAC	500 bp Cx57 LacZ	(Hombach et al., 2004)
GluA4 EF511	CAC TAT GTC TCA GTT CTC TCA AG	380 bp WT 450 bp GluA4 flox	(Fuchs et al., 2007; Ströh et al., 2013, 2018)
GluA4 EF188	ACG ATT GCA ACT AAG TTG ACA C		
GluA2 VM10	GTT GTC TAA CAA GTT GTT GAC C	250 bp WT 350bp GluA2 flox	(Shimshek et al., 2006; Ströh et al., 2018)
GluA2 VM12	GCG TAA GCC TGT GAA ATA CCT G		

7.1.7 Software

Table 10: Software used in this study

Software	Producer	RRID
Adobe Illustrator CC 2019	Adobe Systems Incorporated	SCR_010279
Adobe Photoshop CS6	Adobe Systems Incorporated	SCR_014199
Fiji (ImageJ2)	(Schindelin et al., 2012)	SCR_002285
GraphPad Prism 9	GraphPad Software	SCR_002798
Leica Application Suite X	Leica Microsystems	SCR_013673

7.2 Experimental protocols

7.2.1 Colocalization analysis protocol

The following section outlines the protocol used for the colocalization analysis and the immunoquantification of Cx57 and ZO-1 beneath the cone pedicle area.

Protocol on Fiji:

- Open the confocal Z-stack image
- At the single pedicle level, select a ROI with a diameter of 7.0 μm
- Approximately 20-25 optical sections are selected for the analysis
- Cx57 channel: subtract background function: rolling ball – select the radius
enhance contrast function: saturated 0.01% normalize
- ZO-1 channel: subtract background function: rolling ball - select the radius
enhance contrast function: saturated 0.01% normalize
- Threshold for Colocalization: Cx57 channel / ZO-1 channel, (the threshold must be the same for all the stacks from the same retina)
- Run colocalization Highlighter (Fiji Plugin)
- Invert the 8-bit image stack
- Analyze particle for colocalization: size pixel 3 px to infinity (area in pixel² – converted later in μm^2 , based on the pixel size of the image)
- Control for colocalization area: Cx57 channel flip vertically
- Quantification ZO-1 and Cx57 on the same area and threshold used before.
- Analyze particle for quantification: size 0.04-infinity (area in μm^2)

7.2.2 Anti-Cx57 antibodies validation

The guinea pig polyclonal anti-Cx57 antibodies (Davids Biotechnologie GmbH, Regensburg, Germany) were generated against two C-terminal peptides of mouse Cx57. The first one was generated against a C-terminal of 15 amino acid (aa) residues (CSMSMILELSSIMKK) of carp Cx53,8, which is homologous to 12 aa residues of the C-terminal end of mouse retinal Cx57 (Hombach et al., 2004; Janssen-Bienhold et al., 2009). The second peptide corresponds to a sequence of 16 aa (PGSRKASFLSRLMSEK) homologous of the aa 425-440 of the mouse retina Cx57. They were termed CSM and PGS, respectively.

Their specificity was extensively verified by immunohistochemistry analyses in wildtype and Cx57^{LacZ/LacZ} (Fig. 36). The immunoreactivity of the two antibodies was reduced to background level in retinal sections of Cx57-deficient mice, following standard protocol (see methods section). Under the same conditions in wildtype animals, both antibodies showed strong

immunoreactivity with the typical distribution in the OPL of the mouse retina as previously reported (Hombach et al., 2004; Janssen-Bienhold et al., 2009; Puller et al., 2009).

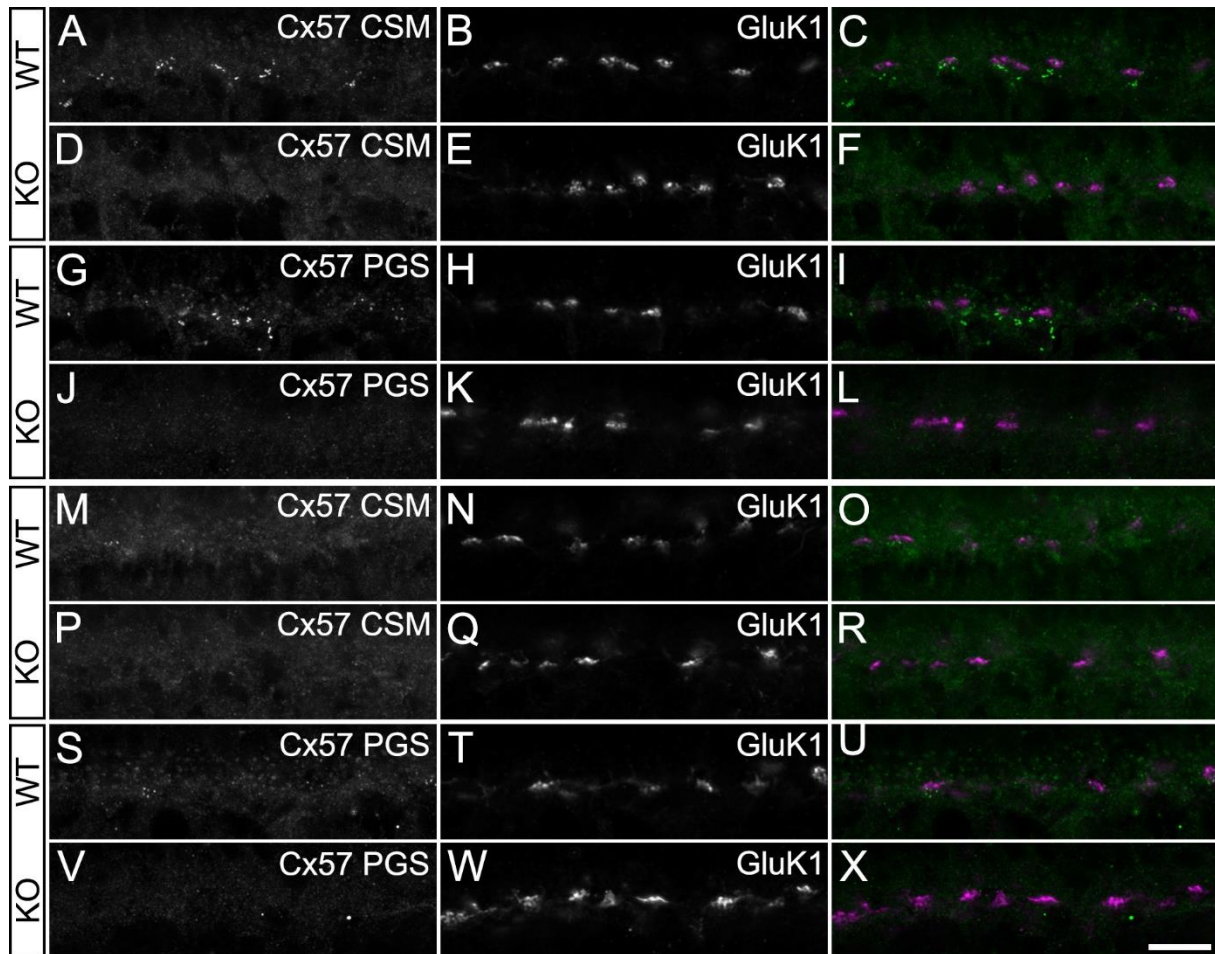


Figure 36: Connexin57 antibody validation

A-F: Maximum intensity projections ($\sim 1 \mu\text{m}$) of confocal image stacks from vertical cryostat sections of dorsal retina, labeled with antibodies against the Cx57 CSM epitope and the kainate receptor subunit 1 (GluK1) in retinas from wild-type (WT, A-C) and Cx57-deficient animals (KO, D-F). **G-L:** As in A-F, but with antibodies against the Cx57 PGS epitope. **M-X:** As in A-F for Cx57 CSM and G-L for Cx57 PGS but from the ventral retina. Scale bar: $10 \mu\text{m}$.

7.2.3 Immunostaining protocols

The following section outlines the main steps involved in the immunohistochemistry protocol for vertical cryosections and whole-mounted retina labeling.

Table 11: Immunostaining protocol for vertical sections

Step	Time	Solution
After sectioning, dry the slide on the heating plate at 35°C	30-45 min	
Encircle the sections with the PAP-pen	Let it dry for 2-3 min	
Rinses	3 X 10 min	PSB pH 7.4 or TBS-Tx pH7.6
Blocking incubation	60 min	NDS or ChemiBLOCKER incubation solution
Incubation of primary antibodies	Overnight at RT	NDS or ChemiBLOCKER incubation solution
Rinses	3 X 10 min	PSB pH 7.4 or TBS-Tx pH7.6
Centrifuge secondary antibodies solution	13000 RPM X 5 min	
Incubation of secondary antibodies	90 min at RT	NDS or ChemiBLOCKER incubation solution
Rinses	3 X 10 min	PSB pH 7.4 or TBS-Tx pH7.6
Coverslip sample with cover glass	Aqua-Poly/Mount	
Storage at 4°C		

NDS incubation solution: 5% NDS, 1% BSA, Tx 0.5% in PBS

ChemiBLOCKER incubation solution: 5% ChemiBLOCKER; 0.02 % Na⁺ Azide, Tx 0.3% in TBS

Table 12: Immunostaining protocol for whole-mounted retinas

Step	Time	Solution
Thaw the eyecup from the cryoprotection solution		
Retina dissection – brushing		PBS pH 7.4
Rinses	4 X 15 min	PBS pH 7.4
Blocking incubation	2 hours	NDS incubation solution
Incubation of primary antibodies	2-3 days at RT	NDS incubation solution
Rinses	3 X 5 min + 3 x 15 min	PBS pH 7.4
Centrifuge secondary antibodies solution	13000 RPM X 5 min	
Incubation of secondary antibodies	2 hours at RT	PBS pH 7.4
Rinses	3 X 5 min + 3 x 15 min	PBS pH 7.4
Place sample between spacers on glass slide		
Coverslip sample with cover glass		Vectashield mounting medium
Sealing		Nail polish
Storage at 4°C		

NDS incubation solution: 5% NDS, 1% BSA, Tx 1% in PBS

7.2.4 Horizontal cell quantification and retina reconstructions

For the large-scale quantification of horizontal cells in whole-mounted retina, the whole tissue was scanned sequentially for each channel in the form of individual squares (Leica DM6, Tlescan) and then stitched together using the LASX software from Leica. The center of each calbindin-positive horizontal cell body was manually identified and counted using the Cell Counter plugin in Fiji, in 5 retinas. The boundary of the S-opsin gradient was manually identified and marked in the same 5 retinas. Immunohistochemistry and large-scale quantification of cells in whole-mounted retina were performed by Lucia Lindenthal and Asli Pektaş. Tissue preparation, immunohistochemistry of one whole-mounted retina and image acquisition were conducted by me, while Christoph Block was responsible for the data presentation. Briefly, the R package “Retistruct” (Sterratt et al., 2013) was used to reconstruct the dissected whole-mounted retinas to the spherical eyecup shape of the intact retina. The reconstructed spherical eyecups were then visualized as azimuthal equal-distance projection. Thereby, the density of horizontal cells was calculated in spherical coordinates by counting the number of cells in a 10° spherical cup. For more information about the methodology of these protocols see the Material and methods section of the publication.

7.2.5 Genotyping protocols

The following section presents the genotyping protocol used to identify and verify the genotypes of the transgenic mouse lines used in the projects.

The protocol consists of two main steps: DNA extraction and DNA amplification by polymerase chain reaction (PCR). For the DNA extraction step from mouse tissue samples, the KAPA HotStart mouse genotyping kit was used. Samples were added to a solution containing the “digestive buffer” and the “enzyme solutions”. The pipetting scheme and the thermocycler setting are listed below (Tab. 13-14).

Table 13: Pipetting scheme for DNA extraction

Volume	Component
22 µl	Nuclease-free water
2.5 µl	Protease solution
2.5 µl	Extract buffer

Table 14: Thermocycler setting for DNA extraction

Step	Temperature	Duration	Cycles
Lysis	75°C	10 min	1
Heat-inactivation	95°C	5 min	1

The initial step is identical for each sample to be analyzed. However, the selective amplification via PCR is tailored to the specific sequence being targeted. In this case, below are listed different pipetting schemes and PCR settings for the different mouse lines used (*Cx57Cre*-PCR Table 15, *Cx57LacZ*-PCR Table 16, *GluA2/GluA4*-PCR Table 17).

The DNA bands were visualized using gel electrophoresis, which separates them by length in base pairs (bp). Samples, ladder, positive and negative controls were made to run in a 2% agarose gel for 40-45 minutes at a constant voltage of 120V. The amplified DNA from the samples and the ladder were finally detected and visualized using a UV transilluminator system.

Table 15: *Cx57Cre* PCR protocol

Pipetting scheme for PCR		PCR program setting			
Volume	Component	Step	Temperature	Duration	Cycles
2.95 μ l	Nuclease-free water	Initial Denaturation	95°C	3 min	1
6.25 μ l	Genotype Mix	Denaturation	95°C	15 sec	35
0.6 μ l	10 μ M Inter-Cre-rev	Primer Annealing	63°C	15 sec	
0.6 μ l	10 μ M Forward primer	Elongation	72°C	20 sec	
0.6 μ l	10 μ M Reverse primer				
1 μ l	Template	Final Elongation	72°C	10 min	1

Table 16: *Cx57LacZ* PCR protocol

Pipetting scheme for PCR		PCR program setting			
Volume	Component	Step	Temperature	Duration	Cycles
2.95 μ l	Nuclease-free water	Initial Denaturation	95°C	3 min	1
6.25 μ l	Genotype Mix	Denaturation	95°C	15 sec	35
0.6 μ l	10 μ M LacZ	Primer Annealing	63°C	15 sec	
0.6 μ l	10 μ M Forward primer	Elongation	72°C	20 sec	
0.6 μ l	10 μ M Reverse primer				
1 μ l	Template	Final Elongation	72°C	10 min	1

Table 17: *GluA2/GluA4* PCR protocol

Pipetting scheme for PCR		PCR program setting			
Volume	Component	Step	Temperature	Duration	Cycles
4.25 μ l	Nuclease-free water	Initial Denaturation	95°C	3 min	1
6.25 μ l	Genotype Mix	Denaturation	95°C	15 sec	37
0.6 μ l	10 μ M Forward primer	Primer Annealing	63°C	15 sec	
0.6 μ l	10 μ M Reverse primer	Elongation	72°C	20 sec	
1 μ l	Template	Final Elongation	72°C	10 min	1

7.3 Supplemental material

7.3.1 Updated nomenclature for ionotropic glutamate receptors

Table S1: NC-IUPHAR recommended and previous nomenclature of ionotropic glutamate receptor subunits.

Ionotropic glutamate family	NC-IUPHAR nomenclature	Previous nomenclatures
AMPA	GluA1	GLU _{A1} , GluR1, GluRA, GluR-A, GluR-K1, HBGR1
	GluA2	GLU _{A2} , GluR2, GluRB, GluR-B, GluR-K2, HBGR2
	GluA3	GLU _{A3} , GluR3, GluRC, GluR-C, GluR-K3
	GluA4	GLU _{A4} , GluR4, GluRD, GluR-D
Kainate	GluK1	GLU _{K5} , GluR5, GluR-5, EAA3
	GluK2	GLU _{K6} , GluR6, GluR-6, EAA4
	GluK3	GLU _{K7} , GluR7, GluR-7, EAA5
	GluK4	GLU _{K1} , KA1, KA-1, EAA1
	GluK5	GLU _{K2} , KA2, KA-2, EAA2
NMDA	GluN1	GLU _{N1} , NMDA-R1, NR1, GluR ξ 1
	GluN2A	GLU _{N2A} , NMDA-R2A, NR2A, GluR ϵ 1
	GluN2B	GLU _{N2B} , NMDA-R2B, NR2B, hNR3, GluR ϵ 2
	GluN2C	GLU _{N2C} , NMDA-R2C, NR2C, GluR ϵ 3
	GluN2D	GLU _{N2D} , NMDA-R2D, NR2D, GluR ϵ 4
	GluN3A	GLU _{N3A} , NMDA-R3A, NMDAR-L, chi-1
	GluN3B	GLU _{N3B} , NMDA-R3B
'Orphan' (GluD)	GluD1	GluR δ 1
	GluD2	GluR δ 2

Greek symbols in NMDA receptor subunit names were applied to the mouse orthologue only. International Union of Pharmacology Committee on Receptor Nomenclature and Drug Classification (NC-IUPHAR) - <http://www.iuphar-db.org/> (from (Collingridge et al., 2009)).

7.3.2 Staining pattern of the anti-GluA2 rabbit monoclonal antibody

The clone 1K4 ZooMAb™ rabbit recombinant monoclonal antibody targets an epitope within 16 amino acids from the C-terminal, cytosolic domain of the glutamate receptor GluA2.

The antibody was tested to detect the spatial distribution and different staining patterns of the AMPA-type glutamate receptors in mouse retina (Fig. S1). The antibody was found to be incapable of detecting the accumulation of the GluA2 subunit below the cone pedicles in the mouse retina. Anti-GluA2 antibodies exhibited robust immunoreactivity at the processes of HC axon terminals invaginating the rod spherules (see Fig. 14). But, in contrast to the monoclonal anti-GluA2 antibody raised in mouse, the rabbit monoclonal anti-GluA2 antibody failed to reveal clusters of AMPA receptors below the cone pedicles. This indicates a disparate recognition of the epitopes on the same proteins, which in turn gives rise to disparate staining patterns.

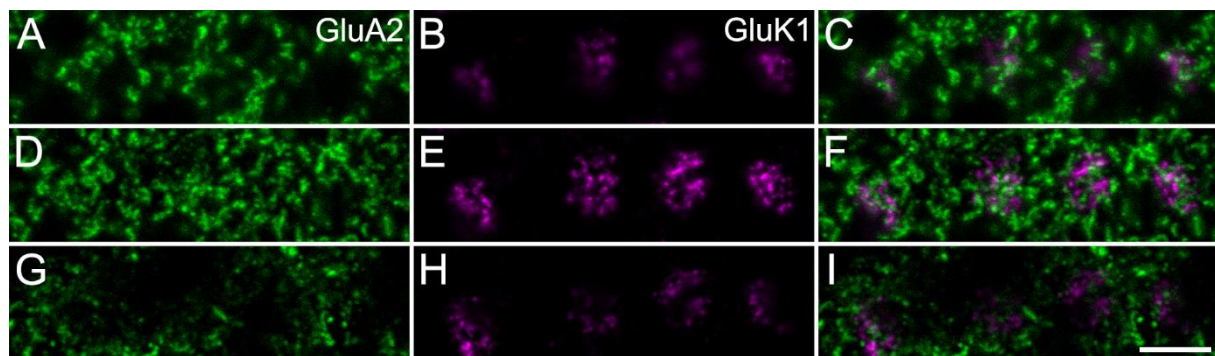


Figure S1: Anti-GluA2 rabbit monoclonal staining pattern in the OPL of the mouse retina

Whole-mounted retina double labeled for GluA2 with the anti-GluA2 rabbit monoclonal and the kainate glutamate receptor subunit 1 (GluK1) used as pedicle marker. Maximum projections of a single image Z-stack of the distal OPL (Z-steps 24-36/36, Z-size ~ 2.6 μm), **A-C**, at the level of invaginating dendrites at the pedicle base (Z-steps 19-23/36, Z-size ~ 1 μm), **D-F** and below the cone pedicle at the putative desmosome-like junctions (Z-steps 12-15/36, Z-size ~ 0.8 μm), **G-I**. Scale bar: 5 μm in I, applies to A-I.

7.3.3 Cx50 immunoreactivity was unchanged in Cx57-deficient mouse retinas

Cx50-containing gap junctions are predominantly expressed on the thick proximal axon terminals of horizontal cells. Immunostaining experiments (Fig. S2), along with previous studies, have demonstrated that these junctions are unable to compensate for a deficiency in dendritic Cx57 (Dorgau et al., 2015).

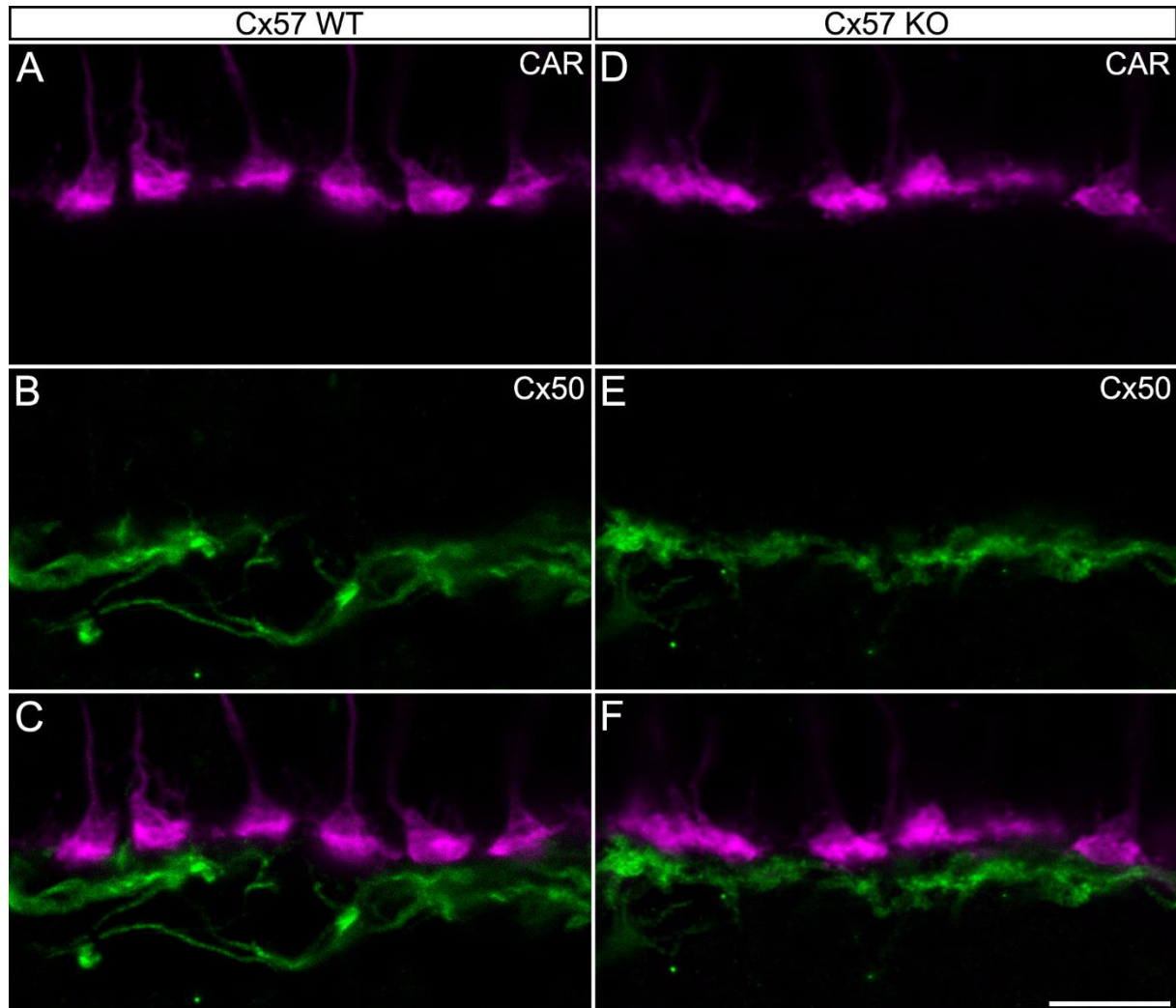


Figure S2: Cx50 immunoreactivity is unchanged in Cx57-deficient mice

Projections of confocal image stacks of vertical cryosections double labeled for the mouse cone arrestin (CAR), and the connexin 50 (Cx50). Images were acquired from the dorsal retina of Cx57^{+/+} (WT) mouse (Z-steps 8-18/27, Z-size ~ 2.2 μm) **A-C**, and from the dorsal retina of Cx57^{LacZ/LacZ} (Cx57 KO) mouse (Z-steps 11-22/31, Z-size ~ 2.4 μm) **D-F**. Scale bar: 10 μm in F, applies to A-F.

7.4 Publication

The following article presents a selection of findings from this thesis. The article is the result of a fruitful collaboration with Dr. Karin Dedek, Dr. Alejandra Acevedo, Dr. Martin Greschner and Christoph Block. The supervision and guidance provided by Dr. Christian Puller, Dr. Karin Dedek, Ulrike Janssen-Bienhold and Dr. Martin Greschner, was fundamental to the success of this project.

- Spinelli, M., Alejandra Acevedo, H., Block, C.T., Lindenthal, L., Schuhmann, F., Greschner, M., Janssen-Bienhold, U., Dedek, K., Puller, C., The first interneuron of the mouse visual system is tailored to the natural environment through morphology and electrical coupling, *ISCIENCE* (2024), doi: <https://doi.org/10.1016/j.isci.2024.111276>

Journal Pre-proof



The first interneuron of the mouse visual system is tailored to the natural environment through morphology and electrical coupling

Matteo Spinelli, H. Alejandra Acevedo, Christoph T. Block, Lucia Lindenthal, Fabian Schuhmann, Martin Greschner, Ulrike Janssen-Bienhold, Karin Dedek, Christian Puller

PII: S2589-0042(24)02501-X

DOI: <https://doi.org/10.1016/j.isci.2024.111276>

Reference: ISCI 111276

To appear in: *ISCIENCE*

Received Date: 15 July 2024

Revised Date: 2 October 2024

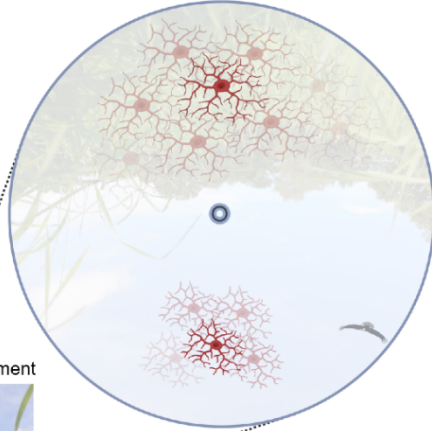
Accepted Date: 25 October 2024

Please cite this article as: Spinelli, M., Alejandra Acevedo, H., Block, C.T., Lindenthal, L., Schuhmann, F., Greschner, M., Janssen-Bienhold, U., Dedek, K., Puller, C., The first interneuron of the mouse visual system is tailored to the natural environment through morphology and electrical coupling, *ISCIENCE* (2024), doi: <https://doi.org/10.1016/j.isci.2024.111276>.

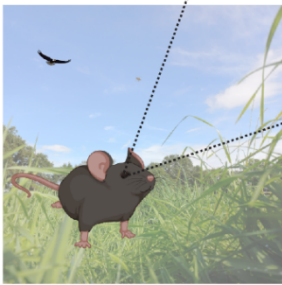
This is a PDF file of an article that has undergone enhancements after acceptance, such as the addition of a cover page and metadata, and formatting for readability, but it is not yet the definitive version of record. This version will undergo additional copyediting, typesetting and review before it is published in its final form, but we are providing this version to give early visibility of the article. Please note that, during the production process, errors may be discovered which could affect the content, and all legal disclaimers that apply to the journal pertain.

© 2024 The Author(s). Published by Elsevier Inc.

Horizontal cell size and electrical coupling



A mouse in its natural environment



Journal Pre-proof

The first interneuron of the mouse visual system is tailored to the natural environment through morphology and electrical coupling

Matteo Spinelli^{1*}, Alejandra Acevedo H.^{2*}, Christoph T. Block¹, Lucia Lindenthal¹, Fabian Schuhmann³, Martin Greschner^{1,4}, Ulrike Janssen-Bienhold¹, Karin Dedek^{2,4} and Christian Puller^{1,5}

*Equal contribution

1 Visual Neuroscience, Department of Neuroscience, Carl von Ossietzky Universität Oldenburg, Oldenburg, Germany

2 Neurosensorics/Animal Navigation, Institute for Biology and Environmental Sciences, Carl von Ossietzky Universität Oldenburg, Oldenburg, Germany,

3 Quantum Biology and Computational Physics, Department of Physics, Carl von Ossietzky Universität Oldenburg, Oldenburg, Germany

4 Research Center Neurosensory Science, University of Oldenburg, Oldenburg, Germany

5 Department of Computational Neuroethology, Max Planck Institute for Neurobiology of Behavior – caesar, Bonn, Germany

Lead Contact

Christian Puller, christian.puller@mpinb.mpg.de

Summary

The topographic complexity of the mouse retina has long been underestimated. However, functional gradients exist, which reflect the non-uniform statistics of the visual environment. Horizontal cells are the first visual interneurons that shape the receptive fields of down-stream neurons. We asked whether regional specializations are present in terms of horizontal cell density distributions, morphological properties, localization of gap junction proteins, and the spatial extent of electrical coupling. These key features were asymmetrically organized along the dorso-ventral axis. Dorsal cells were less densely distributed, had larger dendritic trees, and electrical coupling was more extensive than in ventral cells. The steepest change occurred at the visual horizon. Our results show that the cellular and synaptic organization of the mouse visual system are adapted to the visual environment at the earliest possible level, and that horizontal cells are suited to form the substrate for the global gradient of ganglion cell receptive fields.

Introduction

The topographic organization of neurons in the vertebrate retina reflects the lifestyle and behavior of a given species in its corresponding habitat. Some of the most basic functions of the visual system are supported by distinct cell distributions, such as prey capture or threat detection. One of the most prominent specializations is the human fovea, which provides us with high acuity vision. There, the cell density is extremely high, and the dendritic and corresponding receptive fields of the neurons are accordingly small. Our fovea is only one example of many, as topographic specializations can be found in various other vertebrate species^{1,2}.

One of the most commonly used model systems for the early visual system in vertebrates is the mouse retina. There, a well-known topographic specialization is the pattern of opsin expression in cone photoreceptors³⁻⁵. Green- and UV-sensitive opsins are expressed in a gradient along the dorso-ventral axis with a steep transition zone at the visual horizon of the mouse, reflecting the natural scene properties of its environment^{6,7}. However, the mouse retina has long been thought to lack any further major topographic variations beyond the distribution of opsins. In line with this simplified anatomical perspective, and due to the lack of better knowledge, functional properties of a given cell type have also been assumed to be the same, or at least very similar, across different retinal regions.

Today it is well known that the mouse retina exhibits many different patterns of topographic variations, some are restricted to distinct cell types, whereas others are more global². For instance, retinal ganglion cells show a distinct global density gradient with many more cells located in the ventral retina, i.e. the upper visual field^{8,9}. This is accompanied by complex density arrangements of cells in a type-dependent manner⁹⁻¹³. Functional specializations of individual ganglion cells of a given type across different retinal locations go hand in hand with the anatomical ones and are equally complex¹⁴⁻¹⁸. While some of these functional gradients may be shaped by intrinsic features of ganglion cells^{19,20}, regional changes of their response properties typically originate in the presynaptic circuitry. However, topographic variations of cells upstream of retinal ganglion cells are poorly understood.

One of the most outstanding examples of a functional gradient in retinal ganglion cells is the dorso-ventral change of their receptive field surround structure in terms of amplitude and spatial extent, with remarkable asymmetries in the vicinity of the visual horizon²¹. The origin of this phenomenon remains unknown. Inhibitory amacrine cell signaling in the inner retina contributes to the formation of ganglion cell receptive field surrounds²². Nevertheless, horizontal cells in the outer retina also play a fundamental role in the establishment of the ganglion cell receptive fields, including surround properties²³⁻²⁵. Thus, we hypothesized that horizontal cells contribute to the region-dependent changes of ganglion cell receptive fields.

Horizontal cells are the first inhibitory interneurons in the vertebrate visual system and positioned to indirectly modulate ganglion cell response properties via lateral synaptic interactions with photoreceptors and bipolar cells in the outer retina²⁶. The spatial extent of lateral interactions is determined by horizontal cell dendritic tree size and extensive electrical coupling of dendrites by gap junctions²⁷⁻³⁰. Our analysis of horizontal cell densities and dendritic field sizes, as well as gap junction distribution and the spatial extent of horizontal cell electrical coupling revealed a topographical organization of these features along the dorso-ventral axis of the retina. The most prominent distribution asymmetries occurred at the opsin transition zone, i.e. the mouse visual horizon.

Results

Horizontal cells play a crucial role in shaping the retinal output signals^{23–25}. Moreover, horizontal cells may match the ganglion cell receptive field surround properties with the visual environment: the strength and spatial extent increase along the dorso-ventral axis of the retina²¹. This change should then be reflected in horizontal cell morphological properties to support signaling at different spatial scales, i.e. large in dorsal retina, small in ventral retina, with a distinct transition zone at the visual horizon. Indeed, some evidence suggests that rodent horizontal cells show a certain level of density variation across retinal regions^{40,41} which may affect the sizes of cells. Thus, we analyzed the horizontal cell density distribution in high detail by considering each and every cell body across complete wild-type mouse retinas.

Horizontal cell density and dendritic tree size form a gradient across the retina

Whole-mounted retinas were labeled with antibodies against calbindin (CaBP, Fig. 1A, B), a common mouse horizontal cell marker⁴². The positions of all immunolabeled horizontal cell bodies were manually marked in a merged microscopic tile scan of the flattened retina (Fig. 1C), where each dot indicates the position of a horizontal cell body (17650 ± 1412 , $n=5$ retinas, see supplemental Fig. S2). The cloverleaf shape of the tissue was reconstructed back into the original, almost hemispherical structure of the eyecup with Retistruct to calculate the densities of cells across the complete retinas^{9,32}. The local density was calculated and shown in an azimuthal equal distance projection (Fig. 1D). The 3D reconstruction allowed a proper averaging of data across five retinas independent of the relief cuts in the original whole-mounts. The retinas were counterstained with antibodies against the short-wavelength sensitive (S-)opsin to reveal the transition zone of opsin expression as an indicator of the visual horizon on the retina^{5,7,21}. The transition zone is represented by lines in Fig. 1C-E (see Fig. 4A and D for representative microscopic images). Note that the transition zone was located far above the optic disc, but then it crossed the peripheral ends of the lower leaflets in a typical retinal whole-mount preparation (Fig. 1C). Future studies of retinal whole-mounts may be informed by these regionalization details and ensure a proper interpretation of data collected from definite positions of the mouse retina. The horizontal cell density was low in the dorsal retina and high in the ventral retina. The steepest change in this gradient occurred in the area of the S-opsin transition zone. The general pattern of this density distribution closely resembled the density gradient of mouse cone photoreceptors^{5,43}. Like other retinal cell types, horizontal cells form a mosaic across the retina, where the dendritic trees of the cells exhibit a constant overlap^{44–46}. Thus, a change in cell density should yield a

corresponding change in dendritic field sizes. Individual horizontal cells were dye-injected ($n=69$) to investigate if the density distribution serves as a direct read-out of dendritic field size, and to gain further insights into the horizontal cell dendritic field structure across the retina (Fig. 1F-J, supplemental Fig. S3). Convex hulls that encompassed the dendritic trees of the injected cells were used to measure their dendritic areas. The analysis revealed that horizontal cell dendritic trees located above the transition zone covered a much larger area ($n=25$, $6165\pm 2357 \mu\text{m}^2$) than cells below ($n=44$, $4633\pm 1196 \mu\text{m}^2$), with calculated dendritic field diameters of $87\pm 2 \mu\text{m}$ or $76\pm 9 \mu\text{m}$, respectively (tailed Wilcoxon rank sum $p<0.01$). A fit to explain the relationship between the cell density and the dendritic area (Fig. 1K) predicted a coverage factor of ~ 5 , which is largely in line with previously published results⁴⁵. Horizontal cell morphology is characterized by dense dendritic branching in central parts of the dendritic tree and sparser, less arborized dendrites in the periphery^{47,48}. Here, injected cells were traced through the image stacks ($n=23$, supplemental Fig. S3). A Sholl analysis³⁵ was applied to the resulting skeletons to investigate whether this branching pattern of horizontal cells may differ between cells from different locations (Fig. 1 L,M). This was not the case, as the results showed a constant branching pattern across the retina. The homogeneous morphology of horizontal cells across all dorsal and ventral cells in our sample became even more prominent (except for one outlier) when the data was normalized to account for the different sizes of the cells.

Horizontal cell dendritic gap junction density changes at the visual horizon

The shape and size of a dendritic tree of a given retinal neuron is typically one of the major determinants of its functional receptive field. Thus, based on our findings, one would expect to find much larger horizontal cell receptive fields in the dorsal retina relative to those located below the opsin transition zone. On the other hand, horizontal cells are well known to exhibit extensive electrically coupled networks via gap junctions, which have been shown to directly affect the receptive field properties of the cells^{27,29,30}. Thus, extensive electrical coupling leads to an increase in the spatial extent of receptive fields and lateral signal spread.

Therefore, we analyzed potential differences of horizontal cell dendritic gap junctions across the retina, which may further influence horizontal cell signaling properties in a region-dependent manner. A prerequisite for such an analysis is, of course, a detailed knowledge of the types and positions of horizontal cell gap junctions. Electrical coupling of mouse horizontal cell dendrites is exclusively supported by gap junctions containing connexin 57 (Cx57)^{28,29,36,49}. Together with Cx50, Cx57 is also involved in the formation of gap junctions between horizontal cell axon terminals⁵⁰. However, the latter are only connected to rod photoreceptor terminals and do not

contribute to dendritic signaling⁵¹. Therefore, axon terminal connexins were largely excluded from our study by restricting the analysis to mostly dendritic Cx57 in a volume beneath a given cone pedicle base (Fig. 2).

Individual dendrites of multiple horizontal cells converge beneath the cone pedicles in the proximal part of the outer plexiform layer (OPL) before their tips invaginate into the pedicle at the glutamate release sites. Mammalian horizontal cells are thought to form dendritic gap junctions primarily in this area of the proximal OPL³⁶. Correspondingly, Cx57-immunoreactive plaques were mostly clustered in the proximal OPL beneath the array of cone pedicles (Fig. 2A-C).

Horizontal cells were injected with neurobiotin, a small tracer molecule which can pass through gap junctions between cells to reveal their complete electrically coupled network^{27,30,52,53}. Here, we combined neurobiotin-injected cells with immunolabeling of Cx57 and high-resolution fluorescence imaging to reveal the exact position of horizontal cell gap junctions on their dendrites (Fig. 2D-I). Cx57-positive plaques were colocalized with horizontal cell dendrites in a region ~2 μm beneath the pedicle, where the dendrites converged and exhibited slight swellings. This may correspond to a specialized area where glutamate-receptor containing desmosome-like junctions are closely associated with gap junctions and the tight-junction protein zonula occludens-1 (ZO-1) on horizontal cell dendrites^{36,54}.

Counterstaining of Cx57 with ZO-1 in the dorsal retina (Fig. 3A-H) confirmed previous results where the immunolabeling was largely colocalized beneath mouse cone pedicles³⁶. The same experiment performed on the ventral retina yielded a completely different picture (Fig. 3I-P). While the overall extent of GluK1 as a pedicle marker did not obviously change across regions, ZO-1 was less densely clustered and lacked the typical elongated plaques beneath pedicles and in areas between them. Most importantly, the amount of Cx57 immunoreactive puncta appeared largely reduced, resulting in a decrease of colocalization between Cx57 and ZO-1. Next, the distribution pattern of ZO-1 and Cx57 was investigated in detail relative to the S-opsin gradient with its transition zone as an indicator for the visual horizon of the mouse. It became obvious that the change from dense Cx57 clustering and robust colocalization with ZO-1 toward highly reduced Cx57 and the lack of colocalization occurred only within a few hundred microns at the transition zone (Fig. 4A-C). Colocalization of Cx57 with ZO-1 and measurements of the area covered by the corresponding immunostaining was performed in small image stack volumes collected from circular ROIs beneath each pedicle ("proximal OPL" as in Fig. 2G-I).

The data was collected and pooled from four locations in the dorsal and ventral retina, respectively (example boxes in Fig. 4D; 3 retinas, containing a total of 144 ROIs of dorsal pedicles, 131 ROIs of ventral pedicles). The original notion that ZO-1 and specifically Cx57 were less densely

clustered at ventral cone pedicles was confirmed by the quantification of immunoreactive areas. These areas were measured within individual ROIs beneath single cone pedicles. Thresholding and normalization was applied (Fig. 4E-G, see methods section for details) to account for different signal-to-noise ratios of the immunostainings in the 3 retinas. ZO-1 and Cx57-positive areas were reduced from dorsal to ventral retina by 22% and 35%, respectively ($p < 0.001$, Fig. 4E,F). Furthermore, the colocalization of ZO-1 and Cx57 was reduced by 84% from dorsal to ventral parts of the retina ($p < 0.001$, Fig. 4G). No significant differences were observed between the measurements of immunoreactive areas along the nasal-temporal axis (p -value Cx57: 0.96, ZO-1: 0.20) or along increasing eccentricities (Cx57: 0.80, ZO-1: 0.64).

As control measurements, colocalization was analyzed again in the same images but with one vertically flipped channel per ROI at single cone pedicles³⁹. Colocalization in the flip control of the dorsal retina was significantly reduced by 73%, suggesting that the overlap measured in the original image did not occur randomly. Colocalization in control measurements of the ventral retina was reduced by 45%. This reduction was not significant due to the low amount of colocalization in the original images.

Changes in gap junction organization translates into distinct patterns of electrical coupling

The difference in the gap junction density on horizontal cell dendrites from dorsal and ventral retina was striking. It remained unclear, however, whether this change resulted in a functional difference, i.e. different electrical coupling strengths in dorsal versus ventral regions. Therefore, horizontal cells of wild-type mice were injected with the tracer molecule neurobiotin to visualize the extent of electrical coupling of a given cell in a determined location of dorso- or ventro-nasal retina (Fig. 5A). Beyond the spatial restriction to the nasal retina, each horizontal cell was injected under constant conditions, including current, injection duration, time of day, lighting, and temperature, to allow for proper comparability between the experiments. The results from these experiments confirmed distinct coupling patterns as suggested by our anatomical results. In the dorsal retina, more cells were electrically coupled to a given horizontal cell ($n=7$; 233 ± 45 coupled cells) and the coupling extended across a larger area (0.245 ± 0.039 mm²; Fig. 5B-E). The exact opposite was true for ventral horizontal cells ($n=7$), which exhibited coupling to fewer cells (130 ± 46) in a smaller area (0.111 ± 0.047 mm²).

Discussion

Our study provides evidence for dorso-ventral asymmetries of horizontal cell features in the mouse retina, in terms of I) the cell density and dendritic tree size, II) the density of gap junctions clustered on their dendrites, and III) the extent of electrical coupling regarding the number of coupled cells and the area covered by them. Cell density gradients across the mammalian retina are well known, including corresponding morphological changes of the cells^{1,2}. It is remarkable, however, that the horizontal cell density gradient reported here is accompanied by a matching change in the synaptic architecture of the cells, i.e. the density and distribution of electrical synapses and the corresponding coupling strength. This change will directly affect the spatial range of signaling at the first synapse in the visual system, as a tight relationship between the extent of electrical coupling and receptive field sizes exists in mammalian horizontal cells^{27,29,30}. Moreover, we provide evidence that these asymmetries match the global properties of the visual environment of the animal, where the most prominent transition of the aforementioned horizontal cell features occurs in the area of the visual horizon of the animal.

Horizontal cells support the functional separation of the mouse visual field

Differences in the functional separation of upper and lower mouse visual fields are well known and some neuronal adjustments of the outer retina have already been revealed at the level of photoreceptors and bipolar cells^{3-7,41,55}. To our knowledge, horizontal cells have rarely been considered in this context (but see ⁴¹, their Fig. 3). Horizontal cells located above the photoreceptor transition zone receive visual information from the ground, and they possess large dendritic trees and exhibit extensive electrical coupling. Horizontal cells below this zone are positioned for information from the upper visual field by smaller dendritic trees and reduced spatial extent of electrical coupling. Therefore, the characteristics of large dendritic trees paired with extensive coupling versus small dendritic trees paired with reduced coupling operate hand in hand as complementary phenomena to create large or small functional units in the lower or upper visual field, respectively (Fig. 6). Small functional units can serve high spatial resolution and would be beneficial for the detection of threats from overhead predators, for instance. Previous work has identified the transient OFF alpha ganglion cell as one of the retinal output cell types responsible for triggering innate defensive behaviors upon approach detection⁵⁶⁻⁵⁸. These ganglion cells are prominently affected by horizontal cell signaling²⁵, which is in line with the idea of horizontal cells contributing directly to the processing of the visual scene and to retinal output signaling. On the other hand, integration of signals across a larger area, specifically in the receptive field surround,

may improve signal detection in front of the animal and in the lower visual field assuming more abundant transitions of low and high contrast signals.

The horizontal cell contribution to receptive field properties of mouse ganglion cells in the inner retina has remained a controversial topic, including electrical coupling of horizontal cells, which did not seem to play a dominant role in ganglion cell signaling⁵⁹. However, a series of recent studies from independent research laboratories provided evidence for horizontal cell signaling as a major influence on ganglion cell receptive field surrounds^{23–25} with previous inconsistencies in observations likely originating in experimental stimulus properties, such as spatial scales or light levels and the focus on certain ganglion cell types²⁵. Therefore, the functional consequences of the horizontal cell feature asymmetries observed here would affect the ganglion cell receptive field surround in the upper visual field to be spatially restricted due to smaller cell sizes and lesser extent of electrical coupling (Fig. 6). In the lower visual field, however, the inhibitory feedback signals of horizontal cells distribute across a larger area, causing a much wider surround of postsynaptic cells with potentially lower amplitudes. These ganglion cell receptive field properties have indeed been shown to exist, and they form a gradient across the retina with the most prominent change at the S-opsin transition zone²¹, resembling our findings of the horizontal cell gradient and its gap junction coupling asymmetry.

The cellular basis of the horizontal cell coupling asymmetry

The cellular basis of the difference in electrical coupling is formed by the asymmetric density distribution of the gap junction protein Cx57 at the horizontal cell dendrites. One cannot rule out that some axonal Cx57 has been included in our measurements, but the numbers should be dominated by dendritic gap junctions because of the restricted analysis areas beneath cone pedicles, where most dendritic gap junctions are formed. Interestingly, our observations included a structural change of gap junctions beneath cone pedicles, beyond a mere reduction of Cx57-positive puncta. This was most prominent in the lack of large, elongated ZO-1 plaques. ZO-1 is typically colocalized or closely associated with dendritic horizontal cell gap junctions, where it is thought to form tight junction barriers at the outer perimeter of gap junction plaques at horizontal cell dendrites, but not at their axon terminals³⁶. Thus, both of the most prominent protein components at the horizontal cell dendritic gap junction are regulated to meet the demands of the mouse visual environment. The reduction of ZO-1 in the ventral retina was obvious but less striking than the reduction of Cx57. This is likely resulting from the association of ZO-1 with Cx36-containing gap junctions at OFF bipolar cell dendritic tips beneath the cone pedicle³⁶ combined with an increase in OFF bipolar cell dendritic density in the ventral retina^{41,55}. We did not attempt

to exclude ZO-1 potentially associated with OFF bipolar cell dendrites from our analysis due to the close spatial vicinity of the two layers of gap junction types.

A compensation of the reduced Cx57 expression by a potential upregulation of another connexin subunit can be ruled out. First, we observed a change in the functional coupling pattern of horizontal cells, which supported the anatomical observations and argued against any compensatory mechanism. Second, Cx50 is another gap junction protein expressed by horizontal cell axons, but it has been shown that it does not compensate for a lack of dendritic Cx57⁵⁰.

Conclusions

Mouse horizontal cells are shaping the ganglion cell receptive field surround properties across a spatial gradient of morphological and functional features, which is adapted to the visual scene of the animal. Future studies are required to elucidate the exact interplay of dendritic tree size and potential modulation of electrical coupling, in concert with the complex local and global modes of horizontal cell signaling features^{48,60}. In this context, it would be enticing to analyze horizontal cell features in model species from different habitats and life styles, with natural environments which differ from those of the common C57/Bl6 mouse model in terms of scene statistics and general ecology.

Limitations of the study

We provide evidence for a region-dependent change in the dendritic tree size and electrical coupling of horizontal cells, which likely contributes to the global gradient of ganglion cell receptive fields. However, the possible effects of light adaptation and time of the day have not been explored here. Light adaptation is well known to affect the extent of electrical coupling of horizontal cells via dopamine, which is released by certain amacrine cells, depending on ambient light levels and the circadian rhythm⁶¹. We kept the light adaptation levels and the time of the experiments (during the subjective day) constant to achieve consistent and comparable results. However, mice are nocturnal animals, and regional coupling patterns at nighttime remain elusive.

Author contributions

Conceptualization, U.J.B., K.D., C.P.; Investigation, M.S., A.A.H., L.L.; Formal Analysis, M.S., A.A.H., C.T.B., F.S.; Data Curation, C.T.B.; Writing – Original Draft, C.P.; Writing – Review & Editing, all authors; Supervision, M.G., U.J.B., K.D., C.P.

Acknowledgements

We would like to thank Bettina Kewitz and Hannah Käse for excellent technical assistance, Sabrina Duda for expert support with the acquisition and processing of horizontal cell density data, and Asli Pektaş for help with the large-scale quantification of cells in whole-mounted retinas. We also thank Silke Haverkamp and Ben Reese for valuable comments on an earlier version of the manuscript. We acknowledge the Fluorescence Microscopy Service Unit, Carl von Ossietzky University of Oldenburg, for the use of the imaging facilities. Figure 6 was created with BioRender.com. This work was supported by DFG RTG 1885/2 to M.G., U.J.B., K.D. and DFG SFB1372: Magnetoreception and Navigation in Vertebrates, Project 395940726 to K.D. and M.G..

Declaration of interests

The authors declare no competing interests.

Figure 1. Horizontal cell density and dendritic field size change across the retina

A,B: Confocal images of dorsal (A) and ventral (B) whole-mounted retina labeled against calbindin (CaBP). **C:** Each dot represents the cell body position of a horizontal cell marked with CaBP across a complete retina of a left eye. The red lines in C and D mark the S-opsin transition zone (see also Fig. 4). D, dorsal; V, ventral; N, nasal; T, temporal. **D:** Azimuthal equal-distance projection of the reconstructed retinal sphere of the data shown in C. The color of the dots represents the local density of the corresponding cell body position. **E:** Horizontal cell density distribution averaged across 5 retinas. Black line, mean S-opsin transition zone, gray lines, SD (n=5). Color bars in D and E indicate cells/mm². **F-I:** Dye-injected horizontal cells from dorsal (F) and ventral (H) retina, together with the corresponding skeletons (G, I) traced through confocal image stacks of the cell with convex hulls to determine the dendritic tree area. **J:** Positions and dendritic field sizes of 69 injected horizontal cells, superimposed on the averaged density distribution from E. Circle area represents the relative area of the corresponding horizontal cell; for better visibility circles are not shown to scale. Filled orange and blue circles show the positions of horizontal cells from F and H, respectively. **K:** Relation between horizontal cell dendritic field size and local horizontal cell density. Lines describe the best estimate assuming a constant coverage factor (5.04, 95% CI [4.72, 5.37]). **L:** Sholl analysis of dendritic intersections from 23 horizontal cells. **M:** As in L but data normalized to dendritic area (convex hull). Scale bars: 50 μ m in B, 1 mm in C, 20 μ m in I, applies to F-I.

Figure 2. Spatial localization of horizontal cell gap junctions

A-C: Projections of a confocal image stack of a vertical cryostat section double-labeled for the kainate receptor subunit 1 (GluK1, used as a cone pedicle marker) and the horizontal cell gap junction protein

connexin 57 (Cx57). **D-F**: Maximum intensity projections of a confocal image stack of whole-mounted retina labeled with antibodies against Cx57 and with Alexa Fluor 568-conjugated streptavidin after microinjection of neurobiotin into a horizontal cell. The distribution of Cx57 is shown at the tips of horizontal cell (HC) dendrites invaginating into two cone pedicles. Pedicle positions were identified by these clusters of invaginating dendritic tips and are indicated by dashed circles. **G-I**: As in D-F, but ~2 μm beneath the same pedicle position. INL, inner nuclear layer; OPL, outer plexiform layer. Scale bars: 10 μm in C, applies to A-C; 5 μm in I, applies to D-I.

Figure 3. Clustering of ZO-1 and Cx57 differs in dorsal and ventral retina

A-D: Maximum intensity projections of a confocal stack from a vertical cryostat section of dorsal retina triple-labeled against the kainate receptor subunit 1 (GluK1), the tight junction protein zonula occludens-1 (ZO-1), and connexin 57 (Cx57). Dashed lines indicate pedicle positions marked by GluK1 staining. **E-H**: As in A-D from a piece of whole-mounted retina. Maximum-intensity projections were chosen to cover the proximal OPL beneath cone pedicles. Circles indicate pedicle positions. Arrows indicate an example pedicle of which single optical sections of the corresponding channels are shown in the box (top right). **I-P**: As in A-H but from ventral retina. Scale bars: 5 μm in L, applies to A-D and I-L; 5 μm in P, applies to E-H and M-P; 1 μm box in P, applies for single optical section boxes E-H and M-P.

Figure 4. Clustering density of horizontal cell gap junctions changes at the S-opsin transition zone

A-C: Maximum intensity projections of confocal image stacks from the region of the short-wavelength sensitive (S)-opsin transition zone. The retinal whole-mount was quadruple-labeled with antibodies against S-opsin, GluK1, ZO-1, and Cx57. A, cone outer segments positive for S-opsin at the transition zone. Boxes B and C indicate regions where confocal image stacks (B₁-C₄) were acquired. B₁-B₄ shows GluK1, ZO-1, and Cx57 at the level of the OPL in the position of box B (in A), close to the transition zone but on its dorsal side. Three example pedicles are indicated by circles. C₁-C₄, as in B₁-B₄ but for the area C on the ventral side of the transition zone. **D**: Azimuthal equal-distance projection of tile scans of a complete, whole-mounted retina immunolabeled against S-opsin. Boxes indicate the locations where image stacks were acquired for the quantification of Cx57 and ZO-1 immunostaining. **E-G**: Quantification of the immunolabeled areas (normalized from μm^2) of Cx57 and ZO-1 and their colocalization per circular ROI beneath each pedicle. Measurements were pooled across dorso-peripheral locations (orange, all upper boxes in D combined) and the ventro-peripheral locations (blue, all lower boxes in D combined). Dashed lines in violin plots show median and quartiles. Each data point represents the measurement in a ROI beneath one pedicle. Orig, colocalization analyzed in the original image stack, Flip, control measurement where one channel per ROI was vertically flipped. Unpaired, two-tailed Mann Whitney test (E, F) and one-way ANOVA with a post-hoc Tukey test for multiple comparisons (G), *** $p < 0.001$; ns, not significant. Scale bars: 100 μm in A; 5 μm in C₄ applies to B₁-C₄.

Figure 5. Tracer coupling patterns of horizontal cells differ in dorsal and ventral retina

A: The position of neurobiotin-injected horizontal cells is indicated by circles superimposed on the density distribution disc taken from Fig. 1E. The area of the circles reflects the number of tracer-coupled cell bodies per injected horizontal cell. Orange and blue filled circles represent the example injections in B-E. **B,C**: Example tracer-coupling patterns upon injection of neurobiotin into single cell bodies (B, in dorsal retina; C, ventral). Convex hulls encompassing all neurobiotin-positive cell bodies were used to measure the area of neurobiotin-spread. **D,E**: Quantification of the number of tracer-coupled horizontal cell bodies (D, $p < 0.01$) and the area of tracer-spread (E, $p < 0.001$) per injection (Mann-Whitney tests). Vertical lines indicate median. Scale bar 100 μm in C, applies to B and C.

Figure 6. Horizontal cell feature asymmetry supports a receptive field architecture adapted to the visual environment.

Dendritic tree size and electrical coupling area of horizontal cells is roughly twice as large in the lower visual field than in the upper. The feature asymmetries shown here are well suited to form the cellular substrate underlying the global asymmetry of ganglion cell receptive field surrounds across the retina (right, brown discs, blue discs represent receptive field centers, adopted from ²¹).

STAR Methods**RESOURCE AVAILABILITY**

- Lead Contact

Further information and requests for resources and reagents should be directed to and will be fulfilled by the Lead Contact, Christian Puller, christian.puller@mpinb.mpg.de

- Data and code availability
 - All data reported in this paper will be shared by the lead contact upon request.
 - This paper does not report original code.
 - Any additional information required to reanalyze the data reported in this paper is available from the lead contact upon request.
- Material availability

All unique reagents generated in this study are available from the lead contact with a completed materials transfer agreement.

EXPERIMENTAL MODEL AND STUDY PARTICIPANT DETAILS

Only mice were used and no new human participants were recruited for this study. All procedures were performed in accordance with the law on animal protection (*Tierschutzgesetz*) issued by the German Federal Government and approved by the local animal welfare committee. Mice of either sex were used, including the wild-type (C57BL/6J), Cx57^{lacZ/lacZ}, and Cx57^{+/+} animals on C57BL/6J genetic background²⁸. Wild-type mice were used for all experiments except for the validation of antibody specificity (Fig. S1). Animals were housed under standard conditions, including a 12-hr light/dark cycle with water and food *ad libitum*.

Mice (ages: 2-4 months for quantification of the horizontal cell (HC) density, 3-5 months for immunohistochemistry, 3-4 months for HC injections) were deeply anesthetized with carbon dioxide and killed by cervical dislocation or decapitation.

METHOD DETAILS

Tissue preparations

After ascertaining the death of the animal, eyes were immediately enucleated and lens and vitreous were removed in a 0.01 M phosphate buffered saline (PBS, pH 7.4) or in a 0.1 M phosphate buffer (PB, pH 7.4). For HC injections, animals have been dark adapted for at least 1 hour before they were sacrificed and the subsequent tissue preparation was performed under infrared illumination using night vision goggles (No. G18597, Gutzeit-GmbH). Retinal dissection was performed in Ames medium (Sigma/Biomol) supplemented with sodium bicarbonate and bubbled with carbogen at 30-32 °C, pH 7.4. Fixation of the tissues was performed at room temperature (RT). Posterior eyecups were immersion-fixed in initially cold 2-4% paraformaldehyde (PFA) diluted in PBS for 15-20 min. Injected retinas were fixed in 2% PFA diluted in 0.1 M PB for 20 min.

For immunohistochemistry, retinas were cryoprotected after fixation in sucrose solution (30% w/v) overnight at 4°C and then stored at -20°C until use. To keep track of the retinal orientation, the choroid fissures were used to place marking cuts into the tissue³¹. For cryosections, the tissue was then embedded in Tissue-Tek O.C.T. Compound (Sakura Finetek) and sectioned vertically at 20 µm using a Leica CM1860 cryostat. For whole-mounted retinas, four radial relieving cuts were made without compromising the initial marking. Then, the retinas were dissected in PBS or in Ames depending on the following set of experiments. This was performed in a way that the complete retina was preserved, including the most peripheral region (outer marginal zone). Finally, the tissue was mounted on a black nitrocellulose filter membrane (Millipore) with the ganglion cell side up, for immunohistochemistry or cell injections.

Immunohistochemistry

Immunohistochemical labeling was performed by an indirect fluorescence method. Vertical sections were incubated overnight at RT with primary antibodies (*Primary antibodies* table and supplemental information, Fig. S1). Three different antibodies against Cx57 were used in this study. They were tested extensively and yielded the same Cx57 staining patterns in the mouse retina as previously published^{28,36,49}. Thus, they were used interchangeably in this study. Two of the polyclonal antibodies against C-terminal peptides of mouse Cx57 were newly raised in guinea pigs (Davids Biotechnologie GmbH, Regensburg, Germany). They were termed CSM and PGS (Fig. S1), and their amino acid sequences are listed in the *Primary antibodies* table. The specificity of the antibodies was demonstrated by immunostainings in wild-type (WT, Cx57^{+/+}) and Cx57-

deficient mice (KO, Cx57^{lacZ/lacZ})²⁸. The common Cx57 immunoreactivity of the two different antibodies was readily observed in wild-type animals following standard protocols (see below) but it was absent in retinal sections of Cx57-deficient mice using the same conditions (Fig. S1).

Antibodies were diluted in incubation solutions containing either 5% normal donkey serum (NDS), 1% bovine serum albumin (BSA), 0.5% Triton X-100 in PBS, or 5% Chemiblocker (Millipore) and 0.3% Triton X-100 in Tris-buffered saline (TBS, pH 7.6). Afterward, sections were incubated for 90 min with secondary antibodies diluted in the corresponding incubation solution. Whole-mounted retinas were incubated at RT for 2-3 days in the primary antibody solution containing 5% NDS, 1% BSA, and 1% Triton X-100 in PBS. Secondary donkey antibodies were incubated at RT for 2h or overnight in the same incubation solution. Type and dilution of secondary antibodies was the same for vertical sections and whole-mounts (Alexa Fluor 488, 568, and 647, 1:500, Invitrogen; Alexa Fluor 405, 1:500, Abcam; CF568, 1:500, Sigma).

Retinas where HCs were injected with neurobiotin (see “Horizontal cell injections” below), which were intended for immunostaining of Cx57, were fixed and labeled using the same protocol as described above. Alexa Fluor 568-conjugated streptavidin (1:250, Invitrogen) was used to visualize neurobiotin during the secondary antibody incubation.

Retinas were mounted together with the filter paper on slides in Vectashield (Vector Laboratories). Spacers between glass slides and coverslips were used to avoid squeezing the tissue. Dye-injected specimens were directly mounted on glass slides with Vectashield and coverslipped with spacers as described above. Neurobiotin-injected specimens for the tracer-coupling analysis of HCs were first incubated overnight at 4°C with Alexa Fluor 568-conjugated streptavidin (1:250), diluted in incubation buffer containing 10% NDS, 0.3% Triton X-100 in 0.1 M PB before mounting.

Primary antibodies

Antibody	Host, type	Working dilution	Immunogen	Source, Catalog #
Calbindin	Rabbit, Polyclonal	1:2000	Recombinant rat calbindin D-28k	Swant CB-38A
Cx57	Guinea pig, Polyclonal	1:500(w)/1:100(c)	C-terminal peptide of mouse Cx57 PGSRKASFLSRLMSEK	This study
Cx57	Guinea pig, Polyclonal	1:200(w)/1:100(c)	C-terminal peptide of mouse Cx57 CSMSMILELSSIMKK	This study
Cx57	Rabbit, Polyclonal	1:500	CSMSMILELSSIMKK	Janssen-Bienhold et al., 2009
GluK1	Mouse, Monoclonal	1:2000	aa 869-918 C-terminus of human GluK1	Santa Cruz Biot. sc-393420

S-opsin	Goat, Polyclonal	1:10000	N-terminus of the of human OPN1SW	Santa Cruz Biot. sc-14363
ZO-1	Mouse, Monoclonal	1:100	aa 334–634 of human recombinant ZO-1	Zymed, 33-9100
ZO-1	Rabbit, Polyclonal	1:100	aa 463–1109 of human zonula occludens-1 cDNA	Zymed, 61-7300

Dilutions used for labeling of cryosections (c) or whole-mounted retinas (w) if different depending on condition

Retina reconstructions

For the large-scale quantification of HC densities, the merged tile scans of image stacks from whole retinas were used. The R package Retistruct³² was used to reconstruct the dissected whole-mounts to the spherical cap shape of the intact retina. 3D reconstruction allowed a better estimate especially at the cloverleaf outline and avoided some miscalculation introduced by stress during flattening. In each retina, the tissue outline and the incisions were manually marked. In rare cases of folded, damaged, or missing retinal tissue, the extent of the retina was manually estimated. The rim angle of the reconstructed retina was set to 110° and the radius of the retina to 1.5 mm, as measured from independent cryosections and in accordance with earlier reports³³. The reconstructed spherical caps were visualized as an azimuthal equal-distance projection. Individual calbindin-positive HC bodies were manually marked using the CellCounter plugin in Fiji, in 5 retinas. The boundary of the short-wavelength sensitive (S-)opsin gradient was manually identified in the same 5 retinas and was represented as mean ± standard deviation (SD, Fig. 1, 5, S2, S3). The local density of horizontal cells was calculated in spherical coordinates by counting the number of cells in a 10 degree spherical cap. This radius corresponds to an arc length of ~260 μm and a counting disc area of 0.21 mm². This counting area was corrected to reflect marked regions where data was unattainable. The average density across different retinas was calculated in a fixed regular grid.

Coverage factor was defined as the number of HCs within the dendritic field of one cell and estimated by multiplication of density and convex hull area. Under the assumption of a constant coverage factor, this relation was fitted in MATLAB using the data shown in Fig. 1K.

Horizontal cell injections

Cell nuclei in whole-mounted retinas of wild-type mice were visualized by prior incubation in Ames medium containing 0.3 - 0.5 μM of DAPI (Abcam) for 60 min at 32 °C. Then the retinas were mounted onto black nitrocellulose membrane (see above).

Borosilicate glass electrodes were pulled with a micropipette puller (P-97, Sutter Instrument CO) to obtain sharp electrodes with a resistance between 100 – 200 M Ω . HCs were injected either with a fluorescent dye alone (to analyze the morphology of the cells) or with a mixture of dye and the gap junction tracer molecule neurobiotin (to analyze the electrical coupling).

For fluorescent dye injections, the electrodes were filled with 2 μ l of 5 mM of Alexa Fluor 568 hydrazide (Invitrogen, diluted in 200 mM KCl) and backfilled with 10 μ l of 200 mM KCl. Epifluorescence light was used to identify DAPI-labeled HC bodies based on their location and their relatively large size. Candidate cell bodies were targeted under visual control with epifluorescence illumination and impaled with sharp electrodes for dye iontophoresis using -0.5 nA square pulses of 500 ms at 1 Hz for 3 min. After injections, the retina was fixed in PFA as described above.

Neurobiotin injections were restricted to the nasal side of a given retina. Electrodes were tip-filled with 3 μ l of a 1:1 mixture of 4% neurobiotin (SP1120, Biozol) diluted in 0.1 M Tris buffer (pH 7.3) and 5 mM Alexa Fluor 568 Hydrazide, and back-filled with 10 μ l of 200 mM KCl in Tris buffer. The dye was injected as described above for 1-2 minutes before the current was reversed to inject neurobiotin using +0.5 nA square pulses of 500 ms at 1 Hz for 5 min. Then, a neurobiotin diffusion time of 10 min was granted before fixation. Only a single HC was injected per retina (dorsal n=7, ventral n=7) to provide constant conditions for these experiments to quantify tracer coupling.

Image acquisition

High-resolution fluorescence image stacks were acquired using TC SP8 or TCS SL confocal laser scanning microscopes (Leica). Scanning was performed with 63x/1.32 or with 63x/1.4 oil-immersion objectives and z-axis increments between 0.1 and 0.3 μ m. The SP8 confocal microscope with either 40x/1.3 or 63x/1.4 oil-immersion objectives was also used to acquire image stacks of HC dendritic trees. Image stacks of the coupled HCs were acquired using a 20x/0.70 oil-immersion objective.

Images of entire whole-mounted retinas were obtained with a Leica DM6B epifluorescence microscope equipped with a motorized stage and a 20x/0.5 air objective. Individual image stacks of a tile scan were automatically stitched together in the microscope software (LAS X, Leica). Overviews of the entire retinas were used for the large-scale quantification of HC density and to keep track of the precise location of the injected horizontal cells (see “retinal reconstruction” section).

Images are presented as single optical sections or as maximum intensity projections of image stacks. Some images were further processed with Fiji³⁴ using the “subtract background” (rolling

ball) plugin and intensities were normalized using the “enhance contrast” plugin with 0.01% saturation. Brightness and contrast of the final images were adjusted using Photoshop (Adobe).

QUANTIFICATION AND STATISTICAL ANALYSIS

Tracing and morphometric analysis

Tracer-coupled HCs were manually counted in Fiji using maximum intensity projections of confocal image stacks. Area measurements were based on convex hulls either encompassing dendritic trees of the HCs (Fig. 1) or all neurobiotin-positive cell bodies (Fig. 5).

Horizontal cell coupling was studied in 14 retinas and the positions and coupling strength were shown along with the independently measured horizontal cell density. The dendritic area was studied in 69 injected cells from 20 retinas (18 animals, either eye). The area was measured from convex hulls of the manually marked dendritic tree. A Sholl analysis³⁵ was used to compare the dendritic branching pattern of traced HCs (n=23) across retinal regions. For this, HC skeletons were traced through image stacks using Amira (Thermo Scientific). The number of intersections of dendritic processes with concentric circles was divided by the area of the respective circle. In Fig. 1M, each cell was normalized to equal convex hull area to focus only on the arborization patterns, not on sizes. Cells with overlapping, co-injected cells or any interference from blood vessels, which hindered accurate interpretation, were excluded.

Colocalization analysis

Immunoreactivity of Cx57 and ZO-1 was measured to assess spatial extent and colocalization. Confocal stacks of cone pedicles from the mid-periphery and periphery of dorsal and ventral regions from three retinas were analyzed (see boxed regions in Fig. 4). The total extent in z direction was chosen to capture the entire thickness of the ZO-1 cluster beneath a given cone pedicle³⁶, which typically included 20-25 consecutive optical sections. For each cone pedicle, a circular region of interest (ROI) with a diameter of 7 μm was selected around the ZO-1 cluster. Background and contrast was adjusted as described above, and a global threshold was independently applied. Colocalization of Cx57 and ZO-1 was analyzed with the “colocalization highlighter” plugin in Fiji (MBF collection^{37,38}). Areas of colocalization and areas of individual immunostaining per channel were measured in the same ROIs with the “analyze particles” plugin in Fiji. Colocalization areas smaller than 0.01 μm^2 were excluded from the analysis. Colocalization in images with one vertically flipped channel per ROI at a given cone pedicle position served as control measurements³⁹. For the quantification of the individual immunostainings, particles with a

size smaller than $0.04 \mu\text{m}^2$ were excluded from the analysis. This analysis was applied to 3 retinas. The area measurements were normalized (Fig. 4E-G) to account for differences between the samples regarding staining intensity and the relative background staining levels.

Statistical analysis

The areas of convex hulls that encompassed the dendritic trees of injected cells were compared with a tailed Wilcoxon rank sum test in MATLAB. Further statistical tests were performed using Prism 9 (GraphPad Software) on normalized ZO-1 and Cx57 immunostaining data (Fig. 4). A one-way ANOVA with a post-hoc Tukey test for multiple comparisons was used to compare the colocalized area in the dorsal and ventral retina. Flip controls were used to account for randomly observed colocalization. An unpaired, two-tailed Mann Whitney test was used to compare the immunoreactive areas of Cx57 and ZO-1 between dorsal and ventral measurements. A potential influence of the nasal-temporal axis and increased retinal eccentricity was assessed with a multi-way ANOVA (MATLAB). A p-value < 0.025 was considered statistically significant. Quantitative data was obtained from 3 retinas including 144 dorsal pedicles, 131 ventral pedicles presented as median and quartiles.

A Mann-Whitney test (Prism 7, GraphPad Software) was performed to test for statistical significance ($p < 0.05$) between the number of coupled cell bodies and the area covered by them (Fig. 5). Quantitative data was obtained from 14 retinas (7 retinas for each dorsal and ventral sides) reported as mean \pm SD in the text description and the median is indicated in Fig. 5D, E.

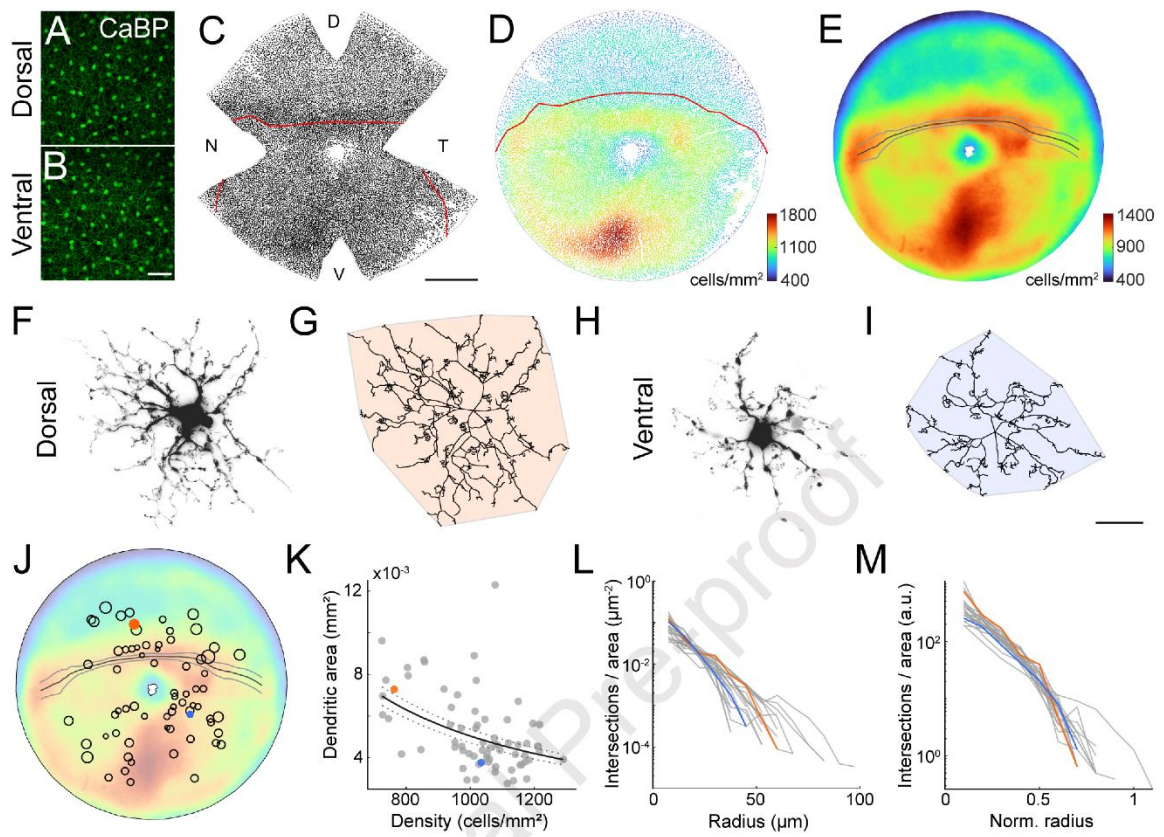
References

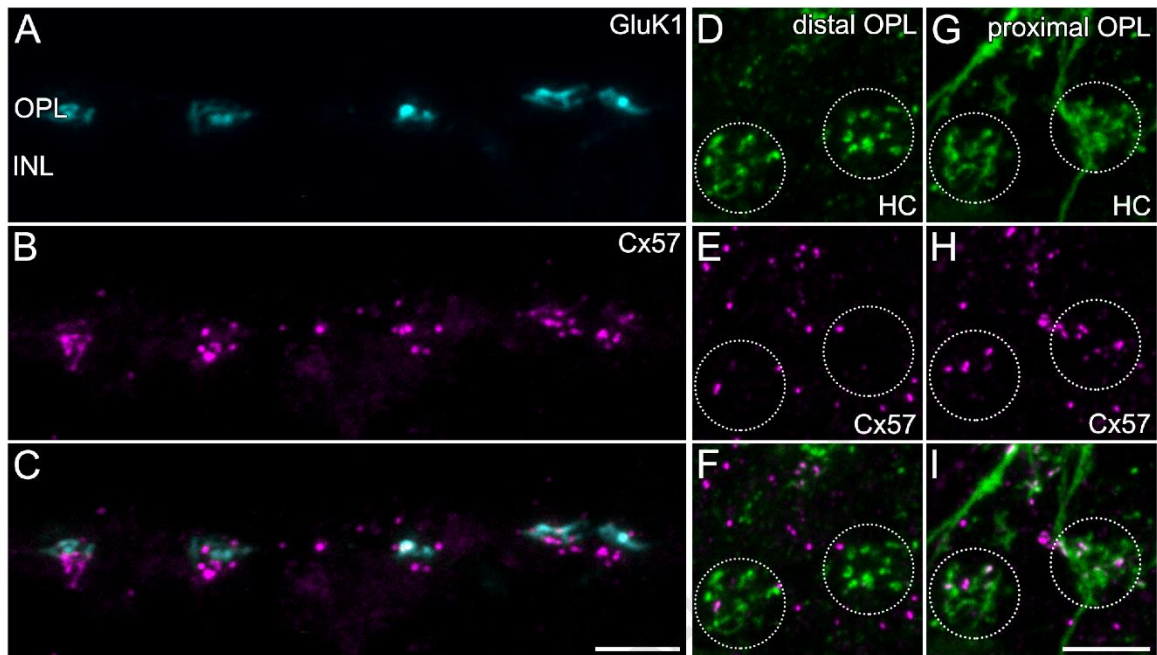
1. Baden, T., Euler, T., and Berens, P. (2020). Understanding the retinal basis of vision across species. *Nat. Rev. Neurosci.* 21, 5–20. <https://doi.org/10.1038/s41583-019-0242-1>.
2. Heukamp, A.S., Warwick, R.A., and Rivlin-Etzion, M. (2020). Topographic Variations in Retinal Encoding of Visual Space. *Annu. Rev. Vis. Sci.* 6, 237–259. <https://doi.org/10.1146/annurev-vision-121219-081831>.
3. Röhlich, P., van Veen, T., and Szél, A. (1994). Two different visual pigments in one retinal cone cell. *Neuron* 13, 1159–1166. [https://doi.org/10.1016/0896-6273\(94\)90053-1](https://doi.org/10.1016/0896-6273(94)90053-1).
4. Applebury, M.L., Antoch, M.P., Baxter, L.C., Chun, L.L., Falk, J.D., Farhangfar, F., Kage, K., Krzystolik, M.G., Lyass, L.A., and Robbins, J.T. (2000). The murine cone photoreceptor: a single cone type expresses both S and M opsins with retinal spatial patterning. *Neuron* 27, 513–523. [https://doi.org/10.1016/s0896-6273\(00\)00062-3](https://doi.org/10.1016/s0896-6273(00)00062-3).
5. Nadal-Nicolás, F.M., Kunze, V.P., Ball, J.M., Peng, B.T., Krishnan, A., Zhou, G., Dong, L., and Li, W. (2020). True S-cones are concentrated in the ventral mouse retina and wired for color detection in the upper visual field. *eLife* 9, e56840. <https://doi.org/10.7554/eLife.56840>.
6. Baden, T., Schubert, T., Chang, L., Wei, T., Zaichuk, M., Wissinger, B., and Euler, T. (2013). A tale of two retinal domains: near-optimal sampling of achromatic contrasts in natural scenes through asymmetric photoreceptor distribution. *Neuron* 80, 1206–1217. <https://doi.org/10.1016/j.neuron.2013.09.030>.
7. Qiu, Y., Zhao, Z., Klindt, D., Kautzky, M., Szatko, K.P., Schaeffel, F., Rifai, K., Franke, K., Busse, L., and Euler, T. (2021). Natural environment statistics in the upper and lower visual field are reflected in mouse retinal specializations. *Curr. Biol. CB* 31, 3233-3247.e6. <https://doi.org/10.1016/j.cub.2021.05.017>.
8. Salinas-Navarro, M., Jiménez-López, M., Valiente-Soriano, F.J., Alarcón-Martínez, L., Avilés-Trigueros, M., Mayor, S., Holmes, T., Lund, R.D., Villegas-Pérez, M.P., and Vidal-Sanz, M. (2009). Retinal ganglion cell population in adult albino and pigmented mice: a computerized analysis of the entire population and its spatial distribution. *Vision Res.* 49, 637–647. <https://doi.org/10.1016/j.visres.2009.01.010>.
9. Duda, S., Block, C.T., Pradhan, D.R., Arzhangnia, Y., Greschner, M., and Puller, C. (2023). Spatial distribution and functional integration of displaced ipRGCs. *bioRxiv*, 2023.09.05.556383. <https://doi.org/10.1101/2023.09.05.556383>.
10. Zhang, Y., Kim, I.-J., Sanes, J.R., and Meister, M. (2012). The most numerous ganglion cell type of the mouse retina is a selective feature detector. *Proc. Natl. Acad. Sci. U. S. A.* 109, E2391-2398. <https://doi.org/10.1073/pnas.1211547109>.
11. Bleckert, A., Schwartz, G.W., Turner, M.H., Rieke, F., and Wong, R.O.L. (2014). Visual space is represented by nonmatching topographies of distinct mouse retinal ganglion cell types. *Curr. Biol. CB* 24, 310–315. <https://doi.org/10.1016/j.cub.2013.12.020>.
12. Rousso, D.L., Qiao, M., Kagan, R.D., Yamagata, M., Palmiter, R.D., and Sanes, J.R. (2016). Two Pairs of ON and OFF Retinal Ganglion Cells Are Defined by Intersectional Patterns of Transcription Factor Expression. *Cell Rep.* 15, 1930–1944. <https://doi.org/10.1016/j.celrep.2016.04.069>.
13. Berry, M.H., Moldavan, M., Garrett, T., Meadows, M., Cravetchi, O., White, E., Leffler, J., von Gersdorff, H., Wright, K.M., Allen, C.N., et al. (2023). A melanopsin ganglion cell subtype forms a dorsal retinal mosaic projecting to the supraoptic nucleus. *Nat. Commun.* 14, 1492. <https://doi.org/10.1038/s41467-023-36955-6>.
14. Chang, L., Breuninger, T., and Euler, T. (2013). Chromatic coding from cone-type unselective circuits in the mouse retina. *Neuron* 77, 559–571. <https://doi.org/10.1016/j.neuron.2012.12.012>.
15. Sabbah, S., Gemmer, J.A., Bhatia-Lin, A., Manoff, G., Castro, G., Siegel, J.K., Jeffery, N., and Berson, D.M. (2017). A retinal code for motion along the gravitational and body axes.

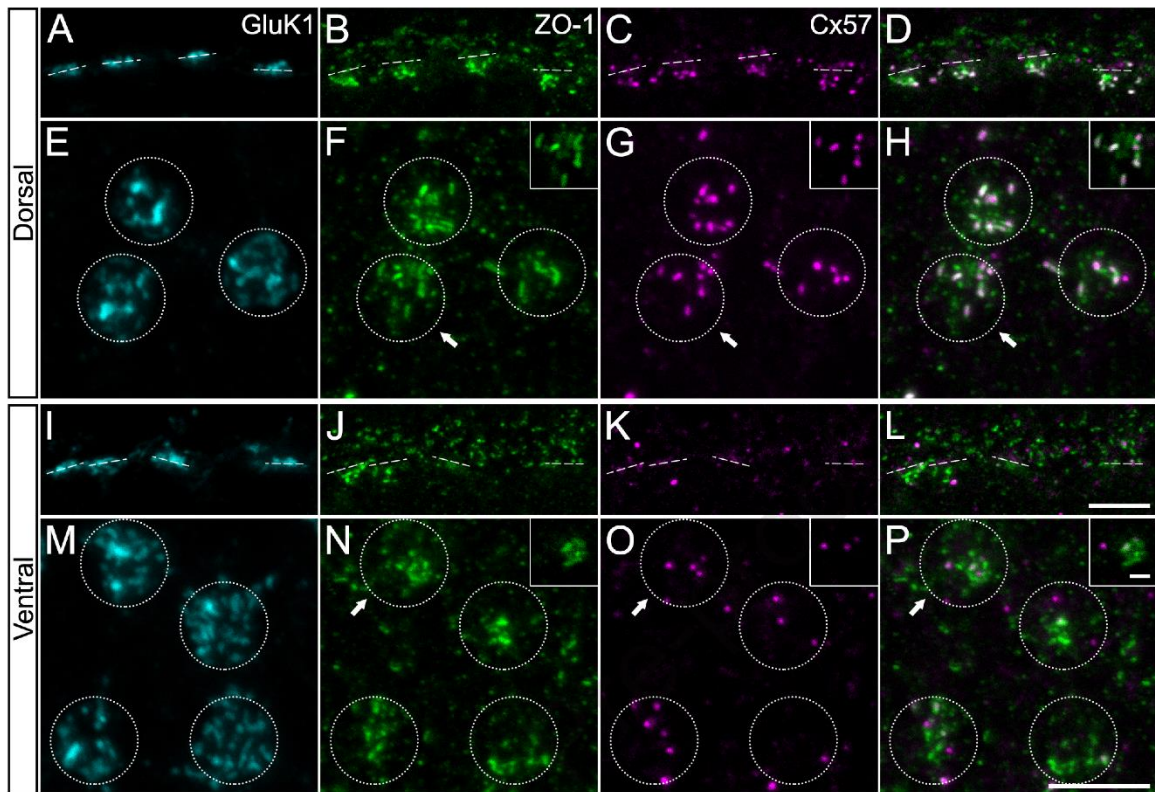
- Nature 546, 492–497. <https://doi.org/10.1038/nature22818>.
16. Warwick, R.A., Kaushansky, N., Sarid, N., Golan, A., and Rivlin-Etzion, M. (2018). Inhomogeneous Encoding of the Visual Field in the Mouse Retina. *Curr. Biol.* CB 28, 655–665.e3. <https://doi.org/10.1016/j.cub.2018.01.016>.
 17. Holmgren, C.D., Stahr, P., Wallace, D.J., Voit, K.-M., Matheson, E.J., Sawinski, J., Bassetto, G., and Kerr, J.N. (2021). Visual pursuit behavior in mice maintains the pursued prey on the retinal region with least optic flow. *eLife* 10, e70838. <https://doi.org/10.7554/eLife.70838>.
 18. Johnson, K.P., Fitzpatrick, M.J., Zhao, L., Wang, B., McCracken, S., Williams, P.R., and Kerschensteiner, D. (2021). Cell-type-specific binocular vision guides predation in mice. *Neuron* 109, 1527–1539.e4. <https://doi.org/10.1016/j.neuron.2021.03.010>.
 19. Raghuram, V., Werginz, P., and Fried, S.I. (2019). Scaling of the AIS and Somatodendritic Compartments in α S RGCs. *Front. Cell. Neurosci.* 13, 436. <https://doi.org/10.3389/fncel.2019.00436>.
 20. Werginz, P., Raghuram, V., and Fried, S.I. (2020). Tailoring of the axon initial segment shapes the conversion of synaptic inputs into spiking output in OFF- α T retinal ganglion cells. *Sci. Adv.* 6, eabb6642. <https://doi.org/10.1126/sciadv.abb6642>.
 21. Gupta, D., Młynarski, W., Sumser, A., Symonova, O., Svatoň, J., and Joesch, M. (2023). Panoramic visual statistics shape retina-wide organization of receptive fields. *Nat. Neurosci.* 26, 606–614. <https://doi.org/10.1038/s41593-023-01280-0>.
 22. Diamond, J.S. (2017). Inhibitory Interneurons in the Retina: Types, Circuitry, and Function. *Annu. Rev. Vis. Sci.* 3, 1–24. <https://doi.org/10.1146/annurev-vision-102016-061345>.
 23. Chaya, T., Matsumoto, A., Sugita, Y., Watanabe, S., Kuwahara, R., Tachibana, M., and Furukawa, T. (2017). Versatile functional roles of horizontal cells in the retinal circuit. *Sci. Rep.* 7, 5540. <https://doi.org/10.1038/s41598-017-05543-2>.
 24. Drinnenberg, A., Franke, F., Morikawa, R.K., Jüttner, J., Hillier, D., Hantz, P., Hierlemann, A., Azeredo da Silveira, R., and Roska, B. (2018). How Diverse Retinal Functions Arise from Feedback at the First Visual Synapse. *Neuron* 99, 117–134.e11. <https://doi.org/10.1016/j.neuron.2018.06.001>.
 25. Ströh, S., Puller, C., Swirski, S., Hölzel, M.-B., van der Linde, L.I.S., Segelken, J., Schultz, K., Block, C., Monyer, H., Willecke, K., et al. (2018). Eliminating Glutamatergic Input onto Horizontal Cells Changes the Dynamic Range and Receptive Field Organization of Mouse Retinal Ganglion Cells. *J. Neurosci. Off. J. Soc. Neurosci.* 38, 2015–2028. <https://doi.org/10.1523/JNEUROSCI.0141-17.2018>.
 26. Thoreson, W.B., and Mangel, S.C. (2012). Lateral interactions in the outer retina. *Prog. Retin. Eye Res.* 31, 407–441. <https://doi.org/10.1016/j.preteyeres.2012.04.003>.
 27. Bloomfield, S.A., Xin, D., and Persky, S.E. (1995). A comparison of receptive field and tracer coupling size of horizontal cells in the rabbit retina. *Vis. Neurosci.* 12, 985–999. <https://doi.org/10.1017/s0952523800009524>.
 28. Hombach, S., Janssen-Bienhold, U., Söhl, G., Schubert, T., Büssow, H., Ott, T., Weiler, R., and Willecke, K. (2004). Functional expression of connexin57 in horizontal cells of the mouse retina. *Eur. J. Neurosci.* 19, 2633–2640. <https://doi.org/10.1111/j.0953-816X.2004.03360.x>.
 29. Shelley, J., Dedek, K., Schubert, T., Feigenspan, A., Schultz, K., Hombach, S., Willecke, K., and Weiler, R. (2006). Horizontal cell receptive fields are reduced in connexin57-deficient mice. *Eur. J. Neurosci.* 23, 3176–3186. <https://doi.org/10.1111/j.1460-9568.2006.04848.x>.
 30. Zhang, A.-J., Jacoby, R., and Wu, S.M. (2011). Light- and dopamine-regulated receptive field plasticity in primate horizontal cells. *J. Comp. Neurol.* 519, 2125–2134. <https://doi.org/10.1002/cne.22604>.
 31. Stabio, M.E., Sondereker, K.B., Haghgou, S.D., Day, B.L., Chidsey, B., Sabbah, S., and Renna, J.M. (2018). A novel map of the mouse eye for orienting retinal topography in anatomical space. *J. Comp. Neurol.* 526, 1749–1759. <https://doi.org/10.1002/cne.24446>.

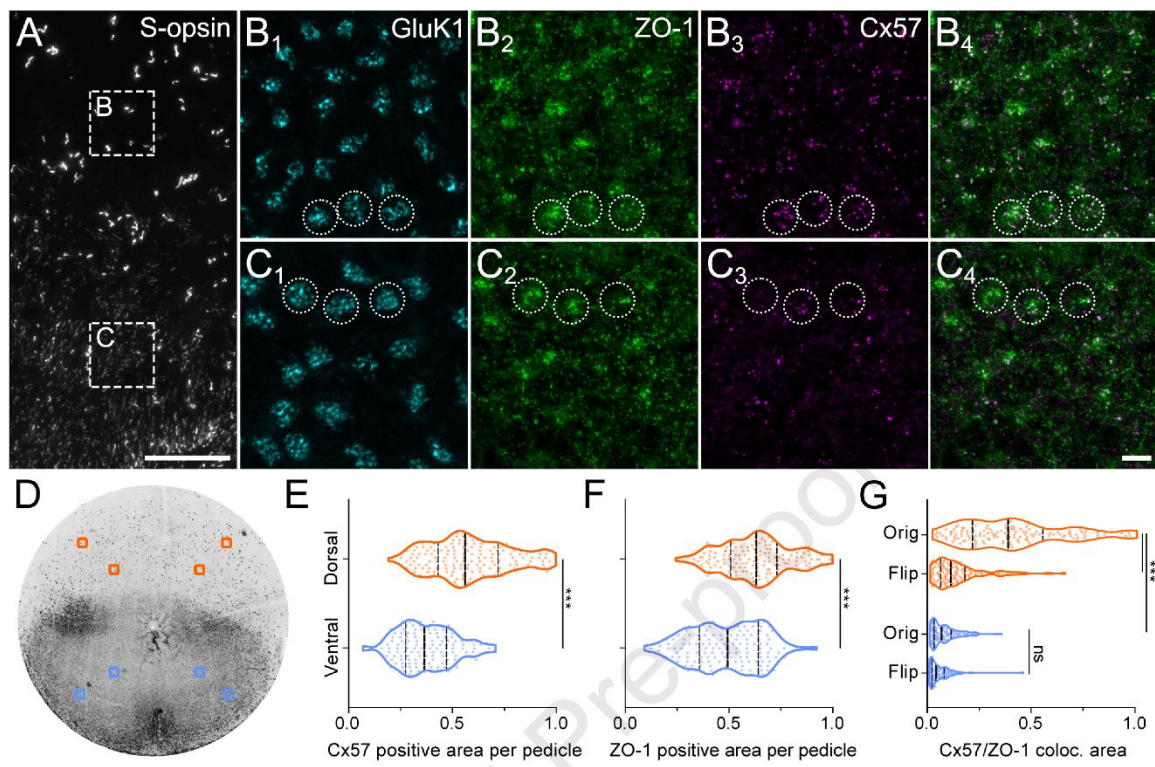
32. Sterratt, D.C., Lyngholm, D., Willshaw, D.J., and Thompson, I.D. (2013). Standard anatomical and visual space for the mouse retina: computational reconstruction and transformation of flattened retinæ with the Retistruct package. *PLoS Comput. Biol.* 9, e1002921. <https://doi.org/10.1371/journal.pcbi.1002921>.
33. Schmucker, C., and Schaeffel, F. (2004). A paraxial schematic eye model for the growing C57BL/6 mouse. *Vision Res.* 44, 1857–1867. <https://doi.org/10.1016/j.visres.2004.03.011>.
34. Schindelin, J., Arganda-Carreras, I., Frise, E., Kaynig, V., Longair, M., Pietzsch, T., Preibisch, S., Rueden, C., Saalfeld, S., Schmid, B., et al. (2012). Fiji: an open-source platform for biological-image analysis. *Nat. Methods* 9, 676–682. <https://doi.org/10.1038/nmeth.2019>.
35. Sholl, D.A. (1953). Dendritic organization in the neurons of the visual and motor cortices of the cat. *J. Anat.* 87, 387–406.1.
36. Puller, C., de Sevilla Müller, L.P., Janssen-Bienhold, U., and Haverkamp, S. (2009). ZO-1 and the spatial organization of gap junctions and glutamate receptors in the outer plexiform layer of the mammalian retina. *J. Neurosci. Off. J. Soc. Neurosci.* 29, 6266–6275. <https://doi.org/10.1523/JNEUROSCI.5867-08.2009>.
37. Collins, T.J. (2007). ImageJ for microscopy. *BioTechniques* 43, 25–30. <https://doi.org/10.2144/000112517>.
38. Tetenborg, S., Yadav, S.C., Hormuzdi, S.G., Monyer, H., Janssen-Bienhold, U., and Dedek, K. (2017). Differential Distribution of Retinal Ca²⁺/Calmodulin-Dependent Kinase II (CaMKII) Isoforms Indicates CaMKII- β and - δ as Specific Elements of Electrical Synapses Made of Connexin36 (Cx36). *Front. Mol. Neurosci.* 10.
39. Puller, C., Haverkamp, S., and Grünert, U. (2007). OFF midget bipolar cells in the retina of the marmoset, *Callithrix jacchus*, express AMPA receptors. *J. Comp. Neurol.* 502, 442–454. <https://doi.org/10.1002/cne.21315>.
40. Gallego-Ortega, A., Norte-Muñoz, M., Miralles de Imperial-Ollero, J.A., Bernal-Garro, J.M., Valiente-Soriano, F.J., de la Villa Polo, P., Avilés-Trigueros, M., Villegas-Pérez, M.P., and Vidal-Sanz, M. (2020). Functional and morphological alterations in a glaucoma model of acute ocular hypertension. *Prog. Brain Res.* 256, 1–29. <https://doi.org/10.1016/bs.pbr.2020.07.003>.
41. Camerino, M.J., Engerbretson, I.J., Fife, P.A., Reynolds, N.B., Berria, M.H., Doyle, J.R., Clemons, M.R., Gencarella, M.D., Borghuis, B.G., and Fuerst, P.G. (2021). OFF bipolar cell density varies by subtype, eccentricity, and along the dorsal ventral axis in the mouse retina. *J. Comp. Neurol.* 529, 1911–1925. <https://doi.org/10.1002/cne.25064>.
42. Haverkamp, S., and Wässle, H. (2000). Immunocytochemical analysis of the mouse retina. *J. Comp. Neurol.* 424, 1–23.
43. Ortín-Martínez, A., Nadal-Nicolás, F.M., Jiménez-López, M., Alburquerque-Béjar, J.J., Nieto-López, L., García-Ayuso, D., Villegas-Pérez, M.P., Vidal-Sanz, M., and Agudo-Barriuso, M. (2014). Number and distribution of mouse retinal cone photoreceptors: differences between an albino (Swiss) and a pigmented (C57/BL6) strain. *PLoS One* 9, e102392. <https://doi.org/10.1371/journal.pone.0102392>.
44. Wässle, H., and Riemann, H.J. (1978). The mosaic of nerve cells in the mammalian retina. *Proc. R. Soc. Lond. B Biol. Sci.* 200, 441–461. <https://doi.org/10.1098/rspb.1978.0026>.
45. Reese, B.E., Raven, M.A., and Stagg, S.B. (2005). Afferents and homotypic neighbors regulate horizontal cell morphology, connectivity, and retinal coverage. *J. Neurosci. Off. J. Soc. Neurosci.* 25, 2167–2175. <https://doi.org/10.1523/JNEUROSCI.4876-04.2005>.
46. Keeley, P.W., Eglén, S.J., and Reese, B.E. (2020). From Random to Regular: Variation in the Patterning of Retinal Mosaics. *J. Comp. Neurol.* 528, 2135–2160. <https://doi.org/10.1002/cne.24880>.
47. Raven, M.A., Oh, E.C.T., Swaroop, A., and Reese, B.E. (2007). Afferent Control of Horizontal Cell Morphology Revealed by Genetic Respecification of Rods and Cones. *J.*

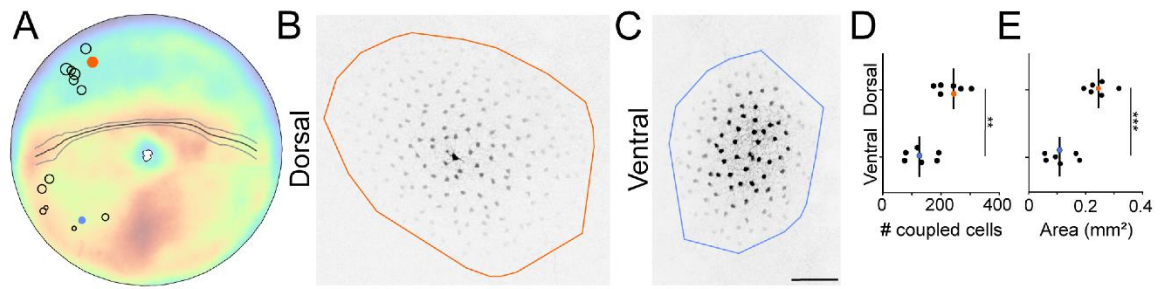
- Neurosci. 27, 3540–3547. <https://doi.org/10.1523/JNEUROSCI.0372-07.2007>.
48. Behrens, C., Yadav, S.C., Korympidou, M.M., Zhang, Y., Haverkamp, S., Irsen, S., Schaedler, A., Lu, X., Liu, Z., Lause, J., et al. (2022). Retinal horizontal cells use different synaptic sites for global feedforward and local feedback signaling. *Curr. Biol. CB* 32, 545–558.e5. <https://doi.org/10.1016/j.cub.2021.11.055>.
 49. Janssen-Bienhold, U., Trümppler, J., Hilgen, G., Schultz, K., Müller, L.P.D.S., Sonntag, S., Dedek, K., Dirks, P., Willecke, K., and Weiler, R. (2009). Connexin57 is expressed in dendro-dendritic and axo-axonal gap junctions of mouse horizontal cells and its distribution is modulated by light. *J. Comp. Neurol.* 513, 363–374. <https://doi.org/10.1002/cne.21965>.
 50. Dorgau, B., Herrling, R., Schultz, K., Greb, H., Segelken, J., Ströh, S., Bolte, P., Weiler, R., Dedek, K., and Janssen-Bienhold, U. (2015). Connexin50 couples axon terminals of mouse horizontal cells by homotypic gap junctions. *J. Comp. Neurol.* 523, 2062–2081. <https://doi.org/10.1002/cne.23779>.
 51. Trümppler, J., Dedek, K., Schubert, T., de Sevilla Müller, L.P., Seeliger, M., Humphries, P., Biel, M., and Weiler, R. (2008). Rod and cone contributions to horizontal cell light responses in the mouse retina. *J. Neurosci. Off. J. Soc. Neurosci.* 28, 6818–6825. <https://doi.org/10.1523/JNEUROSCI.1564-08.2008>.
 52. Vaney, D.I. (1991). Many diverse types of retinal neurons show tracer coupling when injected with biocytin or Neurobiotin. *Neurosci. Lett.* 125, 187–190. [https://doi.org/10.1016/0304-3940\(91\)90024-N](https://doi.org/10.1016/0304-3940(91)90024-N).
 53. He, S., Weiler, R., and Vaney, D.I. (2000). Endogenous dopaminergic regulation of horizontal cell coupling in the mammalian retina. *J. Comp. Neurol.* 418, 33–40. [https://doi.org/10.1002/\(sici\)1096-9861\(20000228\)418:1<33::aid-cne3>3.0.co;2-j](https://doi.org/10.1002/(sici)1096-9861(20000228)418:1<33::aid-cne3>3.0.co;2-j).
 54. Haverkamp, S., Grünert, U., and Wässle, H. (2000). The cone pedicle, a complex synapse in the retina. *Neuron* 27, 85–95. [https://doi.org/10.1016/s0896-6273\(00\)00011-8](https://doi.org/10.1016/s0896-6273(00)00011-8).
 55. Sharpe, Z.J., Shehu, A., and Ichinose, T. (2022). Asymmetric Distributions of Achromatic Bipolar Cells in the Mouse Retina. *Front. Neuroanat.* 15. <https://doi.org/10.3389/fnana.2021.786142>.
 56. Münch, T.A., da Silveira, R.A., Siegert, S., Viney, T.J., Awatramani, G.B., and Roska, B. (2009). Approach sensitivity in the retina processed by a multifunctional neural circuit. *Nat. Neurosci.* 12, 1308–1316. <https://doi.org/10.1038/nn.2389>.
 57. Kim, T., Shen, N., Hsiang, J.-C., Johnson, K.P., and Kerschensteiner, D. (2020). Dendritic and parallel processing of visual threats in the retina control defensive responses. *Sci. Adv.* 6, eabc9920. <https://doi.org/10.1126/sciadv.abc9920>.
 58. Wang, F., Li, E., De, L., Wu, Q., and Zhang, Y. (2021). OFF-transient alpha RGCs mediate looming triggered innate defensive response. *Curr. Biol. CB* 31, 2263–2273.e3. <https://doi.org/10.1016/j.cub.2021.03.025>.
 59. Dedek, K., Pandarinath, C., Alam, N.M., Wellershaus, K., Schubert, T., Willecke, K., Prusky, G.T., Weiler, R., and Nirenberg, S. (2008). Ganglion cell adaptability: does the coupling of horizontal cells play a role? *PLoS One* 3, e1714. <https://doi.org/10.1371/journal.pone.0001714>.
 60. Jackman, S.L., Babai, N., Chambers, J.J., Thoreson, W.B., and Kramer, R.H. (2011). A positive feedback synapse from retinal horizontal cells to cone photoreceptors. *PLoS Biol.* 9, e1001057. <https://doi.org/10.1371/journal.pbio.1001057>.
 61. Ribelayga, C.P., and O'Brien, J. (2017). Chapter 10 - Circadian and Light-Adaptive Control of Electrical Synaptic Plasticity in the Vertebrate Retina. In *Network Functions and Plasticity*, J. Jing, ed. (Academic Press), pp. 209–241. <https://doi.org/10.1016/B978-0-12-803471-2.00010-2>.



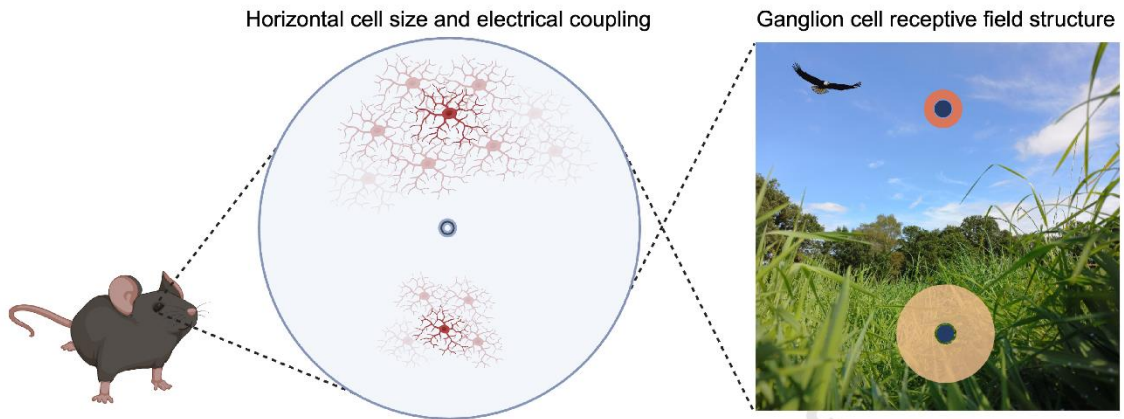








Journal Pre-proof



Journal Pre-proof

- Horizontal cell properties are asymmetrically organized along the dorso-ventral axis
- Dorsal cells are larger than ventral cells
- Dorsal cells are more extensively coupled via gap junctions than ventral cells
- Changes occur at the opsin transition zone of photoreceptors, i.e. the visual horizon

Journal Pre-proof

Key resources table

REAGENT or RESOURCE	SOURCE	IDENTIFIER
Antibodies		
Rabbit polyclonal anti-Calbindin	Swant	Cat#cb38a; RRID: AB_3107026
Guinea pig polyclonal anti-Connexin57-PGS	This paper	N/A
Guinea pig polyclonal anti-Connexin57-CSM	This paper	N/A
Rabbit polyclonal anti-Connexin57	Hombach et al., ²⁸	RRID:AB_2490076
Mouse monoclonal anti-GluK1(E-12)	Santa Cruz Biotechnology	Cat#sc393420; RRID:AB_2716684
Goat polyclonal anti-S-opsin	Santa Cruz Biotechnology	Cat#sc14363; RRID:AB_2158332
Mouse monoclonal anti-ZO-1	Zymed	Cat#33-9100; RRID:AB_87181
Rabbit polyclonal anti-ZO-1	Zymed	Cat#61-7300; RRID:AB_138452
Donkey anti-rabbit IgG (H+L) Alexa Fluor 488	Invitrogen	Cat#A-21206; RRID:AB_2535792
Donkey anti-mouse IgG (H+L) Alexa Fluor 568	Invitrogen	Cat#A10037; RRID:AB_11180865
Donkey anti-goat IgG (H+L) Alexa Fluor 647	Invitrogen	Cat#A-21447; RRID:AB_141844
Donkey anti-mouse IgG (H+L) Alexa Fluor 647	Invitrogen	Cat#A-31571; RRID:AB_162542
Donkey anti-goat IgG (H+L) Alexa Fluor 405	Abcam	Cat#ab175664; RRID:AB_2313502
Donkey anti-guinea pig IgG (H+L) CF568	Sigma-Aldrich	Cat#SAB4600469; RRID:AB_2832959
Chemicals, peptides, and recombinant proteins		
Alexa Fluor 568 Hydrazide	Invitrogen	Cat#A10441
Streptavidin, Alexa Fluor 568 Conjugate	Invitrogen	Cat#S-11226
Ames' Medium	Sigma-Aldrich	Cat#A1420
DAPI	Abcam	Cat#228549
Neurobiotin tracer	Biozol	Cat#SP1120-20
Experimental models: Organisms/strains		
Mouse: C57BL/6J	Tierhaus, Carl von Ossietzky Universität Oldenburg	N/A
Mouse: Cx57 ^{LacZ/LacZ}	Hombach et al., ²⁸	RRID:IMSR_EM:01644
Software and algorithms		
LAS X Software Leica DM6	Leica Microsystems	RRID:SCR_024857
Fiji	Schindelin et al., ³³	RRID:SCR_002285

Journal Pre-proof

GraphPad Prism 7.0	GraphPad Software	RRID:SCR_002798
GraphPad Prism 9.0	GraphPad Software	RRID:SCR_002798
Adobe Photoshop	Adobe	RRID:SCR_014199
Adobe Illustrator	Adobe	RRID:SCR_010279
MATLAB	The MathWorks, Inc.	RRID:SCR_001622
R package RetiStruct	Sterratt et al., ⁴²	N/A

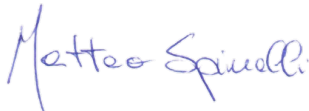
Journal Pre-proof

8. Erklärung

Hiermit erkläre ich, dass ich die vorliegende Arbeit selbstständig verfasst habe und keine, als die angegebenen Quellen und Hilfsmittel verwendet habe. Ich versichere, dass diese Arbeit weder in ihrer Gesamtheit noch in Teilen einer anderen Hochschule zur Begutachtung in einem Promotionsverfahren vorliegt oder vorgelegen hat und dass ich die Leitlinien guter wissenschaftlicher Praxis der Carl von Ossietzky Universität Oldenburg befolgt habe. Weiterhin versichere ich, dass im Zusammenhang mit dem Promotionsvorhaben keine kommerziellen Vermittlungs- oder Beratungsdienste (Promotionsberatung) in Anspruch genommen worden sind.

Oldenburg, 08 November 2024

(Ort, Datum)

 (Matteo Spinelli)